Optimization Algorithms for Realizable Signal-Adapted Filter Banks

Thesis by

Andre Tkacenko

In Partial Fulfillment of the Requirements

for the Degree of

Doctor of Philosophy

California Institute of Technology

Pasadena, California

2004

(Submitted May 12, 2004)

Acknowledgements

First of all, I would like to thank my advisor, Prof. P. P. Vaidyanathan, for the guidance he has given me and for supporting me during my stay at Caltech. I first met P. P. when I was an undergrad at Caltech, when he was assigned to be my advisor. Even though he was rather busy on account of his Option Representative duties at the time, he was always there when I needed to see him and attentative when I spoke with him. My respect for him grew when I took his course on digital signal processing, EE 112. He was always able to take a daunting and difficult to understand concept and simplify it and make it unintimidating. I was so grateful the day that P. P., after finishing his EE 112 lecture for the day, told me that I had been admitted to his group. As my graduate advisor, he was always there for me and had my best interests at heart. He always pointed me in the right direction when I was lost and supported me when I was on the right path. In addition to being my mentor, he has also been a good friend to me. He has a good sense of humor and often times we have exchanged jokes. (In addition to our love for digital signal processing and our sense of humor, P. P. and I also have something else in common: a love for Three's Company!) I will always be grateful for the opportunity that he gave me to teach the multirate part of his signal processing course, EE 112b, in the spring of 2003. Because of him, I aspire to return to academia some day.

I would like to thank the National Science Foundation (NSF) and the Office of Naval Research (ONR) for financially supporting as a graduate student at Caltech. Also, I would like to thank the members of my defense and candidacy examining committees: Prof. Robert J. McEliece, Prof. Babak Hassibi, Prof. Jehoshua Bruck, Dr. Bojan Vrcelj, Dr. Payman Arabshahi, and Prof. Joel N. Franklin. In particular, I would like to thank Prof. McEliece (The Chief) for being my teacher, senior thesis advisor as an undergrad, and good friend. He was always willing to lend an ear to my social travails and offer me good advise on what to do. Though his advise was always sagacious, I unfortunately rarely followed it on account of my being young and näive. I would like to thank him for his advise and friendship by taking him out to a certain restaurant again some time! In addition to the above people, I would like to thank some of my teachers at Wilcox High School

including Al Holland, my calculus teacher, and my gym teacher Jerry Louderback, whose wife was able to procure a Caltech undergraduate application form for me at the proverbial eleventh hour.

I would like to thank my lab mates Bojan Vrcelj, Sony Akkarakaran, Murat Meşe, Byung-Jun Yoon, Sriram Murali, Mike Larsen, and Borching Su for making my time spent in the lab cheerful and fun. My senior lab mates, Bojan, Sony, and Murat, were inspirational to me and helped me mature from the first year graduate student that I once was to the senior leveled one that I am now. In particular, I would especially like to thank Bojan for being both my friend and an elderly brother figure for me. I miss our afternoon trips to Starbucks in Old Town Pasadena where we used to sit, chat, and ogle at all of the pretty girls as they walked by. With any luck, I hope we will be able to resume our old tradition once again. In addition, I would also like to thank Prof. Shayan Mookherjea, my old friend from my undergraduate days at Caltech. I want to thank Shayan for walking with me to all of those restaurants we used to eat at before any of us had cars and also for introducing me to LaTeX. Also, I want to thank Aristotelis Asimakopoulous, and friend of mine from my undergraduate days who came back to Caltech during my graduate studies. He was my partner in crime in various nefarious activities which I elect to omit here.

Also, I would like to thank my parents, Dusanka and Nikola Tkacenko, for their endless love and support. I am indebted to them for the sacrifices that they made to put me through school as an undergraduate. It is my hope that some day I will be able to be as good of a parent to my children as my parents have been to me. I want to thank my brothers Nick, Boris, and Aleks for being the best siblings that I could hope for. In particular, I want to thank my brother Nick for being my best friend (and for introducing me to Buffy and Angel). I hope that we will be able to spend more time with each other after he finishes school at UC Santa Cruz. Furthermore, I would also like to thank my grandparents, Sofija and Nikola Milunovic, for their love and support. In particular, I want to thank my grandfather Nikola, who is a master woodcarver, for offering to carve me a throne for completing my doctorate. As with all of his other works, I am sure that it is the “only one kind on planet [sic]”.

I would like to give a special thanks to my Princessa Victoria Delgadillo. She came into my life when I least expected it and most needed it. It is because of her that I know what it is to feel alive. She has been a light in my darkness and has shown me true happiness. I want to thank her for loving me and supporting me during this tumultuous time in my life. Though I don’t know what the future may hold for us, I want her to know that I love her and that she will always be a part of my heart and my soul, now and forever.

Last, but certainly not least, I would like to thank God, the Infinite Being, for creating this beautiful world in which we all live and beautiful mathematics (some of which I will present here in my thesis). I also want to thank Him for always watching over me and protecting me (even when I didn't deserve it). Whenever I put my faith in His will, He always led me on the right path. I pray that His love and divine presence will be with us all, now and ever, and unto the ages of ages. Amen.

Abstract

Multirate filter banks are fundamental systems commonly used in digital signal processing (DSP). Typically, they are used to decompose a discrete-time signal into a set of frequency selective components called subband signals. Filter banks have been found to be useful for lossy data compression schemes such as MP3 and JPEG 2000, denoising, and signal estimation. In the last decade, transmultiplexers, the dual structures of multirate filter banks, have been shown to be useful in digital communications systems such as discrete multitone (DMT) systems for channel equalization and inter/intra-symbol interference cancellation in the presence of noise.

Recently, a special type of filter bank adapted to its input known as the principal component filter bank (PCFB) has been shown to be simultaneously optimal for a wide variety of objectives. Such filter banks are not only optimal for relevant data compression type objectives such as coding gain and multiresolution, but also for digital communications type objectives such as power minimization, when the filter bank is implemented in its transmultiplexer form. The only problem is that PCFBs, which are defined over classes of paraunitary (PU) filter banks, are only known to exist for certain classes. In particular, PCFBs are in general known to exist only in the extremal cases where the analysis/synthesis polyphase matrix has zero memory and doubly infinite memory, respectively. Furthermore, for many practical cases of inputs, the filters corresponding to the infinite-order PCFB have ideal bandpass response and are as such unrealizable. When the polyphase matrix has finite memory or a finite impulse response (FIR), it is believed that PCFBs do not exist, although this has not yet been formally proven in the literature.

The main contribution of this thesis is to *bridge the gap* between the zero memory PCFB and the infinite-order one. To that end, a variety of methods for the design of *realizable* signal-adapted FIR filter banks is presented. It is shown that a popular conventional method for designing signal-adapted FIR PU filter banks, which only requires the design of an optimal FIR compaction filter, is in fact not well suited for designing good filter banks due to the exponential complexity caused by the nonuniqueness of the FIR compaction filter. To avoid this dilemma, we propose a method by which all of the filters are obtained together. In particular, the method consists of finding an FIR PU least-squares approximant to the infinite-order PCFB polyphase matrix. Using an elegant complete parameterization of FIR PU systems in terms of canonical building blocks, an iterative greedy algorithm for solving the least-squares problem is presented. Simulation results provided here show that as the order or memory of the signal-adapted FIR PU filter bank increases, the filter bank behaves more and more like the infinite-order PCFB in terms of a variety of objectives included coding gain, multiresolution, and power minimization. This serves to *bridge the gap* between the zero memory and infinite memory PCFBs, which previously has not been done in the literature.

In addition to being useful for the design of PCFB-like FIR filter banks, the proposed iterative algorithm can also be used for a variety of other design problems including the FIR PU interpolation problem. Unlike the traditional FIR interpolation problem, whose solution is known in closed form, the FIR PU interpolation problem is far more difficult and is in fact still open. Despite this, the proposed algorithm can be used to find an approximant to an interpolant and sometimes even find an interpolant, as we show here through simulations.

In the second part of the thesis, we focus on the design of realizable signal-adapted quantized filter banks in which the filters are FIR but otherwise unconstrained. The filters are chosen to minimize the mean-squared error of the output, which is shown to be equivalent to maximizing the coding gain of the system. By alternately optimizing the analysis and synthesis filters, an iterative greedy algorithm, different from that mentioned above, is proposed for the design of such filter banks. Simulation results provided show that the filter banks designed exhibit performance close to the information theoretic rate-distortion bound.

Finally, we show how some of the techniques used in the above iterative algorithms can be used for the design of a channel shortening equalizer. Channel shortening equalizers, which arise in the context of digital communications, have been found to be necessary for DMT systems such as the digital subscriber loop (DSL) in which the channel impulse response must be *shortened* to the length of the cyclic prefix. In particular, we show how the eigenfilter technique which is used in the above-mentioned FIR PU iterative greedy algorithm, can be used for the design of a noise optimized channel shortening equalizer. As opposed to other techniques, which require a Cholesky decomposition of a certain matrix for every delay parameter considered, the proposed method is lower in complexity in that it only requires a single such decomposition for all delay values. Despite this significant decrease in complexity, it is shown through simulations that the equalizers designed using this technique perform nearly optimally in terms of observed bit rate.

Contents

List of Figures

List of Tables

Chapter 1

Introduction

Filter banks are common systems that arise in the study of multirate digital signal processing [67, 13] and wavelet theory [32, 47]. Essentially, a multirate filter bank decomposes a given input signal into a set of lower rate components known as subband signals. Often times, some subband signals contain more information about the original input than others. In these cases, the subbands can be easily manipulated to remove some of the redundancy present in the original input signal, resulting in data compression. Popular lossy data compression schemes such as MP3 (for audio signals) as well as JPEG and JPEG 2000 (for image signals) use filter banks in this manner to remove the redundancy present in the original signals [41, 39]. In addition to this, transmultiplexers [67], which are dual structures of multirate filter banks, have been found to be useful in digital communications [46, 15, 16]. By adding a minimal amount of redundancy, transmultiplexers have been found to be able to achieve stable blind channel equalization [14, 42, 43] and the removal of inter/intra-symbol interference [17, 18] all in the presence of noise. Several well known modern communications systems such as digital subscriber loop (DSL) and orthogonal frequency division multiplexing (OFDM), which are examples of discrete multitone (DMT) systems [26], consist of transmultiplexers with redundancy [46].

Recently, a special filter bank adapted to its input statistics known as the principal components filter bank (PCFB) [62, 1, 69] has been found to be *simultaneously* optimal for a wide variety of objectives. In particular, PCFBs are optimal for data compression type objectives such as coding gain and multiresolution, as well as for digital communications type objectives such as power minimization when the filter bank is implemented in its transmultiplexer form [1]. Unfortunately, PCFBs, which are defined over classes of paraunitary (PU) filter banks, are in general only known to exist for two special classes [1]. In particular, PCFBs are known to exist only in the extremal cases where the filter bank analysis/synthesis polyphase matrix has zero memory and doubly infinite memory, respectively. For many practical input signals, this latter class consists of filters that have ideal bandpass characteristics and are as such *unrealizable* [68]. Though several methods for the design of *realizable* signal-adapted filter banks have been proposed (see [35, 37, 79] for example), none have established a connection between their filter banks and the unrealizable PCFB. In particular, though we might expect a realizable filter bank of finite order that is optimized for a particular objective to behave more and more like the unrealizable PCFB as the order increases, this has not yet been shown in the literature.

The thesis presents several optimization algorithms for the design of realizable signal-adapted filter banks in which the filters all have a finite impulse response (FIR). Matlab code for these algorithms will soon be available at [60]. One of the main contributions is to establish a link between realizable signal-adapted filter banks and the unrealizable infinite-order PCFB. In particular, it will be shown that FIR filter banks designed using our methods behave more and more like the infinite-order PCFB as the filter order increases. This serves to *bridge the gap* between the zero memory PCFB and the infinite-order one which previously has not been done in the literature.

The primary purpose of this introductory chapter is to set the stage for the remainder of the thesis. To that end, every attempt has been made to keep the chapter as self-contained as possible. In this chapter, a brief overview of multirate systems and identities which will be used throughout the thesis, as well as commonly used notations and terminology, is given in Sec. 1.1. We formally introduce PCFBs in this chapter (Sec. 1.2.1) and mention problems related to them. In addition, we discuss other problems relevant to the thesis including the FIR paraunitary (PU) interpolation problem in Sec. 1.3 and the channel shortening equalizer problem in Sec. 1.4. The material presented here is by no means a complete coverage of multirate systems and filter banks. For a more comprehensive treatment of multirate system theory and its applications, the reader is referred to [67, 32, 47, 41, 39, 15, 16].

1.1 Review of Multirate Systems

1.1.1 Discrete-Time Signal Processing

All of the signals of interest in DSP are *discrete-time* sequences of either real or complex numbers. These sequences are typically obtained by uniformly sampling a continuous-time signal, such as a voltage signal as a function of time. For example, if $x_c(t)$ denotes a continuous-time signal, then the sequence $x(n) \triangleq x_c(nT_s)$ for $n \in \mathbb{Z}$ denotes a discrete-time signal obtained by uniformly sampling

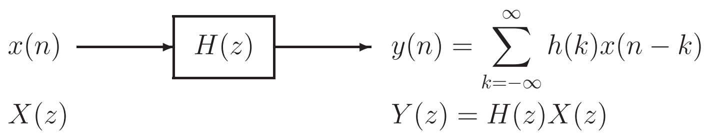

Figure 1.1: Linear time-invariant (LTI) filtering operation.

$x_c(t)$ every T_s units of time.

In order for the discrete-time signal $x(n)$ to be stored digitally on a computer, for example, the value of $x(n)$ at each n must be approximated by a value obtained from a finite set of possible values. This process is called *quantization* or discretization. Typically, we will assume that the number of discretization levels is large enough so as to ignore the effects of quantization (fine quantization). However, in many data compression applications, it becomes necessary to use only a small number of levels (coarse quantization), so as to decrease the overall bit rate and obtain lossy compression [41, 39]. For the remainder of the thesis, we will ignore the effects of quantization unless stated otherwise.

Signal processing analysis is often facilitated by considering alternative representations of discrete-time signals and systems. Perhaps the most commonly used alternative representations of a discrete-time signal $x(n)$ are its z-transform $X(z)$ and its Fourier transform $X(e^{j\omega})$. The z-transform is defined as

$$X(z) \triangleq \sum_{n=-\infty}^{\infty} x(n)z^{-n}$$

for regions of $z \in \mathbb{C}$ for which the above summation converges. Also, the Fourier transform $X(e^{j\omega})$ is simply $X(z)$ evaluated on the unit circle $z = e^{j\omega}$, assuming that the summation converges there. In cases where the Fourier transform $X(e^{j\omega})$ exists but the z-transform $X(z)$ does not [67], we will write $X(z)$ as a shorthand notation for $X(e^{j\omega})$.

1.1.2 Fundamental Building Blocks

The majority of multirate DSP systems consists of three fundamental building blocks. These are the linear time-invariant (LTI) filter, the expander, and the decimator. An LTI filter, such as the one shown in Fig. 1.1, is characterized by its impulse response $h(n)$ (i.e., its response to the unit Kronecker delta impulse function $x(n) = \delta(n)$ [67]), or equivalently by its z-transform $H(z)$, which is called the transfer function. The system of Fig. 1.1 is an example of a single-input single-output (SISO) LTI system. More generally, a multiple-input multiple-output (MIMO) LTI filter, such

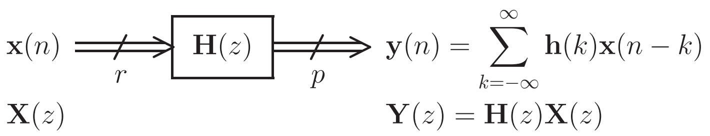
$\mathbf{x}(n)$
r
$\mathbf{H}(z)$
p
$\mathbf{y}(n) = \sum_{k=-\infty}^{\infty} \mathbf{h}(k)\mathbf{x}(n-k)$
$\mathbf{X}(z)$
$\mathbf{Y}(z) = \mathbf{H}(z)\mathbf{X}(z)$

Figure 1.2: Multiple-input multiple-output (MIMO) LTI filtering operation.

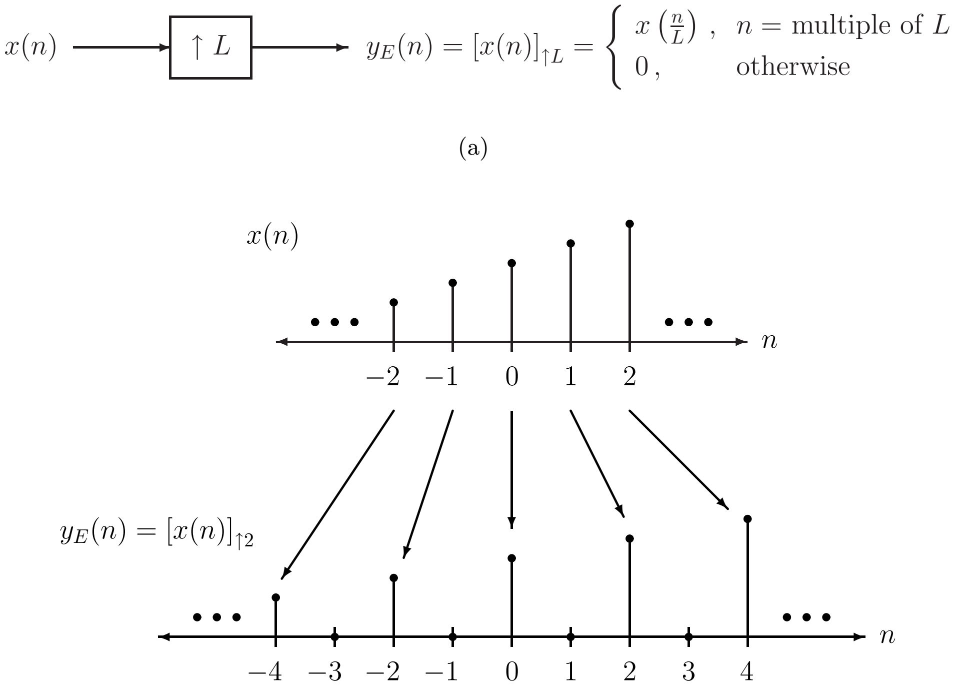
$x(n)$
$\uparrow L$
$y_E(n) = [x(n)]_{\uparrow L} = \begin{cases} x\left(\frac{n}{L}\right), & n = \text{multiple of } L \\ 0, & \text{otherwise} \end{cases}$
$x(n)$
n
-2 -1 0 1 2
$y_E(n) = [x(n)]_{\uparrow 2}$
n
-4 -3 -2 -1 0 1 2 3 4

(a)

(b)

Figure 1.3: L-fold expander input/output relationship: (a) Block diagram, (b) Example for $L = 2$.

as the one shown in Fig. 1.2 operates on a $r \times 1$ vector input $\mathbf{x}(n)$ to produce an $p \times 1$ vector output $\mathbf{y}(n)$. Such a filter is characterized by its $p \times r$ impulse response matrix sequence $\mathbf{h}(n)$ or equivalently by its $p \times r$ transfer function matrix $\mathbf{H}(z)$.

While LTI systems are used to filter discrete-time signals, expanders and decimators are used to alter the *rates* of such signals. An L-fold expander, such as the one shown in Fig. 1.3(a), is used to *increase* the rate by a factor of L. The L-fold expander essentially pads $(L-1)$ zeros between each sample of its input and as such, the output must operate at a rate of L times the input rate in order to maintain the proper sampling rate of the input signal. This is shown in Fig. 1.3(b) for $L = 2$. In contrast to the L-fold expander, the M-fold decimator, such as the one shown in Fig. 1.4(a), is used to *decrease* the rate by a factor of M. The M-fold decimator only preserves every

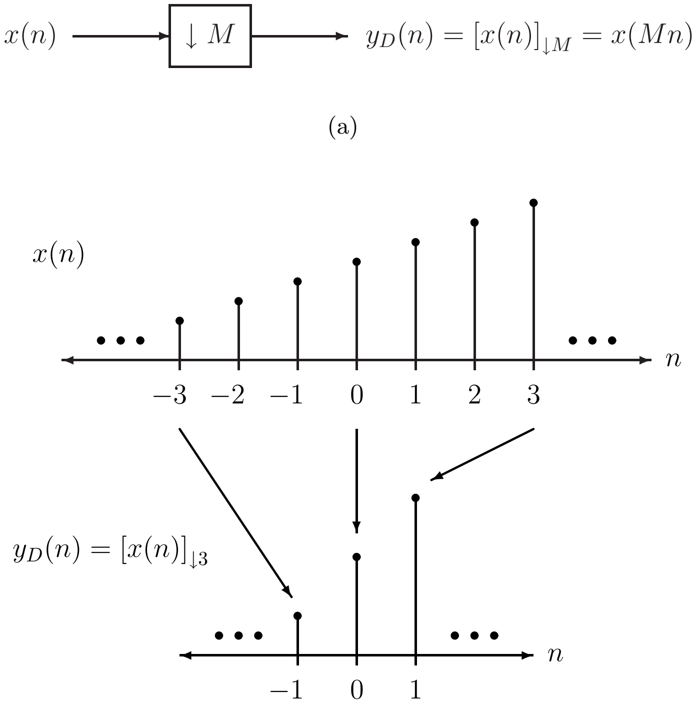

(a)

(b)

Figure 1.4: M-fold decimator input/output relationship: (a) Block diagram, (b) Example for $M = 3$.

M-th sample of its input and as such, the output must operate at an M times lower rate in order to keep the proper sampling rate of the input signal. This is shown in Fig. 1.4(b) for $M = 3$.

Frequency or z-domain representations of the input/output relationships of expanders and decimators provide more insight about the nature of these rate altering building blocks. From Fig. 1.3(a) and 1.4(a), it can be shown [67] that we have

$$\begin{aligned} Y_E(z) &= [X(z)]_{\uparrow L} = X\left(z^L\right) && (L\text{-fold expander}) \\ Y_D(z) &= [X(z)]_{\downarrow M} = \frac{1}{M}\sum_{k=0}^{M-1} X\left(z^{\frac{1}{M}} W_M^k\right) && (M\text{-fold decimator}) \end{aligned} \tag{1.1}$$

where $W_M \triangleq e^{-j\frac{2\pi}{M}}$ denotes the M-th root of unity. In the frequency domain, the L-fold expander output $Y_E(e^{j\omega})$ consists of an L-fold compressed version of $X(e^{j\omega})$ along with $(L-1)$ uniformly shifted copies called *images*. Similarly, the M-fold decimator output $Y_D(e^{j\omega})$ consists of an M-fold stretched version of $X(e^{j\omega})$ (scaled by $1/M$) along with $(M-1)$ uniformly shifted scaled copies called *alias components*. This is shown in Fig. 1.5 for both the expander and decimator for $L = M = 4$. The presence $(L-1)$ images for an L-fold expander indicate a *redundancy* of a factor

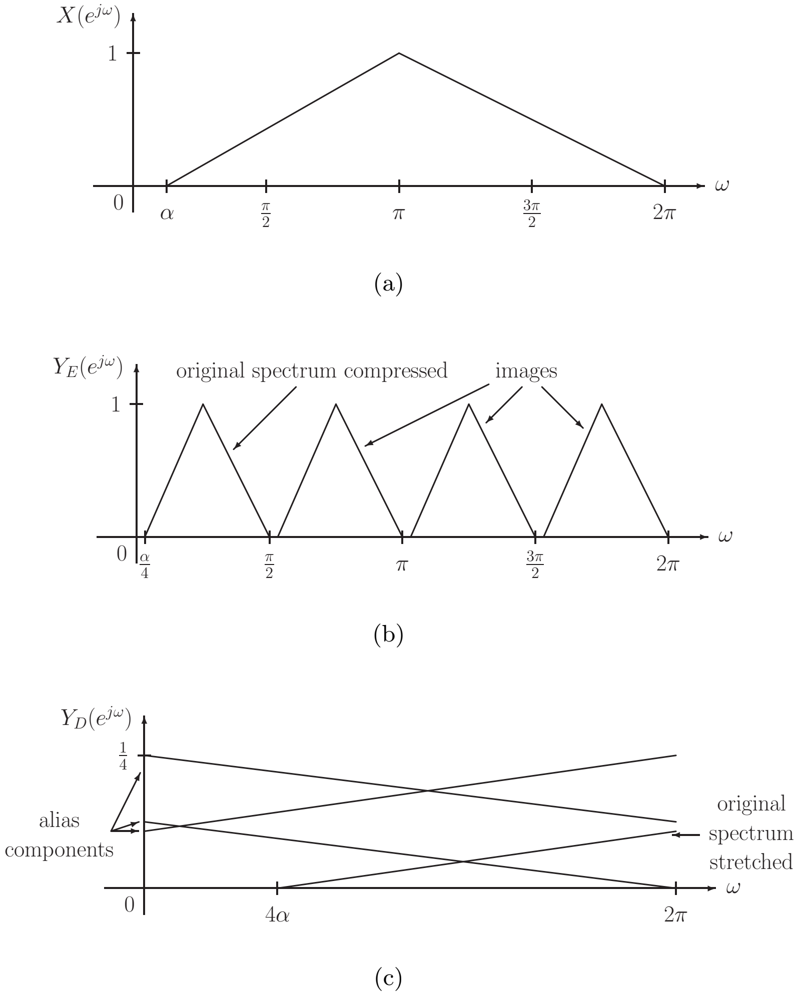

Figure 1.5: (a) Given input signal spectrum $X(e^{j\omega})$, (b) Expanded signal spectrum $Y_E(e^{j\omega})$ $(L = 4)$, (c) Decimated signal spectrum $Y_D(e^{j\omega})$ $(M = 4)$.

of L, whereas the $(M-1)$ alias components for an M-fold decimator indicate a *loss of information* of a factor of M. While the original input $X(z)$ can always be recovered by its L-fold expanded version $Y_E(z)$, it can not in general be recovered by its M-fold decimated version $Y_D(z)$.

Special combinations of LTI systems and decimators/expanders can be used to parallelize/serialize discrete-time operations. One common way of parallelizing or vectorizing a scalar signal is the M-fold *blocking* system shown in Fig. 1.6(a). The blocked signal vector $\mathbf{x}(n)$ is obtained by stacking every nonoverlapping block of M samples of $x(n)$ into a vector. Note that the overall rate of the blocked signal $\mathbf{x}(n)$ is the same as that of the input $x(n)$, since $\mathbf{x}(n)$ consists of M components each operating at $(1/M)$ times the input rate. The dual structure of the blocking system of Fig. 1.6(a) is the L-fold *unblocking* system shown in Fig. 1.6(b). This system is used to serialize or scalarize

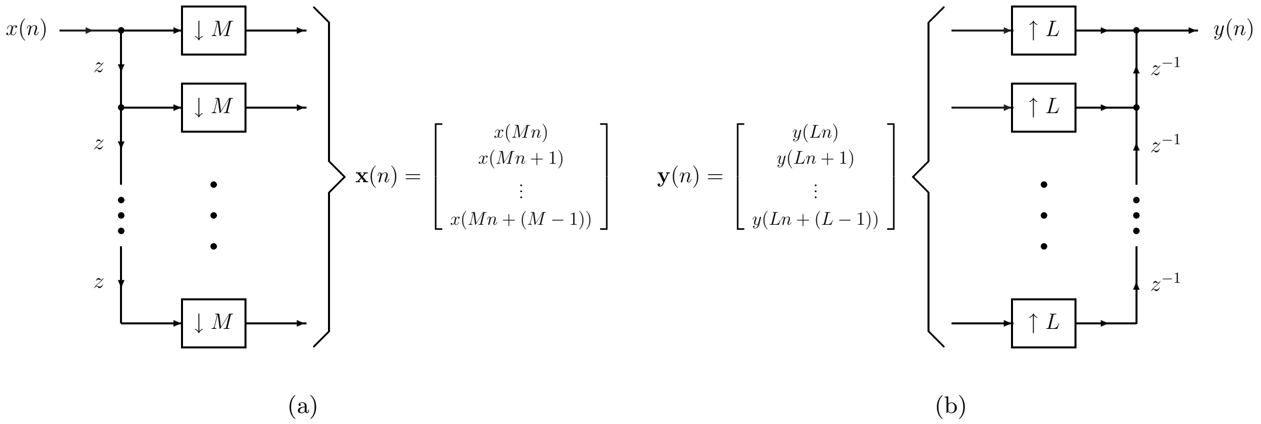
$x(n)$
z
z
z
$\downarrow M$
$\downarrow M$
$\downarrow M$
$\mathbf{x}(n) = \begin{bmatrix} x(Mn) \\ x(Mn+1) \\ \vdots \\ x(Mn+(M-1)) \end{bmatrix}$
$\mathbf{y}(n) = \begin{bmatrix} y(Ln) \\ y(Ln+1) \\ \vdots \\ y(Ln+(L-1)) \end{bmatrix}$
$\uparrow L$
$\uparrow L$
$\uparrow L$
z^{-1}
z^{-1}
z^{-1}
$y(n)$
(a)
(b)

Figure 1.6: (a) M-fold blocking system, (b) L-fold unblocking system.

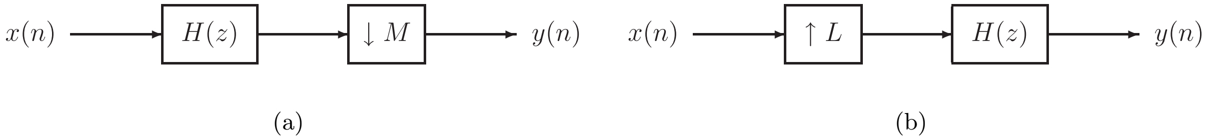

Figure 1.7: (a) M-fold decimation filter system, (b) L-fold interpolation filter system.

a vector signal input $\mathbf{y}(n)$. The components of the input vector $\mathbf{y}(n)$ are interlaced with each other to produce the output $y(n)$. As with the blocking system, the overall rate of the unblocking system output $y(n)$ is the same as its input $\mathbf{y}(n)$, since $y(n)$ consists of $(1/L)$ of the components of $\mathbf{y}(n)$ operating at L times the input rate. Blocking and unblocking systems naturally arise upon exploiting *polyphase decompositions* of LTI systems in conjunction with decimators and expanders, as is shown in the next section.

1.1.3 Decimation/Interpolation Filter Systems

Recall that decimators and expanders are responsible for the undesirable phenomena of aliasing and imaging, respectively. In multirate signal processing, LTI filtering is commonly used to remove these artifacts. To remove the effects of aliasing a signal is filtered *before* being decimated, whereas to counteract the effects of imaging, a signal is filtered *after* being expanded. This is shown in Fig. 1.7(a) and (b), respectively. The system of Fig. 1.7(a) is known as a decimation filter system whereas that shown in Fig. 1.7(b) is known as an interpolation filter system [67].

Though these systems are capable of attenuating or even eliminating the effects of aliasing and imaging, their current implementations shown in Fig. 1.7 are not computationally efficient. This is

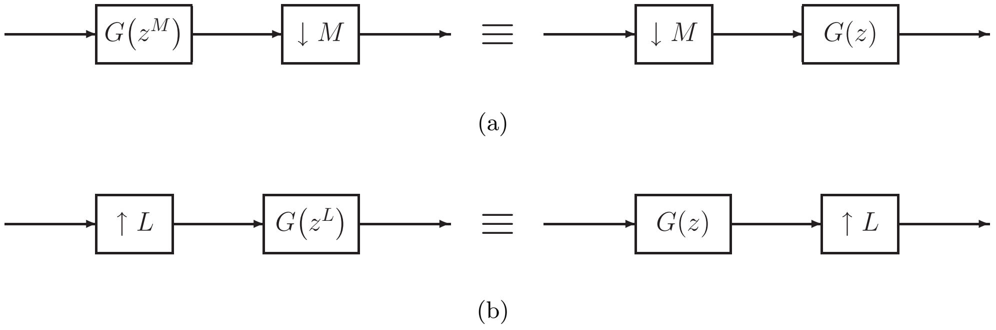

Figure 1.8: (a) Decimator noble identity, (b) Expander noble identity.

because the decimation filter system only keeps every M-th output sample and the interpolation filter system is only feeding a nonzero input to its filter at every L-th instance of time. By using *polyphase decompositions* (Sec. 1.1.3.2) of the filters appearing in the decimation/interpolation filter systems together with the *noble identities* (Sec. 1.1.3.1), we can obtain computationally efficient structures for these systems.

1.1.3.1 Noble Identities

Certain LTI systems can be moved across decimators/expanders by using the *noble identities* [67]. The noble identities are shown in Fig. 1.8 for (a) decimators and (b) expanders. Note that the noble identities, when they can be used, provide computationally efficient implementations, since they give us a way to filter *after* decimating and *before* expanding. However, note that the decimator/expander noble identities only apply when the original filter system is a function of z^M or z^L, respectively. As such, they cannot immediately be applied to the decimation/interpolation filter systems of Fig. 1.7. By using *polyphase decompositions* of the filters appearing in Fig. 1.7, we can overcome this problem.

1.1.3.2 Polyphase Decompositions

A polyphase decomposition of an LTI system $H(z)$ with impulse response $h(n)$ is simply an alternate way of expressing $H(z)$ or $h(n)$. Note that for any integer K, the impulse response $h(n)$ can be expressed as the interlaced sum of K lower rate signals. One example of this is shown in Fig. 1.9 for $K = 3$. This partitioning of $h(n)$ into K lower rate signals is analogous to partitioning the set of integers into K equivalence classes modulo the integer K. Though there are infinitely many ways to express $h(n)$ or $H(z)$ as a sum of K interlaced lower rate signals, the two most common ways

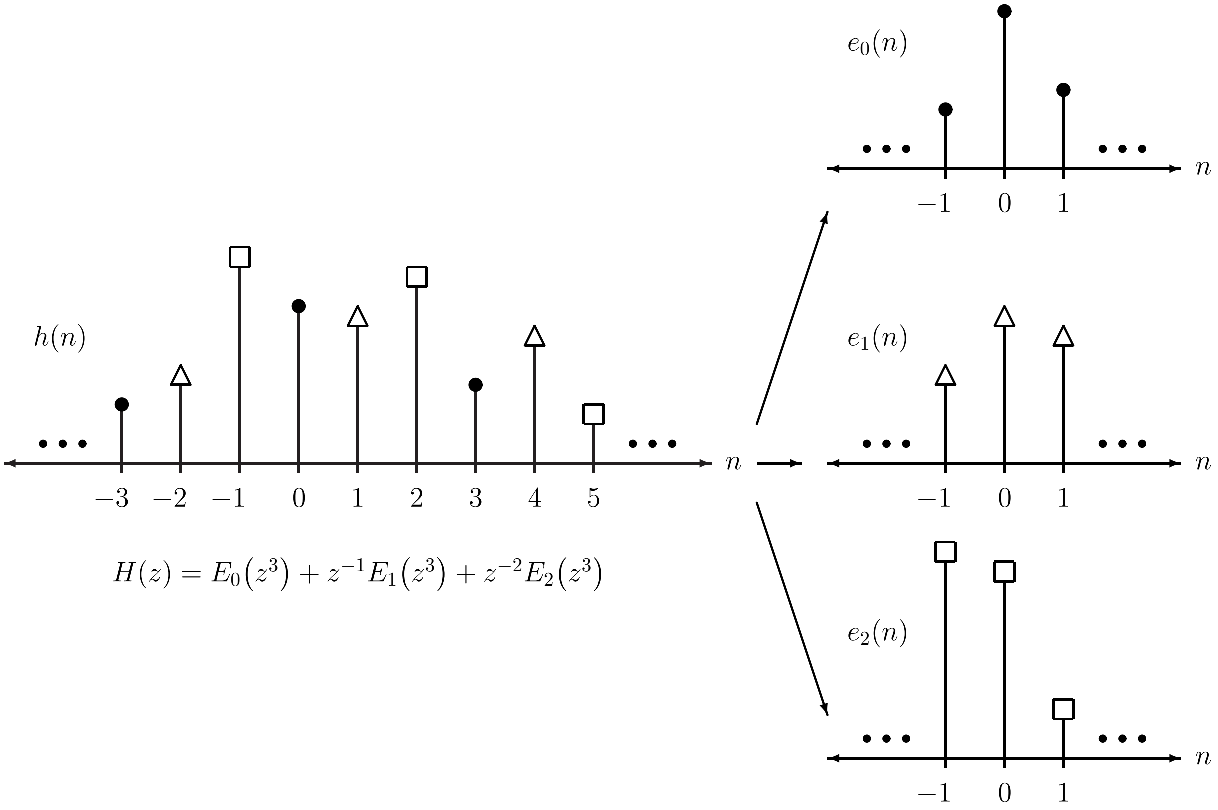

Figure 1.9: Time domain interpretation of the polyphase representation for $K = 3$.

are shown below.

$$\begin{aligned} H(z) &= \sum_{k=0}^{K-1} z^{-k} E_k\big(z^K\big) \quad \text{(Type I)} \\ H(z) &= \sum_{k=0}^{K-1} z^{k} R_k\big(z^K\big) \quad \text{(Type II)} \end{aligned} \tag{1.2}$$

where the impulse responses of the lower rate signals $E_k(z)$ and $R_k(z)$ are given by

$$\begin{aligned} e_k(n) &= h(Kn+k) \iff E_k(z) = \big[z^k H(z)\big]_{\downarrow K} \quad \text{(Type I)} \\ r_k(n) &= h(Kn-k) \iff R_k(z) = \big[z^{-k} H(z)\big]_{\downarrow K} \quad \text{(Type II)} \end{aligned}$$

for $0 \le k \le K-1$. The alternate expressions for $H(z)$ given in (1.2) are known as *polyphase decompositions* of $H(z)$ [67].

Using polyphase decompositions of the filter $H(z)$ appearing in the decimation/interpolation filter systems of Fig. 1.7, we can then apply the noble identities of Fig. 1.8 to obtain computationally

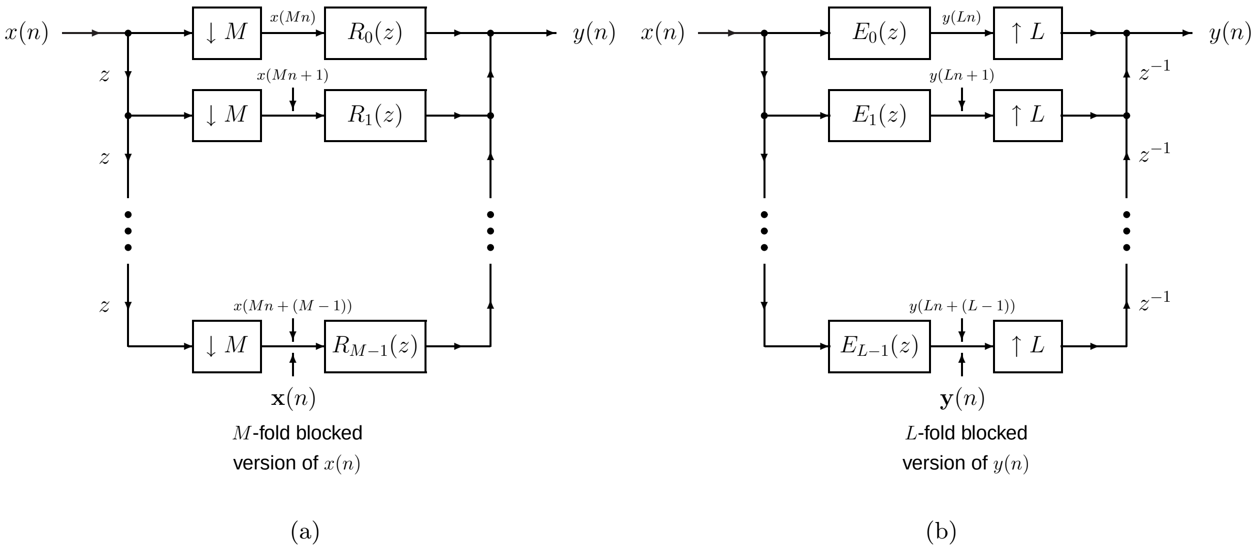

Figure 1.10: Polyphase implementations of (a) decimation filter system (using (1.3)), (b) interpolation filter system (using (1.4)).

efficient structures for these systems. In particular, if we use a Type II decomposition of the form

$$H(z) = \sum_{k=0}^{M-1} z^k R_k\big(z^M\big) \tag{1.3}$$

for the decimation filter system of Fig. 1.7(a) and a Type I decomposition of the form

$$H(z) = \sum_{k=0}^{L-1} z^{-k} E_k\big(z^L\big) \tag{1.4}$$

for the interpolation filter system of Fig. 1.7(b), then the equivalent computationally efficient structures that result upon using the noble identities are shown in Fig. 1.10. Note that the decimation filter system of Fig. 1.10(a) consists of *blocking* the input signal and then filtering the blocked version by a multiple-input single-output (MISO) system. Similarly, the interpolation filter system of Fig. 1.10(b) consists of filtering the input by a single-input multiple-output (SIMO) system followed by *unblocking* the filter output. Since blocking and unblocking operations require no computations, the systems of Fig. 1.10 are indeed more computationally efficient than those shown in Fig. 1.7.

Polyphase decompositions play a prominent role in the study of multirate filter banks and their dual structures transmultiplexers, as will be shown in the next section.

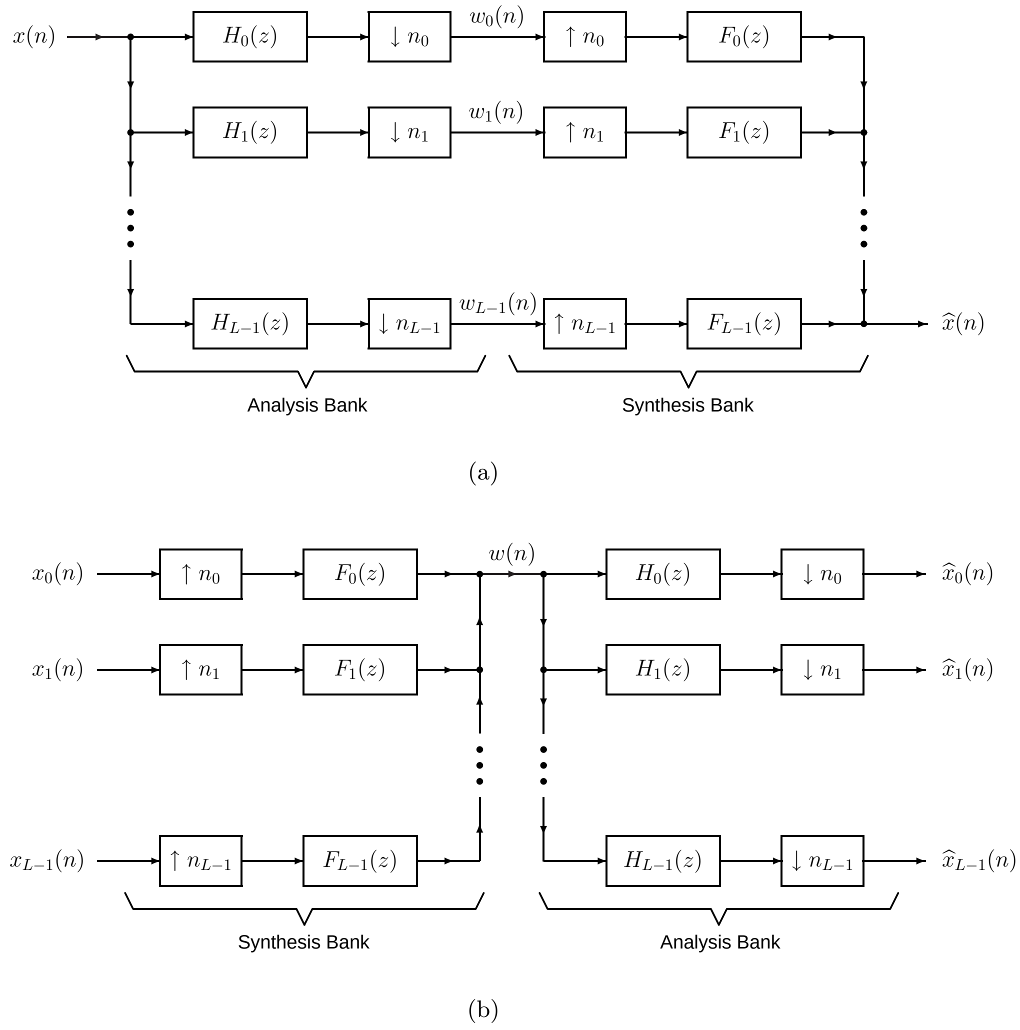

(a)

(b)

Figure 1.11: (a) General nonuniform multirate filter bank, (b) The dual structured transmultiplexer.

1.1.4 Filter Banks and Transmultiplexers

As mentioned above, a multirate filter bank is used to decompose a given input signal into a set of lower rate signals called subbands. This is often done by feeding the input, say $x(n)$, to a bank of *decimation filter systems* called the *analysis bank*, as shown in Fig. 1.11(a). Here, the filters $\{H_k(z)\}$ are called analysis filters. The subbands $\{w_k(n)\}$ are then usually processed in some way, though this is not shown in Fig. 1.11(a). For example, to achieve lossy data compression, $\{w_k(n)\}$ are *quantized* [41, 39]. Afterwards, the subbands are typically used to try to *reconstruct* the original input. This is often done by feeding the subbands $\{w_k(n)\}$ into a bank of *interpolation filter systems* called the *synthesis bank*, as shown in Fig. 1.11(a). Here, the filters $\{F_k(z)\}$ are called synthesis filters. The analysis/synthesis banks of Fig. 1.11(a) together constitute a *multirate filter bank* [67].

By reversing the roles of the analysis and synthesis banks, we obtain the dual to the multirate filter bank known as the *transmultiplexer* [67], as shown in Fig. 1.11(b). Whereas filter banks are typically used for source coding applications such as data compression, transmultiplexers are often used for channel coding applications in digital communications. The transmultiplexer model of Fig. 1.11(b) may represent, for example, a digital communications system in which we have L users $\{x_k(n)\}$ who wish to transmit data over a common path. After passing through the channel, the data from each user must be isolated and recovered, yielding the received signals $\{\widehat{x}_k(n)\}$.

The systems of Fig. 1.11 are given special names according to the overall rate of the subband signals, which depend on the nature of the decimator/expander values $\{n_k\}$ used. Note that the overall rate of the subband signals is simply $\left(\sum_{k=0}^{L-1} \frac{1}{n_k}\right)$ times the input rate. If we have

$$\sum_{k=0}^{L-1} \frac{1}{n_k} = 1$$

then the filter bank is said to be *maximally decimated*, whereas the transmultiplexer will be said to be *minimally expanded*. In this case, we may have neither a loss of information nor redundancy. On the other hand, if we have

$$\sum_{k=0}^{L-1} \frac{1}{n_k} < 1$$

then the filter bank will be said to be *overdecimated*, whereas the transmultiplexer will be said to be *underexpanded*. In this case, the filter bank incurs a *loss of information*, whereas the transmultiplexer system possesses *redundancy*. Finally, if we have

$$\sum_{k=0}^{L-1} \frac{1}{n_k} > 1$$

then the filter bank will be said to be *underdecimated*, whereas the transmultiplexer will be said to be *overexpanded*. In this case, the filter bank system has *redundancy*, whereas the transmultiplexer incurs a *loss of information*.

If $\widehat{x}(n) = x(n)$ for all $x(n)$ for the filter bank system or $\widehat{x}_k(n) = x_k(n)$ for all k and for all $\{x_k(n)\}$ for the transmultiplexer system, then each system is said to possess the *perfect reconstruction* (PR) property[1] [67]. If all of the decimator/expander values $\{n_k\}$ are equal, the systems of Fig. 1.11 are said to be *uniform*. For arbitrary values of $\{n_k\}$, these systems are said to be *nonuniform*.

[1] A more general definition of the PR condition [67] is a *distortionless reconstruction* in which we have $\widehat{x}(n) = cx(n-D)$ for the filter bank system or $\widehat{x}_k(n) = c_k x_k(n-D_k)$ for the transmultiplexer system. Here, c and $\{c_k\}$ represent scale factors, whereas D and $\{D_k\}$ denote delay values. Since scale factors and delays can often easily be absorbed into the analysis/synthesis filters, for the remainder of the thesis, we will only be concerned with the stricter PR property defined above.

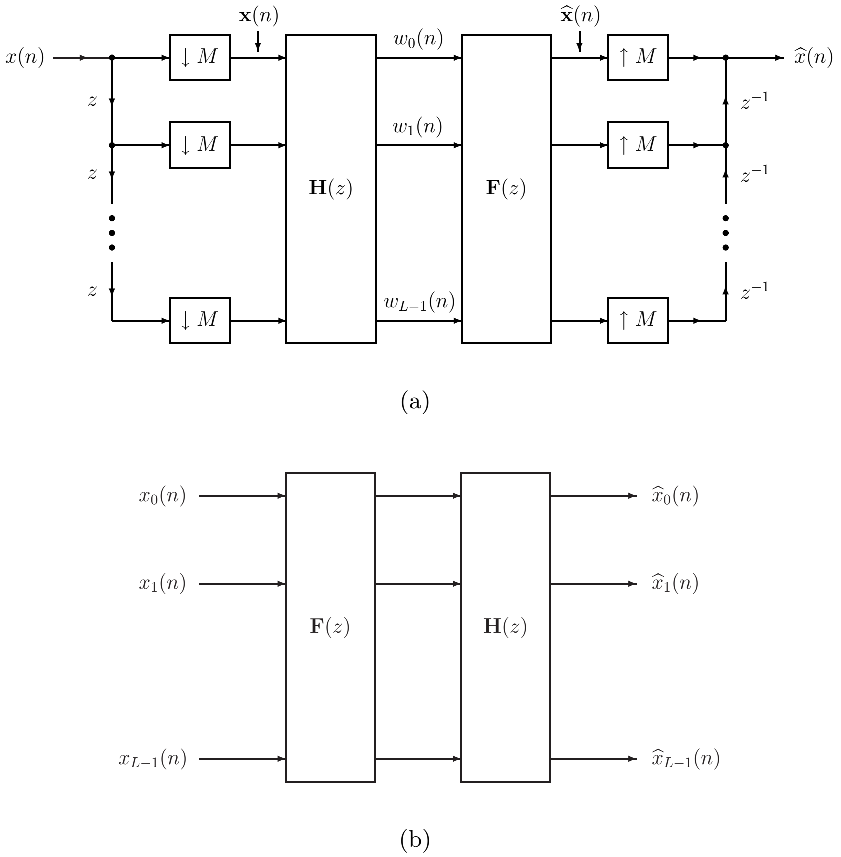

Figure 1.12: Polyphase representations of (a) uniform filter bank, (b) uniform transmultiplexer.

1.1.4.1 Polyphase Representations of Uniform Systems

Suppose that the systems of Fig. 1.11 are uniform with $n_k = M$ for all k. Also, let the Type II and Type I polyphase decompositions of the analysis and synthesis filters, respectively, be given by

$$\begin{aligned} H_k(z) &= \sum_{\ell=0}^{M-1} z^{\ell} H_{k,\ell}\big(z^M\big) \quad \text{(Type II)} \\ F_k(z) &= \sum_{\ell=0}^{M-1} z^{-\ell} F_{k,\ell}\big(z^M\big) \quad \text{(Type I)} \end{aligned}$$

for $0 \leq k \leq L-1$. Using these decompositions, together with the noble identities from Sec. 1.1.3.1, we can redraw the systems of Fig. 1.11(a) and (b) as in Fig. 1.12(a) and (b), respectively, where $\mathbf{H}(z)$ and $\mathbf{F}(z)$ are, respectively, $L \times M$ and $M \times L$ matrices with

$$[\mathbf{H}(z)]_{k,\ell} = H_{k,\ell}(z)\,,\ [\mathbf{F}(z)]_{\ell,k} = F_{k,\ell}(z)$$

for $0 \leq k \leq L-1$ and $0 \leq \ell \leq M-1$. Here, $\mathbf{H}(z)$ is called the *analysis polyphase matrix*, whereas $\mathbf{F}(z)$ is called the *synthesis polyphase matrix*.

Note that the polyphase form of the filter bank system shown in Fig. 1.12(a) consists of blocking the input $x(n)$ by M, filtering the blocked signal $\mathbf{x}(n)$ by the MIMO LTI system $\mathbf{F}(z)\mathbf{H}(z)$, and then unblocking the filtered signal $\widehat{\mathbf{x}}(n)$ by M to obtain the output $\widehat{x}(n)$. Also note that the polyphase form of the transmultiplexer consists of simply filtering the input vector signal $\{x_k(n)\}$ by the MIMO LTI system $\mathbf{H}(z)\mathbf{F}(z)$ to obtain the output vector signal $\{\widehat{x}_k(n)\}$. Analogous properties hold true for the general nonuniform systems shown in Fig. 1.11, although the details are much more involved than for the uniform case [12] (see the Appendix of Chapter 2 for the analysis required in the general nonuniform case).

1.1.4.2 Biorthogonality and Orthonormality

Recall that the filter bank system of Fig. 1.11(a) is said to be PR iff $\widehat{x}(n) = x(n)$ for all $x(n)$. For the polyphase representation of the uniform system of Fig. 1.12(a), it can be shown [67] that PR is equivalent to

$$\mathbf{F}(z)\mathbf{H}(z) = \mathbf{I}_M \quad \textit{(Filter Bank Biorthogonality Condition)} \tag{1.5}$$

The filter bank system described by $\mathbf{F}(z)$ and $\mathbf{H}(z)$ is said to be *biorthogonal* if (1.5) holds. In other words, biorthogonality is equivalent to the PR property. (This is true not only for filter banks, but also for transmultiplexers as discussed below.) Clearly, we must have $L \geq M$ in order for (1.5) to hold, since otherwise the left-hand side of (1.5) can never be of full normal rank M [67]. This is consistent with the fact that the overall rate of the subbands, which is $\frac{L}{M}$ times the input rate, is strictly less than the input rate when $L < M$, indicating a *loss of information.*

If $\mathbf{H}(z)$ satisfies a *paraunitary* (PU) condition [67] of the form

$$\widetilde{\mathbf{H}}(z)\mathbf{H}(z) = \mathbf{I}_M \quad \textit{(Paraunitary Condition)} \tag{1.6}$$

where the tilde notation is defined as $\widetilde{\mathbf{H}}(z) \triangleq \mathbf{H}^{\dagger}(1/z^*)$ [67], a special class of filter banks known as *orthonormal* filter banks are generated upon choosing $\mathbf{F}(z)$ as

$$\mathbf{F}(z) = \widetilde{\mathbf{H}}(z) \quad \text{(Ensures PR)}$$

In other words, the filter bank is said to be *orthonormal* iff

$$\widetilde{\mathbf{H}}(z)\mathbf{H}(z) = \mathbf{I}_M\,, \mathbf{F}(z) = \widetilde{\mathbf{H}}(z) \quad \textit{(Filter Bank Orthonormality Condition)} \tag{1.7}$$

Orthonormal filter banks have been found to be useful for many applications [67] including data compression [47]. Several popular data compression schemes such as JPEG and JPEG 2000 use orthonormal filter banks to obtain good lossy data compression [41, 39]. Orthonormal filter banks have several advantages which make them very attractive to use. For example, orthonormal filter banks preserve the energy of the input signal in the subbands (i.e., the ℓ_2 norm of the subband signals equals that of the input signal [67]), which may be useful if we wish to avoid overamplifying or overattenuating the subbands. Also, orthonormal filter banks only require the design of either the analysis or synthesis polyphase matrix, since the analysis/synthesis polyphase matrices are related as $\mathbf{F}(z) = \widetilde{\mathbf{H}}(z)$. Finally, if the analysis filters $\{H_k(z)\}$ or equivalently the analysis polyphase matrix $\mathbf{H}(z)$ of an orthonormal filter bank are FIR, then the corresponding synthesis filters $\{F_k(z)\}$ and synthesis polyphase matrix $\mathbf{F}(z)$ are also *necessarily* FIR.

Biorthogonality and orthonormality conditions also exist for the transmultiplexer system of Fig. 1.11(b). In particular, for the uniform system of Fig. 1.12(b), the biorthogonality condition becomes

$$\mathbf{H}(z)\mathbf{F}(z) = \mathbf{I}_L \quad \textit{(Transmulitplexer Biorthogonality Condition)} \tag{1.8}$$

Clearly, we must have $L \leq M$ here in order for (1.8) to hold, since otherwise the left-hand side of (1.8) can never be of full normal rank L [67]. Analogous with the filter bank system, this is consistent with the fact that when $L > M$, we have a *loss of information*. Similar to (1.7), the orthonormality condition for the transmultiplexer system of Fig. 1.12(b) is given by

$$\widetilde{\mathbf{F}}(z)\mathbf{F}(z) = \mathbf{I}_L \, , \mathbf{H}(z) = \widetilde{\mathbf{F}}(z) \quad \textit{(Transmultiplexer Orthonormality Condition)} \tag{1.9}$$

It should be noted that biorthogonality and orthonormality conditions analogous to those given in (1.5), (1.8), (1.7), and (1.9) exist for the general nonuniform systems shown in Fig. 1.11. The interested reader is referred to [67, 45, 12] for more details.

1.2 Signal-Adapted Filter Banks

Any filter bank whose filters somehow depend on any knowledge of the input statistics is called a *signal-adapted* filter bank. A typical model for a signal-adapted filter bank that will be used throughout the thesis is the uniform M-channel maximally decimated filter bank shown in Fig. 1.13(a). The M-fold polyphase representation of this filter bank is shown in Fig. 1.13(b). Here, the subband processors $\{\mathcal{P}_k\}$ may be nonlinear systems such as scalar quantizers or thresholding devices or linear filters for denoising.

Throughout the thesis, we will assume that the input signal $x(n)$ is a *cyclo wide sense stationary* process with period M (abbreviated CWSS(M)) [40]. This means that the mean $\mu(n)$ and

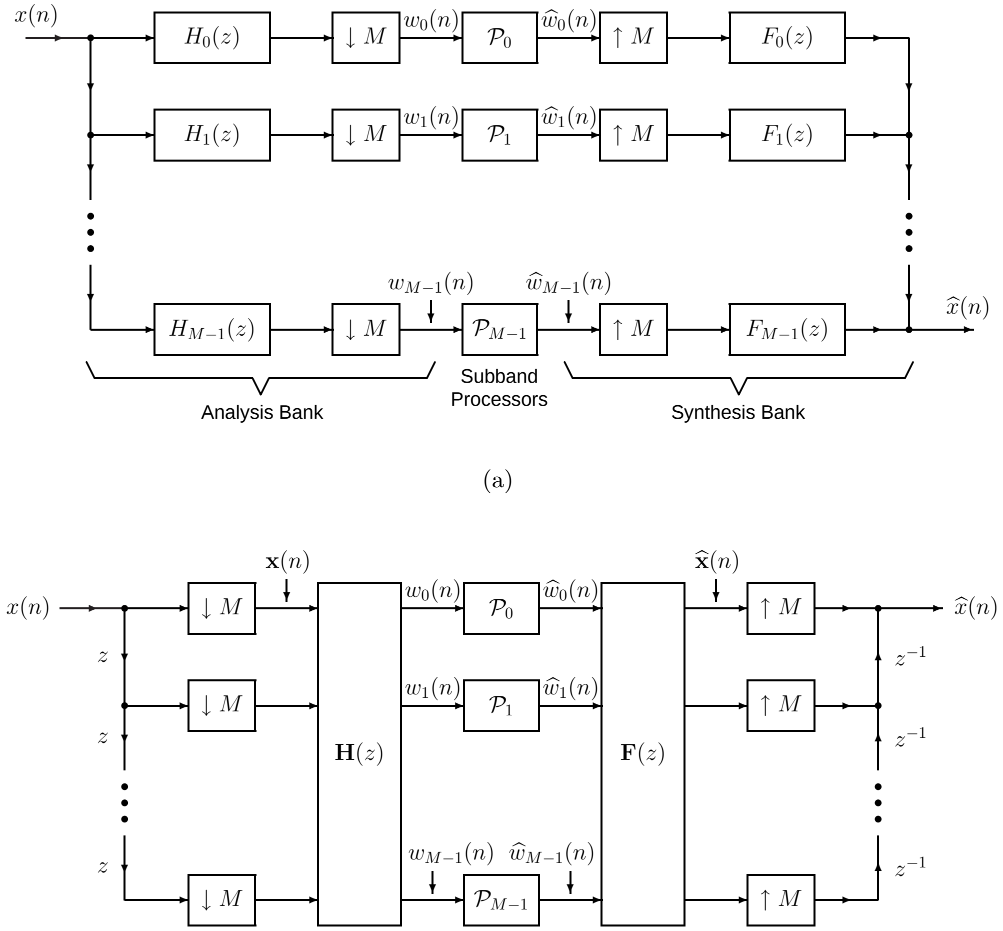

(a)

(b)

Figure 1.13: (a) Typical uniform M-channel maximally decimated filter bank system. (b) Polyphase representation of the filter bank.

autocorrelation $R_{xx}(n,k)$ of $x(n)$, which are given by

$$\begin{aligned} \mu(n) &= E\left[x(n)\right] \\ R_{xx}(n,k) &= E\left[x(n)x^*(n-k)\right] \end{aligned}$$

are *periodic* in n with period M. (Here E denotes the *expectation operator* [67].) It should be noted that $x(n)$ is CWSS(M) iff its M-fold blocked version $\mathbf{x}(n)$ shown in Fig. 1.13(b) is wide sense stationary (WSS) [40], meaning that the mean and autocorrelation of $\mathbf{x}(n)$ do not depend on n. Here, the mean $\boldsymbol{\mu}$ and autocorrelation $\mathbf{R}_{\mathbf{xx}}(k)$ are given by

$$\begin{aligned} \boldsymbol{\mu} &= E\left[\mathbf{x}(n)\right] \\ \mathbf{R}_{\mathbf{xx}}(k) &= E\left[\mathbf{x}(n)\mathbf{x}^\dagger(n-k)\right] \end{aligned}$$

For the remainder of the thesis, we will assume that $x(n)$ and hence $\mathbf{x}(n)$ are *zero mean*. Also, we will assume that we only have knowledge of the second order statistics of $\mathbf{x}(n)$ (namely, $\mathbf{R_{xx}}(k)$), in addition to the given zero mean assumption on $\mathbf{x}(n)$. An equivalent representation of the autocorrelation $\mathbf{R_{xx}}(k)$ that will be commonly used is the *power spectral density* (psd) $\mathbf{S_{xx}}(z)$, which is simply the z-transform of $\mathbf{R_{xx}}(k)$.

1.2.1 Principal Component Filter Banks

Focusing on Fig. 1.13(b), often times, for simplicity of design as well as for other reasons, we will restrict our attention to orthonormal or PU filter banks in which we have[2]

$$\widetilde{\mathbf{F}}(z)\mathbf{F}(z) = \mathbf{I}\,,\ \mathbf{H}(z) = \widetilde{\mathbf{F}}(z) \tag{1.10}$$

Recently, it has been shown that a special type of PU filter bank matched to the input statistics $\mathbf{S_{xx}}(z)$ known as the principal component filter bank (PCFB) [62] is *simultaneously* optimal for a variety of objective functions [1]. Among these objectives are included several important data compression objectives such as mean-squared error under the presence of quantization noise [28] (for any bit allocation) and coding gain [68, 69] (with optimal bit allocation). By definition, a PCFB for an input psd $\mathbf{S_{xx}}(z)$ and for a class $\mathcal{C}$ of filter banks, if it exists, is one whose subband variance vector

$$\boldsymbol{\sigma} \triangleq \begin{bmatrix} \sigma_{w_0}^2 & \sigma_{w_1}^2 & \cdots & \sigma_{w_{M-1}}^2 \end{bmatrix}^T \tag{1.11}$$

majorizes [22] any other subband variance vector arising from any other filter bank in $\mathcal{C}$. (Recall that a vector $\mathbf{a} \triangleq \begin{bmatrix} a_0 & a_1 & \cdots & a_{P-1} \end{bmatrix}^T$ with $a_0 \geq a_1 \geq \cdots \geq a_{P-1} \geq 0$ is said to *majorize* [22] a vector $\mathbf{b} \triangleq \begin{bmatrix} b_0 & b_1 & \cdots & b_{P-1} \end{bmatrix}^T$ with $b_0 \geq b_1 \geq \cdots \geq b_{P-1} \geq 0$ iff we have

$$\sum_{k=0}^{p} a_k \geq \sum_{k=0}^{p} b_k \ \forall\ 0 \leq p \leq P-2\,,\ \sum_{k=0}^{P-1} a_k = \sum_{k=0}^{P-1} b_k\ .)$$

In addition to being optimal for coding gain and mean-squared error in the presence of quantization noise, the PCFB has also been shown to be optimal for any *concave* objective function of $\boldsymbol{\sigma}$ [1].

[2] It should be noted that (1.10) is equivalent to the orthonormality condition given in (1.7) since the filter bank is maximally decimated. Here, we have opted for the form given in (1.10), in which we focus on the design of the synthesis bank, as it will be more natural when we constrain the synthesis filters to be causal FIR. These filters are causal FIR iff $\mathbf{F}(z)$ is as well. This is not however true for the analysis filters and $\mathbf{H}(z)$ on account of the advance chain present in the blocking system.

1.2.1.1 Classes for Which PCFBs Are Known to Exist

Though PCFBs exhibit many optimal characteristics, they are only known to exist for special classes of filter banks [1]. One notable exception to this is for the special case where $M = 2$, in which case a PCFB always exists for any class of PU filter banks [1]. For general M, however, PCFBs are known to exist only for two special classes. If $\mathcal{C}$ is the class of all transform coders $\mathcal{C}^t$, in which $\mathbf{F}(z)$ is a constant unitary matrix $\mathbf{T}$, then the PCFB exists and is the Karhunen-Loève transform (KLT) for the input process $\mathbf{x}(n)$ (i.e., $\mathbf{T}$ *diagonalizes* the autocorrelation matrix $\mathbf{R}_{\mathbf{xx}}(0)$) [23, 1]. Furthermore, if $\mathcal{C}$ is the class of all (unconstrained order) PU filter banks $\mathcal{C}^u$, then the PCFB exists and is the *pointwise in frequency* KLT for $\mathbf{x}(n)$ [68, 1, 69]. By this, we mean that $\mathbf{F}(e^{j\omega})$ diagonalizes (i.e., totally decorrelates) $\mathbf{S}_{\mathbf{xx}}(e^{j\omega})$ for every ω such that the frequency dependent eigenvalues are always arranged in decreasing order, which is a property called spectral majorization [68]. For many practical cases of inputs (for example, if the scalar input signal $x(n)$ is itself WSS), the corresponding analysis and synthesis filters are ideal bandpass filters called compaction filters [68, 66, 65] (see Chapter 2 for more on compaction filters). As such, they are unrealizable in practice. However, they serve to compute an upper bound on the performance that we can expect from a PU filter bank.

1.2.1.2 Difficulties with the Class of FIR PU Systems

The problem with the class of FIR PU filter banks in which $\mathbf{F}(z)$ has finite memory (or more appropriately finite *McMillan degree*[3]) is that it is believed that a PCFB doesn't exist [27, 1, 24], although this has not yet been formally proven. Instead, for this class, $\mathbf{F}(z)$ is typically chosen to optimize a *specific* objective for a given input psd, such as coding gain [11, 8, 35, 79], rate-distortion [36], or a multiresolution energy compaction criterion [37]. All such methods require the numerical optimization of nonlinear and nonconvex objective functions which offer little insight into the behavior of the solutions as the filter order (i.e., the memory of $\mathbf{F}(z)$) increases.

Another common approach is to calculate an optimal FIR compaction filter [64, 59] (for the first filter $F_0(z)$) and then obtain the rest of the filters via an appropriate filter bank completion for a multiresolution criterion [37, 49]. Though elegant in the sense that the filter bank design problem is tantamount to calculating an FIR compaction filter followed by an appropriate KLT, it suffers from the ambiguity caused by the nonuniqueness of the FIR compaction filter. Different compaction

[3] The McMillan degree of a causal MIMO system is defined as the minimum number of delay elements required to implement the system [67].

filter spectral factors lead to different filter banks which in turn yield different performances (as is shown in Chapter 3). As such, all such spectral factors need to be tested for their performance [49], which is *exponentially* computationally complex with respect to the compaction filter order.

Finally, none of the above-mentioned methods for the design of FIR PU signal-adapted filter banks in the literature have been shown to tend toward the infinite-order PCFB solution as the FIR degree or order increases. Intuition tells us that as the order increases, any FIR PU filter bank designed to optimize any one objective for which the PCFB is optimal will tend to behave more and more like the infinite-order PCFB, though this has not previously been shown in the literature. One of the major contributions of this thesis is to show this behavior and to *bridge the gap* between the zeroth-order KLT and infinite-order PCFB (see Chapters 3 and 4).

1.3 The FIR PU Interpolation Problem

In certain applications, it may be necessary for an FIR PU system, say $\mathbf{F}(e^{j\omega})$, to take on a prescribed set of values over a prescribed set of frequencies. For example, suppose that for the frequencies $\omega_0, \omega_1, \ldots, \omega_{L-1}$, we require

$$\mathbf{F}(e^{j\omega_k}) = \mathcal{U}_k \ \ \forall \ 0 \leq k \leq L-1 \tag{1.12}$$

Evidently, the matrices $\{\mathcal{U}_k\}$ must be unitary in light of the PU assumption on $\mathbf{F}(e^{j\omega})$. The problem of finding an FIR PU system of a certain McMillan degree which satisfies (1.12) is known as the FIR PU interpolation problem [71].

In the traditional FIR interpolation problem, in which the only restriction made on the interpolant is the FIR constraint, we can always find an interpolant of length at most equal to the number of interpolation conditions by using the Lagrange interpolation formula [22]. However, for the FIR PU interpolation problem of (1.12), in general, it is not known whether there even exists an interpolant of finite degree which will satisfy all L conditions from (1.12). For the special case in which $\mathbf{F}(e^{j\omega})$ is scalar, it is known that in general, only one condition from (1.12) can be satisfied (since in this case, $\mathbf{F}(z)$ is necessarily a pure delay [71]).

Though there is no known solution to the FIR PU interpolation problem, using the optimization algorithm presented in Chapter 4, we can find an approximant to an interpolant. For cases where an interpolant of a certain degree is known to exist, this algorithm can be used to find the interpolant. One of the contributions of the thesis here is thus a numerical approach to solve a theoretically intractable problem.

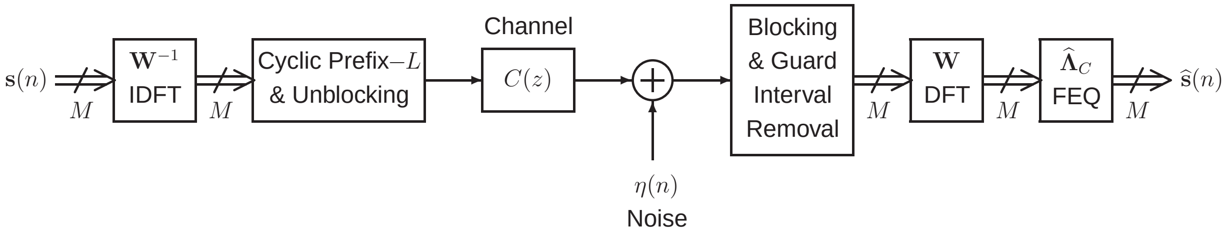

$\widehat{\mathbf{\Lambda}}_C$ is diagonal with

$$\left[\widehat{\mathbf{\Lambda}}_C\right]_{k,k} = \frac{1}{C\left(e^{j\omega_k}\right)}\ ,\ \omega_k = \frac{2\pi k}{M}\ ,\ 0 \leq k \leq M-1$$

Figure 1.14: Typical discrete multitone (DMT) system.

1.4 The Channel Shortening Equalizer Problem

Modern discrete multitone (DMT) digital communications systems such as the digital subscriber loop (DSL) [46] have become popular and have revolutionized telephone wireline communications. With the advent of such systems has come the need for *channel shortening equalizers* [33, 3, 6]. To see this, consider the typical DMT system shown in Fig. 1.14. Here, $\mathbf{s}(n)$ denotes a vector of data corresponding to M users in the communications system. Also, $\mathbf{W}$ denotes the $M \times M$ discrete Fourier transform (DFT) matrix [67], $\mathbf{W}^{-1}$ denotes the inverse DFT (IDFT), and $\widehat{\mathbf{\Lambda}}_C$ is the frequency domain equalizer (FEQ) matrix used to undo the effects of the channel. Perhaps the most important feature of the DMT system of Figure 1.14 is the inclusion of redundancy in the form of a *cyclic prefix* of length L [46]. The beauty of this redundancy is that it can be shown that in the absence of noise, we have perfect reconstruction, i.e., $\widehat{\mathbf{s}}(n) = \mathbf{s}(n)$, if the channel $C(z)$ is of length less than or equal to $L+1$. Essentially, the DMT system is able to equalize an FIR channel using only FIR components (namely, the blocking components along with the DFT matrices $\mathbf{W}$ and $\mathbf{W}^{-1}$ as well as the FEQ). This is only possible because of the inherent redundancy.

From a practical point of view, we want the cyclic prefix length L as small as possible, since it represents a redundancy which hinders the overall rate of the system by a factor of $\frac{M}{(M+L)}$. However, the channel may be very long, as is the case in practical DMT systems such as asymmetric DSL (ADSL) in which the channel is a telephone wire line [46]. For example, in ADSL, $M = 512$ and $L = 32$ [46], although the channels are typically hundreds of samples long. This suggests the need for an equalizer at the receiver which *shortens* the channel, as shown in Figure 1.15. Such an equalizer is typically called a time domain equalizer or TEQ [46]. As the channel may have zeros

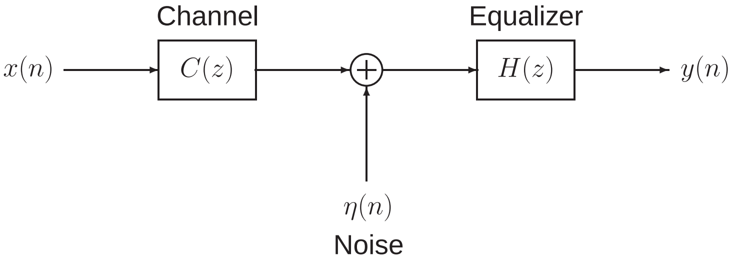

Figure 1.15: Channel shortening equalizer model.

near or outside the unit circle, the equalizer $H(z)$ is usually not chosen to exactly shorten the channel $C(z)$, as this may result in spurious noise amplification. Instead, $H(z)$ is typically an FIR filter chosen to concentrate the energy of the effective channel $C_{\text{eff}}(z) \triangleq H(z)C(z)$ in a window of length $L+1$.

The eigenfilter method [74, 56], which is one of the techniques used in some of the iterative optimization algorithms proposed in the thesis, can be used for the design of channel shortening equalizers. In Chapter 6, we show how the eigenfilter technique can be applied to obtain a low complexity equalizer that accounts for both the effects of the channel length and the noise. There it is shown through simulations that the equalizers designed perform nearly optimally in terms of throughput or bit rate.

1.5 Outline of the Thesis

1.5.1 Eigenfilter Design of Overdecimated Compaction Filter Banks (Chapter 2)

In Chapter 2, we present an iterative method for the design of FIR compaction filters and filter banks. The model used is an overdecimated filter bank in which the PR property can never hold in general. There, it is shown that the compaction filter design problem is tantamount to minimizing the mean-squared error of the output and consists of optimizing a quadratic form subject to quadratic PU constraints. To solve this problem, an iterative method is proposed in which the constraints are linearized at each step. At each iteration, the linearized problem can then be solved using the *eigenfilter method* [74, 54]. The proposed iterative algorithm, though suboptimal, is low in complexity on account of the eigenfilter method, can be used to design more than one filter at a time, and is shown to yield filters that behave like the infinite-order PCFB as the order increases.

1.5.2 Multiresolution Optimal FIR PU Filter Banks (Chapter 3)

Though very low in complexity, the iterative eigenfilter method for compaction filter design suffers from the drawbacks that the quadratic PU constraints may not be satisfied and also that the performance in terms of compaction gain tends to saturate well below that of the infinite-order PCFB as the order increases. To alleviate this problem, in Chapter 3, a different iterative algorithm is proposed for the design of compaction filters. Using a complete parameterization of all FIR PU systems in terms of degree-one Householder building blocks [75, 67], an iterative algorithm for designing an FIR compaction filter is presented in which the objective is to approximate the infinite-order PCFB compaction filter in the least-squares sense. This ensures that the desired PU constraint is always in effect. At each iteration, one set of parameters in the Householder-like characterization of the compaction filter is *globally optimized* assuming all other parameters are fixed. As such, the algorithm is *greedy* and the mean-squared error at every iteration is guaranteed to be monotonic nonincreasing per iteration.

Since the phase of the infinite-order PCFB compaction filter is arbitrary (see Chapters 2 and 4), a modification is proposed in which the phase of the FIR compaction filter is *fed back* to the desired infinite-order compaction filter response. In essence, this modification, which we call the *phase feedback modification*, allows the algorithm to find an easier phase to approximate with an FIR solution. With this modification in effect, it is shown that the algorithm not only still remains greedy, but also results in better FIR compaction filters in terms of compaction gain. Simulation results show a *monotonic* increase in compaction gain as a function of filter order that comes very close to the infinite-order compaction filter bound.

To obtain the rest of the filters of a maximally decimated signal-adapted orthonormal filter bank, a multiresolution optimality criterion [62, 37] is used. With this criterion, the entire filter bank is elegantly designed using only an FIR compaction filter followed by a simple KLT. Though elegant, this criterion is shown to suffer from the inherent nonuniqueness of the FIR compaction filter in terms of its different spectral factors. Different spectral factors lead to different filter banks which in turn yield different performances. By choosing the spectral factor which yields the largest coding gain, it is shown that the FIR filter banks designed perform more and more like the infinite-order PCFB in terms of several objectives as the FIR order increases. This serves to *bridge the gap* between the zeroth-order KLT and infinite-order PCFB.

1.5.3 Direct FIR PU Approximation of the PCFB (Chapter 4)

Due to the inherent nonuniqueness of an FIR compaction filter in terms of its spectral factors, designing signal-adapted filter banks using the multiresolution criterion used in Chapter 3 becomes computationally intractable as the filter order increases. This is because the number of spectral factors and hence filter banks whose performance must be tested grows *exponentially* with order. To avoid this problem, in Chapter 4, the iterative algorithm of Chapter 3 is generalized to obtain all of the synthesis filters at the same time. In particular, a method is proposed for solving the general weighted least-squares approximation problem for the matrix case using an FIR PU approximant. Using the above-mentioned Householder-like factorization of such systems, an iterative algorithm is proposed in which a set of parameters is *globally optimized* at each iteration assuming all others are fixed. As such, the algorithm is greedy in the same way in which the one from Chapter 3 is as well.

To design an FIR PU signal-adapted filter bank, the proposed algorithm is used to approximate the synthesis polyphase matrix of an infinite-order PCFB. With this method, all of the filters are obtained at the same time with only a marginal increase in complexity over the method of Chapter 3. As the infinite-order PCFB synthesis polyphase matrix exhibits a *phase-type ambiguity* (which we formally define in Chapter 4), a generalization of the phase feedback modification from Chapter 3 to the matrix case is proposed. With this modification in effect, the algorithm not only still remains greedy but also yields a better *magnitude-type* fit for the synthesis filters. As all of the filters are found together, this eliminates the need to complete the filter bank using an FIR compaction filter as well as the problems caused by the nonuniqueness of this filter. Simulation results show that the FIR PU signal-adapted filter banks designed using this method behave more and more like the infinite-order PCFB in terms of numerous objectives as the order increases. As with the method proposed in Chapter 3, this serves to *bridge the gap* between the zeroth-order KLT and the infinite-order PCFB. However, this method avoids the need to check the performance of different compaction filter spectral factors, which is *exponentially* computationally complex with filter order.

In addition to being useful for the design of signal-adapted filter banks, the proposed algorithm can also be used for the FIR PU interpolation problem through proper choice of the weight function. Though this problem is still open, the proposed algorithm can always be used to find an approximant to a desired interpolant. For cases where an interpolant is known to exist, the proposed algorithm can be used to find this interpolant, as simulations show.

1.5.4 Coding Gain Optimal FIR Filter Banks (Chapter 5)

In Chapter 5, we consider the optimal design of a signal-adapted filter bank in which the filters are FIR but otherwise unconstrained. The model used is a uniform filter bank with a variable number of channels with scalar quantizers in the subbands and the objective is to minimize the mean-squared error observed at the filter bank output. This is equivalent to maximizing the coding gain of the system. Assuming that the analysis (synthesis) bank is fixed, globally optimizing the corresponding synthesis (analysis) bank is very simple and can be done using the principle of completing the square [22], as is shown. This leads to an iterative greedy algorithm in which the analysis and synthesis banks are alternately optimized. Simulation results verify the greediness of the algorithm and exhibit its usefulness. When we ignore the effects due to quantization, the algorithm can be used to design overdecimated filter banks for optimal reconstruction. In many cases, the filters designed *compact the energy* of the input, much like the compaction filters of an infinite-order PCFB. Upon accounting for the effects of quantization, it is shown that the quantization systems designed come close to the information theoretic rate-distortion bound [10, 7] and coding gain bound [25]. As the filter orders increase, the quantized filter banks designed come closer to these bounds, in line with intuition. This phenomenon has previously not been shown in the literature.

1.5.5 Eigenfilter Channel Shortening Equalizer for DMT Systems (Chapter 6)

Chapter 6 differs in theme from the previous chapters in the sense that it is concerned with the design of *channel shortening equalizers* for DMT systems. There, it is shown that the eigenfilter method used in Chapter 2 can be used for this problem. In particular, we show how the eigenfilter method can be used for the design of a *fractionally spaced equalizer* (FSE) for channel shortening which jointly accounts for the effects due to the channel length as well as noise. One advantage of this method is that it is lower in complexity than other commonly used methods. As opposed to other similar methods which require a different Cholesky decomposition [22] of a certain matrix for every delay parameter chosen, the proposed method only requires one. Despite a significant decrease in complexity, it is shown that there is only a minimal loss in the observed bit rate or throughput. Simulation results for various practical channels encountered in a DSL environment show that the proposed method performs nearly optimally in terms of bit rate.

1.6 Notations

The notation used in the thesis closely parallels that used in [67]. In particular, the subscripts $(^*)$, $(^T)$, and $(^\dagger)$ denote, respectively, the conjugate, transpose, and conjugate transpose of a general matrix quantity. The real and imaginary parts of a complex number c will be denoted by $\mathrm{Re}[c]$ and $\mathrm{Im}[c]$, respectively. Typically, boldface letters are used for matrices and vectors. The (k, ℓ)-th element of a matrix $\mathbf{P}$ will be denoted by $[\mathbf{P}]_{k,\ell}$. The notation $\mathrm{diag}\,(a_0, a_1, \ldots, a_{M-1})$ is used to denote an $M \times M$ diagonal matrix whose diagonal elements are the values $a_0, a_1, \ldots, a_{M-1}$ (i.e., if $\mathbf{\Lambda} = \mathrm{diag}\,(a_0, a_1, \ldots, a_{M-1})$, then $[\mathbf{\Lambda}]_{k,k} = a_k$). Here, $\mathrm{Tr}\,[\mathbf{A}]$ will be used to denote the *trace* of a matrix $\mathbf{A}$, which is the sum of its diagonal elements. Also, we will use $||\mathbf{A}||_F$ to denote the *Frobenius norm* of any matrix $\mathbf{A}$, which is defined as $||\mathbf{A}||_F \triangleq \sqrt{\mathrm{Tr}\,[\mathbf{A}^\dagger \mathbf{A}]}$ [22].

Lowercase letters are commonly used for discrete-time sequences, whereas uppercase letters are often used for Fourier and z-transforms. Together with Fig. 1.3(a) and 1.4(a), (1.1) establishes the notation that will be used for expanders and decimators. For any matrix system $\mathbf{H}(z)$, its *paraconjugate* $\mathbf{H}^\dagger(1/z^*)$ [67] will be denoted by $\widetilde{\mathbf{H}}(z)$.

Finally, in line with standard notation used in statistical signal processing [48], $E\,[\cdot]$ will be used to denote the *expectation operator*.

Chapter 2

Eigenfilter Design of Overdecimated Compaction Filter Banks

In this chapter, a method is proposed for the design of a uniform overdecimated FIR PU filter bank optimized for *energy compaction*. If no FIR constraint is imposed, then the corresponding optimal filters are unconstrained order PCFB filters. For many practical cases of inputs, these filters are ideal bandpass filters called *compaction filters*, as is shown here. As such, these filters are *necessarily* of infinite-order.

When an FIR constraint is imposed on the energy compaction objective, the problem becomes tantamount to maximizing a quadratic form subject to quadratic (and often singular) constraints, as we show here. The method proposed to solve this problem consists of iteratively linearizing the singular quadratic constraints. At each iteration, the *eigenfilter* approach [74, 56] can be used to solve this problem, as is shown. Simulations provided show that the filters designed behave like those of the infinite-order PCFB as the order increases.

Finally, we expand on some of the optimality properties of PU overdecimated filter banks in general. This is shown not only for the uniform overdecimated filter bank considered here, but also for a more general *rational nonuniform* overdecimated synthesis bank signal approximation model. It turns out that for this model, the optimal driving signals are generated by a corresponding overdecimated analysis bank as we show here. If the synthesis bank satisfies a PU condition similar to (1.6), then the corresponding optimal analysis bank is just the paraconjugate of the synthesis bank, yielding an orthonormal overdecimated system.

The content of this chapter is mainly drawn from [54, 49] and portions of it have been presented at [57].

2.1 Outline

In Sec. 2.2, we review the traditional compaction filter problem. The solution in the unconstrained order case is presented in Sec. 2.2.1, with a special emphasis in Sec. 2.2.1.1 for the case in which the input is WSS. An overview of previous work on FIR compaction filters is presented in Sec. 2.2.2.

In Sec. 2.3, we introduce the energy compaction problem for uniform overdecimated PU filter banks. The relation between energy compaction and minimizing the mean-squared error of the output is revealed in Sec. 2.3.1. As shown in the Appendix, this relation holds not only for the uniform overdecimated model, but also for a more general rational nonuniform model as well. In Sec. 2.3.2, the FIR constraint is imposed on the energy compaction problem and it is shown that the problem is quadratic in the filter coefficients with quadratic constraints.

The iterative approach to solving the FIR energy compaction problem by linearizing the singular quadratic constraints is proposed in Sec. 2.4. In Sec. 2.4.1, it is shown that the linearized problem at each iteration can be solved using the eigenfilter method. Simulation results provided in Sec. 2.5 show that the FIR filters designed have a tendency to behave more and more like the corresponding PCFB filters as the order increases. Concluding remarks are made in Sec. 2.6.

Finally, in the Appendix, we focus on the general rational nonuniform overdecimated model for signal approximation and derive the optimal driving signals for this model. First, the optimal driving signals are derived for the deterministic case and then proven to be optimal for the stochastic case as well. When the synthesis bank satisfies a PU condition analogous to (1.6), the optimality of the corresponding orthonormal filter bank is shown as well as the relation between energy compaction and minimizing mean-squared error.

2.2 The Compaction Filter Problem

Consider the one-channel overdecimated filter bank system shown in Fig. 2.1(a). This is essentially an example of the system shown in Fig. 1.13(a) in which the subband processors $\{\mathcal{P}_k\}$ keep only one subband and discard the rest, i.e., $\mathcal{P}_k = \delta(k)$ for $0 \leq k \leq M-1$. As before, we assume that the input $x(n)$ is CWSS(M) whose M-fold blocked version $\mathbf{x}(n)$ has psd $\mathbf{S}_{\mathbf{xx}}(z)$. The compaction filter problem is to maximize the variance of the subband process $w(n)$ subject to an orthonormality condition on the filter bank similar to the one from (1.10). In particular, this condition is

$$H(z) = \widetilde{F}(z)\,,\ \left[\widetilde{F}(z)F(z)\right]_{\downarrow M} = 1 \tag{2.1}$$

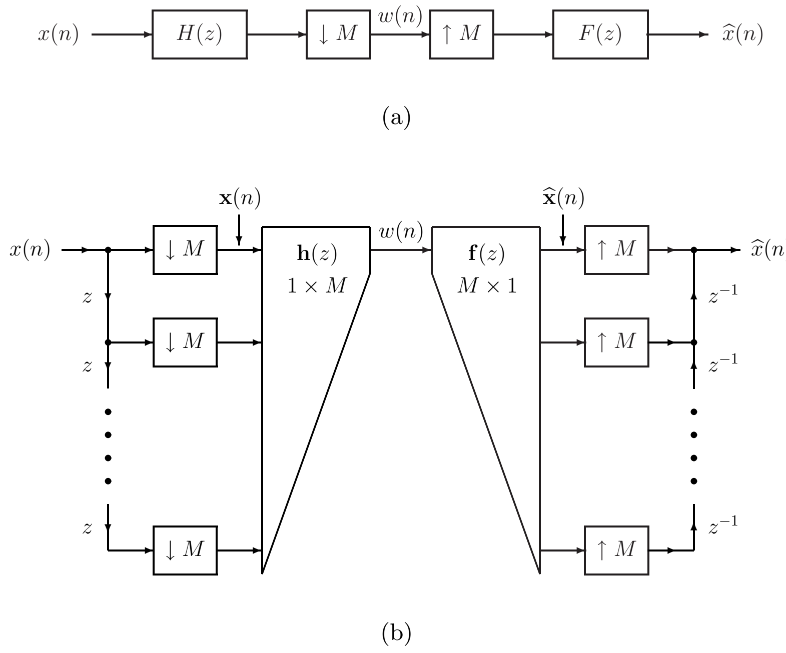

Figure 2.1: (a) One-channel overdecimated filter bank model. (b) Polyphase implementation.

This constraint on $F(z)$ (and hence $H(z)$) is called the *magnitude squared Nyquist(M) constraint*, since the magnitude squared response $\left|F(e^{j\omega})\right|^2$ is Nyquist(M) [67]. It can be shown that the compaction problem is tantamount to minimizing the mean-squared error of the filter bank output in blocked form (see Sec. 2.3.1 and the Appendix). In other words, the error is minimized when we *compact* the energy of the input $x(n)$ in the subband signal $w(n)$.

If we express $H(z)$ and $F(z)$, respectively, in terms of their Type II and Type I M-fold polyphase decompositions, then the system of Fig. 2.1(a) can be redrawn as in Fig. 2.1(b). Here, $\mathbf{h}(z)$ is a row vector consisting of polyphase components of $H(z)$ and $\mathbf{f}(z)$ is a column vector consisting of polyphase components of $F(z)$. In terms of $\mathbf{h}(z)$ and $\mathbf{f}(z)$, the orthonormality condition of (2.1) is

$$\mathbf{h}(z) = \widetilde{\mathbf{f}}(z)\,,\ \widetilde{\mathbf{f}}(z)\mathbf{f}(z) = 1 \tag{2.2}$$

which is similar to the condition of (1.10). With (2.2) in effect, the variance of the subband signal $w(n)$, namely, σ_w^2, becomes the following.

$$\sigma_w^2 = \frac{1}{2\pi}\int_0^{2\pi} \mathbf{f}^\dagger(e^{j\omega})\mathbf{S_{xx}}(e^{j\omega})\mathbf{f}(e^{j\omega})\,d\omega \tag{2.3}$$

Combining (2.3) with (2.2), the compaction filter problem is to choose $F(z)$ or equivalently $\mathbf{f}(z)$ to solve the following problem.

$$\text{Maximize } \sigma_w^2 = \frac{1}{2\pi}\int_0^{2\pi} \mathbf{f}^\dagger(e^{j\omega})\mathbf{S_{xx}}(e^{j\omega})\mathbf{f}(e^{j\omega})\,d\omega \text{ subject to } \mathbf{f}^\dagger(e^{j\omega})\mathbf{f}(e^{j\omega}) = 1\ \forall\ \omega. \tag{2.4}$$

2.2.1 Solution in the Unconstrained Order Case

If no restrictions are made on the order of $F(z)$ (or equivalently $\mathbf{f}(z)$), then the optimal choice of $\mathbf{f}(e^{j\omega})$ which solves the compaction filter problem of (2.4) is any *frequency dependent* unit norm eigenvector $\mathbf{v}(e^{j\omega})$ of the matrix $\mathbf{S}_{\mathbf{xx}}(e^{j\omega})$ which corresponds to its largest frequency dependent eigenvalue $\lambda_{\max}(e^{j\omega})$ [62, 68]. This follows from *Rayleigh's principle* [22], which states that the maximum value of the integrand of (2.3) for any ω, namely, $\mathbf{f}^{\dagger}(e^{j\omega})\mathbf{S}_{\mathbf{xx}}(e^{j\omega})\mathbf{f}(e^{j\omega})$, is simply $\lambda_{\max}(e^{j\omega})$, with the unit norm constraint $\mathbf{f}^{\dagger}(e^{j\omega})\mathbf{f}(e^{j\omega}) = 1$ in effect. This maximum value occurs iff $\mathbf{f}(e^{j\omega})$ is any unit norm vector in the eigenspace corresponding to $\lambda_{\max}(e^{j\omega})$. Since this choice of $\mathbf{f}(e^{j\omega})$ maximizes the integrand of (2.3) for all ω, it hence maximizes its integral σ_w^2 as well. The resulting optimal compaction filter $F(e^{j\omega})$ (or equivalently $F^*(e^{j\omega})$) is in fact the first synthesis (analysis) filter of the unconstrained order PCFB [62, 68, 1]. It should be noted that the remaining synthesis (as well as analysis) filters are themselves optimal compaction filters. In particular, the k-th synthesis (or analysis) filter corresponding to the unconstrained order PCFB is an optimal compaction filter for the psd $\mathbf{S}_{\mathbf{xx}}(e^{j\omega})$ with the k largest eigenvalues removed (i.e., set to zero). This psd will be called the k-th *peeled spectrum* of $\mathbf{x}(n)$, since it represents the psd $\mathbf{S}_{\mathbf{xx}}(e^{j\omega})$ with the largest k eigenvalues *peeled off.* It should be noted here that the optimal filter $F(e^{j\omega})$ can only be expressed in terms of the psd $\mathbf{S}_{\mathbf{xx}}(e^{j\omega})$ *pointwise in frequency.* The order of the optimal $F(e^{j\omega})$ depends greatly on the *nature* of the psd $\mathbf{S}_{\mathbf{xx}}(e^{j\omega})$, as will soon be shown.

2.2.1.1 Special Case of WSS Input

For many practical scenarios, the scalar input signal $x(n)$ is itself WSS. In this case, the psd $\mathbf{S}_{\mathbf{xx}}(z)$ of the blocked version $\mathbf{x}(n)$ specifically has a *pseudocirculant* structure [40] (see the Appendix). If $S_{xx}(z)$ denotes the psd of $x(n)$ here, then the compaction filter problem of (2.4) can be simplified as follows [68].

$$\text{Maximize } \sigma_w^2 = \frac{1}{2\pi}\int_0^{2\pi} S_{xx}(e^{j\omega})\left|F(e^{j\omega})\right|^2 d\omega \text{ subject to } \left[\left|F(e^{j\omega})\right|^2\right]_{\downarrow M} = 1 \ \forall\ \omega. \tag{2.5}$$

Note that in this special case where $x(n)$ is WSS, the compaction filter problem of (2.5) only depends on the magnitude of $F(e^{j\omega})$ and not on its phase. As such, the optimum compaction filter is not unique.

If no order constraint is made on $F(z)$, then the optimum compaction filter is in general an ideal bandpass filter. This was first shown by Unser [66] for the special case of $M = 2$ and later generalized by Vaidyanathan [68] for arbitrary M. In particular, the optimum compaction filter must satisfy

$$\left|F(e^{j\omega})\right|^2 = \begin{cases} M\,, & \omega \in \boldsymbol{\omega}_x \\ 0\,, & \text{otherwise} \end{cases} \tag{2.6}$$

where $\boldsymbol{\omega}_x$ is the set of frequencies defined as follows.

$$\boldsymbol{\omega}_x \triangleq \left\{\omega \in [0, 2\pi) : S_{xx}(e^{j\omega}) \geq S_{xx}\left(e^{j\left(\omega + \frac{2\pi m}{M}\right)}\right) \ \forall \ 1 \leq m \leq M-1\right\} \tag{2.7}$$

If ties exist in (2.7), then only one frequency is chosen. In addition to the nonuniqueness of the compaction filter with respect to phase, there is also a possible nonuniqueness with respect to magnitude if ties exist in the comparison step in (2.7). Regardless of these sources of nonuniqueness, it is clear that when the input is WSS, any unconstrained order optimal compaction filter is necessarily an ideal bandpass filter in general. As such, these filters are unrealizable in practice and only serve as a benchmark for the performance we can expect from practical, realizable filters.

Finally, we should note that when $x(n)$ is WSS, the PCFB analysis/synthesis filters, which are obtained from $\mathbf{S_{xx}}(e^{j\omega})$ and its peeled spectra, are themselves infinite-order bandpass filters whose magnitude responses are similar to the form given in (2.6). Hence, all of the filters of an unconstrained PCFB in this case are *necessarily* infinite in order.

2.2.2 Overview of Previous Work on FIR Compaction Filters

If, in addition to the PU constraint of (2.2), we impose an FIR constraint on $F(z)$ (or equivalently $\mathbf{f}(z)$), the compaction filter problem of (2.4) becomes much more complicated. The reason for this is that, in terms of the filter coefficients, the problem is tantamount to maximizing a quadratic form subject to a quadratic unit norm condition as well as several *singular* quadratic constraints [9], as is shown in Sec. 2.3.2. This problem is *nonconvex* in terms of the filter coefficients [9, 35, 64] and as such, complicated numerical techniques must be employed for the design of FIR compaction filters. A brief survey of some of the methods proposed for their design is given below. It should be noted here that all of these methods apply only for the special case in which the input $x(n)$ is WSS (i.e., the compaction filter problem simplifies to (2.5)).

1. *Quadratically Constrained Optimization:* Several methods were proposed for solving the abovementioned quadratically constrained quadratic form maximization problem numerically using the method of Lagrange multipliers (see [8] for the special case where $M = 2$ and [9] for arbitrary M). Though these methods do not require spectral factorization, they are only guaranteed to reach a local optimum due to the nonconvex nature of the optimization problem.

2. *Optimizing the FIR Lattice Structure:* For the special case where $M = 2$, it is well known that any real coefficient FIR PU filter bank is completely parameterized by a lattice structure [67] which is characterized by a finite set of rotation angles. Several methods were proposed for the optimization of these angles [70, 11]. Though these methods automatically satisfy the desired PU constraint and do not require spectral factorization, they have the drawback that they are only guaranteed to reach a local optimum and only work for the special case of $M = 2$.

3. *Optimizing the Product Filter:* As the compaction filter problem of (2.5) is only in terms of the magnitude squared response $\left|F(e^{j\omega})\right|^2$, several methods have been proposed for the design of the product filter $G(z) \triangleq \widetilde{F}(z)F(z)$. In this case, the objective function σ_w^2 becomes linear in terms of the coefficients of $G(z)$, but, in addition to the usual PU constraint of (2.2), the positivity constraint $G(e^{j\omega}) \geq 0$ must be also be enforced. Hence, the problem is a linear programming (LP) problem with infinitely many positivity inequality constraints (which is typically called a semi-infinite programming (SIP) problem [35]). Several approaches were proposed for finding the optimal product filter, including the window method of [29] and the frequency discretization method of [35, 37], in which the positivity constraints are only satisfied on a finite set of frequency points. These methods have been shown to yield good performance, despite the fact that there is no guarantee of global optimality and a spectral factorization step is required at the end.

4. *State Space Approach:* Recently an elegant method for the design of optimum FIR compaction filters was proposed based on a state space description of the compaction filter [64]. This method, which is based on a semi-definite programming (SDP) technique, ensures a *globally optimal* compaction filter and doesn't require a spectral factorization step. However, this method only applies for WSS inputs $x(n)$ and becomes extremely computationally intensive as the filter order increases.

Using the proposed iterative eigenfilter method for the overdecimated filter bank model of Sec. 2.3, we can design several PCFB-like compaction filters *simultaneously*. Furthermore, since the eigenfilter approach is used here, the method is very low in complexity [74, 56] and also can be used when the input $x(n)$ is CWSS(M).

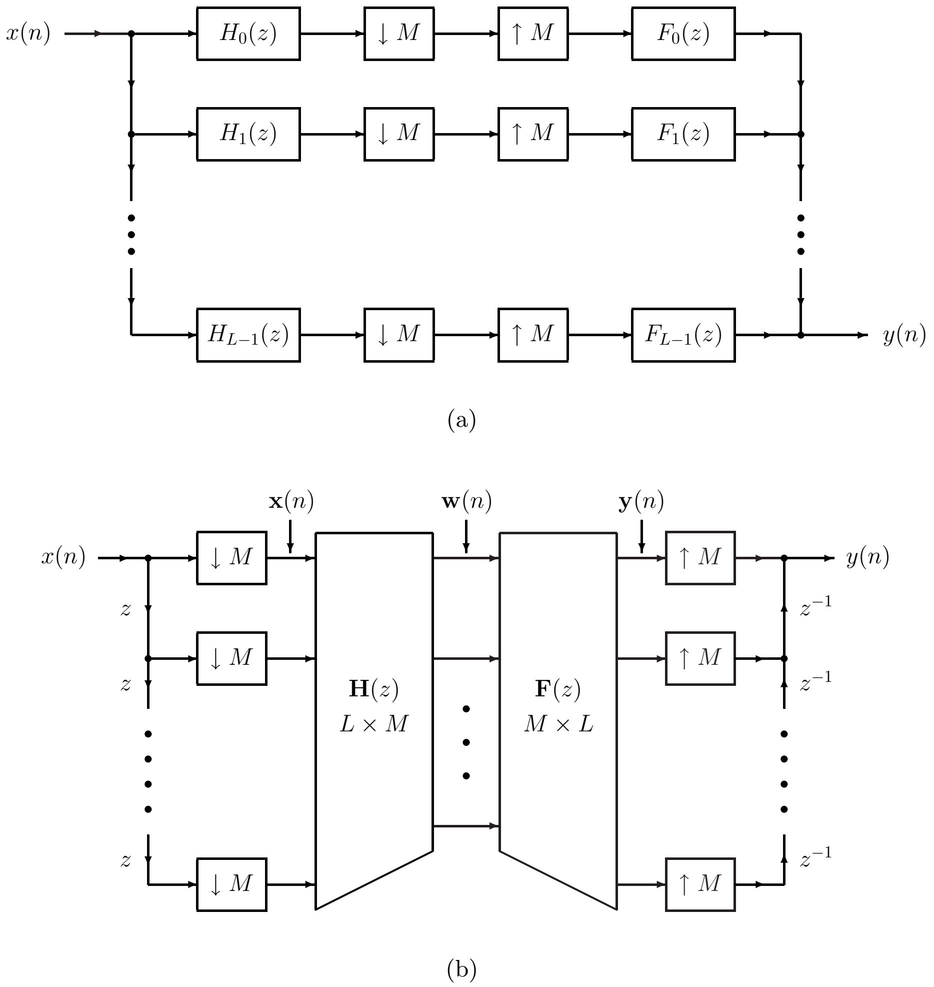

Figure 2.2: (a) Uniform overdecimated filter bank ($L < M$), (b) Polyphase representation.

2.3 Energy Compaction Problem for Overdecimated Filter Banks

Here, we focus on the overdecimated uniform filter bank shown in Fig. 2.2(a). In accordance with Sec. 1.1.4, by overdecimated, we mean that the number of channels L satisfies $L < M$, i.e., the number of subbands is strictly less than the decimation ratio. Also, recall from Sec. 1.1.4 that with such a system, we have a loss of information and properties such as alias cancellation and PR are in general impossible. If we consider the following polyphase decompositions (see Sec. 1.1.3.2) of the analysis filters $H_k(z)$ and synthesis filters $F_k(z)$ for $0 \leq k \leq L-1$,

$$\begin{aligned} H_k(z) &= \sum_{\ell=0}^{M-1} z^{\ell} H_{k,\ell}(z^M) \quad \text{(Type II)} \\ F_k(z) &= \sum_{\ell=0}^{M-1} z^{-\ell} F_{k,\ell}(z^M) \quad \text{(Type I)} \end{aligned}$$

then the system of Fig. 2.2(a) can be redrawn as in Fig. 2.2(b), where

$$[\mathbf{H}(z)]_{\ell,m} = H_{\ell,m}(z)\,,\ [\mathbf{F}(z)]_{m,\ell} = F_{\ell,m}(z)$$

for $0 \leq \ell \leq L-1$ and $0 \leq m \leq M-1$. Note that here, the vector signals $\mathbf{x}(n)$ and $\mathbf{y}(n)$ denote, respectively, the M-fold blocked versions [67] of the filter bank input $x(n)$ and output $y(n)$.

2.3.1 Derivation of the Energy Compaction Problem

Let us denote the autocorrelation sequence and psd of $\mathbf{x}(n)$ by $\mathbf{R}_{\mathbf{xx}}(k)$ and $\mathbf{S}_{\mathbf{xx}}(z)$, respectively. In addition to this stationarity assumption on $\mathbf{x}(n)$, we will also assume that the filter bank is *orthonormal.* This means that the matrices $\mathbf{H}(z)$ and $\mathbf{F}(z)$ from Fig. 2.2(b) satisfy [67]

$$\mathbf{H}(z) = \widetilde{\mathbf{F}}(z)\,,\ \widetilde{\mathbf{F}}(z)\mathbf{F}(z) = \mathbf{I}_L \tag{2.8}$$

With the above assumptions on the input and filter bank, it can easily be shown that minimizing the error of the output is equivalent to *compacting* the energy of the signal $\mathbf{w}(n)$.

Suppose that we wish to choose $\mathbf{H}(z)$ and $\mathbf{F}(z)$ subject to the orthonormality constraint of (2.8) to minimize the expected mean-squared error between $\mathbf{x}(n)$ and $\mathbf{y}(n)$, defined as follows.

$$\xi \triangleq E\left[||\mathbf{x}(n) - \mathbf{y}(n)||^2\right] \tag{2.9}$$

If we define the blocked filter error $\mathbf{e}(n)$ as $\mathbf{e}(n) \triangleq \mathbf{x}(n) - \mathbf{y}(n)$ and denote the psd of $\mathbf{e}(n)$ by $\mathbf{S}_{\mathbf{ee}}(z)$, then from (2.9), we have

$$\xi = \mathrm{Tr}\left[E\left[\mathbf{e}(n)\mathbf{e}^{\dagger}(n)\right]\right] = \frac{1}{2\pi}\int_0^{2\pi} \mathrm{Tr}\left[\mathbf{S}_{\mathbf{ee}}(e^{j\omega})\right]\, d\omega \tag{2.10}$$

From Fig. 2.2(b) and [67], it can be shown that we have

$$\begin{aligned}\mathbf{S}_{\mathbf{ee}}(z) &= \mathbf{S}_{\mathbf{xx}}(z) - \mathbf{F}(z)\mathbf{H}(z)\mathbf{S}_{\mathbf{xx}}(z) - \mathbf{S}_{\mathbf{xx}}(z)\widetilde{\mathbf{H}}(z)\widetilde{\mathbf{F}}(z)\\ &\quad + \mathbf{F}(z)\mathbf{H}(z)\mathbf{S}_{\mathbf{xx}}(z)\widetilde{\mathbf{H}}(z)\widetilde{\mathbf{F}}(z)\end{aligned} \tag{2.11}$$

Imposing the orthonormality constraint of (2.8) in (2.11) yields

$$\mathrm{Tr}\left[\mathbf{S}_{\mathbf{ee}}(z)\right] = \mathrm{Tr}\left[\mathbf{S}_{\mathbf{xx}}(z)\right] - \mathrm{Tr}\left[\widetilde{\mathbf{F}}(z)\mathbf{S}_{\mathbf{xx}}(z)\mathbf{F}(z)\right]$$

Substituting this into (2.10) leads to the following.

$$\begin{aligned}\xi &= \frac{1}{2\pi}\int_0^{2\pi} \mathrm{Tr}\left[\mathbf{S}_{\mathbf{xx}}(e^{j\omega})\right]\, d\omega\\ &\quad \underbrace{- \frac{1}{2\pi}\int_0^{2\pi} \mathrm{Tr}\left[\mathbf{F}^{\dagger}(e^{j\omega})\mathbf{S}_{\mathbf{xx}}(e^{j\omega})\mathbf{F}(e^{j\omega})\right]\, d\omega}_{\sigma_{\mathbf{w}}^2} && (2.12)\\ &= \mathrm{Tr}\left[\mathbf{R}_{\mathbf{xx}}(0)\right] - \sigma_{\mathbf{w}}^2 && (2.13)\end{aligned}$$

Hence, from (2.13), with the orthonormality constraint of (2.8) in effect, minimizing ξ from (2.9) is equivalent to maximizing $\sigma^2_{\mathbf{w}}$. But $\sigma^2_{\mathbf{w}}$ is just the energy of the subband vector process $\mathbf{w}(n)$ from Fig. 2.2(b), i.e., $\sigma^2_{\mathbf{w}} = \mathrm{Tr}\left[\mathbf{R}_{\mathbf{ww}}(0)\right]$, where $\mathbf{R}_{\mathbf{ww}}(k)$ denotes the autocorrelation of $\mathbf{w}(n)$. Thus, minimizing the mean-squared error of the overdecimated filter bank is equivalent to maximizing or *compacting* the energy of the subband process $\mathbf{w}(n)$. It can be shown that if no length constraints are made on the matrix $\mathbf{F}(z)$ from Fig. 2.2(b), then an optimal set of synthesis filters $F_k(z)$ for $0 \leq k \leq L-1$ from Fig. 2.2(a) which maximize $\sigma^2_{\mathbf{w}}$ from (2.13) are the first L ideal compaction filters appearing in the infinite-order PCFB for $\mathbf{S}_{\mathbf{xx}}(z)$ [62, 68].

2.3.2 Imposing the FIR Constraint on the Matrix $\mathbf{F}(z)$

Suppose now that in addition to the orthonormality constraint of (2.8), the matrix $\mathbf{F}(z)$ is causal and FIR of length N. In other words, suppose that we have the following.

$$\mathbf{F}(z) = \sum_{n=0}^{N-1} \mathbf{f}(n) z^{-n} \tag{2.14}$$

where $\mathbf{f}(n)$ is the $M \times L$ impulse response of $\mathbf{F}(z)$. Define the $MN \times L$ impulse response matrix $\widehat{\mathbf{f}}$ and $M \times MN$ block delay matrix $\mathbf{d}(z)$ as follows.

$$\begin{aligned} \widehat{\mathbf{f}} &\triangleq \begin{bmatrix} \mathbf{f}^T(0) & \mathbf{f}^T(1) & \cdots & \mathbf{f}^T(N-1) \end{bmatrix}^T \\ \mathbf{d}(z) &\triangleq \begin{bmatrix} \mathbf{I}_M & z^{-1}\mathbf{I}_M & \cdots & z^{-(N-1)}\mathbf{I}_M \end{bmatrix} \end{aligned}$$

From (2.14), we clearly have $\mathbf{F}(z) = \mathbf{d}(z)\widehat{\mathbf{f}}$ and $\widetilde{\mathbf{F}}(z) = \widehat{\mathbf{f}}^\dagger \widetilde{\mathbf{d}}(z)$. Substituting this into (2.12) yields the following.

$$\sigma^2_{\mathbf{w}} = \mathrm{Tr}\left[\widehat{\mathbf{f}}^\dagger \underbrace{\left(\frac{1}{2\pi} \int_0^{2\pi} \mathbf{d}^\dagger(e^{j\omega}) \mathbf{S}_{\mathbf{xx}}(e^{j\omega}) \mathbf{d}(e^{j\omega})\, d\omega \right) \widehat{\mathbf{f}}}_{\widehat{\mathbf{R}}} \right] \tag{2.15}$$

Here, the $MN \times MN$ matrix $\widehat{\mathbf{R}}$ is positive semidefinite and can be expressed in terms of the autocorrelation of $\mathbf{x}(n)$ as follows.

$$\widehat{\mathbf{R}} = \begin{bmatrix} \mathbf{R}_{\mathbf{xx}}(0) & \mathbf{R}_{\mathbf{xx}}(-1) & \cdots & \mathbf{R}_{\mathbf{xx}}(-(N-1)) \\ \mathbf{R}_{\mathbf{xx}}(1) & \mathbf{R}_{\mathbf{xx}}(0) & \cdots & \mathbf{R}_{\mathbf{xx}}(-(N-2)) \\ \vdots & \vdots & \ddots & \vdots \\ \mathbf{R}_{\mathbf{xx}}(N-1) & \mathbf{R}_{\mathbf{xx}}(N-2) & \cdots & \mathbf{R}_{\mathbf{xx}}(0) \end{bmatrix} \tag{2.16}$$

From (2.16), note that $\widehat{\mathbf{R}}$ is the N-fold block autocorrelation matrix corresponding to $\mathbf{x}(n)$ and that $\widehat{\mathbf{R}}$ is a *block Toeplitz* matrix [22]. In the special case where the scalar input signal $x(n)$ is WSS with autocorrelation $R_{xx}(k)$, then we have

$$[\mathbf{R}_{\mathbf{xx}}(k)]_{\ell,m} = R_{xx}(Mk + \ell - m)\,,\ 0 \leq \ell, m \leq M-1$$

and so $\widehat{\mathbf{R}}$ in this case is actually Toeplitz.

To analyze the orthonormality condition of (2.8) with the FIR constraint on $\mathbf{F}(z)$ in effect, define $\mathbf{G}(z) \triangleq \widetilde{\mathbf{F}}(z)\mathbf{F}(z)$. Then, from (2.8), in the time domain, we require

$$\mathbf{g}(n) = \mathbf{f}^{\dagger}(-n) * \mathbf{f}(n) = \sum_{m} \mathbf{f}^{\dagger}(m)\mathbf{f}(m+n) = \mathbf{I}_L \delta(n) \tag{2.17}$$

where $\mathbf{g}(n)$ is the impulse response of $\mathbf{G}(z)$. Assuming $\mathbf{F}(z)$ to be causal and FIR as in (2.14), then $\mathbf{g}(n)$ can only be nonzero for $-(N-1) \leq n \leq (N-1)$. As $\mathbf{g}^{\dagger}(-n) = \mathbf{g}(n)$, the orthonormality conditions of (2.17) only need to be satisfied for $0 \leq n \leq N-1$. These constraints can be compactly written in terms of the matrix $\widehat{\mathbf{f}}$ as follows [9].

$$\widehat{\mathbf{f}}^{\dagger}\mathcal{S}_k\widehat{\mathbf{f}} = \mathbf{I}_L\delta(k)\,,\ 0 \leq k \leq N-1 \tag{2.18}$$

where $\mathcal{S}_k$ $(MN \times MN)$ is the k-th block shift matrix given by the following.

$$\mathcal{S}_k = \begin{bmatrix} \mathbf{0}_{(N-k)M \times kM} & \mathbf{I}_{(N-k)M} \\ \mathbf{0}_{kM \times kM} & \mathbf{0}_{kM \times (N-k)M} \end{bmatrix}\,,\ 0 \leq k \leq N-1 \tag{2.19}$$

For example, we have

$$\mathcal{S}_1 = \begin{bmatrix} \mathbf{0} & \mathbf{I}_M & \mathbf{0} & \cdots & \mathbf{0} \\ \mathbf{0} & \mathbf{0} & \mathbf{I}_M & \ddots & \vdots \\ \vdots & \vdots & \ddots & \ddots & \mathbf{0} \\ \vdots & \vdots & & \ddots & \mathbf{I}_M \\ \mathbf{0} & \mathbf{0} & \cdots & \cdots & \mathbf{0} \end{bmatrix}$$

Note that for $1 \leq k \leq N-1$, the matrix $\mathcal{S}_k$ from (2.19) is *singular*. Hence, from (2.18), it follows that there are $(N-1)$ *singular quadratic* constraints. The key to deriving the iterative eigenfilter technique lies in linearizing these singular constraints. This is done by expressing the constraints of (2.17) in an *implicit* form. Note that for $n = 0$, (2.17) can be expressed in terms of the matrix $\widehat{\mathbf{f}}$ as follows.

$$\widehat{\mathbf{f}}^{\dagger}\widehat{\mathbf{f}} = \mathbf{I}_L \tag{2.20}$$

Similarly, for $1 \leq n \leq N-1$, (2.17) can be expressed in terms of $\widehat{\mathbf{f}}$ as follows.

$$\underbrace{\begin{bmatrix} \mathbf{0} & \mathbf{f}^{\dagger}(0) & \mathbf{f}^{\dagger}(1) & \cdots & \mathbf{f}^{\dagger}(N-2) \\ \mathbf{0} & \mathbf{0} & \mathbf{f}^{\dagger}(0) & \cdots & \mathbf{f}^{\dagger}(N-3) \\ \vdots & \vdots & \ddots & \ddots & \vdots \\ \mathbf{0} & \mathbf{0} & \cdots & \mathbf{0} & \mathbf{f}^{\dagger}(0) \end{bmatrix}}_{\mathbf{C}} \underbrace{\begin{bmatrix} \mathbf{f}(0) \\ \mathbf{f}(1) \\ \vdots \\ \mathbf{f}(N-1) \end{bmatrix}}_{\widehat{\mathbf{f}}} = \underbrace{\begin{bmatrix} \mathbf{0} \\ \mathbf{0} \\ \vdots \\ \mathbf{0} \end{bmatrix}}_{\mathbf{0}_{L(N-1)\times L}} \tag{2.21}$$

It should be noted that the $L(N-1) \times MN$ matrix $\mathbf{C}$ from (2.21) is a function of the impulse response coefficients $\mathbf{f}(n)$. As such, the constraint in (2.21) is an *implicit quadratic* constraint. Combining (2.15), (2.20), and (2.21), the energy compaction problem in the presence of the FIR constraint on $\mathbf{F}(z)$ can be expressed as follows.

$$\begin{aligned} &\text{Maximize } \sigma_{\mathbf{w}}^2 = \text{Tr}\left[\widehat{\mathbf{f}}^{\dagger}\widehat{\mathbf{R}}\widehat{\mathbf{f}}\right] \\ &\text{subject to } \widehat{\mathbf{f}}^{\dagger}\widehat{\mathbf{f}} = \mathbf{I}_L \text{ and } \mathbf{C}\widehat{\mathbf{f}} = \mathbf{0}_{L(N-1)\times L} \end{aligned} \tag{2.22}$$

with $\widehat{\mathbf{R}}$ and $\mathbf{C}$ as in (2.16) and (2.21), respectively.

In general, the optimization problem of (2.22) is *nonlinear* and *nonconvex* in terms of the elements of the matrix $\widehat{\mathbf{f}}$. What makes the problem difficult to solve is the implicit quadratic constraint $\mathbf{C}\widehat{\mathbf{f}} = \mathbf{0}$ from (2.21). Using the iterative approach for solving the optimization problem of (2.22) to be discussed in the next section, it is possible to turn this implicit quadratic constraint into an *explicit linear* constraint. Once this constraint becomes linear, the optimization at each iteration can be solved exactly using the *eigenfilter* technique [74, 56], which is low in complexity and numerically stable. Before showing this, we will first formally present the iterative algorithm for solving the optimization problem of (2.22).

2.4 Iterative Eigenfilter Method for Solving the FIR Compaction Problem

In what follows, let $\mathbf{f}_k(n)$ denote the impulse response $\mathbf{f}(n)$ at the k-th iteration. Also, define the $MN \times L$ matrix $\widehat{\mathbf{f}}_k$ and $L(N-1) \times MN$ matrix $\mathbf{C}_k$ as follows.

$$\widehat{\mathbf{f}}_k \triangleq \begin{bmatrix} \mathbf{f}_k^T(0) & \mathbf{f}_k^T(1) & \cdots & \mathbf{f}_k^T(N-1) \end{bmatrix}^T \tag{2.23}$$

$$\mathbf{C}_k \triangleq \begin{bmatrix} \mathbf{0} & \mathbf{f}_k^\dagger(0) & \mathbf{f}_k^\dagger(1) & \cdots & \mathbf{f}_k^\dagger(N-2) \\ \mathbf{0} & \mathbf{0} & \mathbf{f}_k^\dagger(0) & \cdots & \mathbf{f}_k^\dagger(N-3) \\ \vdots & \vdots & \ddots & \ddots & \vdots \\ \mathbf{0} & \mathbf{0} & \cdots & \mathbf{0} & \mathbf{f}_k^\dagger(0) \end{bmatrix} \tag{2.24}$$

Then, the proposed iterative algorithm is as follows.

Initialization:

Choose any $\mathbf{f}_0(n)$ which satisfies the orthonormality constraints of (2.17). This can be easily done using the complete characterization of FIR PU systems in terms of degree-one Householder-like building blocks [75, 67]. Compute $\widehat{\mathbf{f}}_0$ from $\mathbf{f}_0(n)$.

Iteration: For $k \geq 1$, do the following.

1. Compute the constraint matrix $\mathbf{C}_{k-1}$.
2. Solve the linearized optimization problem

$$\begin{gathered} \text{Maximize } \sigma^2_{\mathbf{w},k} = \text{Tr}\left[\widehat{\mathbf{f}}_k^\dagger \mathbf{R} \widehat{\mathbf{f}}_k\right] \\ \text{subject to } \widehat{\mathbf{f}}_k^\dagger \widehat{\mathbf{f}}_k = \mathbf{I}_L \text{ and } \mathbf{C}_{k-1}\widehat{\mathbf{f}}_k = \mathbf{0}_{L(N-1)\times L} \end{gathered} \tag{2.25}$$

3. To measure the convergence of the iteration to an orthonormal solution, calculate the *orthonormality error matrix* at the k-th iteration defined by

$$\boldsymbol{\epsilon}_k \triangleq \mathbf{C}_k \widehat{\mathbf{f}}_k \tag{2.26}$$

As we need $\boldsymbol{\epsilon}_k = \mathbf{0}$ in theory (from (2.21), (2.23), (2.24), and (2.26)), terminate the iteration when we have

$$||\boldsymbol{\epsilon}_k||_F < \delta_T \tag{2.27}$$

where $||\boldsymbol{\epsilon}_k||_F$ denotes the *Frobenius norm* of $\boldsymbol{\epsilon}_k$ [22] and δ_T is a some small threshold value.

Before proceeding, it should be noted that there is no guarantee that the iterative algorithm will converge to an orthonormal solution, although in simulations it often does so as shown below. At present, there is no known method as to what should be done if the iteration fails to converge to an orthonormal solution. Furthermore, even if there is convergence, there is no guarantee that the resulting solution is globally optimal.

Despite this, often times in simulations such as those presented below, the algorithm performs well in terms of approaching the behavior of the ideal compaction filters of the infinite-order PCFB. Also, the algorithm can be used for relatively large orders N, as the linearized optimization problem of (2.25) can be solved using the eigenfilter approach [67]. We now proceed to show how to solve the linearized optimization problem of (2.25).

2.4.1 Solution to the Iterative Linearized Optimization Problem

Consider the linear constraint $\mathbf{C}_{k-1}\widehat{\mathbf{f}}_k = \mathbf{0}$ from (2.25). This constraint holds iff the columns of $\widehat{\mathbf{f}}_k$ lie in the *null space* of $\mathbf{C}_{k-1}$ [22]. Let $\mathbf{U}_{k-1}$ denote a unitary matrix whose columns span the null space of $\mathbf{C}_{k-1}$. If ρ denotes the dimension of the null space of $\mathbf{C}_{k-1}$, then $\mathbf{U}_{k-1}$ is $MN \times \rho$. As the columns of $\widehat{\mathbf{f}}_k$ must lie in the null space of $\mathbf{C}_{k-1}$, $\widehat{\mathbf{f}}_k$ must be of the form $\widehat{\mathbf{f}}_k = \mathbf{U}_{k-1}\mathbf{a}$ for some arbitrary $\rho \times L$ matrix $\mathbf{a}$. Hence, we have

$$\mathbf{C}_{k-1}\widehat{\mathbf{f}}_k = \mathbf{0} \Longleftrightarrow \widehat{\mathbf{f}}_k = \mathbf{U}_{k-1}\mathbf{a} \tag{2.28}$$

Given that $\mathbf{C}_{k-1}$ is $L(N-1) \times MN$, we can easily argue that the dimension of its null space ρ satisfies $\rho \geq L$. Hence, the linear constraint $\mathbf{C}_{k-1}\widehat{\mathbf{f}}_k = \mathbf{0}$ transforms the problem of finding $\widehat{\mathbf{f}}_k$ into that of finding the $\rho \times L$ matrix $\mathbf{a}$. The quantity $\mathbf{a}$ is arbitrary but must be such that the unitary constraint $\widehat{\mathbf{f}}_k^\dagger\widehat{\mathbf{f}}_k = \mathbf{I}_L$ from (2.25) is satisfied. Clearly, from (2.28), we have

$$\widehat{\mathbf{f}}_k^\dagger\widehat{\mathbf{f}}_k = \mathbf{I}_L \Longleftrightarrow \mathbf{a}^\dagger\mathbf{a} = \mathbf{I}_L$$

upon exploiting the unitarity of $\mathbf{U}_{k-1}$. As can be seen, the constraints of (2.25) transform the problem of finding $\widehat{\mathbf{f}}_k$ into that of finding $\mathbf{a}$ where $\mathbf{a}$ is allowed to by any $\rho \times L$ unitary matrix. Hence, the optimization problem of (2.25) can be recast as follows.

$$\begin{gathered}\text{Maximize } \sigma_{\mathbf{w},k}^2 = \text{Tr}\left[\mathbf{a}^\dagger\overline{\mathbf{R}}_{k-1}\mathbf{a}\right] \text{ where } \overline{\mathbf{R}}_{k-1} \triangleq \mathbf{U}_{k-1}^\dagger\widehat{\mathbf{R}}\mathbf{U}_{k-1} \\ \text{subject to the constraint } \mathbf{a}^\dagger\mathbf{a} = \mathbf{I}_L\end{gathered} \tag{2.29}$$

The solution to this problem follows from a generalization of Rayleigh's principle [22, p. 191] and is as follows. Suppose that $\overline{\mathbf{R}}_{k-1}$ has the following unitary diagonalization.

$$\overline{\mathbf{R}}_{k-1} = \mathbf{V}_{k-1}\mathbf{\Lambda}_{k-1}\mathbf{V}_{k-1}^\dagger$$

where $\mathbf{V}_{k-1}$ is a $\rho \times \rho$ matrix of eigenvectors of $\overline{\mathbf{R}}_{k-1}$ and $\mathbf{\Lambda}_{k-1}$ is a diagonal matrix consisting of the eigenvalues of $\overline{\mathbf{R}}_{k-1}$. In addition, suppose that $\mathbf{\Lambda}_{k-1} = \text{diag}\left(\lambda_{k-1,0}, \lambda_{k-1,1}, \ldots, \lambda_{k-1,\rho-1}\right)$ and

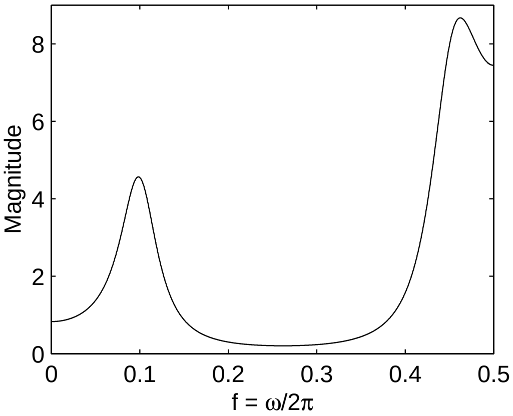

Figure 2.3: Input power spectral density $S_{xx}(e^{j\omega})$.

that the eigenvalues have been ordered in decreasing order, i.e., $\lambda_{k-1,0} \geq \lambda_{k-1,1} \geq \cdots \geq \lambda_{k-1,\rho-1}$. Then, the solution to the optimization problem of (2.29) is given to be [22]

$$\sigma^2_{\mathbf{w},k} = \sum_{i=0}^{L-1} \lambda_{k-1,i}$$

which occurs iff we have

$$\mathbf{a} = \mathbf{V}_{k-1}\mathbf{b}$$

where $\mathbf{b}$ is a $\rho \times L$ matrix of the form

$$\mathbf{b} = \begin{bmatrix} \mathbf{B} \\ \mathbf{0}_{(\rho-L)\times L} \end{bmatrix} \tag{2.30}$$

and $\mathbf{B}$ is any $L \times L$ square unitary matrix. In other words, the optimal $\mathbf{a}$ is a such that its columns are unitary combinations of the first L eigenvectors of $\overline{\mathbf{R}}_{k-1}$. Once an optimal $\mathbf{a}$ has been found, the corresponding optimal $\widehat{\mathbf{f}}_k$ can be found using $\widehat{\mathbf{f}}_k = \mathbf{U}_{k-1}\mathbf{a}$. As computing the optimal synthesis filter matrix $\widehat{\mathbf{f}}_k$ requires the eigendecomposition of a particular matrix, it follows that the original linearized optimization problem of (2.25) is an eigenfilter type problem [74, 56]. The simulation results presented in the next section show the merit of the proposed iterative eigenfilter method.

2.5 Simulation Results

To test the proposed iterative eigenfilter algorithm, the input process $x(n)$ was chosen to be a real WSS autoregressive process of order 4 (AR(4)) whose power spectrum $S_{xx}(e^{j\omega})$ is plotted in Fig. 2.3. For all of the simulation results presented here, we chose $M = 7$, i.e., the block size of the filter bank used was 7. Also, the matrix $\mathbf{B}$ from (2.30) was chosen to be $\mathbf{I}_L$ for all examples.

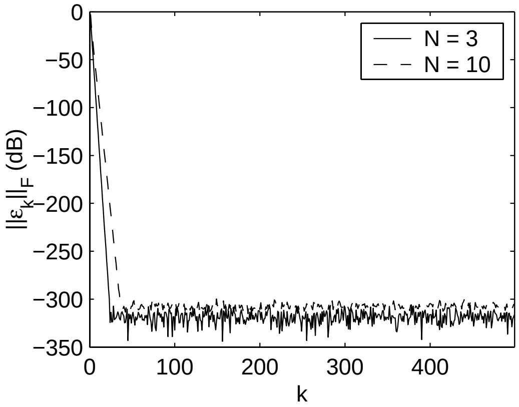

Figure 2.4: Orthonormality error $||\boldsymbol{\epsilon}_k||_F$ vs. the iteration index k $(L = 1,\, M = 7)$.

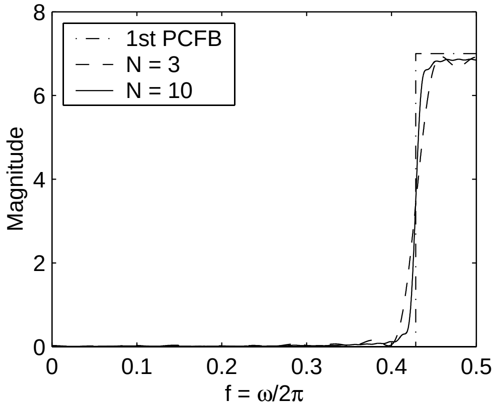

Figure 2.5: Magnitude squared responses of the designed FIR synthesis filter $F_0(z)$ along with the first filter of the infinite-order PCFB $(L = 1,\, M = 7)$.

We first considered the design of a single channel of the overdecimated system (i.e., $L = 1$). The observed error in orthonormality using the iterative eigenfilter method is shown in Fig. 2.4 in dB for two values of orders, namely, $N = 3$ and 10. In order to observe the behavior of our algorithm, we ran it for 500 iterations and opted not to choose a stopping threshold value δ_T from (2.27). As can be seen from Fig. 2.4, the proposed method indeed converged toward an orthonormal solution for both cases of filter orders. The error $||\boldsymbol{\epsilon}_k||_F$ saturated at around −300 dB for both cases, most likely due to quantization effects as a result of finite precision arithmetic.

To gauge the performance of the algorithm, a plot of the magnitude squared response of the resulting synthesis filter $F_0(z)$ from Fig. 2.2(a) is shown in Fig. 2.5 for the two orders $N = 3$ and 10, along with that of the first filter of the infinite-order PCFB. As can be seen, both FIR filters have a response close to that of the ideal compaction filter. Furthermore, the higher order filter offers a better approximation than the lower order one, in line with intuition.

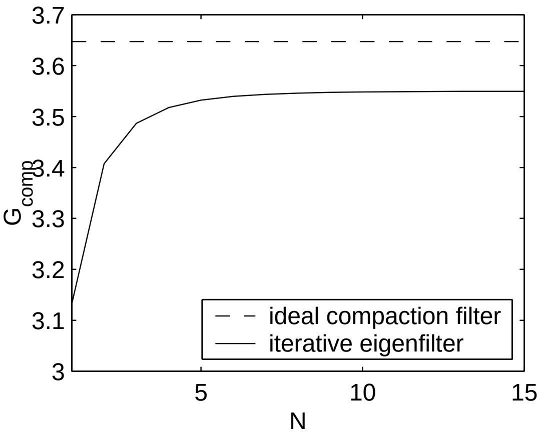

Figure 2.6: Compaction gain G_{comp} vs. the filter order parameter N.

To quantitatively measure the performance of the proposed iterative algorithm, we opted to calculate the *compaction gain* [68] of the designed filters, which is simply the subband variance σ_w^2 from (2.3) normalized by the average input power. Though this quantity has only previously been defined for the case in which the input $x(n)$ is WSS, we extend this definition here for the CWSS(M) case considered in Sec. 2.2 and 2.3. For this case, we define the compaction gain G_{comp} as follows.

$$G_{\text{comp}} \triangleq \frac{\sigma_w^2}{\frac{1}{M}\text{Tr}\left[\mathbf{R_{xx}}(0)\right]} \tag{2.31}$$

In the special case in which $x(n)$ is WSS, (2.31) becomes

$$G_{\text{comp}} = \frac{\sigma_w^2}{\sigma_x^2} = \frac{\dfrac{1}{2\pi}\displaystyle\int_0^{2\pi} S_{xx}(e^{j\omega})\left|F(e^{j\omega})\right|^2\,d\omega}{\dfrac{1}{2\pi}\displaystyle\int_0^{2\pi} S_{xx}(e^{j\omega})\,d\omega} \tag{2.32}$$

which is consistent with the definition given in [68]. The ideal compaction filter maximizes this quantity over all filters satisfying the required orthonormality condition of (2.8) [68]. A plot of the observed compaction gain as a function of the filter order parameter N is shown in Fig. 2.6. Though the compaction gain increases monotonically as N increases, it appears to saturate well below the ideal compaction gain. At this time, it is not known why this phenomenon occurs. Despite this, however, for small orders, the observed compaction gain is reasonably large.

To further test the algorithm, we then considered the design of two channels of the overdecimated system (i.e., $L = 2$) and fixed the order to be $N = 10$. The observed error in orthonormality (in dB) as a function of iteration is shown in Fig. 2.7. As before, it can be seen that the algorithm is converging to an orthonormal solution. The magnitude squared responses of the designed synthesis

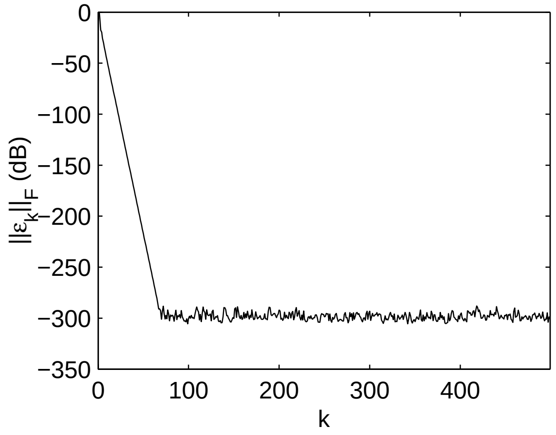

Figure 2.7: Orthonormality error $||\boldsymbol{\epsilon}_k||_F$ vs. the iteration index k ($L = 2$, $M = 7$, $N = 10$).

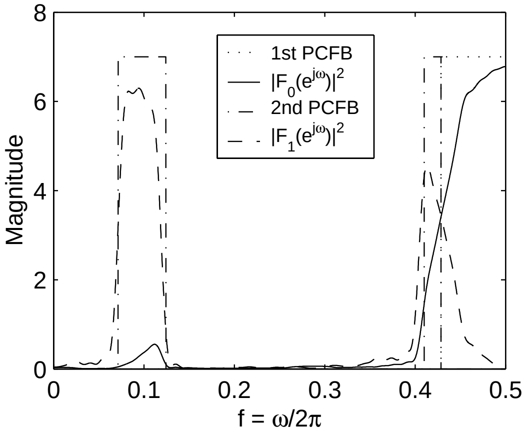

Figure 2.8: Magnitude squared responses of the designed FIR synthesis filters $F_0(z)$ and $F_1(z)$ along with the first two filters of the infinite-order PCFB ($L = 2$, $M = 7$, $N = 10$).

filters $F_0(z)$ and $F_1(z)$ are shown in Fig. 2.8 along with those of the first two filters of the infinite-order PCFB. From this, it is clear that the proposed algorithm is yielding filters close to the ideal compaction filters of the infinite-order PCFB, as desired.

2.6 Concluding Remarks

The iterative eigenfilter method for designing signal-adapted overdecimated filter banks for energy compaction was shown to yield filters similar to the optimal infinite-order compaction filters corresponding to the unconstrained order PCFB. Furthermore, as the eigenfilter approach is used at each iteration, the method is very low in computational complexity. Despite this, however, the iterative eigenfilter method is not without shortcomings. First of all, the method is not guaranteed to yield a PU or orthonormal solution. Though in all of the examples shown in Sec. 2.5, the algorithm converged to an orthonormal solution, there are many examples in which this is not the case. In addition to this, even if we have convergence, there is no guarantee that the resulting solution is optimal. This was best shown in Fig. 2.6, where the compaction gain was shown to saturate at a level well below that of the optimal compaction gain. Finally, the method only applies strictly for the overdecimated case in which the number of channels L satisfies $L < M$, where M is the decimation ratio. If we wish to obtain a maximally decimated system in which $L = M$, then the algorithm breaks down, since the subband variance $\sigma_{\mathbf{w}}^2$ from (2.12) becomes fixed in this case. As such, if we wish to obtain a good maximally decimated system from $L < M$ filters, we must *complete* the filter bank using some criterion to obtain the remaining $(M - L)$ filters.

With the iterative algorithms of Chapters 3 and 4, these problems no longer exist. Using the complete parameterization of FIR PU systems in terms of Householder-like degree-one building blocks [75, 67], the PU constraint is always satisfied as it is *structurally imposed.* Both methods are shown to saturate close to the performance of the infinite-order PCFB with filter order in terms of many objectives including compaction gain and coding gain. Finally, for the method of Chapter 3, a multiresolution criterion, for which the PCFB is optimal, is used to complete the filter bank given only the first compaction filter, whereas in Chapter 4, no filter bank completion is necessary as all of the filters are found *simultaneously.*

Appendix: Least-Squares Signal Model Approximation Problem

For the overdecimated filter bank system of Fig. 2.2(b) in which the orthonormality condition of (2.8) is satisfied, it turns out that the subband vector process $\mathbf{w}(n)$ is the *optimal driving signal* to the synthesis bank for minimizing the mean-squared error between the input $\mathbf{x}(n)$ and output $\mathbf{y}(n)$. This optimality holds not only for the system of Fig. 2.2, but also for a more general model that we will introduce below. We will prove this optimality first for the deterministic case and then for the stochastic case.

Consider the *rational nonuniform* overdecimated synthesis bank shown in Fig. 2.9. By overdecimated, we mean that

$$\sum_{k=0}^{P-1} \frac{m_k}{n_k} < 1$$

and so the inputs $\{c_k(n)\}$ operate at a lower overall rate than the output $y(n)$. As such, for fixed synthesis filters $\{F_k(z)\}$, we cannot *steer* the output $y(n)$ to be any signal which we desire.

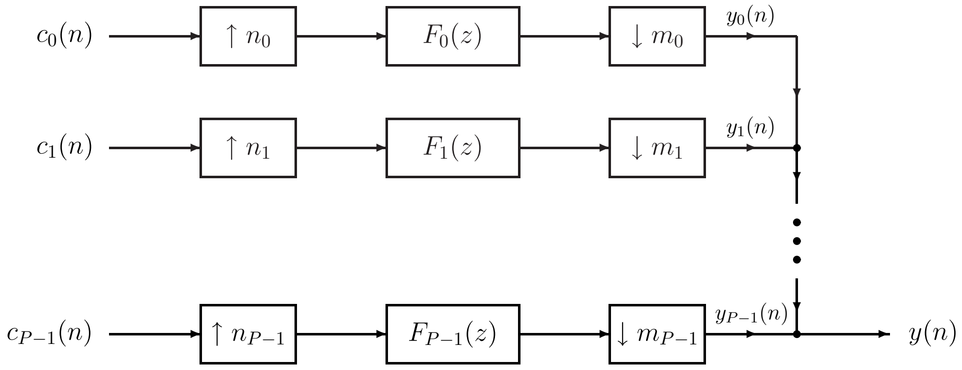

Figure 2.9: Rational nonuniform synthesis bank.

Mathematically, as the synthesis bank is overdecimated, the subspace of signals $\mathcal{V}$ generated by the model given by

$$\mathcal{V} \triangleq \left\{ y(n) : y(n) = \sum_{k=0}^{P-1} \sum_{m=-\infty}^{\infty} c_k(m) f_k(m_k n - n_k m) \,,\; c_k(n) \in \ell_2 \;\; \forall \;\; k \right\} \tag{2.33}$$

is a *proper* subspace of ℓ_2. The question then naturally arises as to how to choose the input driving signals $\{c_k(n)\}$ to minimize the mean-squared error between a desired signal $x(n)$ and the synthesis bank output $y(n)$. In this section, we address this problem first for the deterministic case and then for the stochastic case. This is a generalization of the results given in [77] for integer nonuniform filter banks for the deterministic case. Though rational nonuniform filter banks can be shown to be transformable to integer nonuniform filter banks [30], the approach here avoids this complicated transformation and solves the least-squares problem in a more direct way. Prior to proceeding, we present a few important results of multirate system theory which will be needed here.

Blocked Form of LTI Systems and Pseudocirculant Matrices

Two important multirate identities which will greatly facilitate the least-squares approximation problem we will consider here is the *decimator/expander cascade identity* shown in Fig. 2.10(a) and the *polyphase identity* shown in Fig. 2.10(b) [67]. The decimator/expander cascade identity allows us to interchange the order of decimation and expansion when the ratios are relatively prime, whereas the polyphase identity allows us to replace certain expander/filter/decimator cascades by an LTI system.

In certain cases, we will want to represent an LTI system using multirate building blocks. This can be done by using the *blocked form* of an LTI system. If $H(z)$ represents any LTI system, then it can be implemented in an M-fold blocked form [67] as shown in Fig. 2.11.

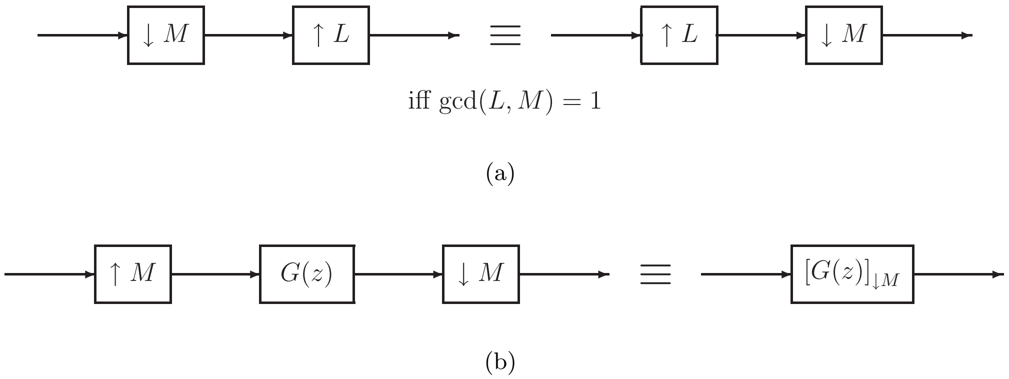

(a)

(b)

Figure 2.10: (a) Decimator/expander cascade identity, (b) Polyphase identity.

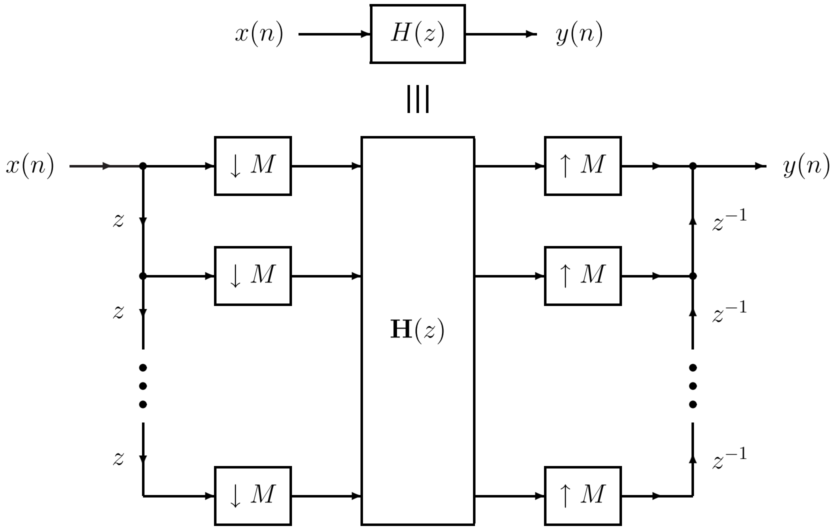

$$[\mathbf{H}(z)]_{k,\ell} = \left[z^{k-\ell}H(z)\right]_{\downarrow M}\ ,\ 0 \le k,\ell \le M-1$$

Figure 2.11: M-fold blocked form of an LTI system $H(z)$.

The matrix $\mathbf{H}(z)$ from Fig. 2.11 is said to be a *pseudocirculant* matrix [67], since it has a form similar to a circulant matrix [22]. To see this, suppose that $H(z)$ has the following M-fold Type I polyphase decomposition.

$$H(z) \quad = \quad \sum_{k=0}^{M-1} z^{-k} E_k\big(z^M\big) \quad \text{(Type I)}$$

Then, from Fig. 2.11, it can be shown that we have

$$\mathbf{H}(z) = \begin{bmatrix} E_0(z) & z^{-1}E_{M-1}(z) & z^{-1}E_{M-2}(z) & \cdots & z^{-1}E_1(z) \\ E_1(z) & E_0(z) & z^{-1}E_{M-1}(z) & \cdots & z^{-1}E_2(z) \\ E_2(z) & E_1(z) & E_0(z) & \ddots & \vdots \\ \vdots & \vdots & \vdots & \ddots & z^{-1}E_{M-1}(z) \\ E_{M-1}(z) & E_{M-2}(z) & E_{M-3}(z) & \cdots & E_0(z) \end{bmatrix}$$

which is simply a down circulant matrix [22] formed from $\{E_0(z), E_1(z), \ldots, E_{M-1}(z)\}$ with z^{-1} delays appearing above the main diagonal. Pseudocirculant matrices play a major role in the study of *alias-free* filter banks [67].

Together with the multirate identities of Fig. 2.10, the blocked form of LTI systems as shown in Fig. 2.11 will greatly facilitate solving the least-squares approximation problem as we now show.

Least-Squares Approximation Problem - Deterministic Case

Consider again the rational nonuniform synthesis bank of Fig. 2.9. We will make the following assumptions here.

- $\gcd(m_k, n_k) = 1 \ \ \forall\ k$ (Coprimeness of m_k and n_k)
- $\displaystyle\sum_{k=0}^{P-1} \frac{m_k}{n_k} < 1$ (Overdecimated system)

There is no loss of generality in making the first assumption, as common factors between m_k and n_k can be absorbed into the filter $F_k(z)$ by using the decimator/expander cascade identity along with the polyphase identity (see Fig. 2.10). The second assumption ensures that the subspace $\mathcal{V}$ in (2.33) is a proper subspace of ℓ_2. Let us define the following integers.

- $N \triangleq \mathrm{lcm}(n_0, n_1, \ldots, n_{P-1})$
- $p_k \triangleq \frac{N}{n_k} \ \ \forall\ k$
- $K \triangleq \displaystyle\sum_{k=0}^{P-1} m_k p_k$

Note that as the system is overdecimated, we have $K < N$.

The goal here is to choose the driving signals $\{c_k(n)\}$ to minimize the *deterministic* mean-squared error objective

$$\xi_{\text{det}} \triangleq \sum_n |x(n) - y(n)|^2$$

where $x(n)$ is any signal in ℓ_2. If $\mathbf{x}(n)$ and $\mathbf{y}(n)$ denote, respectively, the N-fold blocked versions of $x(n)$ and $y(n)$, we have

$$\xi_{\text{det}} = \sum_n ||\mathbf{x}(n) - \mathbf{y}(n)||^2 \tag{2.34}$$

Using Parseval's relation [67], ξ_{det} can be expressed as follows.

$$\xi_{\text{det}} = \frac{1}{2\pi} \int_0^{2\pi} \left|\left|\mathbf{X}(e^{j\omega}) - \mathbf{Y}(e^{j\omega})\right|\right|^2 d\omega \tag{2.35}$$

where $\mathbf{X}(z)$ and $\mathbf{Y}(z)$ denote, respectively, the z-transforms of $\mathbf{x}(n)$ and $\mathbf{y}(n)$.

To simplify $\mathbf{Y}(z)$, consider the k-th branch of the system of Figure 2.9 reproduced in Figure 2.12(a). If we implement $F_k(z)$ in an m_kN-fold block form (see Fig. 2.11), we obtain the system shown in Figure 2.12(b), where $\mathbf{A}_k(z)$ is an $m_kN \times m_kN$ pseudocirculant matrix [67] with

$$[\mathbf{A}_k(z)]_{r,s} = \left[z^{r-s}F_k(z)\right]_{\downarrow m_kN}$$

for $0 \leq r, s \leq m_kN - 1$. By applying the polyphase identity of Fig. 2.10(b), the expander on the left ($\uparrow n_k$) as well as the decimator on the right ($\downarrow m_k$) can be moved across the network resulting in the system of Figure 2.12(c). The $N \times m_kp_k$ transfer matrix $\mathbf{F}_k(z)$ is obtained by preserving only the N rows of $\mathbf{A}_k(z)$ which are multiples of m_k and the m_kp_k columns which are multiples of n_k. In other words,

$$[\mathbf{F}_k(z)]_{c,d} = \left[z^{cm_k - dn_k}F_k(z)\right]_{\downarrow m_kN} = \left[z^c\left[z^{-dn_k}F_k(z)\right]_{\downarrow m_k}\right]_{\downarrow N} \tag{2.36}$$

for $0 \leq c \leq N - 1$ and $0 \leq d \leq m_kp_k - 1$. Note that from Figure 2.12(c), $\mathbf{c}_k(n)$ is simply the m_kp_k-fold blocked version of $c_k(n)$ and $\mathbf{y}_k(n)$ is the N-fold blocked version of $y_k(n)$. Clearly, we have the following.

$$\mathbf{Y}_k(z) = \mathbf{F}_k(z)\mathbf{C}_k(z) \tag{2.37}$$

But note that we have

$$y(n) = \sum_{k=0}^{P-1} y_k(n) \Longleftrightarrow \mathbf{y}(n) = \sum_{k=0}^{P-1} \mathbf{y}_k(n)$$

Thus, using (2.37), we get

$$\mathbf{Y}(z) = \sum_{k=0}^{P-1} \mathbf{Y}_k(z) = \sum_{k=0}^{P-1} \mathbf{F}_k(z)\mathbf{C}_k(z)$$

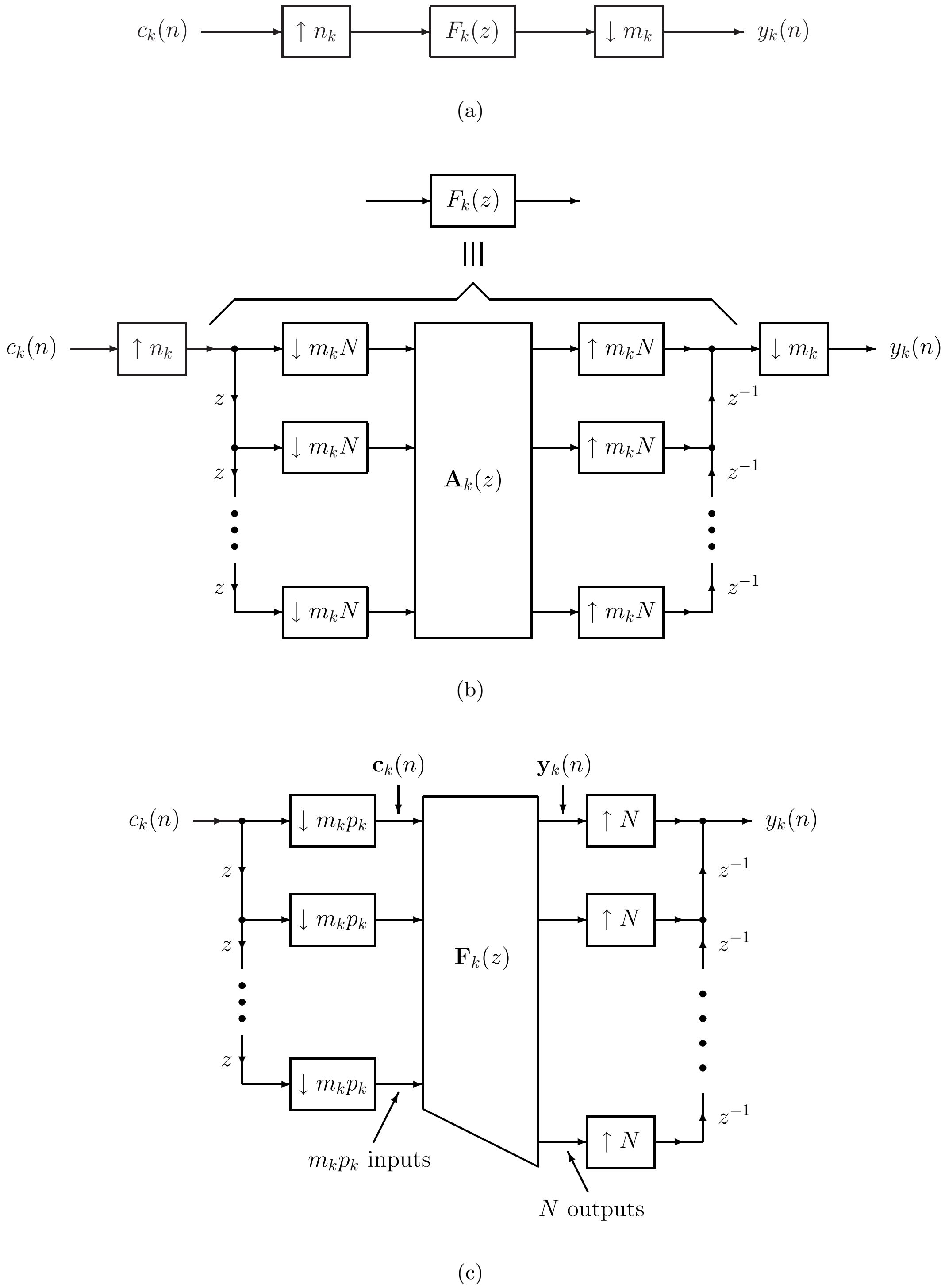

Figure 2.12: (a) The k-th branch of the signal model from Fig. 2.9, (b) With $F_k(z)$ implemented in an m_kN-fold block form, (c) Resulting structure after applying the polyphase identity.

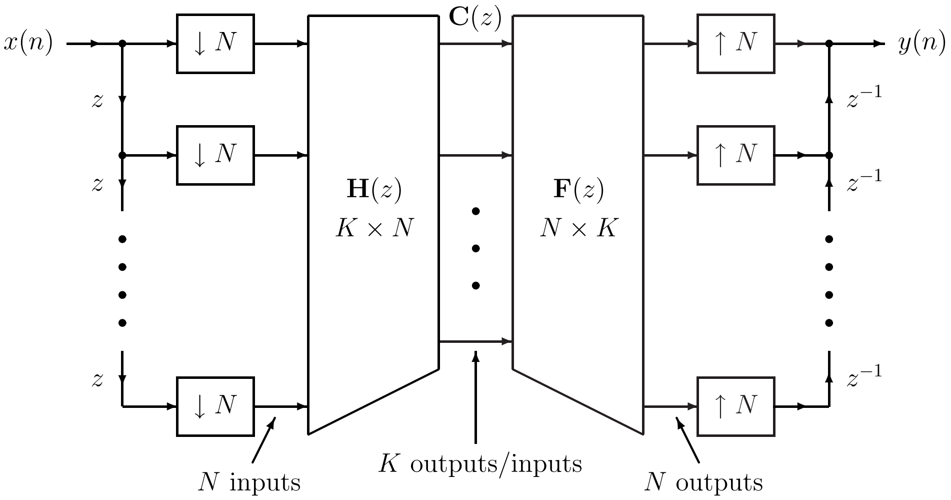

Figure 2.13: System for obtaining the optimal driving signal $\mathbf{C}(z)$.

This can be expressed as

$$\mathbf{Y}(z) = \underbrace{\begin{bmatrix} \mathbf{F}_0(z) & \mathbf{F}_1(z) & \cdots & \mathbf{F}_{P-1}(z) \end{bmatrix}}_{\mathbf{F}(z)} \underbrace{\begin{bmatrix} \mathbf{C}_0(z) \\ \mathbf{C}_1(z) \\ \vdots \\ \mathbf{C}_{P-1}(z) \end{bmatrix}}_{\mathbf{C}(z)} \tag{2.38}$$

where $\mathbf{F}(z)$ is an $N \times K$ matrix and $\mathbf{C}(z)$ is a $K \times 1$ vector. Note that even though the fixed matrix $\mathbf{F}(z)$ has a restricted structure as can be seen from (2.36), the vector $\mathbf{C}(z)$ is completely arbitrary.

Substituting (2.38) into (2.35), we have

$$\xi_{\text{det}} = \frac{1}{2\pi} \int_0^{2\pi} || \underbrace{\mathbf{F}(e^{j\omega})\mathbf{C}(e^{j\omega}) - \mathbf{X}(e^{j\omega})}_{\boldsymbol{\epsilon}(\omega)} ||^2 \, d\omega$$

and so we can minimize ξ_{det} by minimizing $||\boldsymbol{\epsilon}(\omega)||^2$ pointwise in ω. The solution to this well-known least-squares problem is [22]

$$\mathbf{C}(e^{j\omega}) = \mathbf{F}^{\#}(e^{j\omega})\mathbf{X}(e^{j\omega}) = \left[\mathbf{F}^{\dagger}(e^{j\omega})\mathbf{F}(e^{j\omega})\right]^{\#} \mathbf{F}^{\dagger}(e^{j\omega})\mathbf{X}(e^{j\omega})$$

where $\mathbf{A}^{\#}$ denotes the Moore-Penrose pseudoinverse of the matrix $\mathbf{A}$ [22].

In the z-domain, the optimum driving signal $\mathbf{C}(z)$ is given by

$$\boxed{\mathbf{C}(z) = \underbrace{\mathbf{F}^{\#}(z)}_{\mathbf{H}(z)}\mathbf{X}(z) = \underbrace{\left[\widetilde{\mathbf{F}}(z)\mathbf{F}(z)\right]^{\#} \widetilde{\mathbf{F}}(z)}_{\mathbf{H}(z)}\mathbf{X}(z)} \tag{2.39}$$

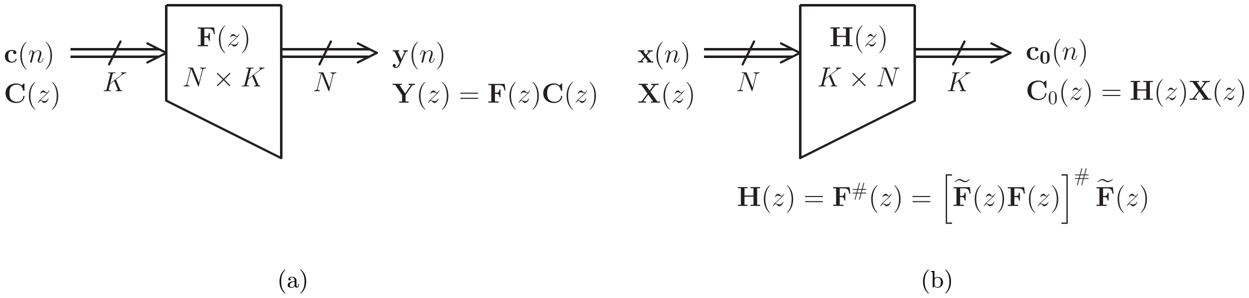
$\mathbf{c}(n)$
$\mathbf{C}(z)$
K
$\mathbf{F}(z)$
$N \times K$
N
$\mathbf{y}(n)$
$\mathbf{Y}(z) = \mathbf{F}(z)\mathbf{C}(z)$
(a)
$\mathbf{x}(n)$
$\mathbf{X}(z)$
N
$\mathbf{H}(z)$
$K \times N$
K
$\mathbf{c_0}(n)$
$\mathbf{C}_0(z) = \mathbf{H}(z)\mathbf{X}(z)$
$\mathbf{H}(z) = \mathbf{F}^{\#}(z) = \left[\widetilde{\mathbf{F}}(z)\mathbf{F}(z)\right]^{\#}\widetilde{\mathbf{F}}(z)$
(b)

Figure 2.14: (a) Equivalent form of Fig. 2.9 with blocking/unblocking elements removed, (b) Method for obtaining the optimal driving signal.

Hence, the optimal $\mathbf{C}(z)$ from (2.39) can be obtained via the system shown in Figure 2.13. In other words, the optimal driving signals to the overdecimated synthesis bank of Fig. 2.9 are the subbands corresponding to an appropriate overdecimated analysis bank as shown in Fig. 2.13. Here, the polyphase matrix $\mathbf{H}(z)$ corresponding to the analysis bank must be the pseudoinverse of the polyphase matrix $\mathbf{F}(z)$ corresponding to the synthesis bank.

Least-Squares Approximation Problem - Stochastic Case

Using several properties of multirate systems, we were able to show that the rational nonuniform overdecimated model of Fig. 2.9 could be equivalently redrawn as the LTI MIMO system model shown in Fig. 2.14(a) in which the blocking/unblocking mechanisms have been omitted for simplicity here. In the previous section, we showed that the optimal driving signal $\mathbf{c}_0(n)$ which minimized the *deterministic* mean-squared error

$$\xi_{\text{det}} = \sum_n ||\mathbf{x}(n) - \mathbf{y}(n)||^2$$

from (2.34) could be obtained by filtering $\mathbf{x}(n)$ as shown in Fig. 2.14(b). The question then naturally arises as to whether the same driving signal will be optimal for the *stochastic* case when we want to minimize the *expected* mean-squared error given by

$$\xi_{\text{sto}} \triangleq E\left[||\mathbf{x}(n) - \mathbf{y}(n)||^2\right] \tag{2.40}$$

where we assume here that the driving signal $\mathbf{c}(n)$ and desired signal $\mathbf{x}(n)$ are *jointly WSS* [67]. It turns out that the answer is in the affirmative, however the proof in this case is far different from the one given in the previous section for the deterministic case. In particular, we will show that the error obtained using the system of Fig. 2.14(b) is less than or equal to the error obtained for any other driving signal $\mathbf{c}(n)$.

To start, first note that since we assume $\mathbf{c}(n)$ and $\mathbf{x}(n)$ are jointly WSS, it follows that the vector

$$\mathbf{v}(n) \triangleq \begin{bmatrix} \mathbf{c}(n) \\ \mathbf{x}(n) \end{bmatrix}$$

is WSS [67]. Its psd $\mathbf{S_{vv}}(z)$ is given by

$$\mathbf{S_{vv}}(z) = \begin{bmatrix} \mathbf{S_{cc}}(z) & \mathbf{S_{cx}}(z) \\ \mathbf{S_{xc}}(z) & \mathbf{S_{xx}}(z) \end{bmatrix} \tag{2.41}$$

As $\mathbf{S_{vv}}(z)$ is a psd, it follows that it is *positive semidefinite* [22] on the unit circle $z = e^{j\omega}$, i.e., $\mathbf{w}^\dagger \mathbf{S_{vv}}(e^{j\omega})\mathbf{w} \geq 0$ for all ω and all nonzero vectors $\mathbf{w}$. This property will prove to be useful here.

To proceed, define the error signal to be $\mathbf{e}(n) \triangleq \mathbf{x}(n) - \mathbf{y}(n)$. As $\mathbf{Y}(z) = \mathbf{F}(z)\mathbf{C}(z)$ from Fig. 2.14(a), it follows that $\mathbf{c}(n)$ and $\mathbf{y}(n)$ are jointly WSS, which implies that $\mathbf{x}(n)$ and $\mathbf{y}(n)$ are also jointly WSS, which in turn implies that $\mathbf{e}(n)$ is WSS [67]. From (2.40), we have

$$\xi_{\text{sto}} = E\left[\mathbf{e}^\dagger(n)\mathbf{e}(n)\right] = \text{Tr}\left[E\left[\mathbf{e}(n)\mathbf{e}^\dagger(n)\right]\right] = \text{Tr}\left[\mathbf{R_{ee}}(0)\right] = \frac{1}{2\pi}\int_0^{2\pi} \text{Tr}\left[\mathbf{S_{ee}}(e^{j\omega})\right]\, d\omega \tag{2.42}$$

where $\mathbf{R_{ee}}(k)$ and $\mathbf{S_{ee}}(z)$ denote, respectively, the autocorrelation and psd of $\mathbf{e}(n)$. Also, using $\mathbf{e}(n) = \mathbf{x}(n) - \mathbf{y}(n)$, we have $\mathbf{S_{ee}}(z) = \mathbf{S_{xx}}(z) - \mathbf{S_{xy}}(z) - \mathbf{S_{yx}}(z) + \mathbf{S_{yy}}(z)$. As $\mathbf{Y}(z) = \mathbf{F}(z)\mathbf{C}(z)$, we have $\mathbf{S_{yy}}(z) = \mathbf{F}(z)\mathbf{S_{cc}}(z)\widetilde{\mathbf{F}}(z)$, $\mathbf{S_{yx}}(z) = \mathbf{F}(z)\mathbf{S_{cx}}(z)$, and $\mathbf{S_{xy}}(z) = \widetilde{\mathbf{S}}_{\mathbf{yx}}(z) = \mathbf{S_{xc}}(z)\widetilde{\mathbf{F}}(z)$ [67]. Hence, we have

$$\mathbf{S_{ee}}(z) = \mathbf{S_{xx}}(z) - \mathbf{S_{xc}}(z)\widetilde{\mathbf{F}}(z) - \mathbf{F}(z)\mathbf{S_{cx}}(z) + \mathbf{F}(z)\mathbf{S_{cc}}(z)\widetilde{\mathbf{F}}(z) \tag{2.43}$$

Now, let $\mathbf{S}_{\mathbf{e}_0\mathbf{e}_0}(z)$ denote the error psd obtained when the driving signal is obtained using the system of Fig. 2.14(b). Also, let $\xi_{\text{sto},0}$ denote the corresponding mean-squared error. Then, from (2.42), we have

$$\xi_{\text{sto},0} = \frac{1}{2\pi}\int_0^{2\pi} \text{Tr}\left[\mathbf{S}_{\mathbf{e}_0\mathbf{e}_0}(e^{j\omega})\right]\, d\omega$$

Hence, we get

$$\xi_{\text{sto}} - \xi_{\text{sto},0} = \frac{1}{2\pi}\int_0^{2\pi} \underbrace{\left\{\text{Tr}\left[\mathbf{S_{ee}}(e^{j\omega})\right] - \text{Tr}\left[\mathbf{S}_{\mathbf{e}_0\mathbf{e}_0}(e^{j\omega})\right]\right\}}_{D(e^{j\omega})}\, d\omega \tag{2.44}$$

Note that from Fig. 2.14(b), we have

$$\mathbf{S}_{\mathbf{e}_0\mathbf{e}_0}(z) = \mathbf{S_{xx}}(z) - \mathbf{S_{xx}}(z)\widetilde{\mathbf{H}}(z)\widetilde{\mathbf{F}}(z) - \mathbf{F}(z)\mathbf{H}(z)\mathbf{S_{xx}}(z) + \mathbf{F}(z)\mathbf{H}(z)\mathbf{S_{xx}}(z)\widetilde{\mathbf{H}}(z)\widetilde{\mathbf{F}}(z) \tag{2.45}$$

Using the following properties of the pseudoinverse [22],

$$\mathbf{A}^{\#}\mathbf{A} = \left(\mathbf{A}^{\#}\mathbf{A}\right)^{\dagger}\ ,\ \mathbf{A}\mathbf{A}^{\#} = \left(\mathbf{A}\mathbf{A}^{\#}\right)^{\dagger} \quad \text{(Hermitian Product Properties)} \tag{2.46}$$

$$\mathbf{A}^{\#}\mathbf{A}\mathbf{A}^{\#} = \mathbf{A}^{\#}\ ,\ \mathbf{A}\mathbf{A}^{\#}\mathbf{A} = \mathbf{A} \quad \text{(Projection Properties)} \tag{2.47}$$

as well as the fact that $\mathrm{Tr}\left[\mathbf{AB}\right] = \mathrm{Tr}\left[\mathbf{BA}\right]$ whenever $\mathbf{A}$ and $\mathbf{B}$ are conformable [22], from (2.45), we get the following.

$$\mathrm{Tr}\left[\mathbf{S}_{\mathbf{e}_0\mathbf{e}_0}(z)\right] = \mathrm{Tr}\left[\mathbf{S}_{\mathbf{xx}}(z)\right] - \mathrm{Tr}\left[\mathbf{F}(z)\mathbf{H}(z)\mathbf{S}_{\mathbf{xx}}(z)\widetilde{\mathbf{H}}(z)\widetilde{\mathbf{F}}(z)\right]$$

Thus, from (2.43) and (2.44), we get

$$\begin{aligned} D(z) &= \mathrm{Tr}\left[\mathbf{S}_{\mathbf{ee}}(z)\right] - \mathrm{Tr}\left[\mathbf{S}_{\mathbf{e}_0\mathbf{e}_0}(z)\right] \\ &= \mathrm{Tr}\left[\mathbf{F}(z)\mathbf{S}_{\mathbf{cc}}(z)\widetilde{\mathbf{F}}(z)\right] - \mathrm{Tr}\left[\mathbf{F}(z)\mathbf{S}_{\mathbf{cx}}(z)\right] - \mathrm{Tr}\left[\mathbf{S}_{\mathbf{xc}}(z)\widetilde{\mathbf{F}}(z)\right] \\ &\quad + \mathrm{Tr}\left[\mathbf{F}(z)\mathbf{H}(z)\mathbf{S}_{\mathbf{xx}}(z)\widetilde{\mathbf{H}}(z)\widetilde{\mathbf{F}}(z)\right] \end{aligned} \tag{2.48}$$

Using (2.47), we have

$$\mathbf{F}(z)\mathbf{S}_{\mathbf{cx}}(z) = \mathbf{F}(z)\mathbf{H}(z)\mathbf{F}(z)\mathbf{S}_{\mathbf{cx}}(z)$$

Then, using (2.46), we get

$$\mathrm{Tr}\left[\mathbf{F}(z)\mathbf{S}_{\mathbf{cx}}(z)\right] = \mathrm{Tr}\left[\mathbf{F}(z)\mathbf{S}_{\mathbf{cx}}(z)\mathbf{F}(z)\mathbf{H}(z)\right] = \mathrm{Tr}\left[\mathbf{F}(z)\mathbf{S}_{\mathbf{cx}}(z)\widetilde{\mathbf{H}}(z)\widetilde{\mathbf{F}}(z)\right] \tag{2.49}$$

Similarly, we have

$$\mathbf{S}_{\mathbf{xc}}(z)\widetilde{\mathbf{F}}(z) = \mathbf{S}_{\mathbf{xc}}(z)\widetilde{\mathbf{F}}(z)\widetilde{\mathbf{H}}(z)\widetilde{\mathbf{F}}(z) = \mathbf{S}_{\mathbf{xc}}(z)\widetilde{\mathbf{F}}(z)\mathbf{F}(z)\mathbf{H}(z)$$

and hence, we get

$$\mathrm{Tr}\left[\mathbf{S}_{\mathbf{xc}}(z)\widetilde{\mathbf{F}}(z)\right] = \mathrm{Tr}\left[\mathbf{F}(z)\mathbf{H}(z)\mathbf{S}_{\mathbf{xc}}(z)\widetilde{\mathbf{F}}(z)\right] \tag{2.50}$$

Combining (2.49) and (2.50) in (2.48), we get

$$\begin{aligned} D(z) &= \mathrm{Tr}\Big[\mathbf{F}(z)\mathbf{S}_{\mathbf{cc}}(z)\widetilde{\mathbf{F}}(z) - \mathbf{F}(z)\mathbf{S}_{\mathbf{cx}}(z)\widetilde{\mathbf{H}}(z)\widetilde{\mathbf{F}}(z) \\ &\quad -\mathbf{F}(z)\mathbf{H}(z)\mathbf{S}_{\mathbf{xc}}(z)\widetilde{\mathbf{F}}(z) + \mathbf{F}(z)\mathbf{H}(z)\mathbf{S}_{\mathbf{xx}}(z)\widetilde{\mathbf{H}}(z)\widetilde{\mathbf{F}}(z)\Big] \\ &= \mathrm{Tr}\left[\mathbf{F}(z)\left(\mathbf{S}_{\mathbf{cc}}(z) - \mathbf{S}_{\mathbf{cx}}(z)\widetilde{\mathbf{H}}(z) - \mathbf{H}(z)\mathbf{S}_{\mathbf{xc}}(z) + \mathbf{H}(z)\mathbf{S}_{\mathbf{xx}}(z)\widetilde{\mathbf{H}}(z)\right)\widetilde{\mathbf{F}}(z)\right] \end{aligned}$$

Note that from (2.41), we can express $D(z)$ as follows.

$$D(z) = \mathrm{Tr}\left[\ \mathbf{F}(z)\underbrace{\begin{bmatrix} \mathbf{I}_K & -\mathbf{H}(z) \end{bmatrix}}_{\mathbf{G}(z)}\underbrace{\begin{bmatrix} \mathbf{S}_{\mathbf{cc}}(z) & \mathbf{S}_{\mathbf{cx}}(z) \\ \mathbf{S}_{\mathbf{xc}}(z) & \mathbf{S}_{\mathbf{xx}}(z) \end{bmatrix}}_{\mathbf{S}_{\mathbf{vv}}(z)}\underbrace{\begin{bmatrix} \mathbf{I}_K \\ -\widetilde{\mathbf{H}}(z) \end{bmatrix}}_{\widetilde{\mathbf{G}}(z)}\widetilde{\mathbf{F}}(z)\ \right] \tag{2.51}$$

But recall that $\mathbf{S}_{\mathbf{vv}}(e^{j\omega})$ is positive semidefinite as it is the psd of $\mathbf{v}(n)$. Thus, from (2.51), we have

$$D(z) = \mathrm{Tr}\left[\,\underbrace{\mathbf{F}(z)\mathbf{G}(z)\mathbf{S}_{\mathbf{vv}}(z)\widetilde{\mathbf{G}}(z)\widetilde{\mathbf{F}}(z)}_{\text{positive semidefinite on } z = e^{j\omega}}\,\right]$$

As the trace of any positive semidefinite matrix is nonnegative [22], $D(e^{j\omega}) \geq 0$. From (2.44), this implies

$$\xi_{\text{sto}} - \xi_{\text{sto},0} = \frac{1}{2\pi}\int_0^{2\pi} D(e^{j\omega})\,d\omega \geq 0 \Longleftrightarrow \xi_{\text{sto},0} \leq \xi_{\text{sto}}$$

Hence, the error obtained using the system of Fig. 2.14(b) is always less than or equal to the error obtained with any other driving signal. Thus, the driving signal $\mathbf{c}_0(n)$ from Fig. 2.14(b) is always an optimal driving signal and so the optimal driving signal in the deterministic case is also an optimal driving signal in the stochastic case. $\bigtriangledown\bigtriangledown\bigtriangledown$

In parting, the following comments are in order. If the synthesis polyphase matrix $\mathbf{F}(z)$ is PU, i.e., $\widetilde{\mathbf{F}}(z)\mathbf{F}(z) = \mathbf{I}_K$, then the optimal analysis bank $\mathbf{H}(z) = \mathbf{F}^{\#}(z) = \left[\widetilde{\mathbf{F}}(z)\mathbf{F}(z)\right]^{\#}\widetilde{\mathbf{F}}(z)$ is simply $\mathbf{H}(z) = \widetilde{\mathbf{F}}(z)$, i.e., $\mathbf{H}(z)$ is the *paraconjugate* of $\mathbf{F}(z)$. In this case, the resulting filter bank system is *orthonormal.* The uniform PU filter bank of Fig. 2.2 is an example of such a filter bank.

In addition to this, with the optimal driving signal $\mathbf{c}(n)$, it can easily be shown that if $\mathbf{F}(z)$ is PU, then minimizing the mean-squared error further by choice of $\mathbf{F}(z)$ is equivalent to *compacting the energy* of $\mathbf{c}(n)$. To see this, note that with the optimal $\mathbf{C}(z)$ from (2.39), the mean-squared error in the deterministic and stochastic cases are respectively given by (2.34) and (2.40) to be

$$\begin{aligned}
\xi_{\text{det}} &= \sum_n |x(n)|^2 - \underbrace{\mathrm{Tr}\left[\frac{1}{2\pi}\int_0^{2\pi}\mathbf{H}(e^{j\omega})\mathbf{X}(e^{j\omega})\mathbf{X}^\dagger(e^{j\omega})\mathbf{F}(e^{j\omega})\,d\omega\right]}_{\sigma^2_{\mathbf{c},\text{det}}} \\
\xi_{\text{sto}} &= \mathrm{Tr}\left[\mathbf{R}_{\mathbf{xx}}(0)\right] - \underbrace{\mathrm{Tr}\left[\frac{1}{2\pi}\int_0^{2\pi}\mathbf{H}(e^{j\omega})\mathbf{S}_{\mathbf{xx}}(e^{j\omega})\mathbf{F}(e^{j\omega})\,d\omega\right]}_{\sigma^2_{\mathbf{c},\text{sto}}}
\end{aligned}$$

where $\mathbf{H}(z) = \mathbf{F}^{\#}(z)$. Clearly, minimizing ξ_{det} and ξ_{sto} is equivalent to *maximizing* $\sigma^2_{\mathbf{c},\text{det}}$ and $\sigma^2_{\mathbf{c},\text{sto}}$, respectively. If $\mathbf{F}(z)$ is PU, then $\mathbf{H}(z) = \widetilde{\mathbf{F}}(z)$ or equivalently $\mathbf{F}(z) = \widetilde{\mathbf{H}}(z)$. In this case, we get

$$\begin{aligned}
\sigma^2_{\mathbf{c},\text{det}} &= \mathrm{Tr}\left[\frac{1}{2\pi}\int_0^{2\pi}\mathbf{H}(e^{j\omega})\mathbf{X}(e^{j\omega})\mathbf{X}^\dagger(e^{j\omega})\mathbf{H}^\dagger(e^{j\omega})\,d\omega\right] \\
\sigma^2_{\mathbf{c},\text{det}} &= \mathrm{Tr}\left[\frac{1}{2\pi}\int_0^{2\pi}\mathbf{H}(e^{j\omega})\mathbf{S}_{\mathbf{xx}}(e^{j\omega})\mathbf{H}^\dagger(e^{j\omega})\,d\omega\right]
\end{aligned}$$

which is simply the *energy* of the optimal driving signal from Fig. 2.14(b) for the deterministic and stochastic cases, respectively. Hence, with the PU constraint in effect, minimizing the mean-squared error is equivalent to *compacting the energy* of the subband vector process, as was shown for the uniform case in Sec. 2.3.1.

Chapter 3

Multiresolution Optimal FIR PU Filter Banks

One major drawback of the iterative eigenfilter method of the previous chapter is that there is no guarantee of convergence to a PU solution for the synthesis bank. In this chapter, an alternate method for designing a compaction filter is proposed in which the PU constraint is *structurally imposed*. This follows from the *complete parameterization* of all 1-D causal FIR PU systems in terms of Householder-like degree-one building blocks [75, 67], which we review here.

Using this characterization, an iterative algorithm is proposed to approximate, in the least-squares sense, any desired response by an FIR filter whose vector of polyphase components is PU. At each iteration, one set of parameters in the characterization of the FIR PU system is *globally* optimized assuming all other parameters to be fixed. As such, the resulting algorithm is *greedy* and so the error is *guaranteed* to be monotonic nonincreasing with iteration.

When the desired response is the response of an optimal infinite-order compaction filter, the algorithm can be used for the design of FIR compaction filters. As the desired response in this case suffers from a *phase ambiguity*, which we show here, a modification to the algorithm is proposed in which the phase of the FIR solution is *fed back* to the desired response. With this modification, which we call the *phase feedback modification*, in effect, the iterative algorithm not only still remains greedy, but also outperforms the unmodified one in terms of compaction gain. In simulations provided, we show that when this modification is used, the compaction gain *monotonically increases* with filter order and comes very close to the performance of the infinite-order compaction filter.

To complete a maximally decimated filter bank given an FIR compaction filter, a *multiresolution* criterion [62, 37] for which the PCFB is optimal, is used. Using the above-mentioned characterization of FIR PU systems, it can be shown that the entire filter bank can be elegantly designed with only one FIR compaction filter followed by an appropriate KLT, as we review here. Though elegant, this approach suffers from the *nonuniqueness* of the FIR compaction filter. Different spectral factors of a given FIR compaction filter lead to different FIR PU filter banks which in turn yield different performances in terms of certain objective functions. This phenomenon has not previously been reported in the literature. By choosing the spectral factor which yields the largest coding gain, in simulations, we show that as the filter order increases, the resulting FIR PU filter bank behaves more and more like the unconstrained or infinite-order PCFB in terms of numerous objectives. In particular, this behavior is shown for coding gain, multiresolution, denoising with zeroth-order Wiener filters in the subbands, and power minimization in nonredundant PU transmultiplexers. This serves to *bridge the gap* between the zeroth-order memory KLT and infinite-order PCFB, which has not previously been reported in the literature.

Since all spectral factors of a given FIR compaction filter must be tested for performance, the computational complexity grows *exponentially* with filter order. As such, designing FIR PU filter banks using the multiresolution criterion of [62, 37] becomes less feasible as the filter order increases. In essence, what we show here is that due to the inherent nonuniqueness of an FIR compaction filter, the FIR compaction filter problem, though elegant and well studied, is *not* well suited for the design of complete signal-adapted FIR PU filter banks. This previously has not been reported in the literature.

The content of this chapter is mainly drawn from [49] and portions of it will been presented at [59].

3.1 Outline

In Sec. 3.2, we review the complete parameterization of 1-D causal FIR PU systems in terms of Householder-like degree-one building blocks. There, the conditions under which the factorization is unique are mentioned, which will be pivotal for designing FIR PU filter banks using only the FIR compaction filter.

With this characterization, in Sec. 3.3, we proceed to the problem of least-squares design of FIR filters whose vector of polyphase components is PU. Such filters have the property that their magnitude squared response satisfies a *Nyquist* condition [67] and hence they are referred to as *magnitude squared Nyquist filters.* The optimal parameters of these filters are derived in Sec. 3.3.1 using the method of Lagrange multipliers. In Sec. 3.3.2, the iterative algorithm for solving the least-squares problem is presented and shown to be *greedy*. Simulation results for the design of FIR compaction filters are shown in Sec. 3.3.3. There, the problems due to the phase ambiguity of the desired infinite-order compaction filter are shown.

The *phase feedback modification*, which we propose to mitigate the effects of phase ambiguity, is introduced in Sec. 3.4. There, it is shown that the iterative algorithm still remains greedy with this modification in effect. Simulations using the phase feedback modification are also provided in Sec. 3.4. It is shown that with the modification in effect, we obtain a *monotonic* increase in compaction gain with filter order which comes very close to the performance of the ideal infinite-order compaction filter, in line with intuition.

In Sec. 3.5, we review the *multiresolution optimality criterion* (MOC) [62, 37] for completing a maximally decimated FIR PU filter bank. This criterion is well suited for the design of signal-adapted filter banks since the PCFB, if it exists, is optimal for this criterion. Using the complete parameterization of FIR PU systems from Sec. 3.2, in Sec. 3.5.1, we show that with this criterion, the entire filter bank can be obtained from a single FIR compaction filter using an appropriate KLT.

In Sec. 3.6, we present simulation results for FIR PU filter banks designed using the MOC. There, the problems associated with the inherent nonuniqueness of the FIR compaction filter become apparent. Different spectral factors lead to different filter banks which in turn lead to different performances. By choosing the spectral factor yielding the largest coding gain, we show that the FIR PU filter banks designed behave more and more like the infinite-order PCFB as the filter order increases. This PCFB-like monotonic behavior is shown in terms of several objectives such as coding gain, multiresolution, denoising with zeroth-order Wiener filters in the subbands, and power minimization for nonredundant PU transmultiplexers. The work here serves to *bridge the gap* between the zeroth-order memory KLT and infinite-order PCFB which previously has not been shown in the literature.

Finally, concluding remarks are made in Sec. 3.7. There, we discuss the merits and shortcomings of the iterative algorithm and MOC for designing FIR PU signal-adapted filter banks.

3.2 Complete Parameterization of 1-D Causal FIR PU Systems

Suppose that $\mathbf{A}(z)$ is a $p \times r$ causal FIR transfer function with $p \geq r$. Then $\mathbf{A}(z)$ is PU with *McMillan degree* $(N-1)$ iff it can be expressed as [75, 67]

$$\mathbf{A}(z) = \mathbf{W}_{N-1}(z)\mathbf{W}_{N-2}(z)\cdots\mathbf{W}_1(z)\mathbf{A}_0 \tag{3.1}$$

where $\mathbf{A}_0$ is a unitary $p \times r$ matrix, i.e., $\mathbf{A}_0^\dagger\mathbf{A}_0 = \mathbf{I}_r$, and $\mathbf{W}_k(z)$ is a $p \times p$ Householder-like PU degree-one building block of the form

$$\mathbf{W}_k(z) = \mathbf{I}_p - \mathbf{w}_k\mathbf{w}_k^\dagger + z^{-1}\mathbf{w}_k\mathbf{w}_k^\dagger\,,\ 1 \leq k \leq N-1 \tag{3.2}$$

and $\mathbf{w}_k$ is a $p \times 1$ unit norm vector for all k.

In general, the matrix $\mathbf{A}_0$ from (3.1) is *unique* [67]. When $r > 1$, the vectors $\mathbf{w}_k$ from (3.2) are in general *not unique*. In contrast to this, when $r = 1$, i.e., when $\mathbf{A}(z)$ is a vector transfer function, the vectors $\mathbf{w}_k$ are unique upto a scale factor of unit magnitude and hence the diadic terms $\mathbf{w}_k\mathbf{w}_k^\dagger$ appearing in (3.2) are *unique*. This uniqueness in the vector case, as will be shown in Sec. 3.5.1, greatly facilitates the design of multiresolution optimal FIR PU filter banks once a suitable compaction filter has been designed.

It should be noted that the factorization of (3.1) is only complete for the one-dimensional case where z is a single complex variable. For D-dimensional FIR PU systems of the form $\mathbf{A}(\mathbf{z})$, where $\mathbf{z}$ is a D-dimensional vector of complex variables, an analogous parameterization to that given in (3.1) is in general *not complete*. The reason for this is that when $D > 1$, the notion of factoring polynomials into roots no longer exists.

We will now proceed to use the factorization of (3.1) for the least-squares design of a causal FIR *magnitude squared Nyquist filter* [67], for which the vector of polyphase components is a causal FIR PU system. As the ultimate goal here will be the design of an FIR compaction filter $F(z)$ for the M-channel maximally decimated filter bank of Fig. 1.13, we will require the orthonormality condition of (2.1) to be satisfied. In other words, we will consider the design of a causal FIR magnitude squared Nyquist(M) filter whose vector of M-fold polyphase components is equivalently a causal FIR PU system.

3.3 Least-Squares Design of FIR Magnitude Squared Nyquist Filters

The design problem we focus on here is as follows. Suppose that $D(e^{j\omega})$ is a desired response that we wish to approximate (in the least-squares sense) with a causal FIR filter $F(e^{j\omega})$ of length MN whose magnitude squared response is Nyquist(M) [67]. For example, $D(e^{j\omega})$ may represent the spectrum of an infinite-order compaction filter. (In the case where the input $x(n)$ to the system of Fig. 2.1 is WSS, then $D(e^{j\omega})$ would represent any spectral factor of the magnitude squared response given in (2.6).) Then, the problem is to minimize the mean-squared error ξ, defined to be

$$\xi \triangleq \frac{1}{2\pi}\int_0^{2\pi} \left|D(e^{j\omega}) - F(e^{j\omega})\right|^2 d\omega \tag{3.3}$$

subject to an FIR constraint on $F(e^{j\omega})$ and the magnitude squared Nyquist(M) constraint [67]

$$\left[\left|F(e^{j\omega})\right|^2\right]_{\downarrow M} = 1 \tag{3.4}$$

Expanding ξ from (3.3) yields

$$\xi = \frac{1}{2\pi}\int_0^{2\pi} \left|D(e^{j\omega})\right|^2 d\omega + \frac{1}{2\pi}\int_0^{2\pi} \left|F(e^{j\omega})\right|^2 d\omega - \frac{1}{2\pi}\int_0^{2\pi} \left(D^*(e^{j\omega})F(e^{j\omega}) + F^*(e^{j\omega})D(e^{j\omega})\right) d\omega \tag{3.5}$$

The first term of the right-hand side of (3.5) is just the ℓ_2 norm squared of the desired impulse response $d(n)$, namely, $||d(n)||_2^2$. Using (3.4), it can be shown that the second term is simply unity [67]. Hence, the only quantities in ξ depending on $F(z)$ are the cross product terms from the third term in (3.5). Thus, the problem is linear in $f(n)$, which greatly simplifies the optimization problem.

In order for $F(z)$ to be a nondegenerate causal FIR filter of length MN which satisfies the magnitude squared Nyquist(M) constraint of (2.1), the $M \times 1$ vector of Type I M-fold polyphase components of $F(z)$, namely, $\mathbf{f}(z)$ from Section 2.2, must be a causal FIR PU vector system with McMillan degree $(N-1)$ [75, 67]. From the results of Sec. 3.2, it follows that we have

$$F(z) = \widetilde{\mathbf{a}}(z)\mathbf{f}\left(z^M\right) \ , \ \text{where } \mathbf{f}(z) = \mathbf{V}(z)\mathbf{u}_0 \tag{3.6}$$

Here $\mathbf{a}(z)$ is the $M \times 1$ advance chain vector given by

$$\mathbf{a}(z) = \left[\begin{array}{cccc} 1 & z & \cdots & z^{M-1} \end{array}\right]^T$$

Also, the quantity $\mathbf{V}(z)$ is an $M \times M$ lossless matrix consisting of $(N-1)$ Householder-like paraunitary degree-one building blocks of the form

$$\mathbf{V}(z) = \prod_{i=N-1}^{1} \mathbf{V}_i(z) \tag{3.7}$$

$$\mathbf{V}_i(z) = \mathbf{I} - \mathbf{v}_i\mathbf{v}_i^\dagger + z^{-1}\mathbf{v}_i\mathbf{v}_i^\dagger\,,\ 1 \leq i \leq N-1 \tag{3.8}$$

where the $M \times 1$ vectors $\mathbf{v}_i$ are unit norm vectors. Finally, the quantity $\mathbf{u}_0$ is some $M \times 1$ unit norm vector.

As can be seen, $F(z)$ in this case is completely characterized by the unit norm vectors $\mathbf{v}_i$ and $\mathbf{u}_0$. Though it is difficult to jointly find the vectors $\mathbf{v}_i$ and $\mathbf{u}_0$ which minimize ξ from (3.3), it will be shown that given the rest of the vectors, optimizing only one vector at a time is very simple. This will serve as the basis for our proposed iterative technique. Prior to proceeding, let us define $\mathcal{V}$ to be the set of all $\mathbf{v}_i$s, i.e., $\mathcal{V} \triangleq \{\mathbf{v}_i : 1 \leq i \leq N-1\}$, and, in accordance with standard set theoretic notation, let $\mathcal{V} \setminus \mathbf{v}_k$ denote the set $\mathcal{V}$ with the element $\mathbf{v}_k$ removed.

3.3.1 Solving the Least-Squares Optimization Problem Using the Method of Lagrange Multipliers

In order to minimize ξ from (3.5) subject to the unit norm constraints on $\mathbf{u}_0$ and the $\mathbf{v}_i$s, we construct the *Lagrangian* objective function [48]

$$J(\mathbf{u}_0, \mathcal{V}) \triangleq \xi(\mathbf{u}_0, \mathcal{V}) + \lambda_0\left(1 - \mathbf{u}_0^\dagger\mathbf{u}_0\right) + \sum_{i=1}^{N-1}\lambda_i\left(1 - \mathbf{v}_i^\dagger\mathbf{v}_i\right) \tag{3.9}$$

where the λ_is are *Lagrange multipliers* chosen to satisfy the unit norm constraints. In what follows, we consider the problem of optimizing one vector at a time, assuming that the rest of the vectors are fixed.

3.3.1.1 Optimal Choice of $\mathbf{u}_0$

To find the optimal choice of $\mathbf{u}_0$, we set the conjugate gradient of $J(\mathbf{u}_0, \mathcal{V})$ with respect to $\mathbf{u}_0$ to be the zero vector [48]. From (3.9), we have [48]

$$\nabla_{\mathbf{u}_0^\dagger} J = \nabla_{\mathbf{u}_0^\dagger}\xi - \lambda_0\mathbf{u}_0 = \mathbf{0} \tag{3.10}$$

Here, the notation $\nabla_{\mathbf{x}^\dagger} f$ denotes a $p \times 1$ column vector whose k-th component is given by

$$[\nabla_{\mathbf{x}^\dagger} f]_k \triangleq \frac{\partial f}{\partial\left[[\mathbf{x}]_k^*\right]}$$

where $\mathbf{x}$ is a $p \times 1$ column vector. Using (3.6) in (3.5) yields

$$\xi(\mathbf{u}_0, \mathcal{V}) = ||d(n)||_2^2 + 1 - \mathbf{b}^\dagger(\mathcal{V})\mathbf{u}_0 - \mathbf{u}_0^\dagger\mathbf{b}(\mathcal{V}) \tag{3.11}$$

where $\mathbf{b}(\mathcal{V})$ is the $M \times 1$ vector

$$\mathbf{b}(\mathcal{V}) \triangleq \frac{1}{2\pi}\int_0^{2\pi} \mathbf{V}^\dagger\left(e^{j\omega M}\right)\mathbf{a}(e^{j\omega})D(e^{j\omega})\,d\omega \tag{3.12}$$

Differentiating ξ from (3.11) with respect to $\mathbf{u}_0^\dagger$ yields [48]

$$\nabla_{\mathbf{u}_0^\dagger}\xi = -\mathbf{b}(\mathcal{V})$$

Substituting this into (3.10) yields the optimal choice of $\mathbf{u}_0$ given by $\mathbf{u}_0 = -\frac{1}{\lambda_0}\mathbf{b}(\mathcal{V})$. In order to satisfy the unit norm constraint $\mathbf{u}_0^\dagger\mathbf{u}_0 = 1$, it follows that the optimal $\mathbf{u}_0$ is of the form

$$\mathbf{u}_0 = e^{j\alpha}\left(\frac{\mathbf{b}(\mathcal{V})}{||\mathbf{b}(\mathcal{V})||}\right) \tag{3.13}$$

where $\alpha \in [0, 2\pi)$ is some phase factor. To find the optimal choice of α here, we substitute (3.13) into (3.11). This yields

$$\xi = ||d(n)||_2^2 + 1 - 2\,||\mathbf{b}(\mathcal{V})||\cos\alpha$$

Clearly, to minimize ξ, we must maximize the third term, which occurs when we choose $\alpha = 0$. Hence, the optimal choice of $\mathbf{u}_0$ and corresponding ξ are given by the following.

$$\boxed{\mathbf{u}_{0,\text{opt}} = \frac{\mathbf{b}(\mathcal{V})}{||\mathbf{b}(\mathcal{V})||}\,,\ \xi_{\text{opt}} = ||d(n)||_2^2 + 1 - 2\,||\mathbf{b}(\mathcal{V})||} \tag{3.14}$$

3.3.1.2 Optimal Choice of $\mathbf{v}_k$

In order to find the optimal choice of $\mathbf{v}_k$ assuming that all other vectors are fixed, we must cleverly extract only those portions of ξ which depend on $\mathbf{v}_k$. For simplicity, let us define the following $M \times M$ matrices.

$$\mathcal{L}_k(z) \triangleq \begin{cases} \displaystyle\prod_{i=N-1}^{k+1} \mathbf{V}_i(z)\,, & 0 \le k \le N-2 \\ \mathbf{I}\,, & k = N-1 \end{cases} \tag{3.15}$$

$$\mathcal{R}_k(z) \triangleq \begin{cases} \mathbf{I}\,, & k = 1 \\ \displaystyle\prod_{i=k-1}^{1} \mathbf{V}_i(z)\,, & 2 \le k \le N \end{cases} \tag{3.16}$$

Note that $\mathcal{L}_k(z)$ and $\mathcal{R}_k(z)$ are, respectively, the left and right neighbors of the matrix $\mathbf{V}_k(z)$ for $1 \le k \le N-1$ appearing in $\mathbf{V}(z)$ from (3.7). In other words, we have

$$\mathbf{V}(z) = \mathcal{L}_k(z)\mathbf{V}_k(z)\mathcal{R}_k(z)\,,\ 1 \le k \le N-1 \tag{3.17}$$

Also note that by construction, we have $\mathcal{L}_0(z) = \mathcal{R}_N(z) = \mathbf{V}(z)$. Substituting (3.17) and (3.8) into (3.6) and (3.5) yields

$$\xi = ||d(n)||_2^2 + 1 - 2\,\mathrm{Re}\left[c(\mathbf{u}_0, \mathcal{V} \setminus \mathbf{v}_k)\right] + \mathbf{v}_k^\dagger \mathbf{T}(\mathbf{u}_0, \mathcal{V} \setminus \mathbf{v}_k)\mathbf{v}_k \tag{3.18}$$

where the 1×1 scalar $c(\mathbf{u}_0, \mathcal{V} \setminus \mathbf{v}_k)$ and $M \times M$ matrix $\mathbf{T}(\mathbf{u}_0, \mathcal{V} \setminus \mathbf{v}_k)$ are defined as follows.

$$\begin{aligned}
c(\mathbf{u}_0, \mathcal{V} \setminus \mathbf{v}_k) &\triangleq \frac{1}{2\pi}\int_0^{2\pi} D^*(e^{j\omega})\mathbf{a}^\dagger(e^{j\omega})\mathcal{L}_k\big(e^{j\omega M}\big)\,\mathcal{R}_k\big(e^{j\omega M}\big)\,\mathbf{u}_0\,d\omega && (3.19)\\
\mathbf{T}(\mathbf{u}_0, \mathcal{V} \setminus \mathbf{v}_k) &\triangleq \mathbf{A}(\mathbf{u}_0, \mathcal{V} \setminus \mathbf{v}_k) + \mathbf{A}^\dagger(\mathbf{u}_0, \mathcal{V} \setminus \mathbf{v}_k), \text{ where we have,} \\
\mathbf{A}(\mathbf{u}_0, \mathcal{V} \setminus \mathbf{v}_k) &\triangleq \frac{1}{2\pi}\int_0^{2\pi} \mathcal{R}_k\big(e^{j\omega M}\big)\,\mathbf{u}_0\left(1 - e^{-j\omega M}\right) D^*(e^{j\omega})\mathbf{a}^\dagger(e^{j\omega})\mathcal{L}_k\big(e^{j\omega M}\big)\;d\omega && (3.20)
\end{aligned}$$

It should be emphasized that from (3.19) and (3.20) the quantities $c(\mathbf{u}_0, \mathcal{V} \setminus \mathbf{v}_k)$ and $\mathbf{T}(\mathbf{u}_0, \mathcal{V} \setminus \mathbf{v}_k)$ *do not* depend on the vector $\mathbf{v}_k$.

As before, to find the optimal choice of $\mathbf{v}_k$, we set the conjugate gradient of the Lagrangian $J(\mathbf{u}_0, \mathcal{V})$ from (3.9) with respect to $\mathbf{v}_k$ to be the zero vector. From (3.9), we have [48]

$$\nabla_{\mathbf{v}_k^\dagger} J = \nabla_{\mathbf{v}_k^\dagger} \xi - \lambda_k \mathbf{v}_k = \mathbf{0} \tag{3.21}$$

Differentiating ξ from (3.18) with respect to $\mathbf{v}_k$ yields [48]

$$\nabla_{\mathbf{v}_k^\dagger} \xi = \mathbf{T}(\mathbf{u}_0, \mathcal{V} \setminus \mathbf{v}_k)\mathbf{v}_k$$

Substituting this into (3.21) yields

$$\mathbf{T}(\mathbf{u}_0, \mathcal{V} \setminus \mathbf{v}_k)\mathbf{v}_k = \lambda_k \mathbf{v}_k$$

which is just an eigenvector equation. In order to minimize ξ from (3.18), by *Rayleigh's principle* [48, 67], $\mathbf{v}_k$ must be a unit norm eigenvector corresponding to the smallest eigenvalue of $\mathbf{T}(\mathbf{u}_0, \mathcal{V} \setminus \mathbf{v}_k)$, which we will denote here by $\mu_{k,\min}$. If $\mathbf{w}_{k,\min}$ denotes any unit norm eigenvector corresponding to $\mu_{k,\min}$, then the optimal $\mathbf{v}_k$ and corresponding error ξ are given by the following.

$$\boxed{\begin{gathered} \mathbf{v}_{k,\mathrm{opt}} = \mathbf{w}_{k,\min}\,, \\ \xi_{\mathrm{opt}} = ||d(n)||_2^2 + 1 - 2\,\mathrm{Re}\left[c(\mathbf{u}_0, \mathcal{V} \setminus \mathbf{v}_k)\right] + \mu_{k,\min} \end{gathered}} \tag{3.22}$$

To summarize the results of this section, using the complete factorization of causal FIR magnitude squared Nyquist(M) systems in terms of Householder-like building blocks, the optimal parameter vectors ($\mathbf{u}_0$ and the $\mathbf{v}_i$s) can be easily found one at a time assuming that the rest of the vectors are fixed. This property forms the basis of the proposed iterative algorithm for solving the original least-squares problem.

3.3.2 Iterative Gradient Optimization Algorithm

Let ξ_m denote the mean-squared error at the m-th iteration for $m \geq 0$. Then, the iterative gradient optimization algorithm is as follows.

Initialization:

1. Generate N random unit norm vectors $\mathbf{u}_0$, $\mathbf{v}_i, 1 \leq i \leq N-1$.
2. Compute the matrix $\mathcal{R}_N(z)$ using (3.16).

Iteration: For $m \geq 0$, do the following.

1. *If* m *is a multiple of* N:
   (a) Calculate the optimal vector $\mathbf{u}_0$ and corresponding error ξ_m using (3.14) and (3.12) with $\mathbf{V}(z) = \mathcal{R}_N(z)$.
   (b) Compute $\mathcal{L}_0(z) = \mathbf{V}(z)$ and $\mathcal{R}_1(z) = \mathbf{I}$.

   Otherwise, if $m \equiv k \bmod N$ *where* $1 \leq k \leq N-1$:
   (a) From (3.15), update the left matrix as $\mathcal{L}_k(z) = \mathcal{L}_{k-1}(z)\widetilde{\mathbf{V}}_k(z)$.
   (b) Calculate the optimal vector $\mathbf{v}_k$ and corresponding error ξ_m using (3.22), (3.19), and (3.20).
   (c) From (3.16), update the right matrix as $\mathcal{R}_{k+1}(z) = \mathbf{V}_k(z)\mathcal{R}_k(z)$.
2. Increment m by 1 and return to Step 1.

As the iterations progress, the left matrix is shortened by the old optimal vectors $\mathbf{v}_k$ whereas the right matrix is lengthened by the newly computed ones. After all of the $\mathbf{v}_k$s have been optimized, the left matrix assumes the value of the right matrix while the right matrix is then refreshed to be the identity matrix.

Since at each stage in the iteration, we are globally optimizing one vector while fixing the rest, the above technique is a *greedy algorithm.* As such, the mean-squared error ξ_m is guaranteed to be monotonic nonincreasing as a function of the iteration index m. Furthermore, as ξ_m has a lower bound (i.e., we always have $\xi_m \geq 0$), ξ_m is guaranteed to have a limit as $m \to \infty$ [67]. Simulation results provided here verify this monotonic and limiting behavior as we now show.

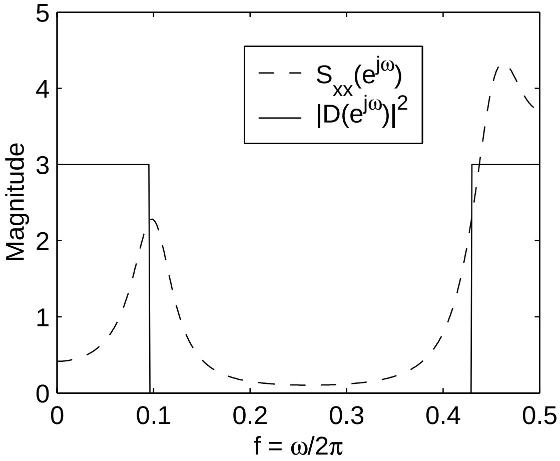

Figure 3.1: Input psd $S_{xx}(e^{j\omega})$ and ideal compaction filter magnitude squared response $\left|D(e^{j\omega})\right|^2$ for $M = 3$.

3.3.3 Simulation Results for Designing FIR Compaction Filters

Here, we considered the design of an FIR compaction filter $F(z)$ of length MN for the system of Fig. 2.1 for a WSS input $x(n)$ with psd $S_{xx}(e^{j\omega})$. As such, we chose the desired response $D(e^{j\omega})$ to be any optimal unconstrained order compaction filter. From (2.6), we know that we must have

$$\left|D(e^{j\omega})\right| = \begin{cases} \sqrt{M}\,, & \omega \in \boldsymbol{\omega}_x \\ 0\,, & \text{otherwise} \end{cases}$$

where $\boldsymbol{\omega}_x$ is the set of frequencies given by (2.7). Though the phase of the ideal compaction filter is arbitrary in this case, we opted to choose a linear phase spectral factor with a delay equal to half of the FIR filter order. Namely, we chose

$$D(e^{j\omega}) = \left|D(e^{j\omega})\right| e^{j\phi(\omega)}\,,\ \text{where } \phi(\omega) = \left(\frac{MN-1}{2}\right)\omega \tag{3.23}$$

For the simulation results here, we chose $x(n)$ to be a real autoregressive order 4 (AR(4)) process with psd $S_{xx}(e^{j\omega})$ as shown in Fig. 3.1. Due to symmetry, only the region $\omega \in [0, \pi]$ is shown. Also in Fig. 3.1, we have plotted the magnitude squared response of the ideal compaction filter for $M = 3$. In accordance with intuition, the compaction filter preserves the significant portions of $S_{xx}(e^{j\omega})$ while discarding the rest.

To test the proposed iterative algorithm, we considered designing an FIR compaction filter with $N = 16$ (implying a filter length of $MN = 48$). All integrals were evaluated numerically using 1,024 uniformly spaced frequency samples. A plot of the observed error ξ_m as a function of the iteration index m is shown in Fig. 3.2 for a total of KN iterations, where we chose $K = \left\lceil \frac{1{,}000}{N} \right\rceil$. (We

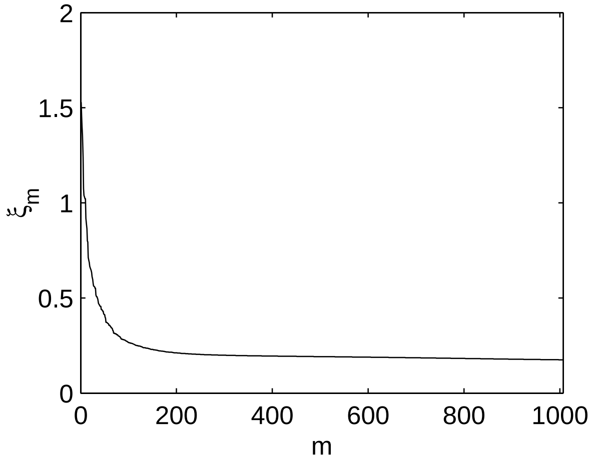

Figure 3.2: Mean-squared error ξ_m vs. the iteration index m.

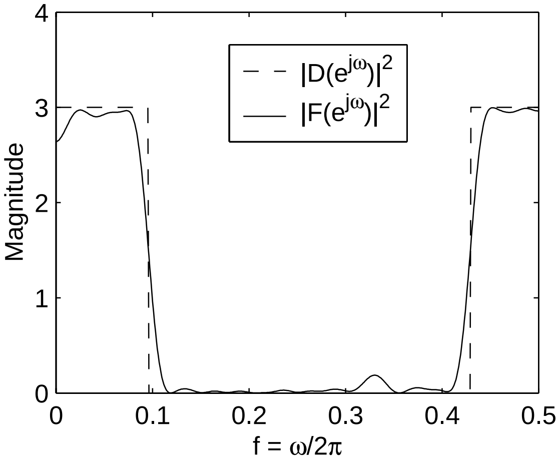

Figure 3.3: Magnitude squared responses of the ideal compaction filter $D(e^{j\omega})$ and the designed FIR compaction filter $F(e^{j\omega})$.

opted for an integer multiple of N iterations to ensure that all of the vectors were optimized the same number of times.) As can be seen from Fig. 3.2, the observed mean-squared error is indeed monotonic nonincreasing and appears to be approaching a limit. In Fig. 3.3, plots of the magnitude squared responses of the ideal and FIR compaction filters are shown. As can be seen, the FIR filter designed here is a good approximation to the ideal response.

To quantitatively measure the performance of the proposed algorithm, we opted to calculate the *compaction gain* [68] of the designed filters. Recall from (2.32) that this quantity is given by

$$G_{\text{comp}} = \frac{\sigma_w^2}{\sigma_x^2} = \frac{\dfrac{1}{2\pi}\displaystyle\int_0^{2\pi} S_{xx}(e^{j\omega})\left|F(e^{j\omega})\right|^2 d\omega}{\dfrac{1}{2\pi}\displaystyle\int_0^{2\pi} S_{xx}(e^{j\omega})\, d\omega}$$

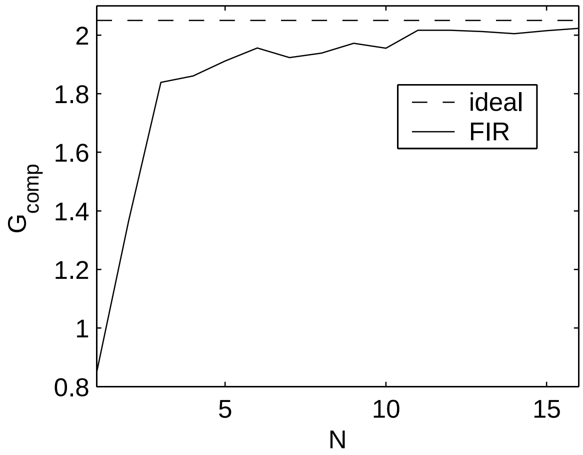

Figure 3.4: Compaction gain G_{comp} vs. the filter order parameter N.

when the input $x(n)$ is WSS. Also recall that the ideal compaction filter maximizes this quantity over all magnitude squared Nyquist(M) filters. A plot of the observed compaction gain as a function of the filter order parameter N is shown in Fig. 3.4. The compaction gain often comes close to the optimal gain, but does not monotonically increase with N. Though counterintuitive, it is most likely due to the fact that we are constraining the desired response to have linear phase as in (3.23). Despite this, the observed compaction gain in many cases comes close to the ideal one. Here, the largest compaction gain observed was 2.0230 for $N = 16$ compared to the ideal one of 2.0501.

3.4 Phase Feedback Modification for Improving Compaction Gain

One of the problems which arose in the design of FIR compaction filters for WSS inputs using the proposed iterative method was the fact that the phase of the desired response $D(e^{j\omega})$ is arbitrary. For the linear phase choice of (3.23), it was qualitatively seen that the iterative method yielded filters close to the ideal compaction filter. However, quantitatively, the algorithm yielded a nonmonotonic behavior with compaction gain as a function of the polyphase order parameter N, contrary to intuition. As the mean-squared error ξ_m is monotonic nonincreasing with m, this suggests that the algorithm is often times putting more of an emphasis on trying to match the phase of $D(e^{j\omega})$ as opposed to its magnitude. This is undesirable for designing compaction filters here since all of the emphasis should be focused on the magnitude.

To mitigate this effect, we propose a modification to the iterative algorithm whereby the phase of the desired response $D(e^{j\omega})$ is changed to match that of the FIR filter $F(e^{j\omega})$. We call this the *phase feedback modification*, since after a certain number of iterations, the phase of $F(e^{j\omega})$ is *fed back* as the phase of $D(e^{j\omega})$. Heuristically, we should expect that with the phase of the desired response matched to that of the FIR filter, the design emphasis for future iterations will be more focused on magnitude than phase.

Suppose that we wish to update the phase after every N_{PF} iterations (i.e., N_{PF} denotes the number of iterations to run before performing a phase feedback). Then, the modification is as follows. If $F_m(e^{j\omega}) = \left|F_m(e^{j\omega})\right| e^{j\phi_m(\omega)}$ denotes the FIR filter obtained at the m-th iteration, then when $m = kN_{\text{PF}}$, where k is some nonnegative integer, we update the desired response as follows.

$$D(e^{j\omega}) \Longrightarrow \left|D(e^{j\omega})\right| e^{j\phi_{kN_{\text{PF}}}(\omega)}$$

If K_{PF} denotes the number of phase feedback cycles desired, then the total number of iterations is $K_{\text{PF}}N_{\text{PF}}$.

Prior to showing design examples with the phase feedback modification, we should note the following. With the modification in effect, it can be shown that the proposed algorithm still remains greedy. To see this, suppose that a phase feedback is performed at the m-th iteration and let $\xi_{m,\text{before}}$ and $\xi_{m,\text{after}}$ denote, respectively, the error before and after the phase feedback. From (3.5), we have

$$\begin{aligned}
\xi_{m,\text{before}} &= ||d(n)||_2^2 + 1 - \frac{1}{\pi}\int_0^{2\pi} \left|D(e^{j\omega})\right| \left|F_m(e^{j\omega})\right| \cos\left(\phi_D(\omega) - \phi_m(\omega)\right)\, d\omega \\
\xi_{m,\text{after}} &= ||d(n)||_2^2 + 1 - \frac{1}{\pi}\int_0^{2\pi} \left|D(e^{j\omega})\right| \left|F_m(e^{j\omega})\right| d\omega
\end{aligned}$$

Clearly we have $\xi_{m,\text{after}} \leq \xi_{m,\text{before}}$. As $\xi_{m+1,\text{after}} \leq \xi_{m,\text{after}}$, since the unmodified algorithm is greedy, we thus have $\xi_{m+1,\text{after}} \leq \xi_{m,\text{before}}$. Hence, the algorithm remains greedy even with the phase feedback modification in effect.

For the simulations run using the phase feedback modification, we choose $N_{\text{PF}} = N$ and $K_{\text{PF}} = \left\lceil \frac{1{,}000}{N} \right\rceil$ here, corresponding to same number of iterations considered without the modification. This corresponds to feeding back the phase each time all of the vectors ($\mathbf{u}_0$ and the $\mathbf{v}_i$s) have been updated once. A plot of the compaction gain observed using the phase feedback modification as a function of the polyphase order N is shown in Fig. 3.5. The compaction gain observed without the modification is also included here for comparison. As can be seen, the phase feedback modification yielded a much better compaction gain than without, especially at low filter orders. Furthermore, here, the observed gain was *monotonically increasing* with N. It should be noted that this behavior did not always occur in our simulations. Due to the fact that the initial conditions were always

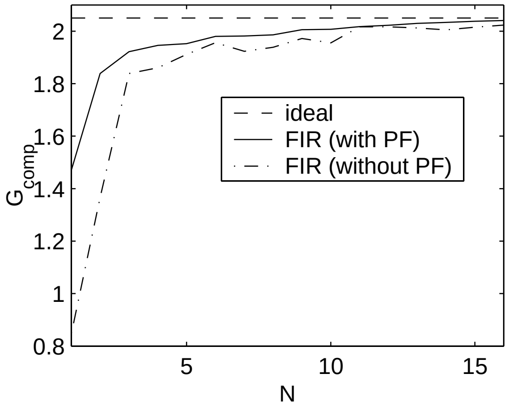

Figure 3.5: Compaction gain G_{comp} vs. the filter order parameter N using the phase feedback modification.

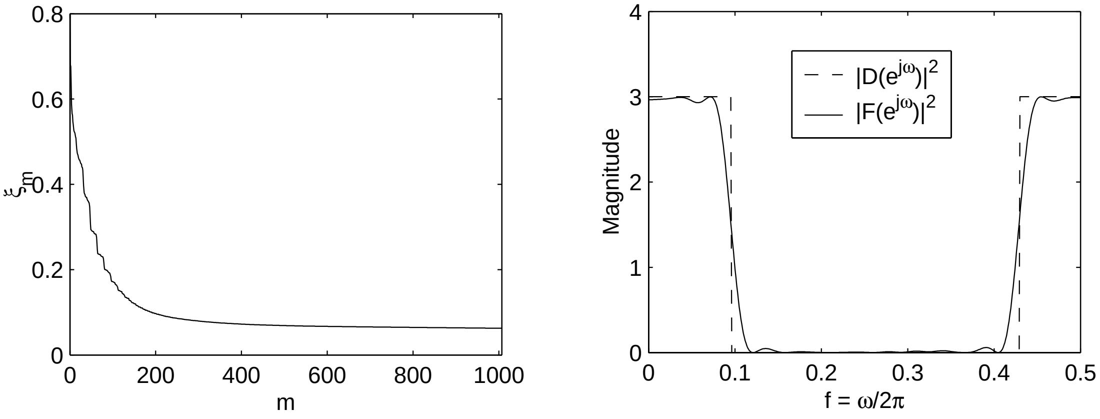

(a)

(b)

Figure 3.6: Compaction filter design using the phase feedback modification. (a) Mean-squared error vs. iteration. (b) Magnitude squared response.

randomly chosen, there were some fluctuations with the compaction gain. However, even with the fluctuations, the phase feedback modification always yielded a larger gain than that observed without it. Here, the largest gain observed was 2.0403 for $N = 16$, which is very close to the ideal one of 2.0501. In Fig. 3.6(a) and (b), respectively, we have plotted the mean-squared error versus iteration and the magnitude squared response of the optimal filter obtained for $N = 16$. From Fig. 3.3 and Fig. 3.6(b), it can be seen that the optimal filter designed using the phase feedback approach yielded a better approximation to the ideal compaction filter than that without it.

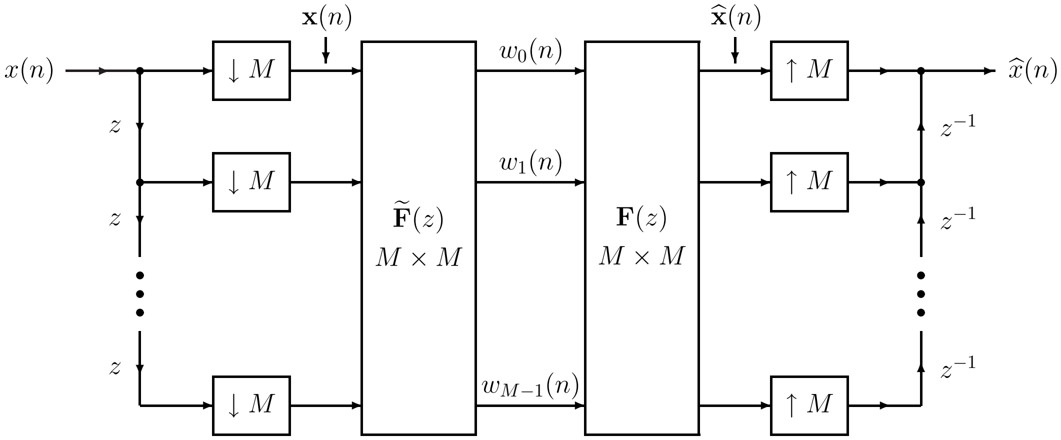

Figure 3.7: Uniform M-channel maximally decimated PU filter bank.

3.5 Design of Signal-Adapted FIR PU Filter Banks Using a Multiresolution Criterion

In this section, we focus on the PU filter bank shown in Fig. 3.7 in which the $M \times M$ synthesis polyphase matrix $\mathbf{F}(z)$ satisfies $\widetilde{\mathbf{F}}(z)\mathbf{F}(z) = \mathbf{I}$ and the synthesis filters are given by [67]

$$\left[\begin{array}{cccc} F_0(z) & F_1(z) & \cdots & F_{M-1}(z) \end{array}\right] = \widetilde{\mathbf{a}}(z)\mathbf{F}\left(z^M\right) \tag{3.24}$$

Note that this filter bank is just a special case of the system shown in Fig. 1.13. In order to mimic the behavior of the infinite-order PCFB for the case where $\mathbf{F}(z)$ is FIR, we will opt to design $\mathbf{F}(z)$ according to the following *multiresolution optimality criterion* originally considered by Moulin and Mıhçak [37].

Multiresolution Optimality Criterion (MOC):

1. Maximize $\sigma^2_{w_0}$ subject to $\left[\widetilde{F}_0(z)F_0(z)\right]_{\downarrow M} = 1$ *(Compaction Filter Problem)*

2. For $i = 1, 2, \ldots, M-1$, successively maximize $\sigma^2_{w_i}$ subject to

$$\left[\widetilde{F}_i(z)F_i(z)\right]_{\downarrow M} = 1 \qquad \textit{(Nyquist(M) Criterion)}$$

$$\left[\widetilde{F}_k(z)F_i(z)\right]_{\downarrow M} = 0 \ \forall \ 0 \le k \le i-1 \qquad \textit{(Orthogonality Criterion)}$$

As can be seen, the MOC consists of optimizing the filters one at a time starting with the design of the compaction filter. At each stage, the next filter is chosen to maximize its subband variance subject to the remaining degrees of freedom dictated by the PU constraint and the other filters already designed. A multiresolution optimal filter bank is also said to be optimal in terms of *scalability* [24] since such a filter bank represents the best approximation for any given scale (i.e., number of subband signals kept). It can easily be shown that the PCFB, if it exists for a class of PU filter banks considered, is multiresolution optimal, by virtue of the fact that it majorizes the vector of subband variances. As we might expect, FIR filter banks designed using the MOC should exhibit infinite-order PCFB-like behavior as the filter order increases. This will be seen via simulation examples presented later in the chapter.

Moulin and Mıhçak [37] were the first to use the MOC for the design of FIR PU filter banks. By using the complete parameterization of FIR PU systems from Sec. 3.2, they showed that the design process for a multiresolution optimal filter bank elegantly consisted of the construction of an FIR compaction filter, followed by an appropriate KLT. However, contrary to intuition, they found that filter banks constructed in this manner were not exhibiting PCFB-like behavior. In particular, it was shown that traditional nonadaptive filter banks (i.e., filter banks with uniformly stacked frequency support) performed better than those designed to satisfy the MOC in terms of coding gain. This is most likely because they did not exploit the *nonuniquness* of the compaction filter for the WSS inputs they considered. Given any valid FIR compaction filter, any spectral factor of it is also a valid compaction filter since both have the same magnitude response. As we might expect, different spectral factors lead to different filter bank parameterizations which in turn yield different performance with respect to the MOC. In [37], the authors only chose the *minimum-phase* spectral factor as their compaction filter. As we will show below through simulation examples, this spectral factor is often *far* from being optimal in terms of the MOC.

Prior to presenting our simulation results for the different compaction filter spectral factors, we show how the parameterization of FIR PU systems from Sec. 3.2 can be applied to the MOC. In particular, we will show that using the MOC, the FIR PU filter bank design problem is tantamount to designing an FIR compaction filter followed by an appropriate KLT.

3.5.1 Application of the Factorization of FIR PU Systems to the MOC

Suppose that $\mathbf{F}(z)$ from Fig. 3.7 is a causal FIR PU $M \times M$ system with McMillan degree $(N-1)$. This implies that the synthesis filters $\{F_k(z)\}$ are causal and FIR of length MN by using (3.24). Then, from (3.1), $\mathbf{F}(z)$ has a factorization of the form

$$\mathbf{F}(z) = \underbrace{\mathbf{V}_{N-1}(z)\mathbf{V}_{N-2}(z)\cdots\mathbf{V}_1(z)}_{\mathbf{V}(z)}\mathbf{U} \qquad (3.25)$$

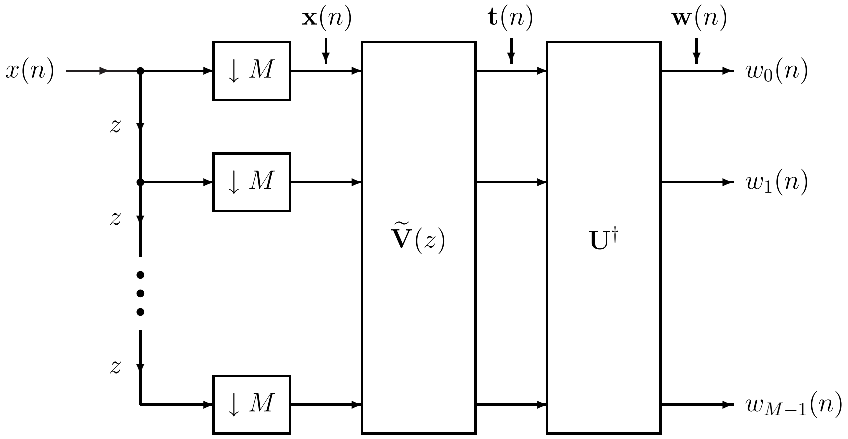

Figure 3.8: Implementation of the analysis bank using the factorization of $\mathbf{F}(z)$ from (3.25).

where $\mathbf{U}$ is an $M \times M$ unitary matrix and $\mathbf{V}_k(z)$ is an $M \times M$ degree-one system of the form

$$\mathbf{V}_k(z) = \mathbf{I} - \mathbf{v}_k\mathbf{v}_k^{\dagger} + z^{-1}\mathbf{v}_k\mathbf{v}_k^{\dagger}\,,\ 1 \leq k \leq N-1 \tag{3.26}$$

where $\mathbf{v}_k$ is a unit norm $M \times 1$ vector for all k. The implementation of the analysis bank $\widetilde{\mathbf{F}}(z)$ using the factorization of (3.25) is shown in Fig. 3.8. Assuming $\mathbf{x}(n)$ is WSS, then so is $\mathbf{t}(n)$ and hence $\mathbf{w}(n)$. Clearly, we have [67]

$$\mathbf{S}_{\mathbf{ww}}(z) = \mathbf{U}^{\dagger}\mathbf{S}_{\mathbf{tt}}(z)\mathbf{U} \Longrightarrow \mathbf{R}_{\mathbf{ww}}(0) = \mathbf{U}^{\dagger}\mathbf{R}_{\mathbf{tt}}(0)\mathbf{U} \tag{3.27}$$

where $\mathbf{S}_{\mathbf{ww}}(z)$ and $\mathbf{S}_{\mathbf{tt}}(z)$ denote, respectively, the psds of $\mathbf{w}(n)$ and $\mathbf{t}(n)$. From Fig. 3.8, we get [67]

$$\mathbf{S}_{\mathbf{tt}}(z) = \widetilde{\mathbf{V}}(z)\mathbf{S}_{\mathbf{xx}}(z)\mathbf{V}(z) \Longrightarrow \mathbf{R}_{\mathbf{tt}}(0) = \frac{1}{2\pi}\int_0^{2\pi} \mathbf{V}^{\dagger}(e^{j\omega})\mathbf{S}_{\mathbf{xx}}(e^{j\omega})\mathbf{V}(e^{j\omega})\,d\omega \tag{3.28}$$

To simplify the MOC using the factorization of $\mathbf{F}(z)$ from (3.25), partition $\mathbf{U}$ into its columns as

$$\mathbf{U} = \begin{bmatrix} \mathbf{u}_0 & \mathbf{u}_1 & \cdots & \mathbf{u}_{M-1} \end{bmatrix} \tag{3.29}$$

Then, from (3.27), we have

$$\sigma_{w_i}^2 = \left[\mathbf{R}_{\mathbf{ww}}(0)\right]_{i,i} = \mathbf{u}_i^{\dagger}\mathbf{R}_{\mathbf{tt}}(0)\mathbf{u}_i \tag{3.30}$$

Furthermore, note that from (3.24) the Nyquist(M) and orthogonality constraints appearing in the MOC have the following equivalent expressions.

$$\left[\widetilde{F}_i(z)F_i(z)\right]_{\downarrow M} = 1 \quad \Longleftrightarrow \quad \mathbf{u}_i^{\dagger}\mathbf{u}_i = 1 \tag{3.31}$$

$$\left[\widetilde{F}_k(z)F_i(z)\right]_{\downarrow M} = 0\ \forall\ 0 \leq k \leq i-1 \quad \Longleftrightarrow \quad \mathbf{u}_k^{\dagger}\mathbf{u}_i = 0\ \forall\ 0 \leq k \leq i-1 \tag{3.32}$$

These constraints are in addition to the constraint that the vectors $\mathbf{v}_k$ from (3.26) be of unit norm.

Recall that Step 1 of the MOC requires the computation of a compaction filter. Suppose that a causal FIR compaction filter $F_0(z)$ of length MN has already been designed using either the proposed iterative algorithm or any of the methods described in Section 2.2.2. Substituting (3.25) and (3.29) in (3.24), it follows that we know the value of

$$F_0(z) = \widetilde{\mathbf{a}}(z) \underbrace{\mathbf{V}\left(z^M\right) \mathbf{u}_0}_{\mathbf{f}_0(z^M)} \tag{3.33}$$

where $\mathbf{f}_0(z) = \mathbf{V}(z)\mathbf{u}_0$ is an $M \times 1$ causal FIR PU vector system of degree $(N-1)$ consisting of Type I polyphase components of $F_0(z)$. As $\mathbf{f}_0(z)$ is a *vector* system, it follows from Sec. 3.2 that the diadic forms present in $\mathbf{V}(z)$, namely, the quantities $\mathbf{v}_k\mathbf{v}_k^\dagger$ for $1 \leq k \leq N-1$, are *unique*. Hence, the matrix $\mathbf{V}(z)$ itself is unique. Thus, a given compaction filter $F_0(z)$ corresponds to a unique $\mathbf{V}(z)$. It should be noted here that this uniqueness holds iff $F_0(z)$ is a *nondegenerate* causal FIR filter of length MN, i.e., the length of $F_0(z)$ can not be less than MN. In all practical cases, however, including the FIR compaction filters designed here, this is never a problem since the filters are always nondegenerate.

To summarize, once a nontrivial FIR compaction filter $F_0(z)$ has been designed, we know the *unique* value of the matrix $\mathbf{V}(z)$ appearing in Fig. 3.8. Hence, the second order statistics of the process $\mathbf{t}(n)$ from Fig. 3.8 are known, namely, the autocorrelation sequence $\mathbf{R}_{\mathbf{tt}}(k)$.

It should also be noted that with $F_0(z)$ given, we also know the first column $\mathbf{u}_0$ of the matrix $\mathbf{U}$ from (3.29). By Rayleigh's principle [22], it follows that $\mathbf{u}_0$ must be a unit norm eigenvector corresponding to the largest eigenvalue of the matrix $\mathbf{R}_{\mathbf{tt}}(0)$ given by (3.27) and (3.28). To see this, note that with $\mathbf{R}_{\mathbf{tt}}(0)$ uniquely determined, using (3.30) and (3.31), Step 1 of the MOC becomes

$$\text{Maximize } \sigma_{w_0}^2 = \mathbf{u}_0^\dagger \mathbf{R}_{\mathbf{tt}}(0)\mathbf{u}_0 \text{ subject to } \mathbf{u}_0^\dagger\mathbf{u}_0 = 1.$$

which is precisely the problem statement in Rayleigh's principle [22].

To determine the other columns $\mathbf{u}_1, \mathbf{u}_2, \ldots, \mathbf{u}_{M-1}$ of the matrix $\mathbf{U}$ from (3.29), note that with $\mathbf{R}_{\mathbf{tt}}(0)$ uniquely determined, from (3.30), (3.31), and (3.32), Step 2 of the MOC becomes

$$\text{Maximize } \sigma_{w_i}^2 = \mathbf{u}_i^\dagger \mathbf{R}_{\mathbf{tt}}(0)\mathbf{u}_i \text{ subject to } \mathbf{u}_i^\dagger\mathbf{u}_i = 1 \text{ and } \mathbf{u}_k^\dagger\mathbf{u}_i = 0 \ \forall \ 0 \leq k \leq i-1.$$

This is done successively for $i = 1, 2, \ldots, M-1$. As such, the vectors $\mathbf{u}_1, \mathbf{u}_2, \ldots, \mathbf{u}_{M-1}$ are found sequentially beginning with $\mathbf{u}_1$ and ending with $\mathbf{u}_{M-1}$. By an extension of Rayleigh's principle [22], it follows that $\mathbf{u}_1$ must be a unit norm eigenvector corresponding to the second largest eigenvalue of $\mathbf{R}_{\mathbf{tt}}(0)$. Similarly, by extension of Rayleigh's principle, $\mathbf{u}_i$ must be a unit norm eigenvector corresponding to the i-th largest eigenvalue of $\mathbf{R}_{\mathbf{tt}}(0)$ for all i. In other words, the optimal matrix $\mathbf{U}$ from (3.29) is the unitary matrix which *diagonalizes* $\mathbf{R}_{\mathbf{tt}}(0)$. Hence, the optimal $\mathbf{U}$ is a KLT for the process $\mathbf{t}(n)$ from Fig. 3.8. Furthermore, the subband variances $\sigma^2_{w_i}$ are simply the *eigenvalues* of $\mathbf{R}_{\mathbf{tt}}(0)$.

In conclusion, designing an FIR PU filter bank using the MOC consists of computing an optimal FIR compaction filter followed by an appropriate KLT. A summary of this design algorithm is given below.

3.5.2 Algorithm for the Design of FIR PU Multiresolution Optimal Filter Banks

1. Design an optimal causal FIR compaction filter $F_0(z)$ of length MN. Identify the $M\times 1$ causal PU vector $\mathbf{f}_0(z)$ of degree $(N-1)$ from (3.33) via a Type I M-fold polyphase decomposition.

2. Find the *unique* $\mathbf{V}_k(z)$ from (3.26) corresponding to $\mathbf{f}_0(z)$ as follows. Define the $M\times 1$ vector system $\mathbf{P}_k(z)$ from $k = N-1, N-2, \ldots, 1$ as

$$\mathbf{P}_{N-1}(z) \triangleq \mathbf{f}_0(z)\,,\;\; \mathbf{P}_{k-1}(z) \triangleq \widetilde{\mathbf{V}}_k(z)\mathbf{P}_k(z) \tag{3.34}$$

Then, in order for $\mathbf{P}_k(z)$ to be a polynomial in z^{-1} of degree k of the form

$$\mathbf{P}_k(z) = \sum_{n=0}^{k} \mathbf{p}_k(n) z^{-n} \tag{3.35}$$

we must have

$$\mathbf{v}_k = c_k \frac{\mathbf{p}_k(k)}{||\mathbf{p}_k(k)||} \text{ for some } c_k \text{ with } |c_k| = 1 \Longrightarrow \mathbf{v}_k\mathbf{v}_k^\dagger = \frac{\mathbf{p}_k(k)\mathbf{p}_k^\dagger(k)}{||\mathbf{p}_k(k)||^2} = \frac{\mathbf{p}_k(k)\mathbf{p}_k^\dagger(k)}{\mathbf{p}_k^\dagger(k)\mathbf{p}_k(k)} \tag{3.36}$$

Hence, the diadic terms $\mathbf{v}_k\mathbf{v}_k^\dagger$ appearing in $\mathbf{V}_k(z)$ from (3.26) are found recursively starting from $k = N-1$ and ending at $k = 1$ using (3.34), (3.35), and (3.36) successively.

3. Compute $\mathbf{V}(z) = \mathbf{V}_{N-1}(z)\mathbf{V}_{N-2}(z)\cdots\mathbf{V}_1(z)$. Then calculate $\mathbf{R}_{\mathbf{tt}}(0)$ using (3.28).

4. Choose $\mathbf{U}$ to be the KLT of $\mathbf{t}(n)$, i.e., the unitary matrix which *diagonalizes* $\mathbf{R}_{\mathbf{tt}}(0)$.

5. Compute the synthesis polyphase matrix $\mathbf{F}(z)$ using $\mathbf{F}(z) = \mathbf{V}(z)\mathbf{U}$.

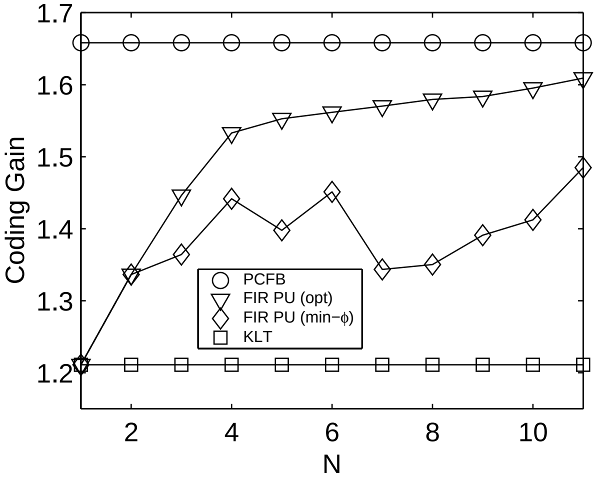

Figure 3.9: Observed coding gain G_{code} as a function of the synthesis polyphase order N.

3.6 Simulation Results for MOC Designed FIR PU Filter Banks

3.6.1 Coding Gain Results

Suppose that the input $x(n)$ to the PU filter bank of Fig. 3.7 is the real AR(4) process considered in Sec. 3.3.3, whose psd $S_{xx}(e^{j\omega})$ is shown in Fig. 3.1. Here, we considered the design of an $M = 3$ channel system. For each filter bank designed, the filters designed in Sec. 3.4 using the proposed iterative algorithm with the phase feedback modification were used as the optimum FIR compaction filter required for multiresolution optimality. The synthesis polyphase matrix order N was varied from 1 to 11 in order to see the behavior of the filter banks designed. For each N, the filter banks corresponding to all compaction filter spectral factors were computed and the one judged to be optimal was the one which yielded the largest coding gain. (See Chapter 5 for more on coding gain.) Assuming optimal bit allocation, the coding gain is given by [67]

$$G_{\text{code}} = \frac{\dfrac{1}{M}\displaystyle\sum_{i=0}^{M-1} \sigma_{w_i}^2}{\left(\displaystyle\prod_{i=0}^{M-1} \sigma_{w_i}^2\right)^{\frac{1}{M}}}$$

In this case, the coding gain is simply the arithmetic mean/geometric mean (AM/GM) ratio of the subband variances. Due to the subband variance majorization property of the PCFB, it can be shown that the PCFB, if it exists for a class of filter banks under consideration, maximizes this quantity [1]. Hence, the coding gain is lower bounded by unity (because of the AM/GM inequality [67]) and upper bounded by the gain produced by the PCFB.

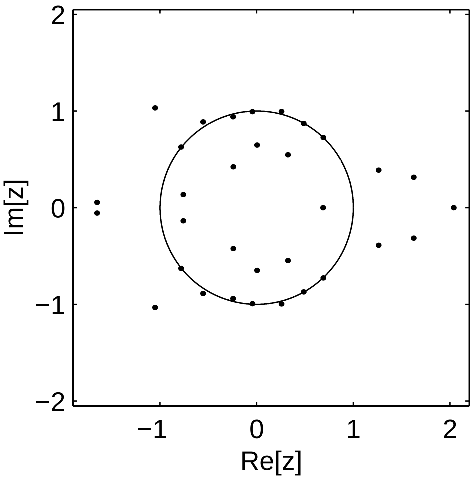

Figure 3.10: Zero locations of the optimal spectral factor for $N = 11$.

A plot of the largest coding gain observed as a function of N is shown in Fig. 3.9[1]. Along with the coding gain of the optimal filter bank, the coding gain of the filter bank yielded by the minimum-phase spectral factor is also shown. As can be seen, there is a large gap between these two solutions. Furthermore, the optimal filter bank always exhibited a *monotonically increasing* coding gain, whereas the minimum-phase filter bank had a fluctuating one.

From Fig. 3.9, it appears as though the optimal filter bank is approaching the performance of the infinite-order PCFB as N increases. It would be interesting to view the behavior for much larger N, however this is not feasible since the number of compaction filter spectral factors increases *exponentially* with N. In general, a compaction filter of order $MN - 1$ has 2^{MN-1} spectral factors. For sake of simplicity, since the input process $x(n)$ is real here, we only considered real coefficient spectral factors. In this case, if the compaction filter has N_r real roots and N_c complex roots (with N_c being even here of course), then only $2^{N_r+(N_c/2)}$ real coefficient spectral factors exist. For $N = 11$ ($MN = 33$), there were a total of $2^{2+\frac{30}{2}} = 2^{17} = 131,072$ different spectral factors that needed to be computed! The locations of the zeros corresponding to the best spectral factor for $N = 11$ is shown in Fig. 3.10. In Fig. 3.11 and 3.12, the magnitude squared responses of the analysis filters is shown for the optimal spectral factor and the minimum-phase one, respectively. As can be seen, the filter responses corresponding to the optimal spectral factor appear to be a better fit to the infinite-order PCFB compaction filters than those of the minimum-phase one.

[1] For $N = 1$, the KLT of $\mathbf{x}(n)$ was chosen as the optimal solution, since it is the PCFB for this class of filter banks.

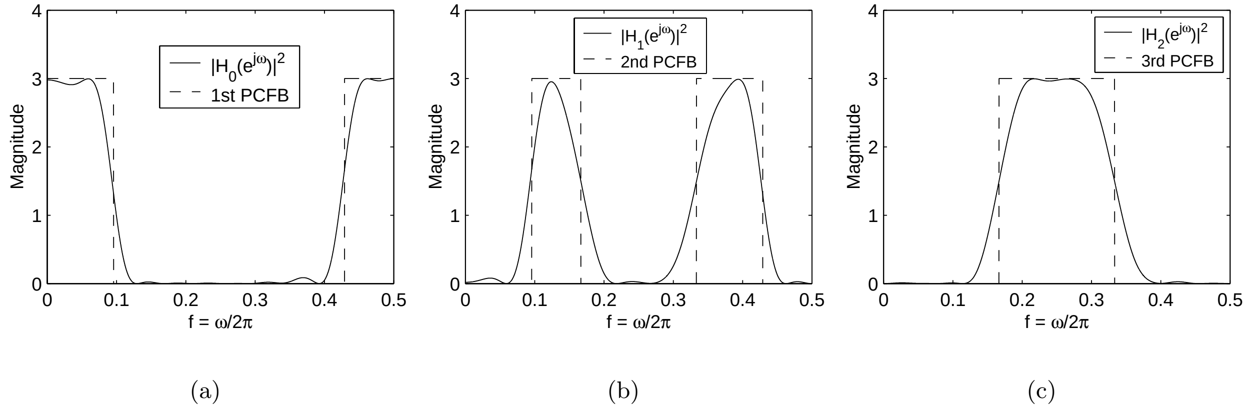

(a) (b) (c)

Figure 3.11: Analysis filter magnitude squared responses for the optimal spectral factor for $N = 11$. (a) First channel. (b) Second channel. (c) Third channel.

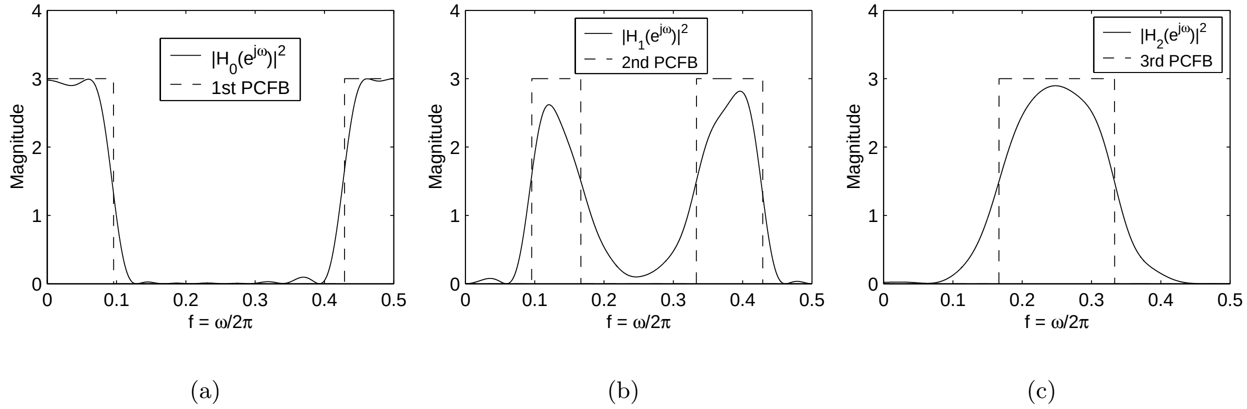

(a) (b) (c)

Figure 3.12: Analysis filter magnitude squared responses for the minimum-phase spectral factor for $N = 11$. (a) First channel. (b) Second channel. (c) Third channel.

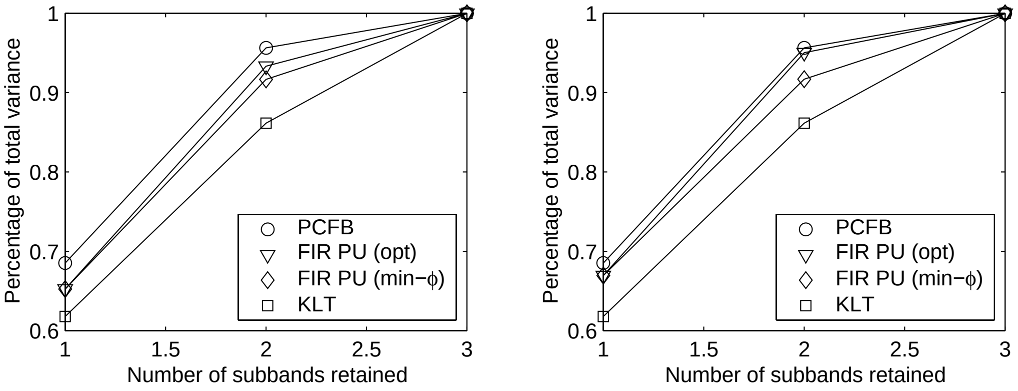

(a)

(b)

Figure 3.13: Proportion $P(L)$ of the total variance as a function of the number of subbands kept L for (a) $N = 3$ and (b) $N = 9$.

3.6.2 Multiresolution Optimality Results

In addition to being good for coding gain, the spectral factor optimized for coding gain also yielded good performance with respect to the MOC. As a measure of multiresolution optimality, we opted to consider the proportion of the partial subband variances to the total. By preserving only L out of M subbands, the proportion of the total variance carried by these L subbands is given by

$$P(L) \triangleq \frac{\sum\limits_{i=0}^{L-1} \sigma_{w_i}^2}{\sum\limits_{i=0}^{M-1} \sigma_{w_i}^2}\,,\ 1 \leq L \leq M$$

Due to the subband variance majorization property of the PCFB (see Sec. 1.2.1), the PCFB maximizes $P(L)$ for all L. The proportion $P(L)$ as a function of the number of subbands kept L is shown in Fig. 3.13 for $N = 3$ and $N = 9$. As can be seen, the variances of the optimized filter bank are closer to the infinite-order PCFB variances than those obtained using the minimum-phase spectral factor. From Fig. 3.13(b), we see that the difference in performance between these two solutions is rather noticable. In line with intuition, it can be seen that as N increases from 4 to 9, the optimized filter bank subband variances are trying to come closer and closer to the PCFB ones.

3.6.3 Noise Reduction Using Zeroth-Order Wiener Filters

Recall from Sec. 1.2.1, that the PCFB, if it exists, is optimal for a wide variety of objective functions. In particular, it has been shown [1] that the PCFB is optimal for noise reduction with zeroth-order

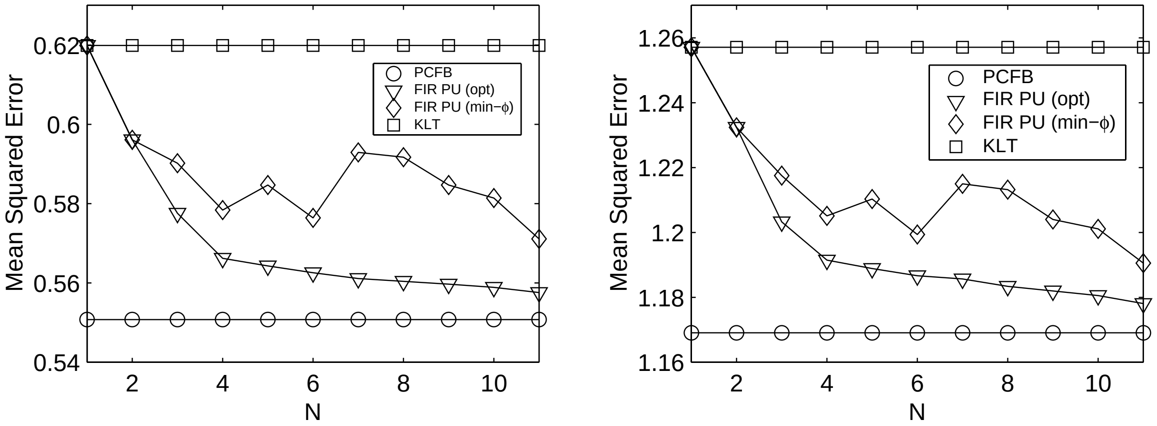

(a)

(b)

Figure 3.14: Mean-squared error ϵ from (3.37) as a function of N for (a) $\eta^2 = 1$ and (b) $\eta^2 = 4$.

Wiener filters in the subbands if the noise is white. In other words, if the input to the filter bank of Fig. 1.13(a) is $x(n) = s(n) + \mu(n)$, where $s(n)$ is a pure signal and $\mu(n)$ is a white noise process and if the subband processors $\{\mathcal{P}_k\}$ are taken to be zeroth-order Wiener filters (i.e., multipliers), then the PCFB for $x(n)$ (which is also the PCFB for $s(n)$ in this case) is optimal in terms of minimizing the mean-squared value of the error $e(n) \triangleq s(n) - \widehat{x}(n)$ [1]. In general, the mean-squared error ϵ in the presence of zeroth-order Wiener filters is given by

$$\epsilon = \frac{1}{M} \sum_{i=0}^{M-1} \frac{\sigma_{w_i}^2 \eta^2}{\sigma_{w_i}^2 + \eta^2} \tag{3.37}$$

where $\sigma_{w_i}^2$ denotes the variance of the i-th subband when the input is the desired signal $s(n)$ and η^2 denotes the variance of the white noise process $\mu(n)$. As ϵ is a *concave* function of the subband variance vector $\boldsymbol{\sigma}$ from (1.11), the PCFB for $s(n)$, if it exists, is optimal for this objective [1].

Interestingly enough, the filter banks optimized over different spectral factors for coding gain yielded PCFB-like performance with respect to the mean-squared error ξ from (3.37). The observed mean-squared errors as a function of the synthesis polyphase order N is shown in Fig. 3.14 for (a) $\eta^2 = 1$ and (b) $\eta^2 = 4$. As can be seen in both cases, the observed mean-squared error for the optimum spectral factor filter bank noticably outperforms the minimum-phase one. Furthermore, in both cases, it can be seen that the error for the optimized filter bank *monotonically decreased* as N increased. Finally, in accordance with our intuition, the optimized filter bank is trying to emulate the behavior of the infinte order PCFB.

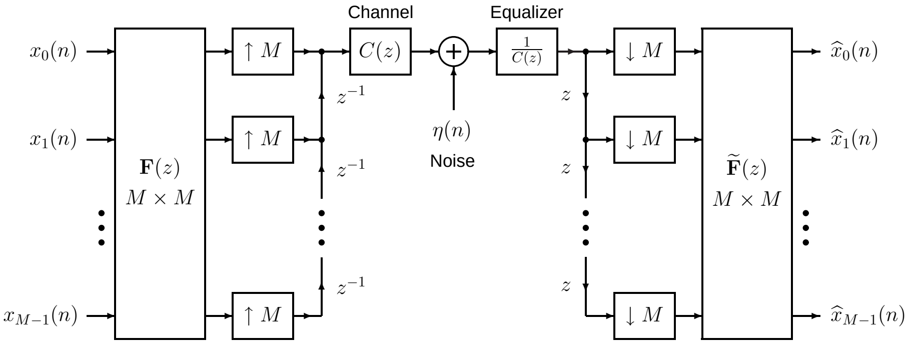

Figure 3.15: Uniform PU nonredundant transmultiplexer.

3.6.4 Power Minimization for Nonredundant PU Transmultiplexers

In addition to applications in data compression, the theory of PCFBs has also been found useful in digital communications involving the design of optimal PU transmultiplexers [73]. A typical nonredundant PU transmultiplexer [67] in polyphase form is shown in Fig. 3.15. We distinguish nonredundant transmultiplexers from redundant ones such as those used in DMT transceivers in which the polyphase matrix $\mathbf{F}(z)$ is $L \times M$ with $L < M$. The system of Fig. 3.15 represents a digital communications system in which M users $\{x_k(n)\}$ transmit data over a common path. Prior to receiving the data and separating the users at the receiver, the incoming signal undergoes a linear distortion in the form of the channel $C(z)$ and a noise process $\eta(n)$ is added to it. To undo the effects of the channel, we assume that a *zero-forcing equalizer* [38, 73] of $\frac{1}{C(z)}$ has been used here.

Assuming that the k-th input signal $x_k(n)$ consists of pulse amplitude modulated (PAM) symbols [38] with b_k bits and power P_k, then if the noise $\eta(n)$ is *Gaussian*, the probability of error in detecting the symbol $x_k(n)$ is given by [73]

$$\mathcal{P}_e(k) = 2\left(1 - 2^{-b_k}\right) \mathcal{Q}\left(\sqrt{\frac{3P_k}{\left(2^{2b_k} - 1\right)\sigma_{q_k}^2}}\right) \tag{3.38}$$

Here $\mathcal{Q}(x)$ is the *Marcum* $\mathcal{Q}$ *function* which is frequently used in communications [38]. Also, $\sigma_{q_k}^2$ denotes the noise power seen at the k-th output $\widehat{x}_k(n)$. Solving (3.38) for P_k yields

$$P_k = \beta\left(\mathcal{P}_e(k), b_k\right)\sigma_{q_k}^2 \text{ where } \beta\left(\mathcal{P}_e(k), b_k\right) = \frac{\left(2^{2b_k} - 1\right)}{3}\left[\mathcal{Q}^{-1}\left(\frac{\mathcal{P}_e(k)}{2\left(1 - 2^{-b_k}\right)}\right)\right]^2 \tag{3.39}$$

As P_k is a *linear* function of $\sigma_{q_k}^2$, it follows that the total power P given by

$$P = \sum_{k=0}^{M-1} P_k \tag{3.40}$$

is a *convex* function of the variances $\left\{\sigma_{q_k}^2\right\}$. As such, this power is minimized if $\mathbf{F}(z)$ is chosen to be a PCFB for the effective noise process seen at the input to the receiver [73]. If $\eta(n)$ is a

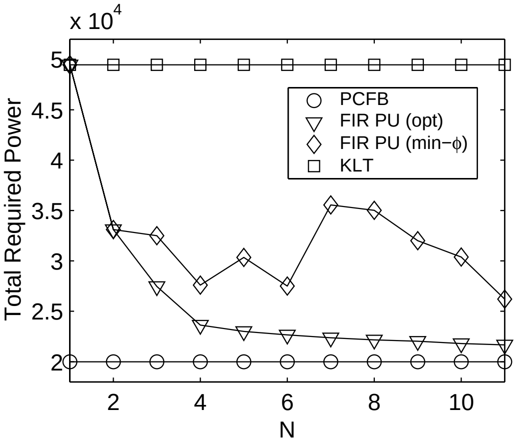

Figure 3.16: Total required power P from (3.40) as a function of N.

WSS process with psd $S_{\eta\eta}(e^{j\omega})$, then the effective noise seen at the receiver input is WSS with psd $\frac{S_{\eta\eta}(e^{j\omega})}{|C(e^{j\omega})|^2}$. Hence, the total power P from (3.40) is minimized if $\mathbf{F}(z)$ is a PCFB for the psd $\frac{S_{\eta\eta}(e^{j\omega})}{|C(e^{j\omega})|^2}$.

As an example, suppose that the desired probability of error is $\mathcal{P}_e(k) = 10^{-9}$ for all k. Also, suppose that $b_0 = 2$, $b_1 = 4$, and $b_2 = 6$. (This is a not an optimal bit allocation [73] and is only chosen as such for simplicity.) Finally, suppose that the effective noise psd $\frac{S_{\eta\eta}(e^{j\omega})}{|C(e^{j\omega})|^2}$ is simply the psd $S_{xx}(e^{j\omega})$ shown in Fig. 3.1. Then, the observed required powers as a function of the synthesis polyphase order N is shown in Fig. 3.16. As can be seen, the optimal spectral factor not only outperforms the minimum-phase one, but also monotonically decreases with N. The optimized filter bank appears to be approaching the performance of the infinite-order, in line with intuition.

3.7 Concluding Remarks

In this chapter, we presented a method for the design of FIR compaction filters based on the complete parameterization of FIR PU systems shown in Sec. 3.2. Using this same characterization, we constructed FIR PU signal-adapted filter banks based on the MOC of Sec. 3.5 using only these filters. Through simulations provided, we showed examples of FIR PU filter banks exhibiting an increasingly PCFB-like behavior as the filter order increased. This behavior has not previously been seen in the literature. However, this came at the expense of an *exponential* increase in complexity on account of the *nonuniqueness* of the FIR compaction filter. In the next chapter, we present a direct method for the design of signal-adapted FIR PU filter banks that avoids the problems caused by the ambiguity of the compaction filter. Furthermore, with this new method, the above-mentioned PCFB-like behavior continues to hold true.

Chapter 4

Direct FIR PU Approximation of the PCFB

Though the signal-adapted filter bank design algorithm of the previous chapter was shown to yield FIR PU filter banks that behaved more like the infinite-order PCFB as the filter order increased, it was shown to suffer from one major drawback. In particular, it was shown that the inherent *nonuniqueness* of the FIR compaction filter in terms of its spectral factors added an *exponential* increase in computational complexity, since each spectral factor needed to be tested for its performance. This suggests that the FIR compaction filter problem is perhaps *not well suited* for the design of complete signal-adapted filter banks. To avoid this dilemma, in this chapter, we present a signal-adapted filter bank design algorithm in which *all* of the filters are found *simultaneously.*

In particular, using the complete parameterization of FIR PU systems given in [75, 67], an iterative algorithm is proposed to approximate, in a weighted least-squares sense, any MIMO desired response by an FIR PU MIMO approximant. This is both a generalization of and departure from the FIR compaction filter design method from the previous chapter in the sense that it applies to general MIMO systems and allows for the incorporation of a weight function. As with the previous method, at each iteration, one set of parameters in the characterization of the FIR PU system is *globally* optimized assuming all other parameters to be fixed. Because of this, as before, the resulting algorithm is *greedy* and so the error is *guaranteed* to be monotonic nonincreasing with iteration.

When the desired response is the synthesis polyphase matrix of an infinite-order PCFB, the algorithm can be used for the design of the entire FIR PU synthesis bank. As the desired response in this case suffers from a *phase-type ambiguity*, which we define here, a modification to the algorithm is proposed in which the phase of the FIR approximant is cleverly *fed back* to the desired response.

With this *phase feedback modification*, which is a generalization of the one proposed in the previous chapter, the iterative algorithm not only still remains greedy, but also yields a better *magnitude-type* fit to the desired response. Simulation results provided here show that, with the phase feedback modification in effect, the FIR PU filter banks designed exhibit an increasingly PCFB-like behavior as the filter order increases. In particular, in terms of objectives such as coding gain, denoising using zeroth-order Wiener filters in the subbands, and power minimization for nonredundant PU transmultiplexers, the FIR PU filter banks designed *monotonically* approached the performance of the infinite-order PCFB as the filter order increased. As with the method presented in the previous chapter, this serves to *bridge the gap* between the zeroth-order KLT and infinite-order PCFB. However, unlike the previous method, there is no additional exponential overhead as we are no longer plagued by the nonuniqueness of the FIR compaction filter as before. In fact, the algorithm proposed here is only nominally more computationally complex than the compaction filter design algorithm of the previous chapter.

As we are able to incorporate a weight function in the design algorithm, in addition to being useful for the design of signal-adapted filter banks, the algorithm can also be used for the FIR PU interpolation problem mentioned in Sec. 1.3. Though this problem is still open, the iterative greedy algorithm proposed here can always be used to approximate a desired interpolant. Furthermore, for cases in which an interpolant is known to exist, the algorithm can be used to find the interpolant, as shown through simulations presented. Thus, the main contribution of the proposed algorithm here is a numerical approach to solve a theoretically intractable problem.

The content of this chapter is drawn from [50].

4.1 Outline

In Sec. 4.2, we analyze the weighted least-squares FIR PU approximation problem. Using the complete parameterization of FIR PU systems introduced in Sec. 3.2, we show how to obtain the optimal parameters in Sec. 4.2.1 and 4.2.2. The iterative algorithm for obtaining the FIR PU approximant is formally introduced in Sec. 4.2.3 and is shown to be greedy there.

In Sec. 4.3, we introduce the phase feedback modification to the iterative algorithm for cases in which the desired response has a phase-type ambiguity. We begin by formally defining the phase-type ambiguity in Sec. 4.3.1 and then proceed to derive the phase feedback modification in Sec. 4.3.2. In Sec. 4.3.3, we show that the iterative algorithm continues to be greedy with the phase feedback modification in effect.

Simulation results for the proposed iterative greedy algorithm are presented in Sec. 4.4. In Sec. 4.4.1, we focus on the design of infinite-order PCFB-like FIR PU filter banks. There, the FIR PU filter banks designed are shown to monotonically behave more and more like the infinite-order PCFB in terms of several objectives. In Sec. 4.4.2, simulation results are presented for the FIR PU interpolation problem.

Finally, concluding remarks are made in Sec. 4.5. There, we discuss the *bridging of the gap* between the zeroth-order KLT and infinite-order PCFB presented here, which has not been previously reported in the literature.

4.2 The FIR PU Approximation Problem

Let $\mathbf{D}(e^{j\omega})$ be any $p\times r$ desired response matrix that we wish to approximate with a $p\times r$ causal FIR PU system $\mathbf{F}(e^{j\omega})$ of McMillan degree $(N-1)$. Note that we require $p \geq r$ in order to satisfy the PU condition $\widetilde{\mathbf{F}}(z)\mathbf{F}(z) = \mathbf{I}_r$. Here, we opt to choose $\mathbf{F}(e^{j\omega})$ to minimize a weighted mean-squared Frobenius norm error between $\mathbf{D}(e^{j\omega})$ and $\mathbf{F}(e^{j\omega})$ given by

$$\xi \triangleq \frac{1}{2\pi}\int_0^{2\pi} W(\omega)\left|\left|\mathbf{D}(e^{j\omega}) - \mathbf{F}(e^{j\omega})\right|\right|_F^2 \, d\omega \tag{4.1}$$

Here, $W(\omega)$ is a scalar nonnegative weight function and $||\mathbf{A}||_F$ denotes the *Frobenius norm* of any matrix $\mathbf{A}$ given by $||\mathbf{A}||_F = \sqrt{\mathrm{Tr}\left[\mathbf{A}^\dagger\mathbf{A}\right]}$ [22]. If we only impose an FIR constraint on $\mathbf{F}(z)$, then the optimal filter coefficients of $\mathbf{F}(z)$ can be found in *closed form* in terms of an appropriate matrix inverse as shown by Tufts and Francis in 1970 [63]. With the additional PU constraint that we impose here, however, this problem becomes more complicated as we show.

Expanding (4.1) and using the PU condition $\widetilde{\mathbf{F}}(z)\mathbf{F}(z) = \mathbf{I}_r$ on $\mathbf{F}(z)$ yields the following.

$$\begin{aligned}\xi \;&=\; \underbrace{\frac{1}{2\pi}\int_0^{2\pi} W(\omega)\left|\left|\mathbf{D}(e^{j\omega})\right|\right|_F^2 \, d\omega + \frac{r}{2\pi}\int_0^{2\pi} W(\omega)\, d\omega}_{a} \\ &\quad - \frac{1}{2\pi}\int_0^{2\pi} W(\omega)\,\mathrm{Tr}\Big[\mathbf{D}^\dagger(e^{j\omega})\mathbf{F}(e^{j\omega}) + \mathbf{F}^\dagger(e^{j\omega})\mathbf{D}(e^{j\omega})\Big] \, d\omega \end{aligned} \tag{4.2}$$

Note that the quantity a in (4.2) is simply a constant and that the only quantity that depends on the system $\mathbf{F}(z)$ is the last term of (4.2). Hence, with the PU constraint in effect, the error ξ is *linear* or first-order in $\mathbf{F}(z)$. This will greatly simplify the optimization problem as will soon be shown.

To help solve this optimization problem with the PU constraint on $\mathbf{F}(z)$, we exploit the complete parameterization of causal FIR PU systems in terms of Householder-like degree-one building blocks [75, 67]. In particular, $\mathbf{F}(z)$ is a causal FIR PU system of McMillan degree $(N-1)$ iff it is of the form

$$\mathbf{F}(z) = \mathbf{V}(z)\mathbf{U} \tag{4.3}$$

where $\mathbf{V}(z)$ is a $p \times p$ PU matrix consisting of $(N-1)$ degree-one Householder-like building blocks of the form

$$\mathbf{V}(z) = \prod_{i=N-1}^{1} \mathbf{V}_i(z)\,,\ \mathbf{V}_i(z) = \mathbf{I}_p - \mathbf{v}_i\mathbf{v}_i^\dagger + z^{-1}\mathbf{v}_i\mathbf{v}_i^\dagger\,,\ 1 \leq i \leq N-1 \tag{4.4}$$

where the vectors $\mathbf{v}_i$ are unit norm vectors, i.e., $\mathbf{v}_i^\dagger\mathbf{v}_i = 1$ for all i. Also, the matrix $\mathbf{U}$ is some $p \times r$ unitary matrix, i.e., $\mathbf{U}^\dagger\mathbf{U} = \mathbf{I}_r$.

Though it is difficult to jointly optimize the parameters $\mathbf{U}$ and $\{\mathbf{v}_k\}$ which minimize ξ from (4.2), it will be shown that optimizing each parameter separately while holding all other parameters fixed is very simple. This will lead to the proposed iterative algorithm whereby the parameters are individually optimized at each iteration.

4.2.1 Optimal Choice of U

Substituting (4.3) into (4.2) yields the following.

$$\begin{aligned}
\xi &= a - \frac{1}{2\pi}\int_0^{2\pi} W(\omega)\,\mathrm{Tr}\Big[\mathbf{D}^\dagger(e^{j\omega})\mathbf{V}(e^{j\omega})\mathbf{U} + \mathbf{U}^\dagger\mathbf{V}^\dagger(e^{j\omega})\mathbf{D}(e^{j\omega})\Big]\,d\omega \\
&= a - \mathrm{Tr}\left[\,\underbrace{\left(\frac{1}{2\pi}\int_0^{2\pi} W(\omega)\mathbf{D}^\dagger(e^{j\omega})\mathbf{V}(e^{j\omega})\,d\omega\right)}_{\mathbf{A}^\dagger}\mathbf{U}\,\right] \\
&\qquad - \mathrm{Tr}\left[\,\mathbf{U}^\dagger\underbrace{\left(\frac{1}{2\pi}\int_0^{2\pi} W(\omega)\mathbf{V}^\dagger(e^{j\omega})\mathbf{D}(e^{j\omega})\,d\omega\right)}_{\mathbf{A}}\,\right] &(4.5)\\
&= a - 2\underbrace{\mathrm{Re}\Big[\,\mathrm{Tr}\Big[\mathbf{U}^\dagger\mathbf{A}\Big]\Big]}_{\mu} &(4.6)
\end{aligned}$$

Note that minimizing ξ from (4.6) is equivalent to maximizing μ. To find the optimal $p \times r$ unitary matrix $\mathbf{U}$ which maximizes μ, we must exploit the singular value decomposition (SVD) [22] of $\mathbf{A}$. Suppose that $\mathbf{A}$ has the following SVD.

$$\mathbf{A} = \mathbf{T}\mathbf{\Sigma}\mathbf{W}^\dagger \tag{4.7}$$

Here, $\mathbf{T}$ and $\mathbf{W}$ are, respectively, $p \times p$ and $r \times r$ unitary matrices. The quantity $\mathbf{\Sigma}$ is a $p \times r$ diagonal matrix of the form

$$\mathbf{\Sigma} = \begin{bmatrix} \mathbf{\Sigma}_0 & \mathbf{0}_{\rho \times (r-\rho)} \\ \mathbf{0}_{(p-\rho)\times\rho} & \mathbf{0}_{(p-\rho)\times(r-\rho)} \end{bmatrix} \tag{4.8}$$

where $\rho = \operatorname{rank}(\mathbf{A})$ and $\mathbf{\Sigma}_0$ is a diagonal matrix of the singular values of $\mathbf{A}$. In other words, we have $\mathbf{\Sigma}_0 = \operatorname{diag}(\sigma_0, \sigma_1, \ldots, \sigma_{\rho-1})$ where $\{\sigma_i\}$ are the singular values of $\mathbf{A}$ which satisfy $\sigma_i > 0$ for all $0 \leq i \leq \rho - 1$. Substituting (4.7) into (4.6) yields the following.

$$\mu = \operatorname{Re}\Big[\operatorname{Tr}\Big[\mathbf{U}^\dagger\mathbf{T}\mathbf{\Sigma}\mathbf{W}^\dagger\Big]\Big] = \operatorname{Re}\Big[\operatorname{Tr}\Big[\mathbf{\Sigma}\underbrace{\mathbf{W}^\dagger\mathbf{U}^\dagger\mathbf{T}}_{\mathbf{G}^\dagger}\Big]\Big] \tag{4.9}$$

Note that the $p \times r$ matrix $\mathbf{G} = \mathbf{T}^\dagger\mathbf{U}\mathbf{W}$ is unitary, i.e., $\mathbf{G}^\dagger\mathbf{G} = \mathbf{I}_r$. As such, the components of $\mathbf{G}$ satisfy

$$\operatorname{Re}\Big[[\mathbf{G}]_{k,\ell}\Big] \leq 1 \tag{4.10}$$

with equality iff $[\mathbf{G}]_{k,q} = \delta(q-\ell)$ and $[\mathbf{G}]_{p,\ell} = \delta(p-k)$, since the columns of $\mathbf{G}$ form an orthonormal set of vectors [22]. Using (4.8) in (4.9) yields

$$\mu = \operatorname{Re}\Big[\operatorname{Tr}\Big[\mathbf{\Sigma}\mathbf{G}^\dagger\Big]\Big] = \operatorname{Re}\left[\sum_{i=0}^{\rho-1}\sigma_i\,[\mathbf{G}]_{i,i}^*\right] = \sum_{i=0}^{\rho-1}\sigma_i\operatorname{Re}\Big[[\mathbf{G}]_{i,i}^*\Big] = \sum_{i=0}^{\rho-1}\sigma_i\operatorname{Re}\Big[[\mathbf{G}]_{i,i}\Big] \tag{4.11}$$

In light of (4.10) and the fact that $\sigma_i > 0$ for all i, from (4.11), we have

$$\mu \leq \sum_{i=0}^{\rho-1}\sigma_i \tag{4.12}$$

with equality iff $[\mathbf{G}]_{i,q} = \delta(q-i)$ and $[\mathbf{G}]_{p,i} = \delta(p-i)$ for all $0 \leq i \leq \rho - 1$. Since $\mathbf{G}$ is unitary, we have equality iff

$$\mathbf{G} = \mathbf{G}_{\text{opt}} = \begin{bmatrix} \mathbf{I}_\rho & \mathbf{0}_{\rho\times(r-\rho)} \\ \mathbf{0}_{(p-\rho)\times\rho} & \mathbf{G}_0 \end{bmatrix} \tag{4.13}$$

where $\mathbf{G}_0$ is an arbitrary $(p-\rho)\times(r-\rho)$ unitary matrix, i.e., $\mathbf{G}_0^\dagger\mathbf{G}_0 = \mathbf{I}_{(r-\rho)}$. As $\mathbf{G} = \mathbf{T}^\dagger\mathbf{U}\mathbf{W}$, we have $\mathbf{U} = \mathbf{T}\mathbf{G}\mathbf{W}^\dagger$, and so the optimum $\mathbf{U}$ and corresponding optimal value of ξ is given by (4.12) and (4.6) to be the following.

$$\boxed{\mathbf{U}_{\text{opt}} = \mathbf{T}\mathbf{G}_{\text{opt}}\mathbf{W}^\dagger \text{ with } \mathbf{G}_{\text{opt}} \text{ as in (4.13)}\,,\ \xi_{\text{opt}} = a - 2\left(\sum_{i=0}^{\rho-1}\sigma_i\right)} \tag{4.14}$$

In the special case where $\rho = r$ (i.e., $\mathbf{A}$ has full rank), we have

$$\mathbf{U}_{\text{opt}} = \mathbf{T} \begin{bmatrix} \mathbf{W}^{\dagger} \\ \\ \mathbf{0}_{(p-r)\times r} \end{bmatrix} \,, \ \xi_{\text{opt}} = a - 2\left(\sum_{i=0}^{r-1} \sigma_i\right)$$

Since the matrices $\mathbf{T}$ and $\mathbf{W}$ from (4.14) depend on $\mathbf{V}(z)$, the choice of $\mathbf{U}$ from (4.14) is optimal for *fixed* $W(\omega)$, $\mathbf{D}(e^{j\omega})$, and $\mathbf{V}(z)$.

4.2.2 Optimal Choice of $\mathbf{v}_k$

In order to find the optimal choice of $\mathbf{v}_k$ assuming that all other parameters are fixed, we must cleverly extract only those portions of ξ which depend on $\mathbf{v}_k$. Similar to what was done for the iterative method of the previous chapter (see (3.15) and (3.16)), for simplicity, let us define the following $p \times p$ matrices.

$$\mathcal{L}_k(z) \triangleq \begin{cases} \displaystyle\prod_{i=N-1}^{k+1} \mathbf{V}_i(z)\,, & 0 \le k \le N-2 \\ \mathbf{I}_p\,, & k = N-1 \end{cases} \tag{4.15}$$

$$\mathcal{R}_k(z) \triangleq \begin{cases} \mathbf{I}_p\,, & k = 1 \\ \displaystyle\prod_{i=k-1}^{1} \mathbf{V}_i(z)\,, & 2 \le k \le N \end{cases} \tag{4.16}$$

As before, note that $\mathcal{L}_k(z)$ and $\mathcal{R}_k(z)$ are, respectively, the left and right neighbors of the matrix $\mathbf{V}_k(z)$ for $1 \le k \le N-1$ appearing in $\mathbf{V}(z)$ from (4.4). In other words, the following relation holds true here.

$$\mathbf{V}(z) = \mathcal{L}_k(z)\mathbf{V}_k(z)\mathcal{R}_k(z)\,, \ 1 \le k \le N-1 \tag{4.17}$$

Also note that by construction, we have $\mathcal{L}_0(z) = \mathcal{R}_N(z) = \mathbf{V}(z)$. Substituting (4.17) and (4.4) into (4.3) and (4.2) yields the following.

$$\begin{aligned}
\xi \;&=\; \underbrace{a - \frac{1}{2\pi}\int_0^{2\pi} W(\omega)\,\mathrm{Tr}\Big[\mathbf{D}^\dagger(e^{j\omega})\mathcal{L}_k(e^{j\omega})\mathcal{R}_k(e^{j\omega})\mathbf{U}\Big]\;d\omega}_{c} \\
&\quad + \frac{1}{2\pi}\int_0^{2\pi} W(\omega)\,\mathrm{Tr}\Big[\mathbf{D}^\dagger(e^{j\omega})\mathcal{L}_k(e^{j\omega})\left(1 - e^{-j\omega}\right)\mathbf{v}_k\mathbf{v}_k^\dagger\mathcal{R}_k(e^{j\omega})\mathbf{U}\Big]\;d\omega \\
&\quad \underbrace{- \frac{1}{2\pi}\int_0^{2\pi} W(\omega)\,\mathrm{Tr}\Big[\mathbf{U}^\dagger\mathcal{R}_k^\dagger(e^{j\omega})\mathcal{L}_k^\dagger(e^{j\omega})\mathbf{D}(e^{j\omega})\Big]\;d\omega}_{c^*} \\
&\quad + \frac{1}{2\pi}\int_0^{2\pi} W(\omega)\,\mathrm{Tr}\Big[\mathbf{U}^\dagger\mathcal{R}_k^\dagger(e^{j\omega})\left(1 - e^{j\omega}\right)\mathbf{v}_k\mathbf{v}_k^\dagger\mathcal{L}_k^\dagger(e^{j\omega})\mathbf{D}(e^{j\omega})\Big]\;d\omega \qquad (4.18) \\
&=\; a - 2\,\mathrm{Re}\,[c] + \mathbf{v}_k^\dagger\underbrace{\left[\frac{1}{2\pi}\int_0^{2\pi} W(\omega)\left(1 - e^{-j\omega}\right)\mathcal{R}_k(e^{j\omega})\mathbf{U}\mathbf{D}^\dagger(e^{j\omega})\mathcal{L}_k(e^{j\omega})\,d\omega\right]}_{\mathbf{B}}\mathbf{v}_k \\
&\quad + \mathbf{v}_k^\dagger\underbrace{\left[\frac{1}{2\pi}\int_0^{2\pi} W(\omega)\left(1 - e^{j\omega}\right)\mathcal{L}_k^\dagger(e^{j\omega})\mathbf{D}(e^{j\omega})\mathbf{U}^\dagger\mathcal{R}_k^\dagger(e^{j\omega})\,d\omega\right]}_{\mathbf{B}^\dagger}\mathbf{v}_k \qquad (4.19) \\
&=\; a - 2\,\mathrm{Re}\,[c] + \mathbf{v}_k^\dagger\underbrace{\left(\mathbf{B} + \mathbf{B}^\dagger\right)}_{\mathbf{Q}}\mathbf{v}_k = a - 2\,\mathrm{Re}\,[c] + \underbrace{\mathbf{v}_k^\dagger\mathbf{Q}\mathbf{v}_k}_{\nu} \qquad (4.20)
\end{aligned}$$

Here, the quantity c defined in (4.18) depends on all of the parameters *except* $\mathbf{v}_k$. Hence, to minimize ξ with respect to $\mathbf{v}_k$, we must minimize the quantity ν from (4.20). But note that $\nu = \mathbf{v}_k^\dagger\mathbf{Q}\mathbf{v}_k$ is simply a *quadratic form* corresponding to the Hermitian matrix $\mathbf{Q}$ [22]. As $\mathbf{v}_k$ must satisfy $\mathbf{v}_k^\dagger\mathbf{v}_k = 1$, it follows from *Rayleigh's principle* [22] that the optimal $\mathbf{v}_k$ must be a unit norm eigenvector corresponding to the smallest eigenvalue of $\mathbf{Q}$. If $\lambda_{\min}$ denotes the smallest eigenvalue of $\mathbf{Q}$ and $\mathbf{w}_{\min}$ is any unit norm eigenvector corresponding to $\lambda_{\min}$, then the optimum choice of $\mathbf{v}_k$ and corresponding optimal ξ are given by (4.20) to be the following.

$$\boxed{\mathbf{v}_{k,\mathrm{opt}} = \mathbf{w}_{\min}\,,\ \ \xi_{\mathrm{opt}} = a - 2\,\mathrm{Re}\,[c] + \lambda_{\min}} \qquad (4.21)$$

Note that since $\mathbf{w}_{\min}$ from (4.21) depends on $\mathcal{L}_k(z)$, $\mathcal{R}_k(z)$, and $\mathbf{U}$, it follows that the choice of $\mathbf{v}_k$ from (4.21) is optimal for *fixed* $W(\omega)$, $\mathbf{D}(e^{j\omega})$, $\mathbf{U}$, and all $\mathbf{v}_i$ for which $i \neq k$.

In summary, finding the optimal parameters corresponding to the Householder-like factorization of causal FIR PU systems is simple if the parameters are optimized individually. The process of updating the individual parameters to their optimal values forms the basis of the proposed iterative algorithm for solving the FIR PU approximation problem, which we now present.

4.2.3 Iterative Greedy Algorithm for Solving the Approximation Problem

Let ξ_m denote the mean-squared error at the m-th iteration for $m \geq 0$. Then, the iterative algorithm for solving the FIR PU approximation problem is as follows.

Initialization:

1. Generate a random $p \times r$ unitary matrix $\mathbf{U}$ and $(N-1)$ $p \times 1$ random unit norm vectors $\mathbf{v}_i, 1 \leq i \leq N-1$.
2. Compute the matrix $\mathcal{R}_N(z)$ using (4.16).

Iteration: For $m \geq 0$, do the following.

1. *If m is a multiple of N:*
   (a) Calculate the optimal $\mathbf{U}$ and corresponding ξ_m using (4.14), (4.7), and (4.5) with $\mathbf{V}(z) = \mathcal{R}_N(z)$.
   (b) Compute $\mathcal{L}_0(z) = \mathbf{V}(z)$ and $\mathcal{R}_1(z) = \mathbf{I}_p$.

   Otherwise, if $m \equiv k \bmod N$ where $1 \leq k \leq N-1$:
   (a) From (4.15), update the left matrix as $\mathcal{L}_k(z) = \mathcal{L}_{k-1}(z)\widetilde{\mathbf{V}}_k(z)$.
   (b) Calculate the optimal $\mathbf{v}_k$ and corresponding ξ_m using (4.21), (4.20), (4.19), and (4.18).
   (c) From (4.16), update the right matrix as $\mathcal{R}_{k+1}(z) = \mathbf{V}_k(z)\mathcal{R}_k(z)$.
2. Increment m by 1 and return to Step 1.

Note that like the iterative algorithm of the previous chapter (see Sec. 3.3.2), as the iterations progress, the left matrix is shortened by the old optimal vectors $\mathbf{v}_k$ whereas the right matrix is lengthened by the newly computed ones. After all $\mathbf{v}_k$s have been optimized, the left matrix assumes the value of the right matrix while the right matrix is then refreshed to be the identity matrix.

Similar to the iterative algorithm of Sec. 3.3.2, at each stage in the iteration, we are optimizing one parameter while fixing the rest, and so the above technique is a *greedy algorithm*. As such, the error ξ_m is guaranteed to be monotonic nonincreasing as a function of m. Furthermore, as ξ_m has a lower bound (i.e., we always have $\xi_m \geq 0$), ξ_m is guaranteed to have a limit as $m \to \infty$ [67]. Thus, the algorithm is guaranteed to converge monotonically to a local optimum. Prior to presenting simulation results for the iterative algorithm, we introduce the phase feedback modification for cases in which the desired response $\mathbf{D}(e^{j\omega})$ has a *phase-type ambiguity*, which we will define shortly.

4.3 Phase Feedback Modification

4.3.1 Phase-Type Ambiguity

Referring back to Fig. 1.13(b), suppose that we would like to design an FIR PU synthesis polyphase matrix approximant to that of the infinite-order PCFB as described in Section 1.2.1. In this case, the desired response $\mathbf{D}(e^{j\omega})$ is any system that totally decorrelates and spectrally majorizes the blocked input signal $\mathbf{x}(n)$ (i.e., $\mathbf{D}(e^{j\omega})$ diagonalizes $\mathbf{S}_{\mathbf{xx}}(e^{j\omega})$ for every ω in such a way that the eigenvalues are arranged in descending order [68, 1]). This implies a *nonuniqueness* for the desired response $\mathbf{D}(e^{j\omega})$. To see this, note that $\mathbf{D}(e^{j\omega})$ must contain the unit norm eigenvectors of $\mathbf{S}_{\mathbf{xx}}(e^{j\omega})$ arranged in some order to preserve the spectral majorization property. Partitioning $\mathbf{D}(e^{j\omega})$ into its columns as

$$\mathbf{D}(e^{j\omega}) = \left[\begin{array}{cccc} \mathbf{d}_0(e^{j\omega}) & \mathbf{d}_1(e^{j\omega}) & \cdots & \mathbf{d}_{M-1}(e^{j\omega}) \end{array}\right] \tag{4.22}$$

it follows that $\mathbf{d}_k(e^{j\omega})$ is a unit norm eigenvector of $\mathbf{S}_{\mathbf{xx}}(e^{j\omega})$ for all ω. As any unit magnitude scale factor of a unit norm eigenvector is itself a unit norm eigenvector, it follows that any system of the form

$$\begin{aligned} \mathbf{D}_a(e^{j\omega}) &= \left[\begin{array}{cccc} \mathbf{d}_0(e^{j\omega})e^{j\phi_0(\omega)} & \mathbf{d}_1(e^{j\omega})e^{j\phi_1(\omega)} & \cdots & \mathbf{d}_{M-1}(e^{j\omega})e^{j\phi_{M-1}(\omega)} \end{array}\right] \\ &= \mathbf{D}(e^{j\omega})\mathbf{\Lambda}(e^{j\omega})\,,\ \text{where } \mathbf{\Lambda}(e^{j\omega}) = \text{diag}\Big(e^{j\phi_0(\omega)}, e^{j\phi_1(\omega)}, \ldots, e^{j\phi_{M-1}(\omega)}\Big) \end{aligned} \tag{4.23}$$

is a valid desired response for an infinite-order PCFB. If the eigenvalues of $\mathbf{S}_{\mathbf{xx}}(e^{j\omega})$ are distinct for all ω, then all valid desired responses are related to each other as in (4.23). On the other hand, if the eigenvalues are not distinct at some frequency, say ω_0, then at that frequency, the columns of any one desired response corresponding to the nondistinct eigenvalues can be expressed as a *unitary* combination of the same columns of any other desired response. As an example, suppose that at ω_0, the largest eigenvalue of $\mathbf{S}_{\mathbf{xx}}(e^{j\omega})$ has multiplicity 2. Then, given any desired response $\mathbf{D}(e^{j\omega})$

of the form given in (4.22), we can obtain another desired response $\mathbf{D}_a(e^{j\omega})$ in which we have

$$\begin{aligned}\mathbf{D}_a(e^{j\omega_0}) &= \Big[\Big[\begin{array}{cc} \mathbf{d}_0(e^{j\omega_0}) & \mathbf{d}_1(e^{j\omega_0}) \end{array} \Big] \mathbf{\Phi}(\omega_0) \quad \mathbf{d}_2(e^{j\omega_0})e^{j\phi_2(\omega_0)} \quad \cdots \quad \mathbf{d}_{M-1}(e^{j\omega_0})e^{j\phi_{M-1}(\omega_0)} \Big] \\ &= \mathbf{D}(e^{j\omega_0}) \underbrace{\begin{bmatrix} \mathbf{\Phi}(\omega_0) & \mathbf{0} & \cdots & \cdots & \mathbf{0} \\ \mathbf{0} & e^{j\phi_2(\omega_0)} & 0 & \cdots & 0 \\ \vdots & 0 & \ddots & \ddots & \vdots \\ \vdots & \vdots & \ddots & \ddots & 0 \\ \mathbf{0} & 0 & \cdots & 0 & e^{j\phi_{M-1}(\omega_0)} \end{bmatrix}}_{\mathbf{\Lambda}(e^{j\omega_0})}\end{aligned}$$

where $\mathbf{\Phi}(\omega_0)$ is a 2×2 unitary matrix. In general, for an eigenvalue with multiplicity μ, the corresponding eigenvectors of one desired response can be related in terms of any other via a $\mu \times \mu$ unitary matrix.

Any $p \times r$ desired response $\mathbf{D}_a(e^{j\omega})$ which has a nonuniqueness of the form

$$\mathbf{D}_a(e^{j\omega}) = \mathbf{D}(e^{j\omega})\mathbf{\Lambda}(e^{j\omega}) \tag{4.24}$$

where $\mathbf{D}(e^{j\omega})$ is some $p \times r$ given desired response and $\mathbf{\Lambda}(e^{j\omega})$ is an $r \times r$ block diagonal matrix of unitary matrices will be said to have a *phase-type ambiguity*, since the phases of the columns are arbitrary in this case. (In the PCFB example described here, the number of blocks of $\mathbf{\Lambda}(e^{j\omega})$ is equal to the number of distinct eigenvalues of $\mathbf{S}_{\mathbf{xx}}(e^{j\omega})$ and the size of each block is equal to the multiplicity of each of these eigenvalues.) When the desired response has a phase-type ambiguity, some desired responses may yield a better overall FIR PU approximant than others. The reason for this is that the causal FIR constraint we assume here imposes severe restrictions on the allowable phase of the FIR PU approximant. Since we do not know the best desired response to choose a priori, we propose a *phase feedback modification* to the iterative greedy algorithm of Section 4.2.3 in order to *learn* the proper desired response.

4.3.2 Derivation of the Phase Feedback Modification

Suppose that we are given a desired response $\mathbf{D}(e^{j\omega})$ with a phase-type ambiguity as in (4.24). In addition, suppose that the matrix $\mathbf{\Lambda}(e^{j\omega})$ from (4.24) corresponds only to a simple phase-type ambiguity of the form

$$\mathbf{\Lambda}(e^{j\omega}) = \operatorname{diag}\Big(e^{j\phi_0(\omega)}, e^{j\phi_1(\omega)}, \ldots, e^{j\phi_{r-1}(\omega)}\Big) \quad \forall\ \omega$$

The question then arises as to how to choose the phases $\{\phi_k(\omega)\}$ to minimize the mean-squared error in (4.1) with the desired response $\mathbf{D}(e^{j\omega})$ replaced by $\mathbf{D}_a(e^{j\omega})$, which is given to be

$$\xi = \frac{1}{2\pi}\int_0^{2\pi} W(\omega)\left|\left|\mathbf{D}_a(e^{j\omega}) - \mathbf{F}(e^{j\omega})\right|\right|_F^2 \, d\omega \tag{4.25}$$

To solve this problem, we partition the old given desired response $\mathbf{D}(e^{j\omega})$ and the FIR PU approximant $\mathbf{F}(e^{j\omega})$ as follows.

$$\begin{aligned}
\mathbf{D}(e^{j\omega}) &= \begin{bmatrix} \mathbf{d}_0(e^{j\omega}) & \mathbf{d}_1(e^{j\omega}) & \cdots & \mathbf{d}_{r-1}(e^{j\omega}) \end{bmatrix} \\
\mathbf{F}(e^{j\omega}) &= \begin{bmatrix} \mathbf{f}_0(e^{j\omega}) & \mathbf{f}_1(e^{j\omega}) & \cdots & \mathbf{f}_{r-1}(e^{j\omega}) \end{bmatrix}
\end{aligned}$$

Then, from (4.25), it can easily be shown that we have

$$\xi = \frac{1}{2\pi}\int_0^{2\pi} W(\omega)\left(\sum_{k=0}^{r-1}\left|\left|\mathbf{d}_k(e^{j\omega})e^{j\phi_k(\omega)} - \mathbf{f}_k(e^{j\omega})\right|\right|_2^2\right) d\omega \tag{4.26}$$

Note that we can minimize ξ from (4.26) by minimizing each term of the summation *pointwise in frequency.* This can be done here since the phases $\{\phi_k(\omega)\}$ are independent functions of k that have arbitrary response (in terms of ω). Hence, minimizing ξ is tantamount to minimizing

$$\ell_k(\omega) \triangleq \left|\left|\mathbf{d}_k(e^{j\omega})e^{j\phi_k(\omega)} - \mathbf{f}_k(e^{j\omega})\right|\right|_2^2 \tag{4.27}$$

for each k. Upon expanding $\ell_k(\omega)$ in (4.27), we get the following.

$$\ell_k(\omega) = \left|\left|\mathbf{d}_k(e^{j\omega})\right|\right|_2^2 + \left|\left|\mathbf{f}_k(e^{j\omega})\right|\right|_2^2 - e^{-j\phi_k(\omega)}\mathbf{d}_k^\dagger(e^{j\omega})\mathbf{f}_k(e^{j\omega}) - \mathbf{f}_k^\dagger(e^{j\omega})\mathbf{d}_k(e^{j\omega})e^{j\phi_k(\omega)} \tag{4.28}$$

Expressing $\mathbf{d}_k^\dagger(e^{j\omega})\mathbf{f}_k(e^{j\omega})$ as

$$\mathbf{d}_k^\dagger(e^{j\omega})\mathbf{f}_k(e^{j\omega}) = \left|\mathbf{d}_k^\dagger(e^{j\omega})\mathbf{f}_k(e^{j\omega})\right| e^{j\theta_k(\omega)} \tag{4.29}$$

then we have $\mathbf{f}_k^\dagger(e^{j\omega})\mathbf{d}_k(e^{j\omega}) = \left|\mathbf{d}_k^\dagger(e^{j\omega})\mathbf{f}_k(e^{j\omega})\right| e^{-j\theta_k(\omega)}$, and so from (4.28), we get

$$\ell_k(\omega) = \left|\left|\mathbf{d}_k(e^{j\omega})\right|\right|_2^2 + \left|\left|\mathbf{f}_k(e^{j\omega})\right|\right|_2^2 - 2\left|\mathbf{d}_k^\dagger(e^{j\omega})\mathbf{f}_k(e^{j\omega})\right| \cos(\theta_k(\omega) - \phi_k(\omega)) \tag{4.30}$$

Hence, to minimize $\ell_k(\omega)$, we must choose $\phi_k(\omega)$ as follows.

$$\phi_{k,\text{opt}}(\omega) = \theta_k(\omega) \tag{4.31}$$

Thus, from (4.31) and (4.29), it can be seen that the optimal thing to do for each column of the desired response is to *mix* its phase with that of the FIR PU approximant. In other words, the phase of the FIR PU approximant must be fed back to the desired response in order to minimize the mean-squared error.

4.3.3 Greediness of the Phase Feedback Modification

With the phase feedback modification of (4.31) in effect, it can be shown that the iterative algorithm from Section 4.2.3 still remains greedy. To see this, suppose that a phase feedback is performed at the m-th iteration and let $\xi_{m,\text{before}}$ and $\xi_{m,\text{after}}$ denote, respectively, the error before and after the phase feedback. Note that $\xi_{m,\text{before}}$ and $\xi_{m,\text{after}}$ are given by (4.1) and (4.25), respectively. For simplicity of notation, let $\mathbf{f}_{k;m}(e^{j\omega})$ denote the k-th column of $\mathbf{F}(e^{j\omega})$ at the m-th iteration and let $\theta_{k;m}(\omega)$ denote the phase of the inner product $\mathbf{d}_k^\dagger(e^{j\omega})\mathbf{f}_{k;m}(e^{j\omega})$ as in (4.29). Using (4.30) and (4.27) in (4.26), we get

$$\xi_{m,\text{before}} - \xi_{m,\text{after}} = \frac{1}{\pi}\int_0^{2\pi} W(\omega)\left(\sum_{k=0}^{r-1}\left|\mathbf{d}_k^\dagger(e^{j\omega})\mathbf{f}_{k;m}(e^{j\omega})\right|(1-\cos(\theta_{k;m}(\omega)))\right)d\omega \geq 0$$

since the integrand from above is always nonnegative. Hence, it follows that $\xi_{m,\text{after}} \leq \xi_{m,\text{before}}$. As $\xi_{m+1,\text{after}} \leq \xi_{m,\text{after}}$, since the unmodified algorithm is greedy, we have $\xi_{m+1,\text{after}} \leq \xi_{m,\text{before}}$. Thus, the algorithm remains greedy even with the phase feedback modification in effect. As will be shown in Sec. 4.4.1 regarding the design of PCFB-like FIR PU filter banks, the phase feedback modification can offer a better *magnitude-type* fit to the desired response than the unmodified algorithm.

4.4 Simulation Results

4.4.1 Design of PCFB-like FIR PU Filter Banks

Recall that the proposed iterative algorithm can be used to design a PCFB-like FIR PU filter bank when the desired response $\mathbf{D}(e^{j\omega})$ is the synthesis polyphase matrix of any infinite-order PCFB for the psd $\mathbf{S}_{\mathbf{xx}}(z)$ of the blocked filter bank input $\mathbf{x}(n)$ from Fig. 1.13(b). Suppose that the unblocked scalar input signal $x(n)$ from Fig. 1.13 is a real WSS autoregressive order 4 (AR(4)) process whose psd $S_{xx}(e^{j\omega})$ is as shown in Fig. 4.1. From Sec. 2.2.1.1, recall that if $x(n)$ is itself WSS with psd $S_{xx}(z)$, then the psd of the blocked process $\mathbf{S}_{\mathbf{xx}}(z)$ is a pseudocirculant matrix (see the Appendix of Chapter 2) formed from $S_{xx}(z)$. In this case, the synthesis filters $\{F_k(z)\}$ corresponding to any infinite-order PCFB are ideal bandpass compaction filters corresponding to $S_{xx}(e^{j\omega})$ and its *peeled spectra* [68]. Also recall that because of the assumed orthonormality condition of (1.10), it follows that the corresponding analysis filters $\{H_k(z)\}$ are also ideal compaction filters.

Here, we considered the design of an $M = 4$ channel system. To first test the proposed algorithm, we opted to see the effects of the phase-type ambiguity of (4.24) on the desired response $\mathbf{D}(e^{j\omega})$ for a fixed synthesis polyphase matrix length of $N = 10$ and fixed weight function $W(\omega) \equiv 1$. This implies

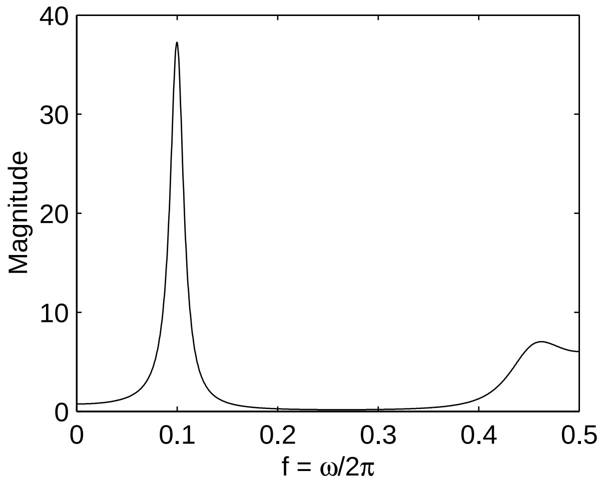

Figure 4.1: Input psd $S_{xx}(e^{j\omega})$ of the AR(4) process $x(n)$.

that the corresponding synthesis filters $\{F_k(z)\}$ are causal and FIR of length $MN = 40$. All integrals were evaluated numerically using 1,024 uniformly spaced frequency samples. A plot of the observed error ξ_m as a function of the iteration index m for both the unmodified and phase feedback modified algorithms is shown in Fig. 4.2(a) for a total of KN iterations[1], where we chose $K = \left\lceil \frac{3{,}000}{N} \right\rceil$. A magnified plot of the first 20 iterations is shown in Fig. 4.2(b). For the phase feedback modified algorithm, a phase feedback was performed at every iteration. As can be seen in Fig. 4.2(a), both algorithms exhibit a monotonically nonincreasing error that appears to be approaching a limit as expected. Both errors appear to saturate after about 500 iterations. In addition, it can be seen that the error for the phase feedback modified algorithm is much lower overall than that of the unmodified one. Though it is difficult to see (view Fig. 4.2(b) for more clarity), with the randomly chosen initial conditions, we had $\xi_0 = 6.8570$ for the unmodified algorithm and $\xi_0 = 7.2634$ for the phase feedback modified one. Clearly, the phase feedback modification here yielded an overall lower mean-squared error by finding, in some sense, the best PCFB to accomodate the causal FIR PU constraint in effect.

To see the effects of the phase feedback modification more clearly, in Figs. 4.3 and 4.4, we have plotted, respectively, the magnitude squared responses of the resulting synthesis filters $\{F_k(z)\}$ for the original and modified algorithms together with the responses of the infinite-order PCFB synthesis filters. (Due to the phase-type ambiguity present in $\mathbf{D}(e^{j\omega})$ here, only the magnitude has

[1] We opted for an integer multiple of N iterations to ensure that all of the parameters were optimized the same number of times. Also, for all of the simulation results presented in this section, a total of KN iterations was used each time, where $K = \left\lceil \frac{3{,}000}{N} \right\rceil$.

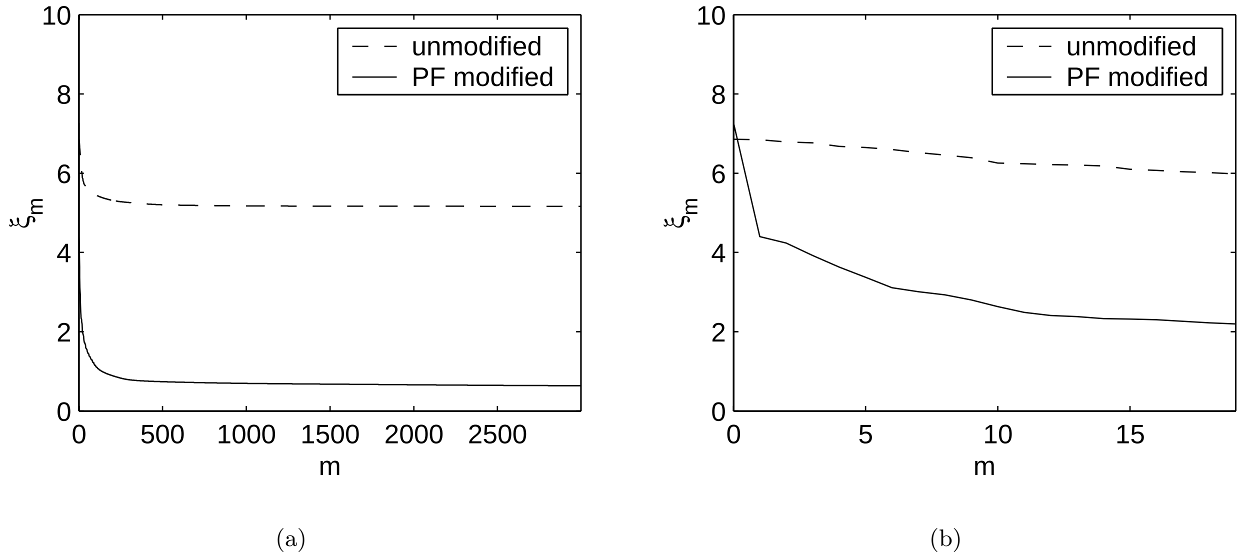

Figure 4.2: Mean-squared error ξ_m vs. iteration m for both the unmodified and phase feedback modified iterative algorithms. (a) Plot of $KN = 3,000$ iterations, (b) Magnified plot of the first 20 iterations.

been plotted since the infinite-order PCFB filters can have arbitrary phase.) As can be seen, the FIR synthesis filters designed with the phase feedback modification offer a better *magnitude-type* fit to the infinite-order PCFB filters than those designed with the unmodified algorithm. Due to this observed phenomenon, we opted to carry out the rest of the PCFB simulations using the phase feedback modification. It should also be noted that the remainder of the PCFB simulations in this section were carried out for the real AR(4) process $x(n)$ with psd $S_{xx}(e^{j\omega})$ as in Fig. 4.1.

4.4.1.1 Multiresolution Optimality Results

Recall from Sec. 1.2.1 and 3.6.2 that due to the subband majorization property of the PCFB, the PCFB is optimal for maximizing the proportion of the partial subband variances to the total variance. By preserving only L out of M subbands, this proportion is given by

$$P(L) \triangleq \frac{\displaystyle\sum_{i=0}^{L-1} \sigma_{w_i}^2}{\displaystyle\sum_{i=0}^{M-1} \sigma_{w_i}^2}\ ,\ 1 \leq L \leq M$$

Note that $P(L)$ for each L is a measure of multiresolution optimality as it measures the amount of signal energy compacted into the first L subbands of the filter bank.

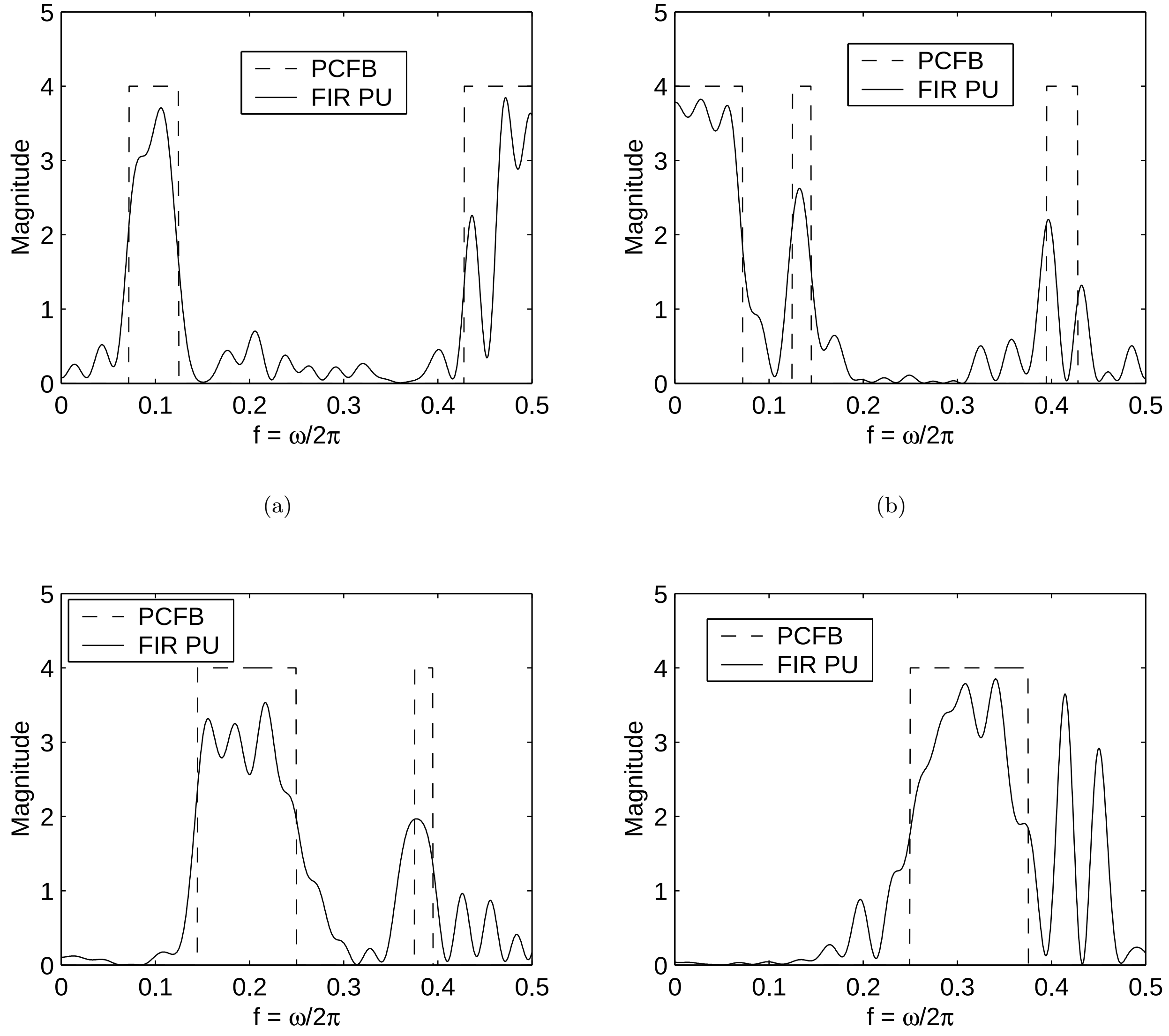

(a)

(b)

(c)

(d)

Figure 4.3: Magnitude squared responses of the PCFB and FIR PU synthesis filters using the unmodified iterative algorithm. (a) $F_0(z)$, (b) $F_1(z)$, (c) $F_2(z)$, (d) $F_3(z)$.

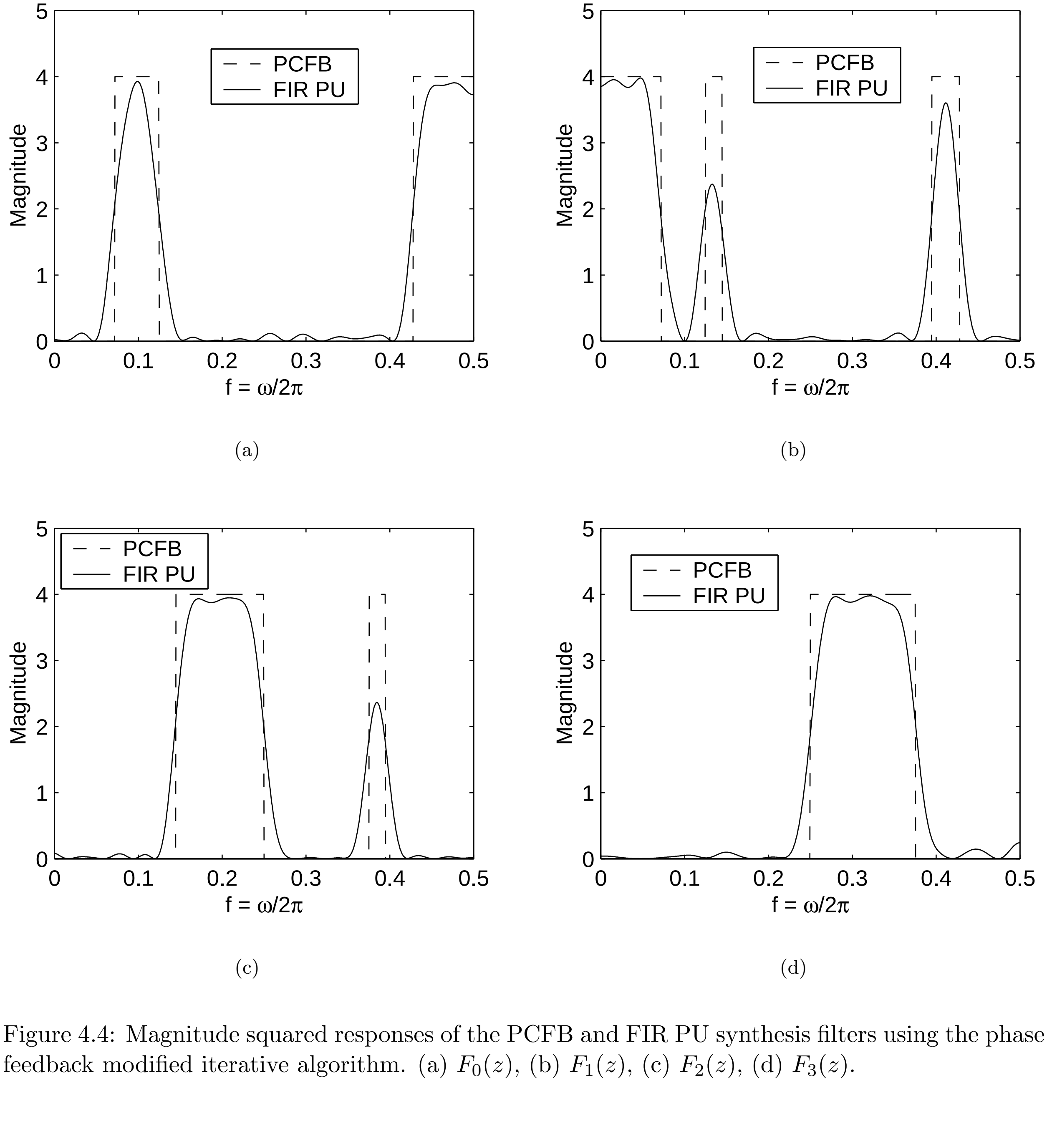

(a)

(b)

(c)

(d)

Figure 4.4: Magnitude squared responses of the PCFB and FIR PU synthesis filters using the phase feedback modified iterative algorithm. (a) $F_0(z)$, (b) $F_1(z)$, (c) $F_2(z)$, (d) $F_3(z)$.

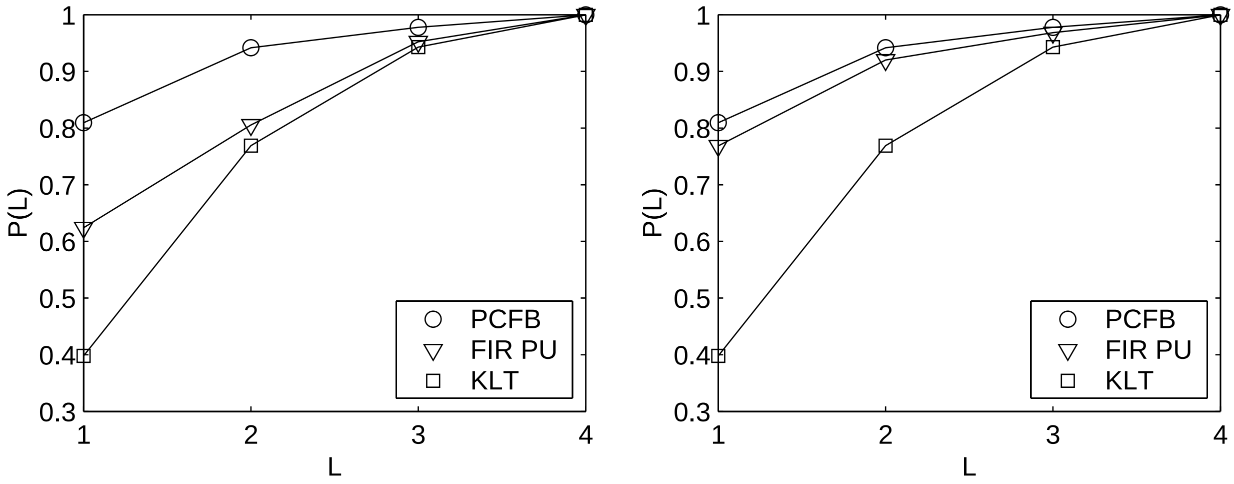

(a)

(b)

Figure 4.5: Proportion of the total variance $P(L)$ as a function of the number of subbands kept L for an $M = 4$ channel system with (a) $N = 3$ and (b) $N = 10$.

Using the proposed iterative algorithm for the design of a PCFB-like filter bank for the real AR(4) process $x(n)$ considered here, a plot of the observed proportion $P(L)$ as a function of the number of subbands preserved L is shown in Fig. 4.5 for $N = 3$ and $N = 10$. Included in Fig. 4.5 are the performances of the zeroth-order PCFB (namely, the KLT) as well as the infinite-order one. As can be seen, both FIR filter banks designed outperform the KLT. Furthermore, by comparing Fig. 4.5(a) and (b), it can be seen that as the filter order increased, the subband variances came closer to those of the infinite-order PCFB.

To show another example of this phenomenon, we considered the design of an $M = 8$ channel system. For this case, a plot of $P(L)$ as a function of L is shown in Fig. 4.6(a) and (b) for $N = 3$ and $N = 10$, respectively. As before, it can be seen that as the filter order increased, the subband variances of the FIR filter banks came closer to those of the infinite-order PCFB[2]. This is in accordance with intuition which states that as the filter order increases, the designed FIR PU filter banks should behave more and more like the infinite-order PCFB.

[2] It should be noted that this phenomenon continues to hold true for larger M, however the results become less dramatic since the gap between the KLT and infinite-order PCFB shrinks as M increases.

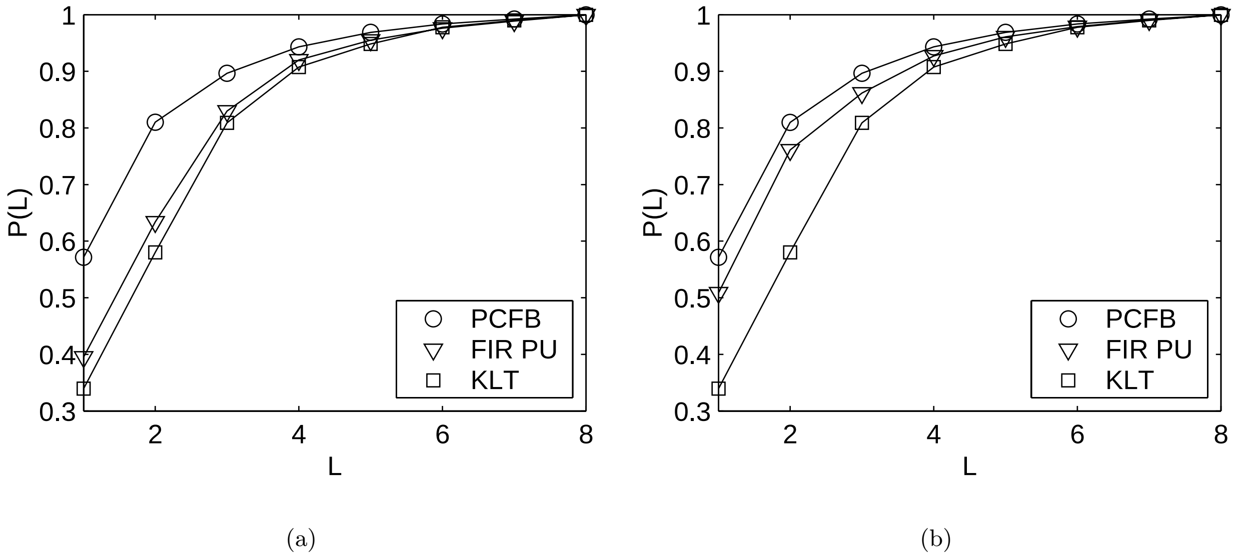

Figure 4.6: Proportion of the total variance $P(L)$ as a function of the number of subbands kept L for an $M = 8$ channel system with (a) $N = 3$ and (b) $N = 10$.

4.4.1.2 Coding Gain Results

From Sec. 1.2.1 and 3.6.1, recall that the PCFB is optimal for coding gain with optimal bit allocation in the subbands [62, 1]. Assuming optimal bit allocation, the coding gain is given by [67]

$$G_{\text{code}} = \frac{\dfrac{1}{M}\displaystyle\sum_{i=0}^{M-1} \sigma_{w_i}^2}{\left(\displaystyle\prod_{i=0}^{M-1} \sigma_{w_i}^2\right)^{\frac{1}{M}}}$$

Here, the proposed iterative algorithm was used to design an $M = 4$ channel PCFB-like filter bank in which the synthesis polyphase matrix length N was varied from 1 to 10. A plot of the coding gain observed as a function of N is shown in Fig. 4.7[3]. In addition, we have included the coding gain of the KLT (2.1276 dB) along with that of the infinite-order PCFB (8.3081 dB). From Fig. 4.7, we can see that even at small filter orders the FIR PU filter banks designed yielded a much larger coding gain than the KLT. Furthermore, the optimized FIR filter banks exhibited a *monotonically increasing* coding gain. This is consistent with intuition which dictates that as the filter order increases, the FIR filter banks designed should become more and more PCFB-like. From Fig. 4.7, it appears as though the coding gain of the FIR filter banks will asymptotically achieve the infinite-order PCFB performance as $N \to \infty$.

[3] For $N = 1$, the KLT of $\mathbf{x}(n)$ was chosen as the optimal solution, since it is the PCFB for this class of filter banks.

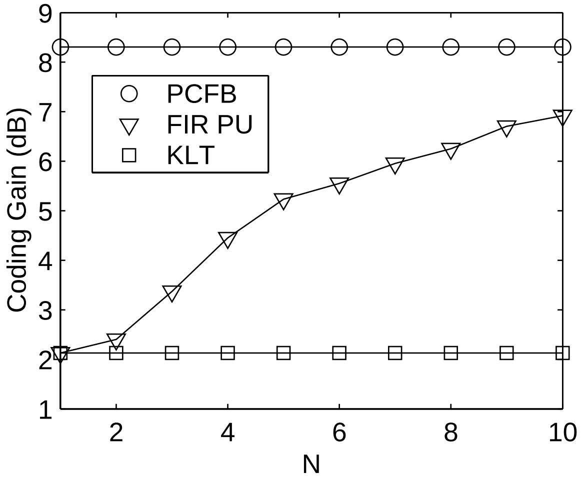

Figure 4.7: Observed coding gain G_{code} as a function of the FIR PU filter order parameter N.

4.4.1.3 Noise Reduction Using Zeroth-Order Wiener Filters

In addition to being optimal for coding gain, recall from Sec. 3.6.3 that the PCFB is optimal for denoising of white noise with zeroth-order Wiener filters in the subbands. From (3.37), recall that the mean-squared error in the presence of zeroth-order Wiener filters is given by

$$\epsilon = \frac{1}{M}\sum_{i=0}^{M-1}\frac{\sigma_{w_i}^2\eta^2}{\sigma_{w_i}^2+\eta^2}$$

where $\sigma_{w_i}^2$ denotes the desired signal variance of the i-th subband and η^2 denotes the variance of the white noise process.

Using the same FIR PU filter banks as those computed in Section 4.4.1.2, the observed mean-squared error ϵ from (3.37) as a function of N is shown in Fig. 4.8 for (a) $\eta^2 = 1$ and (b) $\eta^2 = 4$. As can be seen in both cases, the FIR filter banks significantly outperform the KLT. Furthermore, it can be seen that the error *monotonically decreased* as N increased, in accordance with intuition. Asymptotically, it appears as though the optimized FIR filter bank is trying to emulate the behavior of the infinte order PCFB.

4.4.1.4 Power Minimization for DMT-Type Transmultiplexers

From Sec. 3.6.4, recall that the PCFB is optimal for minimizing the total power of a PU transmultiplexer digital communications system in which the noise is Gaussian, the input signals consist of PAM symbols [38], a zero-forcing equalizer [38] has been used, and the symbol error probabilities

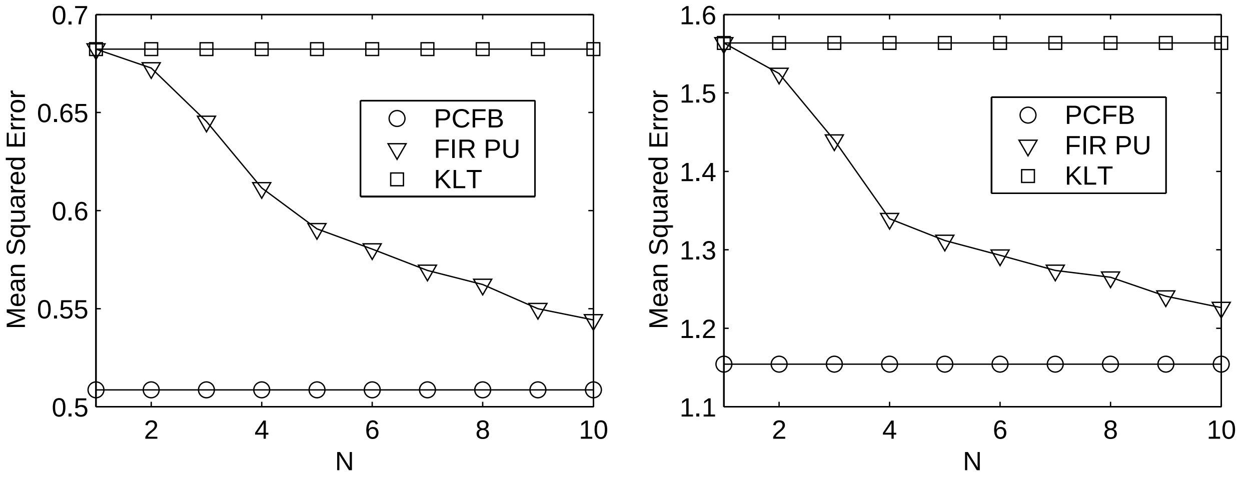

(a)

(b)

Figure 4.8: Noise reduction performance (ϵ from (3.37)) with zeroth-order subband Wiener filters as a function of the FIR PU filter order parameter N for (a) noise variance (η^2) of 1 and (b) noise variance of 4.

and bit allocations are fixed. Recall from (3.39) and (3.40) that the total power is given by

$$P = \sum_{k=0}^{M-1} \beta\left(\mathcal{P}_e(k), b_k\right) \sigma_{q_k}^2$$

where $\beta\left(\mathcal{P}_e(k), b_k\right)$ is a constant that depends only on the symbol error probability and bit allocation for the k-th subband and $\sigma_{q_k}^2$ denotes the noise power seen at the k-th output. As P is a *convex* function of the variances $\sigma_{q_k}^2$, it is minimized if the transmultiplexer polyphase matrix $\mathbf{F}(z)$ is chosen to be a PCFB for the effective noise process seen at the input to the receiver (i.e., the original noise filtered by the zero-forcing equalizer).

As an example, suppose that the desired probability of error is $\mathcal{P}_e(k) = 10^{-9}$ for all k. Also, suppose that we have $b_0 = 2$, $b_1 = 3$, $b_2 = 4$, and $b_3 = 5$. It should be noted that this is a not an optimal bit allocation [73] and is only chosen here as such for simplicity. Finally, suppose that the effective noise psd is simply the psd $S_{xx}(e^{j\omega})$ shown in Fig. 4.1. Then, using the proposed iterative algorithm, the required powers as a function of the synthesis polyphase order N is shown in Fig. 4.9. As can be seen, the FIR filter banks designed here significantly outperform the KLT and exhibit a *monotonically decreasing* power as a function of N, in accordance with intuition. Furthermore, as before, the optimized FIR filter bank appears to be approaching the performance of the infinite-order PCFB as the order increases.

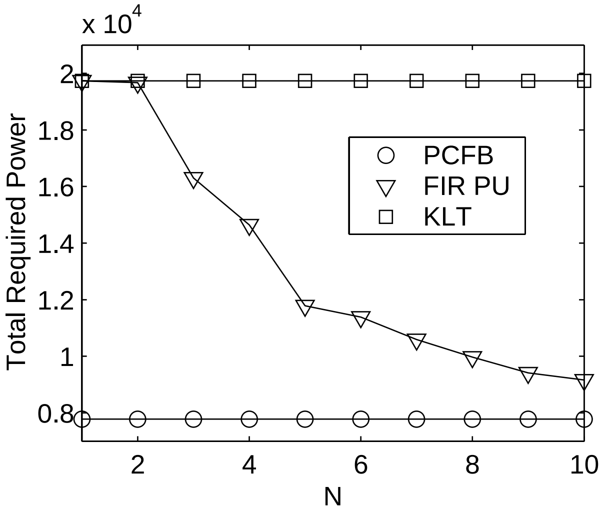

Figure 4.9: Nonredundant DMT-type transmultiplexer total required power P as a function of the FIR PU filter order parameter N.

4.4.2 The FIR PU Interpolation Problem

Recall from Section 1.3 that the FIR PU interpolation problem involves finding an FIR PU system of a certain McMillan degree, say $\mathbf{F}(e^{j\omega})$, which takes on a prescribed set of L values, say $\mathcal{U}_0, \mathcal{U}_1, \ldots, \mathcal{U}_{L-1}$, over a prescribed set of L frequencies, say $\omega_0, \omega_1, \ldots, \omega_{L-1}$. In other words, we seek an FIR PU $\mathbf{F}(z)$ of a certain degree such that $\mathbf{F}(e^{j\omega_k}) = \mathcal{U}_k$ for all $0 \leq k \leq L-1$. (Clearly the matrices $\{\mathcal{U}_k\}$ must be unitary.) As mentioned in Section 1.3, there is no known solution to the FIR PU interpolation problem. However, for this problem, the proposed iterative algorithm can be used to approximate an interpolant. In this case, the desired response $\mathbf{D}(e^{j\omega})$ is as follows.

$$\mathbf{D}(e^{j\omega}) = \begin{cases} \mathcal{U}_k\,, & \omega = \omega_k \ \forall \ 0 \leq k \leq L-1 \\ \text{don't care}, & \text{otherwise} \end{cases}$$

As we don't care about the response at all frequencies not in the set $\{\omega_k\}$, it only makes sense that these regions be given no weight in the approximation problem. One weight function which accomodates this need is the interpolation weight function $W_{\text{int}}(\omega)$, given by the following.

$$W_{\text{int}}(\omega) = 2\pi \sum_{k=0}^{L-1} p_k \delta(\omega - \omega_k) \tag{4.32}$$

Here, the p_ks are *discrete* weight parameters used to emphasize the design of some interpolation conditions over others which satisfies

$$p_k \geq 0\,, \ \sum_{k=0}^{L-1} p_k = 1$$

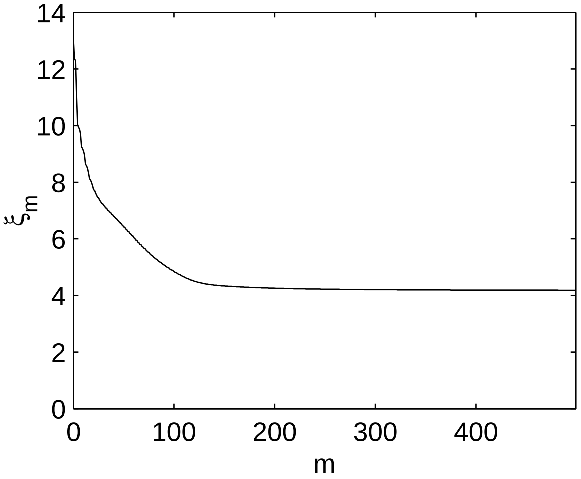

Figure 4.10: FIR PU interpolation problem - Example 1: Mean-squared error ξ_m vs. iteration m.

In other words, $\{p_k\}$ is a discrete probability density function (pdf). Substituting (4.32) into the expression for the weighted mean-squared error ξ from (4.1) yields

$$\xi = \sum_{k=0}^{L-1} p_k \left|\left|\mathbf{D}(e^{j\omega_k}) - \mathbf{F}(e^{j\omega_k})\right|\right|_F^2 = \sum_{k=0}^{L-1} p_k \left|\left|\mathcal{U}_k - \mathbf{F}(e^{j\omega_k})\right|\right|_F^2$$

Hence, with the interpolation weight function $W_{\text{int}}(\omega)$ from (4.32), the mean-squared error integral becomes a *discrete summation.* This simplifies the proposed iterative algorithm since no numerical integration is required.

4.4.2.1 FIR PU Interpolation - Example 1

As an example, suppose that we seek a 3×2 FIR PU system $\mathbf{F}(z)$ such that $\mathbf{F}(e^{j\omega}) = \mathcal{U}_k$ for $0 \leq k \leq 3$, where $\mathcal{U}_0, \ldots, \mathcal{U}_3$ are randomly chosen 3×2 unitary matrices. Furthermore, suppose that the frequencies are chosen as

$$\omega_0 = 0\,,\ \omega_1 = \frac{\pi}{2}\,,\ \omega_2 = \frac{3\pi}{4}\,,\ \omega_3 = \frac{5\pi}{4}$$

Since there are 4 interpolation conditions, we might expect that we need $N \geq 4$ for the FIR PU interpolant in general. Using the proposed iterative algorithm for $N = 4$, the observed mean-squared error ξ_m as a function of iteration m is shown in Fig. 4.10. Here, we used $p_0 = p_1 = p_2 = p_3 = \frac{1}{4}$ (i.e., uniform weighting) and KN iterations, where we chose $K = \left\lceil \frac{500}{N} \right\rceil$. As the error appears to have saturated at a nonzero value (in this case 4.1844), this suggests that there may not exist an FIR PU system with $N = 4$ that satisfies the desired interpolation conditions. Despite this, the algorithm has found a good approximant to the desired interpolant.

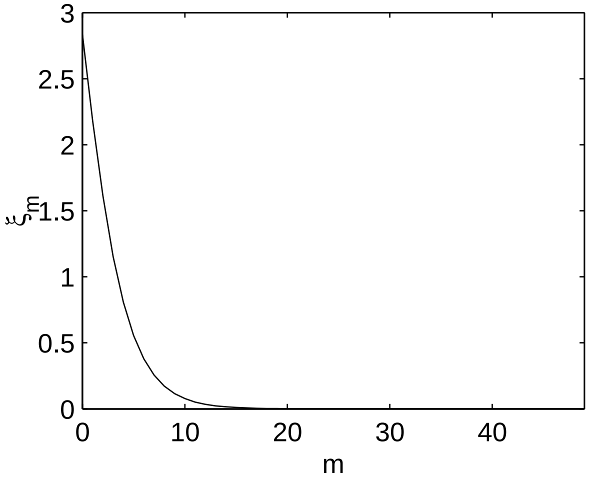

Figure 4.11: FIR PU interpolation problem - Example 2: Mean-squared error ξ_m vs. iteration m.

4.4.2.2 FIR PU Interpolation - Example 2

To further test the performance of the proposed iterative algorithm, we can use it to obtain an FIR PU system for which we know that an interpolant exists. For example, suppose that we seek a 3×2 FIR PU system $\mathbf{F}(z)$ such that

$$\begin{aligned}\mathbf{F}(e^{j\omega_0}) &= \mathcal{U}_0 = \left(\mathbf{I} - \mathbf{v}\mathbf{v}^\dagger + e^{-j\omega_0}\mathbf{v}\mathbf{v}^\dagger\right)\mathbf{U} \\ \mathbf{F}(e^{j\omega_1}) &= \mathcal{U}_1 = \left(\mathbf{I} - \mathbf{v}\mathbf{v}^\dagger + e^{-j\omega_1}\mathbf{v}\mathbf{v}^\dagger\right)\mathbf{U}\end{aligned}$$

Here, $\mathbf{v}$ is an arbitrary 3×1 unit norm vector and $\mathbf{U}$ is a 3×2 arbitrary unitary matrix. As there are 2 interpolation conditions, we expect that in general, we need $N \geq 2$ here. Clearly, for $N = 2$, the choice

$$\mathbf{F}(z) = \left(\mathbf{I} - \mathbf{v}\mathbf{v}^\dagger + z^{-1}\mathbf{v}\mathbf{v}^\dagger\right)\mathbf{U} \tag{4.33}$$

satisfies the desired interpolation conditions. Using the proposed iterative algorithm, we can see if the algorithm can *converge* to the interpolant of (4.33). For this simulation, we chose $\omega_0 = 0$ and $\omega_1 = \frac{3\pi}{4}$ and $p_0 = p_1 = \frac{1}{2}$ (i.e., uniform weighting). A plot of the observed mean-squared error as a function of iteration is shown in Fig. 4.11 for KN iterations, where we chose $K = \left\lceil \frac{50}{N} \right\rceil$. As we can see, it appears as though the algorithm does in fact converge to the interpolant of (4.33).

In summary, even though there is no general solution to the FIR PU interpolation problem, the proposed algorithm offers a way to *approximate* a suitable interpolant.

4.5 Concluding Remarks

Using the complete characterization of FIR PU systems in terms of Householder-like degree-one building blocks, in this chapter we proposed an iterative greedy algorithm for solving a general matrix version of the weighted least-squares approximation problem for an FIR PU approximant. For cases in which the desired response matrix exhibited a *phase-type ambiguity*, which we formally defined here, a phase feedback modification was proposed in which the phase of the FIR PU approximant was fed back to the desired response. With this modification in effect, the resulting algorithm was shown to still remain greedy and provide a better *magnitude-type* fit of the desired response.

As opposed to most traditional signal-adapted filter bank design methods which optimize a specific objective for which the PCFB is optimal, the method used here was to approximate the infinite-order PCFB itself using a realizable FIR PU filter bank. In contrast to popular criteria for signal-adapted design, such as the MOC of Chapter 3, which require a filter bank completion step after a suitable FIR compaction filter has been computed, the method used here avoids this entirely as all of the filters are found *simultaneously.* The advantage of this is that we avoid the problems due to the *nonuniqueness* of the compaction filter, which plagued the method presented in Chapter 3 with an *exponential* increase in complexity. Through simulations presented here, it was shown that the FIR PU filter banks designed *monotonically* behaved more and more like the infinite-order PCFB as the filter order increased in terms of numerous objectives. This serves to *bridge the gap* between the zeroth-order KLT and infinite-order PCFB. Together with the results of the design method of Chapter 3, this phenomenon has not previously been reported in the literature.

In addition to being useful for the design of signal-adapted filter banks, we showed that the iterative algorithm could also be used for the FIR PU interpolation problem. Though this problem is still open, the algorithm always offers a way to approximate a desired interpolant, which may or may not even exist. With simulations provided here, we showed that the algorithm could converge to an interpolant, when one was known to exist. In essence, the algorithm provides us with a numerical approach to solve a theoretically open problem.

Chapter 5

Coding Gain Optimal FIR Filter Banks

This chapter differs somewhat in theme from the rest of the chapters in that we focus on the design of FIR signal-adapted filter banks in which no PU constraint is enforced. As opposed to traditional filter bank design algorithms which enforce a PU or biorthogonality condition to be satisfied, we make no such constraints here. The only constraint that we adhere to is that the analysis/synthesis filters be FIR and hence realizable.

Here, the model we focus on is a uniform filter bank with scalar quantizers in the subbands. Such a model is commonly used to achieve good lossy data compression in methods such as JPEG and MP3 [41, 39]. The goal here is to choose the best analysis/synthesis filters, subject to an FIR constraint, to minimize the filter bank mean-squared reconstruction error for a fixed bit allocation among the quantizers. This is shown to be equivalent to maximizing the coding gain of the system. Under the *high bit rate assumption* [25], we show how to derive the optimal analysis/synthesis bank assuming that the corresponding synthesis/analysis bank is fixed. This will lead to an iterative *greedy* algorithm for designing the filter bank where the analysis and synthesis banks are alternately optimized.

Simulation results presented here show the versatility and merit of the proposed greedy algorithm. By neglecting the effects of the quantizers, we show how the method can be used to design an *overdecimated* filter bank which minimizes the mean-squared error of its output. Though the PU constraint is not enforced here, we show that many similarities exist between these FIR filter banks designed and optimal PU filter banks or PCFBs. In particular, we show that the FIR filters designed appear to *compact* the energy of the input process, a property which is also shared with the PCFB.

When we account for the effects of the quantizers, we show how the algorithm can be used to design optimal FIR pre/postfilters for quantization. The performance in this case is measured in terms of coding gain and distortion or mean-squared error. We compare the distortion observed to the rate-distortion bound given by information theory [25, 10, 7]. It is shown that the method comes close to this bound and comes closer when we increase the filter orders, as expected.

Finally, we consider the design of a maximally decimated system with quantizers in the subbands. As before, the performance is measured in terms of coding gain and distortion. When compared to the rate-distortion bound, it is shown that the method comes closer to the bound as we increase the filter orders, in line with intuition. Furthermore, we show that the quantized filter bank system outperforms the scalar pre/postfiltering quantization system, as expected.

The content of portions of this chapter will be presented at [58].

5.1 Outline

In Sec. 5.2, we present the quantized filter bank model which we will focus on here. There, we review the high bit rate assumption for scalar quantizers, which greatly simplifies the mathematical analysis required for the objective under consideration.

In Sec. 5.3, we derive the optimal analysis/synthesis banks for minimizing the reconstruction error at the output. The optimal synthesis bank for a fixed analysis bank is derived in Sec. 5.3.1, whereas the optimal analysis bank for a fixed synthesis bank is derived in Sec. 5.3.2. In Sec. 5.3.3, we formally present an iterative greedy algorithm for obtaining the optimal FIR filter bank for minimizing the reconstruction error.

Simulation results are presented in Sec. 5.4. In Sec. 5.4.1, we neglect the effects due to quantization and show how the algorithm can be used to design an overdecimated filter bank. There, in Sec. 5.4.1.1 and Sec. 5.4.1.2, the similarities and differences between the FIR filter banks designed and the PCFB are shown. The effects of quantization are discussed in Sec. 5.4.2 along with several important measures of optimality. In Sec. 5.4.2.1, we use the iterative algorithm to design optimal FIR pre/postfilters for quantization. The method is shown there to exhibit distortion behavior close to the rate-distortion bound. In Sec. 5.4.2.2, we consider the design of a maximally decimated filter bank with quantizers in the subbands. There, it is shown that such filter banks yield performance close to the rate-distortion bound and outperform the scalar pre/postfiltering quantization system.

Finally, concluding remarks are made in Sec. 5.5.

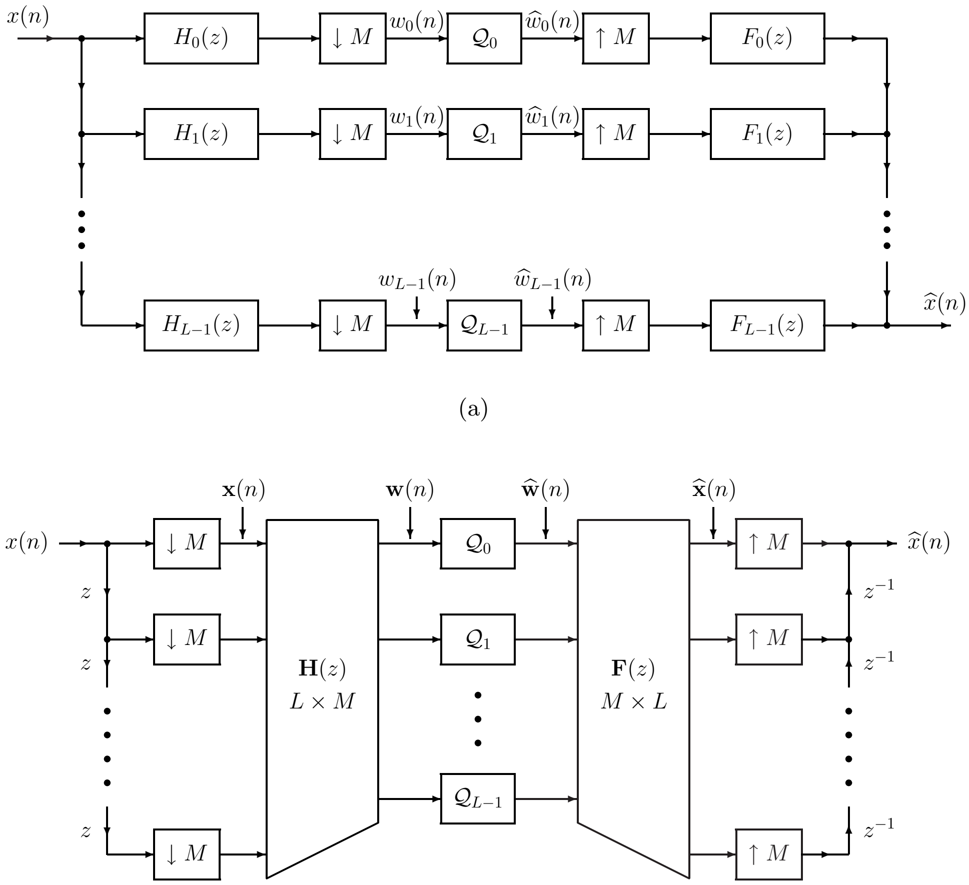

(b)

Figure 5.1: (a) Uniform filter bank with scalar quantizers in the subbands, (b) Polyphase representation of the filter bank.

5.2 Uniform Quantized Filter Bank Model

The model we focus on here is a uniform filter bank with *scalar quantizers* in the subbands as shown in Fig. 5.1(a). This model is often used in data compression to achieve good lossy compression [41, 39]. Here, the number of channels L is variable, but for the purposes of data compression, we will often desire $L \leq M$, since if $L > M$, we are introducing an unnecessary redundancy into the system. If we consider the following M-fold polyphase decompositions of the analysis filters $H_k(z)$ and synthesis filters $F_k(z)$ for $0 \leq k \leq L-1$,

$$\begin{aligned} H_k(z) &= \sum_{\ell=0}^{M-1} z^{\ell} H_{k,\ell}\big(z^M\big) \quad \text{(Type II)} \\ F_k(z) &= \sum_{\ell=0}^{M-1} z^{-\ell} F_{k,\ell}\big(z^M\big) \quad \text{(Type I)} \end{aligned}$$

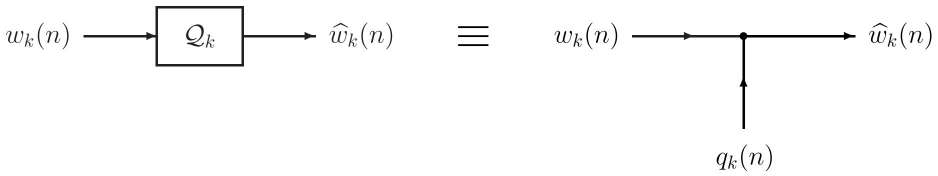

Figure 5.2: High bit rate quantizer model.

then the system of Fig. 5.1(a) can be redrawn as in Fig. 5.1(b), where we have

$$[\mathbf{H}(z)]_{\ell,m} = H_{\ell,m}(z)\,,\ [\mathbf{F}(z)]_{m,\ell} = F_{\ell,m}(z) \ \text{ for } \ 0 \leq \ell \leq L-1\,,\ 0 \leq m \leq M-1$$

Here, $\mathbf{x}(n)$ and $\widehat{\mathbf{x}}(n)$ denote, respectively, the M-fold blocked versions of the filter bank input $x(n)$ and $\widehat{x}(n)$. Also, $\mathbf{w}(n)$ and $\widehat{\mathbf{w}}(n)$ denote, respectively, the vector of quantizer inputs and outputs given by

$$\mathbf{w}(n) \triangleq \begin{bmatrix} w_0(n) & w_1(n) & \cdots & w_{L-1}(n) \end{bmatrix}^T\,,\ \widehat{\mathbf{w}}(n) \triangleq \begin{bmatrix} \widehat{w}_0(n) & \widehat{w}_1(n) & \cdots & \widehat{w}_{L-1}(n) \end{bmatrix}^T$$

The quantizer $\mathcal{Q}_k$ is used to limit the number of possible output values of each sample of its input $w_k(n)$ to a finite amount of possibilities. Most often, the quantizer *approximates* $w_k(n)$ using a finite amount of discrete levels. For example, if the sample $w_k(n)$ is a 16 bit word stored on a computer in memory, the quantizer $\mathcal{Q}_k$ may truncate $w_k(n)$ to 4 bits by preserving only the 4 most significant bits of $w_k(n)$. Since the quantizer output requires less information to store than its input in general, it allows us to achieve data compression. As can be seen, the quantizer decreases the *rate* of the overall system while introducing *distortion*, since we are always discarding information in general. Hence, any compression achieved by the quantizer is necessarily *lossy*.

Since most if not all digital signals are processed on computers, quantizers are typically characterized by the number of bits that have been allocated to it. For example, if the quantizer $\mathcal{Q}_k$ from Fig. 5.1 is allocated b_k bits, then its output $\widehat{w}_k(n)$ can take on 2^{b_k} possible values. Though quantizers are nonlinear devices which often become mathematically intractable to account for exactly, under certain assumptions and approximations, they become very simple to analyze.

For the remainder of the thesis, we will assume that the *high bit rate assumption* [25] is valid for each quantizer $\mathcal{Q}_k$ here. The high bit rate assumption, which approximately holds true if the number of bits b_k is large enough [25], allows us to treat the quantizer $\mathcal{Q}_k$ as an additive zero mean white noise process. This is shown in Fig. 5.2. The variance of the additive white noise $q_k(n)$ is given by

$$\sigma_{q_k}^2 = c_k 2^{-2b_k} \sigma_{w_k}^2 \tag{5.1}$$

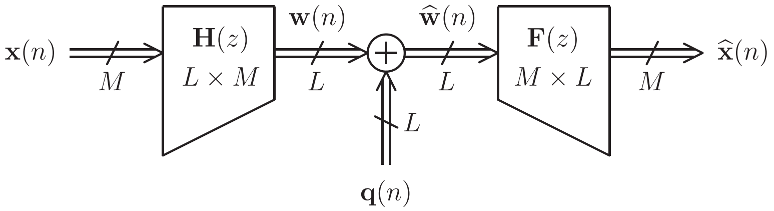

Figure 5.3: Equivalent quantized filter bank model under the high bit rate assumption.

Here, c_k is a quantity called the *quantizer performance factor* that depends on the coding method used as well as the probability density function (pdf) of the quantizer input sample $w_k(n)$ [25] (which is assumed to be the same for all n). For example, if $\mathcal{Q}_k$ is a *Lloyd-Max* quantizer [25], which is optimized for the input pdf, then $c_k = 1.00$ for a uniform pdf and $c_k = 2.71$ for a Gaussian pdf [25]. In addition to the above assumptions on $q_k(n)$, it is assumed that $q_k(n)$ is uncorrelated with the other noise processes $q_\ell(n)$ for all $\ell \neq k$ as well as the input signals $w_k(n)$ for all k.

Using the high bit rate additive noise quantizer model of Fig. 5.2, the filter bank model of Fig. 5.1(b) can be redrawn as in Fig. 5.3. The vector $\mathbf{q}(n)$ simply consists of the noise processes $q_k(n)$ and is given by

$$\mathbf{q}(n) \triangleq \begin{bmatrix} q_0(n) & q_1(n) & \cdots & q_{L-1}(n) \end{bmatrix}^T$$

Here, we have removed the blocking/unblocking structures used to obtain the scalar signals $x(n)$ and $\widehat{x}(n)$, as we will only be concerned about their respective equivalent M-fold blocked versions $\mathbf{x}(n)$ and $\widehat{\mathbf{x}}(n)$.

As before, we will assume that $\mathbf{x}(n)$ is WSS with psd $\mathbf{S}_{\mathbf{xx}}(z)$. From the above assumptions, it follows that the vector $\mathbf{q}(n)$ is WSS with psd $\mathbf{S}_{\mathbf{qq}}(z)$, where we have

$$\mathbf{S}_{\mathbf{qq}}(z) = \mathbf{Q} \text{ where } \mathbf{Q} = \text{diag}\left(\sigma_{q_0}^2, \sigma_{q_1}^2, \ldots, \sigma_{q_{L-1}}^2\right) \tag{5.2}$$

Also, the processes $\mathbf{q}(n)$ and $\mathbf{w}(n)$ are uncorrelated here.

5.3 Optimizing the Mean-Squared Reconstruction Error

The quantized filter bank model of Fig. 5.1 is plagued with distortion introduced by the quantizers as well as errors caused by aliasing, amplitude, and phase distortions. As we wish to minimize these effects, we will consider the problem of minimizing the expected M-fold blocked mean-squared error ξ given by

$$\xi \triangleq E\left[||\mathbf{x}(n) - \widehat{\mathbf{x}}(n)||^2\right] \tag{5.3}$$

for a fixed bit allocation $\{b_k\}$. Using the high bit rate model of the quantized filter bank shown in Fig. 5.3, it follows that $\mathbf{x}(n)$ and $\widehat{\mathbf{x}}(n)$ are jointly WSS. Hence, the error $\mathbf{e}(n) \triangleq \mathbf{x}(n) - \widehat{\mathbf{x}}(n)$ is WSS. We have

$$\xi = E\left[\mathbf{e}^\dagger(n)\mathbf{e}(n)\right] = \mathrm{Tr}\left[E\left[\mathbf{e}(n)\mathbf{e}^\dagger(n)\right]\right] = \mathrm{Tr}\left[\mathbf{R}_{\mathbf{ee}}(0)\right] = \mathrm{Tr}\left[\frac{1}{2\pi}\int_0^{2\pi} \mathbf{S}_{\mathbf{ee}}(e^{j\omega})\,d\omega\right] \tag{5.4}$$

where $\mathbf{R}_{\mathbf{ee}}(k)$ and $\mathbf{S}_{\mathbf{ee}}(z)$ denote, respectively, the autocorrelation and psd of $\mathbf{e}(n)$. As $\mathbf{e}(n) = \mathbf{x}(n) - \widehat{\mathbf{x}}(n)$, we have

$$\mathbf{S}_{\mathbf{ee}}(z) = \mathbf{S}_{\mathbf{xx}}(z) - \mathbf{S}_{\mathbf{x}\widehat{\mathbf{x}}}(z) - \mathbf{S}_{\widehat{\mathbf{x}}\mathbf{x}}(z) + \mathbf{S}_{\widehat{\mathbf{x}}\widehat{\mathbf{x}}}(z) \tag{5.5}$$

where $\mathbf{S}_{\mathbf{x}\widehat{\mathbf{x}}}(z)$ and $\mathbf{S}_{\widehat{\mathbf{x}}\mathbf{x}}(z)$ denote the cross psds of $\mathbf{x}(n)$ and $\widehat{\mathbf{x}}(n)$ [48], and $\mathbf{S}_{\widehat{\mathbf{x}}\widehat{\mathbf{x}}}(z)$ denotes the psd of $\widehat{\mathbf{x}}(n)$. Note that from Fig. 5.3, we have

$$\widehat{\mathbf{X}}(z) = \mathbf{F}(z)\mathbf{H}(z)\mathbf{X}(z) + \mathbf{F}(z)\mathbf{Q}(z)$$

Thus, assuming $\mathbf{x}(n)$ and $\mathbf{q}(n)$ are uncorrelated, we have [67]

$$\begin{aligned} \mathbf{S}_{\mathbf{x}\widehat{\mathbf{x}}}(z) &= \mathbf{S}_{\mathbf{xx}}(z)\widetilde{\mathbf{H}}(z)\widetilde{\mathbf{F}}(z) && (5.6)\\ \mathbf{S}_{\widehat{\mathbf{x}}\mathbf{x}}(z) &= \widetilde{\mathbf{S}}_{\mathbf{x}\widehat{\mathbf{x}}}(z) = \mathbf{F}(z)\mathbf{H}(z)\mathbf{S}_{\mathbf{xx}}(z) && (5.7)\\ \mathbf{S}_{\widehat{\mathbf{x}}\widehat{\mathbf{x}}}(z) &= \mathbf{F}(z)\mathbf{H}(z)\mathbf{S}_{\mathbf{xx}}(z)\widetilde{\mathbf{H}}(z)\widetilde{\mathbf{F}}(z) + \mathbf{F}(z)\mathbf{S}_{\mathbf{qq}}(z)\widetilde{\mathbf{F}}(z) \\ &= \mathbf{F}(z)\mathbf{H}(z)\mathbf{S}_{\mathbf{xx}}(z)\widetilde{\mathbf{H}}(z)\widetilde{\mathbf{F}}(z) + \mathbf{F}(z)\mathbf{Q}\widetilde{\mathbf{F}}(z) && (5.8) \end{aligned}$$

Here, we used (5.2) in (5.8). Substituting (5.6), (5.7), and (5.8) in (5.5), we get

$$\begin{aligned} \mathbf{S}_{\mathbf{ee}}(z) &= \mathbf{S}_{\mathbf{xx}}(z) - \mathbf{S}_{\mathbf{xx}}(z)\widetilde{\mathbf{H}}(z)\widetilde{\mathbf{F}}(z) - \mathbf{F}(z)\mathbf{H}(z)\mathbf{S}_{\mathbf{xx}}(z) \\ &\quad + \mathbf{F}(z)\mathbf{H}(z)\mathbf{S}_{\mathbf{xx}}(z)\widetilde{\mathbf{H}}(z)\widetilde{\mathbf{F}}(z) + \mathbf{F}(z)\mathbf{Q}\widetilde{\mathbf{F}}(z) \end{aligned} \tag{5.9}$$

Though it is difficult to jointly choose $\mathbf{H}(z)$ and $\mathbf{F}(z)$ subject to FIR constraints to optimize ξ (see [20, 19, 21] for a Lagrange multiplier technique for a fixed quantization term $\mathbf{Q}$), doing so one at a time is simple and can be done globally. This will lead to an iterative algorithm whereby the analysis and synthesis banks are alternately optimized. Before proceeding, note that the matrix $\mathbf{Q}$ from (5.9) *depends* on the analysis bank $\mathbf{H}(z)$. To see this, note that from (5.2) and (5.1), we have

$$\mathbf{Q} = \mathrm{diag}\left(c_0 2^{-2b_0}\sigma_{w_0}^2, c_1 2^{-2b_1}\sigma_{w_1}^2, \ldots, c_{L-1}2^{-2b_{L-1}}\sigma_{w_{L-1}}^2\right) \tag{5.10}$$

where we have, from Fig. 5.3,

$$\sigma_{w_k}^2 = \frac{1}{2\pi}\int_0^{2\pi} \left[\mathbf{H}(e^{j\omega})\mathbf{S}_{\mathbf{xx}}(e^{j\omega})\mathbf{H}^\dagger(e^{j\omega})\right]_{k,k} d\omega \tag{5.11}$$

Hence, optimizing the analysis bank $\mathbf{H}(z)$ for a fixed synthesis bank $\mathbf{F}(z)$ is more mathematically challenging than optimizing $\mathbf{F}(z)$ for a fixed $\mathbf{H}(z)$. As such, we first consider optimizing $\mathbf{F}(z)$ for a fixed $\mathbf{H}(z)$ and then move on to the more challenging task of optimizing $\mathbf{H}(z)$ for a fixed $\mathbf{F}(z)$.

5.3.1 Optimal Synthesis Bank $\mathbf{F}(z)$ for Fixed Analysis Bank $\mathbf{H}(z)$

Suppose that the analysis bank $\mathbf{H}(z)$ is fixed and that the synthesis bank $\mathbf{F}(z)$ is FIR of length N_f and of the form

$$\mathbf{F}(z) = z^P \mathbf{F}_c(z)$$

where P is an advance parameter and $\mathbf{F}_c(z)$ is a *causal* FIR system of the form

$$\mathbf{F}_c(z) = \sum_{n=0}^{N_f-1} \mathbf{f}_c(n) z^{-n}$$

Note that the impulse response $\mathbf{f}_c(n)$ is an $M \times L$ sequence. If we define the $M \times LN_f$ matrix $\overline{\mathbf{f}}_c$ and $LN_f \times L$ delay matrix $\mathbf{d}(z)$ as

$$\begin{aligned} \overline{\mathbf{f}}_c &\triangleq \begin{bmatrix} \mathbf{f}_c(0) & \mathbf{f}_c(1) & \cdots & \mathbf{f}_c(N_f-1) \end{bmatrix} \\ \mathbf{d}(z) &\triangleq \begin{bmatrix} z^P \mathbf{I}_L & z^{P-1}\mathbf{I}_L & \cdots & z^{P-(N_f-1)}\mathbf{I}_L \end{bmatrix}^T \end{aligned}$$

then clearly we have $\mathbf{F}(z) = \overline{\mathbf{f}}_c \mathbf{d}(z)$ and all of the degrees of freedom in choosing $\mathbf{F}(z)$ with the FIR constraint lie in the choice of the constant matrix $\overline{\mathbf{f}}_c$. From (5.9), we have

$$\begin{aligned} \mathbf{S}_{\mathbf{ee}}(z) &= \mathbf{S}_{\mathbf{xx}}(z) - \mathbf{S}_{\mathbf{xx}}(z)\widetilde{\mathbf{H}}(z)\widetilde{\mathbf{d}}(z)\overline{\mathbf{f}}_c^\dagger - \overline{\mathbf{f}}_c\mathbf{d}(z)\mathbf{H}(z)\mathbf{S}_{\mathbf{xx}}(z) \\ &\quad + \overline{\mathbf{f}}_c\mathbf{d}(z)\left[\mathbf{H}(z)\mathbf{S}_{\mathbf{xx}}(z)\widetilde{\mathbf{H}}(z) + \mathbf{Q}\right]\widetilde{\mathbf{d}}(z)\overline{\mathbf{f}}_c^\dagger \end{aligned} \tag{5.12}$$

Substituting (5.12) into (5.4) yields

$$\xi = \mathrm{Tr}\left[\mathbf{R}_{\mathbf{xx}}(0) - \mathbf{B}^\dagger\overline{\mathbf{f}}_c^\dagger - \overline{\mathbf{f}}_c\mathbf{B} + \overline{\mathbf{f}}_c\mathbf{A}\overline{\mathbf{f}}_c^\dagger\right] \tag{5.13}$$

where $\mathbf{R}_{\mathbf{xx}}(k)$ denotes the autocorrelation of $\mathbf{x}(n)$ and the $LN_f \times LN_f$ matrix $\mathbf{A}$ and $LN_f \times M$ matrix $\mathbf{B}$ are defined as follows.

$$\mathbf{A} \triangleq \frac{1}{2\pi}\int_0^{2\pi} \mathbf{d}(e^{j\omega})\left[\mathbf{H}(e^{j\omega})\mathbf{S}_{\mathbf{xx}}(e^{j\omega})\mathbf{H}^\dagger(e^{j\omega}) + \mathbf{Q}\right]\mathbf{d}^\dagger(e^{j\omega})\, d\omega \tag{5.14}$$

$$\mathbf{B} \triangleq \frac{1}{2\pi}\int_0^{2\pi} \mathbf{d}(e^{j\omega})\mathbf{H}(e^{j\omega})\mathbf{S}_{\mathbf{xx}}(e^{j\omega})\, d\omega \tag{5.15}$$

Note that $\mathbf{A}$ is simply the N_f-fold block autocorrelation matrix of the process $\widehat{\mathbf{w}}(n)$ from Fig. 5.3 [48]. In other words, if $\mathbf{R}_{\widehat{\mathbf{w}}\widehat{\mathbf{w}}}(k)$ denotes the autocorrelation of $\widehat{\mathbf{w}}(n)$, then we have

$$\mathbf{A} = \begin{bmatrix} \mathbf{R}_{\widehat{\mathbf{w}}\widehat{\mathbf{w}}}(0) & \mathbf{R}_{\widehat{\mathbf{w}}\widehat{\mathbf{w}}}(1) & \cdots & \mathbf{R}_{\widehat{\mathbf{w}}\widehat{\mathbf{w}}}(N_f-1) \\ \mathbf{R}_{\widehat{\mathbf{w}}\widehat{\mathbf{w}}}(-1) & \mathbf{R}_{\widehat{\mathbf{w}}\widehat{\mathbf{w}}}(0) & \cdots & \mathbf{R}_{\widehat{\mathbf{w}}\widehat{\mathbf{w}}}(N_f-2) \\ \vdots & \vdots & \ddots & \vdots \\ \mathbf{R}_{\widehat{\mathbf{w}}\widehat{\mathbf{w}}}(-(N_f-1)) & \mathbf{R}_{\widehat{\mathbf{w}}\widehat{\mathbf{w}}}(-(N_f-2)) & \cdots & \mathbf{R}_{\widehat{\mathbf{w}}\widehat{\mathbf{w}}}(0) \end{bmatrix}$$

As such, the matrix $\mathbf{A}$ is strictly positive definite and hence invertible [48]. Since $\mathbf{A}$ is invertible, using the trick of *completing the square* [22, 34], we can express ξ in (5.13) as follows

$$\xi = \mathrm{Tr}\left[\underbrace{\left(\overline{\mathbf{f}}_c - \mathbf{B}^\dagger \mathbf{A}^{-1}\right) \mathbf{A} \left(\overline{\mathbf{f}}_c - \mathbf{B}^\dagger \mathbf{A}^{-1}\right)^\dagger}_{\text{positive semidefinite}} + \mathbf{R}_{\mathbf{xx}}(0) - \mathbf{B}^\dagger \mathbf{A}^{-1} \mathbf{B} \right]$$

As we wish to minimize ξ, this can only be done by setting the first term on the right-hand side of the above equation equal to the zero matrix. This yields the following optimal choice of $\overline{\mathbf{f}}_c$ and corresponding optimal ξ.

$$\boxed{\overline{\mathbf{f}}_{c,\mathrm{opt}} = \mathbf{B}^\dagger \mathbf{A}^{-1}\ ,\ \xi_{\mathrm{opt}} = \mathrm{Tr}\left[\mathbf{R}_{\mathbf{xx}}(0) - \mathbf{B}^\dagger \mathbf{A}^{-1} \mathbf{B}\right]} \tag{5.16}$$

Here, $\mathbf{A}$ and $\mathbf{B}$ are as in (5.14) and (5.15), respectively. The choice of $\overline{\mathbf{f}}_c$ given in (5.16) is optimal for a fixed $\mathbf{S}_{\mathbf{xx}}(z)$, $\mathbf{H}(z)$, and $\mathbf{Q}$.

5.3.2 Optimal Analysis Bank $\mathbf{H}(z)$ for Fixed Synthesis Bank $\mathbf{F}(z)$

5.3.2.1 Simplifying the Quantization Noise Term

Prior to optimizing the mean-squared error ξ with respect to the analysis bank $\mathbf{H}(z)$, it will help to simplify the quantization noise term that appears in the expression for $\mathbf{S}_{\mathbf{ee}}(z)$ given in (5.9). Note that from (5.4), we have

$$\xi = \frac{1}{2\pi} \int_0^{2\pi} \mathrm{Tr}\left[\mathbf{S}_{\mathbf{ee}}(e^{j\omega})\right]\, d\omega \tag{5.17}$$

Also, from (5.9), we have

$$\begin{aligned} \mathrm{Tr}\left[\mathbf{S}_{\mathbf{ee}}(z)\right] \;=\;& \mathrm{Tr}\left[\mathbf{S}_{\mathbf{xx}}(z)\right] - \mathrm{Tr}\left[\mathbf{S}_{\mathbf{xx}}(z)\widetilde{\mathbf{H}}(z)\widetilde{\mathbf{F}}(z)\right] - \mathrm{Tr}\left[\mathbf{F}(z)\mathbf{H}(z)\mathbf{S}_{\mathbf{xx}}(z)\right] \\ & + \mathrm{Tr}\left[\mathbf{F}(z)\mathbf{H}(z)\mathbf{S}_{\mathbf{xx}}(z)\widetilde{\mathbf{H}}(z)\widetilde{\mathbf{F}}(z)\right] + \underbrace{\mathrm{Tr}\left[\mathbf{F}(z)\mathbf{Q}\widetilde{\mathbf{F}}(z)\right]}_{G(z)} \end{aligned} \tag{5.18}$$

Before simplifying $\mathrm{Tr}\left[\mathbf{S}_{\mathbf{ee}}(z)\right]$ further, we will simplify the term $G(z)$, which is due to the quantization noise $\mathbf{q}(n)$ filtered by the synthesis bank $\mathbf{F}(z)$ as can be seen in Fig. 5.3. The reason for this is that the matrix $\mathbf{Q}$ appearing in $G(z)$ *depends* on the analysis bank $\mathbf{H}(z)$ as can be seen from (5.10) and (5.11). Using the fact that $\mathrm{Tr}\left[\mathbf{AB}\right] = \mathrm{Tr}\left[\mathbf{BA}\right]$ whenever $\mathbf{A}$ and $\mathbf{B}$ are conformable [22], we have

$$G(z) = \mathrm{Tr}\left[\mathbf{Q}\widetilde{\mathbf{F}}(z)\mathbf{F}(z)\right]$$

Upon using (5.10), we get

$$G(z) = \sum_{k=0}^{L-1} c_k 2^{-2b_k} \sigma_{y_k}^2 \left[\widetilde{\mathbf{F}}(z)\mathbf{F}(z)\right]_{k,k} = \sum_{k=0}^{L-1} c_k 2^{-2b_k} \left[\widetilde{\mathbf{F}}(z)\mathbf{F}(z)\right]_{k,k} \sigma_{y_k}^2$$

As $\sigma^2_{y_k}$ is given by (5.11), we have

$$\begin{aligned} G(z) &= \sum_{k=0}^{L-1} c_k 2^{-2b_k} \left[\widetilde{\mathbf{F}}(z)\mathbf{F}(z)\right]_{k,k} \left(\frac{1}{2\pi}\int_0^{2\pi} \left[\mathbf{H}(e^{j\lambda})\mathbf{S}_{\mathbf{xx}}(e^{j\lambda})\mathbf{H}^{\dagger}(e^{j\lambda})\right]_{k,k} d\lambda\right) \\ &= \frac{1}{2\pi}\int_0^{2\pi} \left(\sum_{k=0}^{L-1} c_k 2^{-2b_k} \left[\widetilde{\mathbf{F}}(z)\mathbf{F}(z)\right]_{k,k} \left[\mathbf{H}(e^{j\lambda})\mathbf{S}_{\mathbf{xx}}(e^{j\lambda})\mathbf{H}^{\dagger}(e^{j\lambda})\right]_{k,k}\right) d\lambda \qquad (5.19) \end{aligned}$$

Define the $L \times L$ matrix $\mathbf{\Lambda}(z)$ as follows.

$$\mathbf{\Lambda}(z) \triangleq \text{diag}\left(c_0 2^{-2b_0}\left[\widetilde{\mathbf{F}}(z)\mathbf{F}(z)\right]_{0,0}, c_1 2^{-2b_1}\left[\widetilde{\mathbf{F}}(z)\mathbf{F}(z)\right]_{1,1}, \ldots, c_{L-1} 2^{-2b_{L-1}}\left[\widetilde{\mathbf{F}}(z)\mathbf{F}(z)\right]_{L-1,L-1}\right) \qquad (5.20)$$

Note that $\mathbf{\Lambda}(z)$ *does not depend* on $\mathbf{H}(z)$. Using $\mathbf{\Lambda}(z)$ in (5.19), we can express $G(z)$ as

$$G(z) = \frac{1}{2\pi}\int_0^{2\pi} \text{Tr}\left[\mathbf{\Lambda}(z)\mathbf{H}(e^{j\lambda})\mathbf{S}_{\mathbf{xx}}(e^{j\lambda})\mathbf{H}^{\dagger}(e^{j\lambda})\right] d\lambda \qquad (5.21)$$

With the simplification of the noise term $G(z)$ given in (5.21), we are now ready to optimize ξ with respect to $\mathbf{H}(z)$ with an FIR constraint in effect.

5.3.2.2 Imposing the FIR Constraint on $\mathbf{H}(z)$

Suppose now that the synthesis bank $\mathbf{F}(z)$ is fixed and that the analysis bank $\mathbf{H}(z)$ is FIR of length N_h and of the form

$$\mathbf{H}(z) = z^Q \mathbf{H}_c(z)$$

where Q is an advance parameter and $\mathbf{H}_c(z)$ is a *causal* FIR system of the form

$$\mathbf{H}_c(z) = \sum_{n=0}^{N_h-1} \mathbf{h}_c(n) z^{-n}$$

Note that the impulse response $\mathbf{h}_c(n)$ is an $L \times M$ sequence and that there are N_h such matrix coefficients. Hence, $\mathbf{H}(z)$ is characterized by a total of LMN_h degrees of freedom with the FIR constraint in effect. In order to minimize ξ from (5.17) in this case, we need to group all of these degrees of freedom together, which can be done through the use of the *vec* operator [34].

Recall that if $\mathbf{A}$ is any $M \times N$ matrix, then vec($\mathbf{A}$) is an $MN \times 1$ column vector with [34]

$$\left[\text{vec}(\mathbf{A})\right]_k \triangleq \left[\mathbf{A}\right]_{k \bmod M, \left\lfloor \frac{k}{M} \right\rfloor}, \quad 0 \leq k \leq MN-1$$

In other words, the vec operator *stacks* the columns of any matrix on top of each other creating a large column vector. Through clever use of the vec operator, we can express ξ from (5.17) as a quadratic function in terms of the filter coefficients of $\mathbf{H}(z)$.

For simplicity, define the $LM \times 1$ column vectors $\overline{\mathbf{h}}_n$ as follows.

$$\overline{\mathbf{h}}_n \triangleq \text{vec}\left(\mathbf{h}_c(n)\right) \ , \ 0 \le n \le N_h - 1$$

Furthermore, define the $LMN_h \times 1$ vector $\overline{\mathbf{h}}$, the $LM \times 1$ vector $\mathbf{v}(z)$ and the $LMN_h \times LM$ advance matrix $\mathbf{a}(z)$ as follows.

$$\begin{aligned} \overline{\mathbf{h}} &\triangleq \begin{bmatrix} \overline{\mathbf{h}}_0^T & \overline{\mathbf{h}}_1^T & \cdots & \overline{\mathbf{h}}_{N_h-1}^T \end{bmatrix}^T \\ \mathbf{v}(z) &\triangleq \text{vec}\left(\widetilde{\mathbf{F}}(z)\mathbf{S}_{\mathbf{xx}}(z)\right) \\ \mathbf{a}(z) &\triangleq \begin{bmatrix} z^{-Q}\mathbf{I}_{LM} & z^{1-Q}\mathbf{I}_{LM} & \cdots & z^{N_h-1-Q}\mathbf{I}_{LM} \end{bmatrix}^T \end{aligned}$$

Note that $\overline{\mathbf{h}}$ contains all of the degrees of freedom of $\mathbf{H}(z)$ here. Also note that due to the linearity property of the vec operator [34], we have

$$\text{vec}\left(\mathbf{H}(z)\right) = \sum_{n=0}^{N_h-1} z^{Q-n} \underbrace{\text{vec}\left(\mathbf{h}_c(n)\right)}_{\overline{\mathbf{h}}_n} = \underbrace{\begin{bmatrix} z^{Q}\mathbf{I}_{LM} & z^{Q-1}\mathbf{I}_{LM} & \cdots & z^{Q-(N_h-1)}\mathbf{I}_{LM} \end{bmatrix}}_{\widetilde{\mathbf{a}}(z)} \underbrace{\begin{bmatrix} \overline{\mathbf{h}}_0 \\ \overline{\mathbf{h}}_1 \\ \vdots \\ \overline{\mathbf{h}}_{N_h-1} \end{bmatrix}}_{\overline{\mathbf{h}}} \tag{5.22}$$

By exploiting the following properties of the trace and vec operators [34],

$$\text{Tr}\left[\mathbf{A}^\dagger\mathbf{B}\right] = \left(\text{vec}(\mathbf{A})\right)^\dagger \text{vec}(\mathbf{B}) \tag{5.23}$$

$$\text{vec}(\mathbf{AXB}) = \left(\mathbf{B}^T \otimes \mathbf{A}\right) \text{vec}(\mathbf{X}) \tag{5.24}$$

where $\otimes$ denotes the *Kronecker product* operator [34], we can express the error ξ as a quadratic function of the vector $\overline{\mathbf{h}}$, which can then be minimized by completing the square as was done in Sec. 5.3.1. Note that for any $M \times N$ matrix $\mathbf{A}$ and $P \times Q$ matrix $\mathbf{B}$, the Kronecker product $\mathbf{A} \otimes \mathbf{B}$ is a $MP \times NQ$ matrix defined as follows [34].

$$\mathbf{A} \otimes \mathbf{B} \triangleq \begin{bmatrix} [\mathbf{A}]_{0,0}\,\mathbf{B} & [\mathbf{A}]_{0,1}\,\mathbf{B} & \cdots & [\mathbf{A}]_{0,N-1}\,\mathbf{B} \\ [\mathbf{A}]_{1,0}\,\mathbf{B} & [\mathbf{A}]_{1,1}\,\mathbf{B} & \cdots & [\mathbf{A}]_{1,N-1}\,\mathbf{B} \\ \vdots & \vdots & \ddots & \vdots \\ [\mathbf{A}]_{M-1,0}\,\mathbf{B} & [\mathbf{A}]_{M-1,1}\,\mathbf{B} & \cdots & [\mathbf{A}]_{M-1,N-1}\,\mathbf{B} \end{bmatrix}$$

Substituting (5.21) into (5.18) and exploiting (5.23), (5.24), and (5.22), we have the following.

$$
\begin{aligned}
\mathrm{Tr}\left[\mathbf{S}_{\mathbf{ee}}(z)\right] &= \mathrm{Tr}\left[\mathbf{S}_{\mathbf{xx}}(z)\right] - \mathrm{Tr}\left[\widetilde{\mathbf{H}}(z)\widetilde{\mathbf{F}}(z)\mathbf{S}_{\mathbf{xx}}(z)\right] - \mathrm{Tr}\left[\mathbf{S}_{\mathbf{xx}}(z)\mathbf{F}(z)\mathbf{H}(z)\right] \\
&\quad + \mathrm{Tr}\left[\widetilde{\mathbf{H}}(z)\widetilde{\mathbf{F}}(z)\mathbf{F}(z)\mathbf{H}(z)\mathbf{S}_{\mathbf{xx}}(z)\right] \\
&\quad + \frac{1}{2\pi}\int_0^{2\pi} \mathrm{Tr}\left[\mathbf{H}^\dagger(e^{j\lambda})\mathbf{\Lambda}(z)\mathbf{H}(e^{j\lambda})\mathbf{S}_{\mathbf{xx}}(e^{j\lambda})\right]\, d\lambda \\
&= \mathrm{Tr}\left[\mathbf{S}_{\mathbf{xx}}(z)\right] - \overline{\mathbf{h}}^\dagger\mathbf{a}(z)\mathbf{v}(z) - \widetilde{\mathbf{v}}(z)\widetilde{\mathbf{a}}(z)\overline{\mathbf{h}} \\
&\quad + \overline{\mathbf{h}}^\dagger\mathbf{a}(z)\,\mathrm{vec}\left(\widetilde{\mathbf{F}}(z)\mathbf{F}(z)\mathbf{H}(z)\mathbf{S}_{\mathbf{xx}}(z)\right) \\
&\quad + \frac{1}{2\pi}\int_0^{2\pi} \overline{\mathbf{h}}^\dagger\mathbf{a}(e^{j\lambda})\,\mathrm{vec}\left(\mathbf{\Lambda}(z)\mathbf{H}(e^{j\lambda})\mathbf{S}_{\mathbf{xx}}(e^{j\lambda})\right)\, d\lambda \\
&= \mathrm{Tr}\left[\mathbf{S}_{\mathbf{xx}}(z)\right] - \overline{\mathbf{h}}^\dagger\mathbf{a}(z)\mathbf{v}(z) - \widetilde{\mathbf{v}}(z)\widetilde{\mathbf{a}}(z)\overline{\mathbf{h}} \\
&\quad + \overline{\mathbf{h}}^\dagger\mathbf{a}(z)\left(\mathbf{S}^T_{\mathbf{xx}}(z)\otimes\widetilde{\mathbf{F}}(z)\mathbf{F}(z)\right)\widetilde{\mathbf{a}}(z)\overline{\mathbf{h}} \\
&\quad + \overline{\mathbf{h}}^\dagger\left(\frac{1}{2\pi}\int_0^{2\pi}\mathbf{a}(e^{j\lambda})\left(\mathbf{S}^T_{\mathbf{xx}}(e^{j\lambda})\otimes\mathbf{\Lambda}(z)\right)\mathbf{a}^\dagger(e^{j\lambda})\,d\lambda\right)\overline{\mathbf{h}}
\end{aligned}
\tag{5.25}
$$

Upon substituting (5.25) into (5.17), we get the following.

$$
\xi = \mathrm{Tr}\left[\mathbf{R}_{\mathbf{xx}}(0)\right] - \overline{\mathbf{h}}^\dagger\mathbf{g} - \mathbf{g}^\dagger\overline{\mathbf{h}} + \overline{\mathbf{h}}^\dagger\mathbf{C}\overline{\mathbf{h}} \tag{5.26}
$$

where the $LMN_h \times 1$ vector $\mathbf{g}$ and $LMN_h \times LMN_h$ matrix $\mathbf{C}$ are defined as

$$
\mathbf{g} \triangleq \frac{1}{2\pi}\int_0^{2\pi}\mathbf{a}(e^{j\omega})\mathbf{v}(e^{j\omega})\,d\omega \tag{5.27}
$$

$$
\mathbf{C} \triangleq \frac{1}{2\pi}\int_0^{2\pi}\mathbf{a}(e^{j\omega})\left(\mathbf{S}^T_{\mathbf{xx}}(e^{j\omega})\otimes\left(\mathbf{F}^\dagger(e^{j\omega})\mathbf{F}(e^{j\omega})+\mathbf{D}\right)\right)\mathbf{a}^\dagger(e^{j\omega})\,d\omega \tag{5.28}
$$

and the $L \times L$ matrix $\mathbf{D}$ is defined to be

$$
\mathbf{D} \triangleq \frac{1}{2\pi}\int_0^{2\pi}\mathbf{\Lambda}(e^{j\omega})\,d\omega
$$

where $\mathbf{\Lambda}(z)$ is as in (5.20).

As can be seen from (5.26), the mean-squared error ξ is a quadratic function of the coefficients of $\mathbf{H}(z)$ which are contained in the vector $\overline{\mathbf{h}}$. To minimize ξ from (5.26), we can complete the square as was done in Sec. 5.3.1. In order to do so, first note that the matrix $\mathbf{C}$ from (5.28) is invertible. To see this, note that from (5.8), $\overline{\mathbf{h}}^\dagger\mathbf{C}\overline{\mathbf{h}}$ represents the energy of $\widehat{\mathbf{x}}(n)$ from Fig. 5.3, i.e., $\overline{\mathbf{h}}^\dagger\mathbf{C}\overline{\mathbf{h}} = \mathrm{Tr}\left[\mathbf{R}_{\widehat{\mathbf{x}}\widehat{\mathbf{x}}}(0)\right] > 0$ for all $\overline{\mathbf{h}} \neq \mathbf{0}$, since we assume that the energy of $\widehat{\mathbf{x}}(n)$ is nonzero here. Hence, by completing the square [22], the optimal $\overline{\mathbf{h}}$ and corresponding optimal ξ are given by

$$
\boxed{\overline{\mathbf{h}}_{\mathrm{opt}} = \mathbf{C}^{-1}\mathbf{g}\,,\ \xi_{\mathrm{opt}} = \mathrm{Tr}\left[\mathbf{R}_{\mathbf{xx}}(0)\right] - \mathbf{g}^\dagger\mathbf{C}^{-1}\mathbf{g}} \tag{5.29}
$$

Here, $\mathbf{g}$ and $\mathbf{C}$ are given by (5.27) and (5.28), respectively. The choice of $\overline{\mathbf{h}}$ given in (5.29) is optimal for a fixed $\mathbf{S}_{\mathbf{xx}}(z)$, $\mathbf{F}(z)$, $\{c_k\}$, and $\{b_k\}$.

5.3.3 Iterative Greedy Analysis/Synthesis Filter Bank Optimization Algorithm

By alternately optimizing the analysis and synthesis banks, we obtain an iterative *greedy* algorithm for designing an FIR filter bank adapted to the psd $\mathbf{S}_{\mathbf{xx}}(z)$ and the bit allocation $\{b_k\}$. In what follows, let $\mathbf{F}_k(z)$, $\mathbf{H}_k(z)$, and ξ_k denote, respectively, the synthesis bank, analysis bank, and reconstruction error at the k-th iteration for $k \geq 0$. Then, the iterative filter bank optimization algorithm is as follows.

Initialization:

1. Select a set of values for the desired filter bank parameters L, M, P, N_f, Q, and N_h.
2. Select a desired bit allocation $\{b_k\}$ along the subbands and choose appropriate quantizer performance factors $\{c_k\}$ for the subband pdfs.
3. Choose an initial synthesis bank $\mathbf{F}_0(z)$.
4. Compute the corresponding optimal analysis bank $\mathbf{H}_0(z)$ and reconstruction error ξ_0 using (5.29).

Iteration: For $k \geq 1$, do the following.

1. With a fixed analysis bank $\mathbf{H}_{k-1}(z)$, compute the optimal synthesis bank $\mathbf{F}_k(z)$ using (5.16).
2. With a fixed synthesis bank $\mathbf{F}_k(z)$, compute the optimal analysis bank $\mathbf{H}_k(z)$ and corresponding reconstruction error ξ_k using (5.29).
3. Increment k by 1 and return to Step 1.

Since this algorithm is greedy, the error ξ_k is guaranteed to be a monotonic nonincreasing function of the iteration index k. As the error is always lower bounded by zero (i.e., $\xi_k \geq 0$), ξ_k is also guaranteed to have a limit as $k \to \infty$ [67]. Simulation results provided here verify this monotonic and limiting behavior. In particular, it will be seen that the error appears to quickly converge to its limit after only a few iterations.

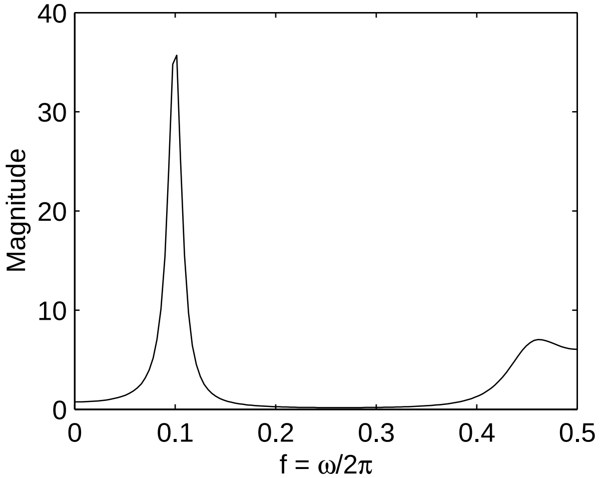

Figure 5.4: Input psd $S_{xx}(e^{j\omega})$ to the system of Fig. 5.1.

5.4 Simulation Results

5.4.1 Overdecimated Filter Bank Design

The proposed iterative algorithm of this chapter can be used for the design of overdecimated compaction-like filter banks in which the only constraint made on the analysis and synthesis filters is that they be FIR. This is done by setting $L < M$ and the quantizer performance factors $c_k = 0$. In this case, the filter bank only suffers from aliasing, amplitude, and phase distortions due to the fact that the filter bank is overdecimated (see Chapter 2). Even though we are not enforcing a PU condition here, it will be seen that in some instances, the filters designed share something in common with those of the infinite-order PCFB. In particular, it will be seen that in some cases, the filters designed try to *compact the energy* of the input signal, a property shared by the PCFB filters.

5.4.1.1 Single Subband Design Example

Suppose that the input $x(n)$ to Fig. 5.1 is a real WSS AR(4) process whose psd $S_{xx}(e^{j\omega})$ is shown in Fig. 5.4. Furthermore, suppose that we chose the following filter bank parameters here.

- Number of channels – $L = 1$, Decimation ratio – $M = 3$.
- Synthesis advance parameter – $P = 0$, Synthesis polyphase matrix length – $N_f = 7$.
- Analysis advance parameter – $Q = N_h - 1$, Analysis polyphase matrix length – $N_h = 7$.

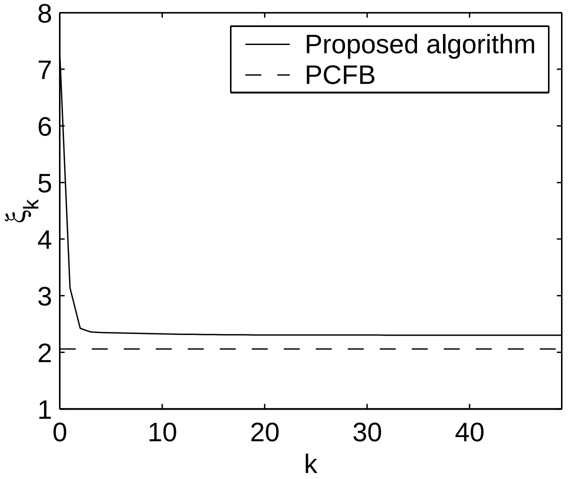

Figure 5.5: Mean-squared reconstruction error ξ_k as a function of the iteration index k. (Single subband example)

In other words, for this example, we have opted to design one subband of a three channel system in which the synthesis filter $F_0(z)$ is a *causal* FIR filter of length $MN_f = 21$ and the analysis filter is an *anticausal* FIR filter of length $MN_h = 21$. Here, we chose the synthesis filter to be causal and the analysis filter to be anticausal and of the same length as the synthesis filter so as not to introduce a temporal bias into the filter bank. For the initialization, the initial synthesis bank $\mathbf{F}_0(z)$ was chosen to be a random causal FIR PU system of degree $(N_f - 1)$ using the complete parameterization of such systems given in Sec. 3.2. All integrals required in the proposed algorithm were computed numerically using 256 uniformly spaced frequency samples.

A plot of the reconstruction error ξ_k as a function of the iteration index k is shown in Fig. 5.5 for a total of 50 iterations. In addition to the FIR filter bank error, we have shown the error obtained using the infinite-order PCFB compaction filters for comparison. As can be seen, the error ξ_k indeed is monotonic nonincreasing and appears to be approaching a limit. After the last iteration, the error was 2.3026, which is close to the corresponding PCFB error of 2.0583. As we increase the order of the filters N_f and N_h, the observed error comes closer to the PCFB error and may in fact surpass this error since outside of the inherent FIR constraint, we are imposing no other constraints such as orthonormality or biorthogonality. When we ran the same simulations but increased N_f and N_h both to 10, the observed reconstruction error after 50 iterations was found to be 2.2163.

It would be interesting to further increase N_f and N_h to see their asymptotic behavior. However, the proposed algorithm becomes excessively computationally intensive in this case and more prone

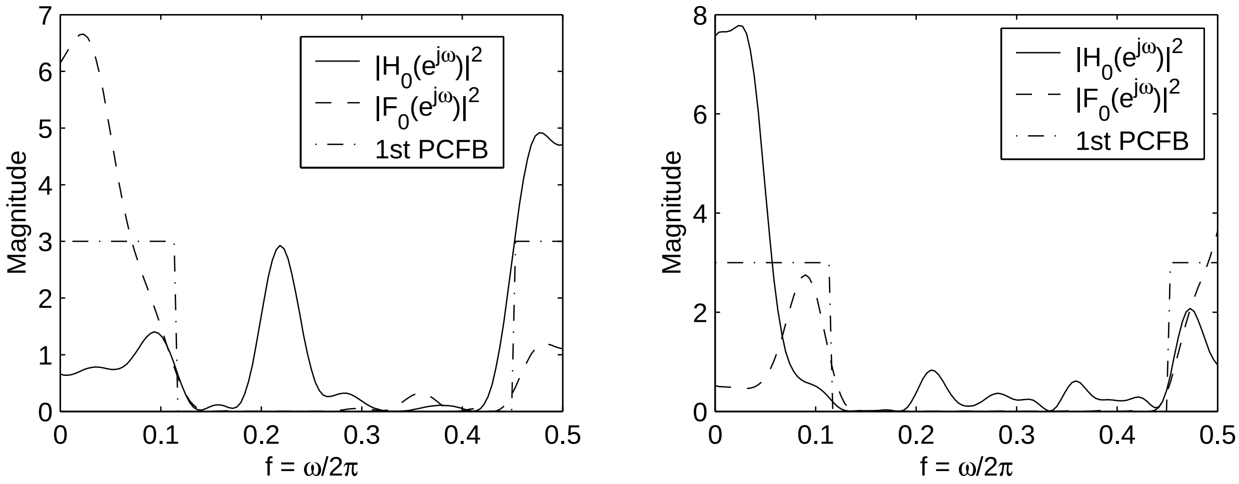

(a)

(b)

Figure 5.6: Magnitude squared responses of the analysis and synthesis filters for (a) $N_f = N_h = 7$ and (b) $N_f = N_h = 10$. (Single subband example)

to numerical inaccuracies. This is because the matrices required to be inverted, namely, $\mathbf{A}$ in (5.14) and $\mathbf{C}$ in (5.28), grow linearly in size with N_f and N_h, respectively, and hence become more complex to invert and more susceptible to numerical errors as a result.

A plot of the magnitude squared responses of the analysis and synthesis filters designed is shown in Fig. 5.6 for (a) $N_f = N_h = 7$ and (b) $N_f = N_h = 10$. In addition, we have also plotted the magnitude squared response of the first PCFB analysis/synthesis filter, which is an ideal compaction filter. As can be seen, the filters designed appear to have most of their energy contained in the same frequency support region as that of the ideal compaction filter. Though no PU constraint was enforced here, the filters designed appear to be *compacting the energy* of the input signal, much like the ideal compaction filter of the PCFB.

In order to gauge the behavior of the solutions obtained with the proposed algorithm, we opted to calculate the deviation of the observed solutions from orthonormality and biorthogonality. To measure the deviation from orthonormality, we considered the metric

$$\delta_{\perp,k} \triangleq \frac{1}{2\pi} \int_0^{2\pi} \left|\left|\mathbf{I}_L - \mathbf{F}_k^{\dagger}(e^{j\omega})\mathbf{F}_k(e^{j\omega})\right|\right|_2^2 d\omega$$

whereas to measure the deviation from biorthogonality, we used

$$\delta_{\mathrm{BIO},k} \triangleq \frac{1}{2\pi} \int_0^{2\pi} \left|\left|\mathbf{I}_L - \mathbf{H}_k(e^{j\omega})\mathbf{F}_k(e^{j\omega})\right|\right|_2^2 d\omega$$

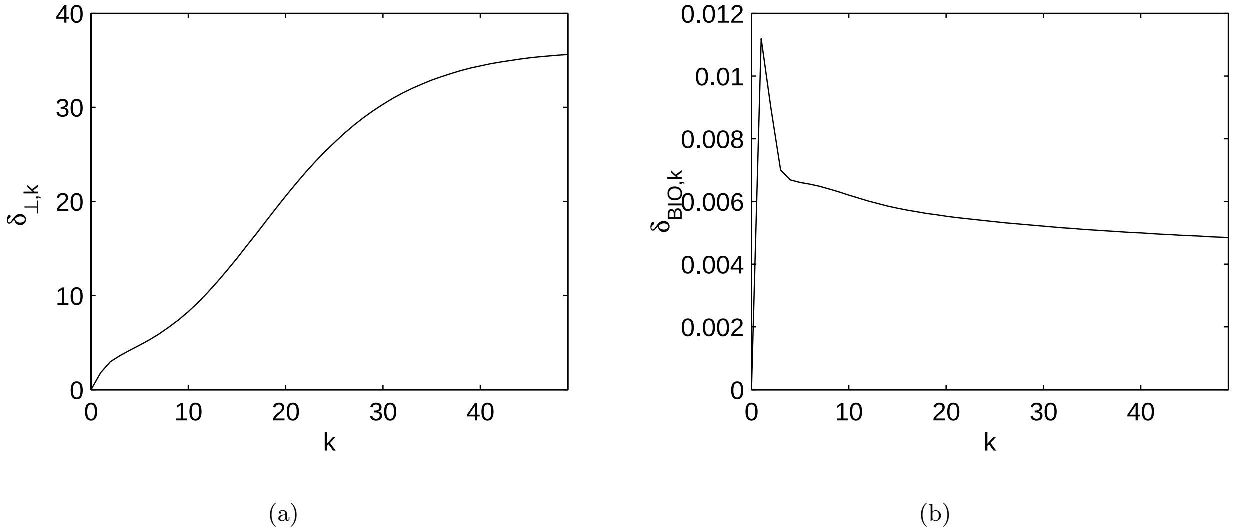

Figure 5.7: Deviation from (a) orthonormality $\delta_{\perp,k}$ and (b) biorthogonality $\delta_{\mathrm{BIO},k}$ as a function of the iteration index k. (Single subband example)

In Fig. 5.7(a) and (b), we have plotted, respectively, $\delta_{\perp,k}$ and $\delta_{\mathrm{BIO},k}$ as functions of k for the case $N_f = N_h = 7$. From Fig. 5.7(a), it can be seen that the solution obtained deviates monotonically from orthonormality, whereas from Fig. 5.7(b), the solution fluctuates but appears approximately biorthogonal. Similar phenomena occurred for $N_f = N_h = 10$ but the results are omitted here for sake of brevity.

5.4.1.2 Multiple Subband Design Example

For this section, we consider the same design example considered in Sec. 5.4.1.1, except that this time, we will take $L = 2$ here. In other words, we consider here the design of two subbands of a three channel system. As before, we ignore the effects due to quantization and so the only sources of error are those due to aliasing, amplitude, and phase distortions as the filter bank is overdecimated.

A plot of the observed reconstruction error ξ_k as a function of the iteration index k is shown in Fig. 5.8 for 50 iterations. As before, we have included the corresponding error obtained with the PCFB. After the last iteration, the error was 0.2455, which is close to the corresponding PCFB error of 0.2294. Note that, as before, if we increase the filter order parameters N_f and N_h, the error comes closer to the PCFB error and may surpass it. Here, when we chose $N_f = N_h = 10$, the observed error after 50 iterations was 0.2377, which indeed is closer to the PCFB error than 0.2455, which was obtained for $N_f = N_h = 7$.

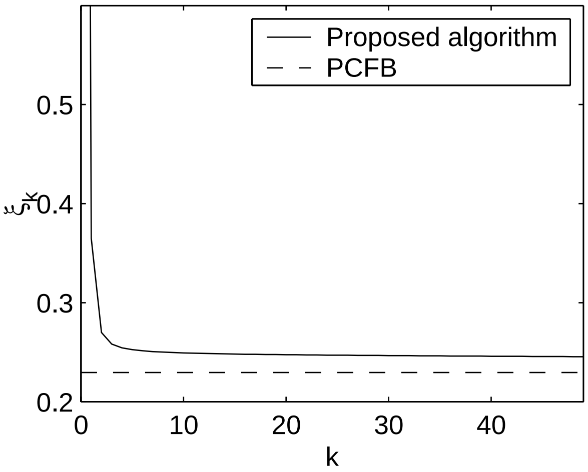

Figure 5.8: Mean-squared reconstruction error ξ_k as a function of the iteration index k. (Multiple subband example)

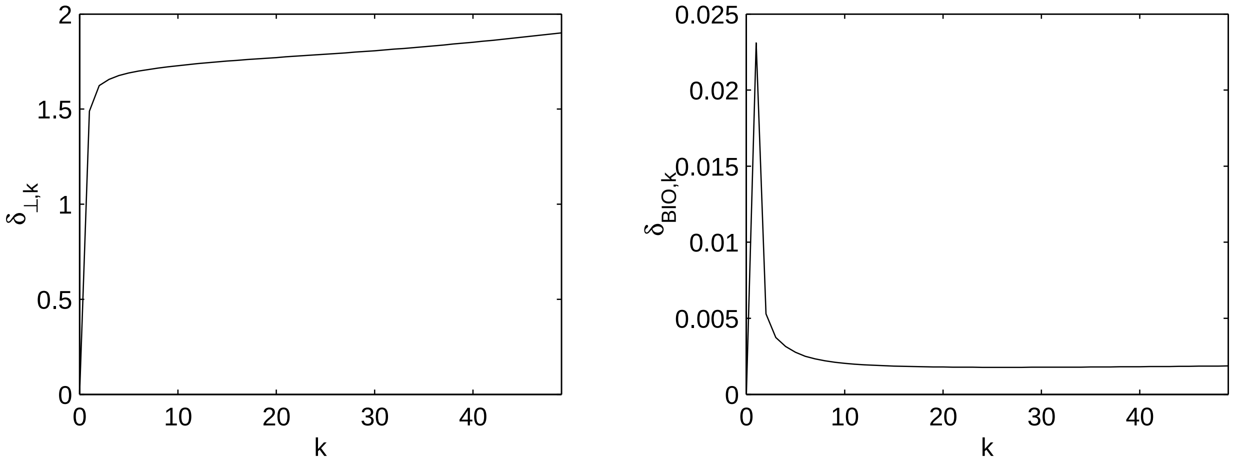

(a)

(b)

Figure 5.9: Deviation from (a) orthonormality $\delta_{\perp,k}$ and (b) biorthogonality $\delta_{\mathrm{BIO},k}$ as a function of the iteration index k. (Multiple subband example)

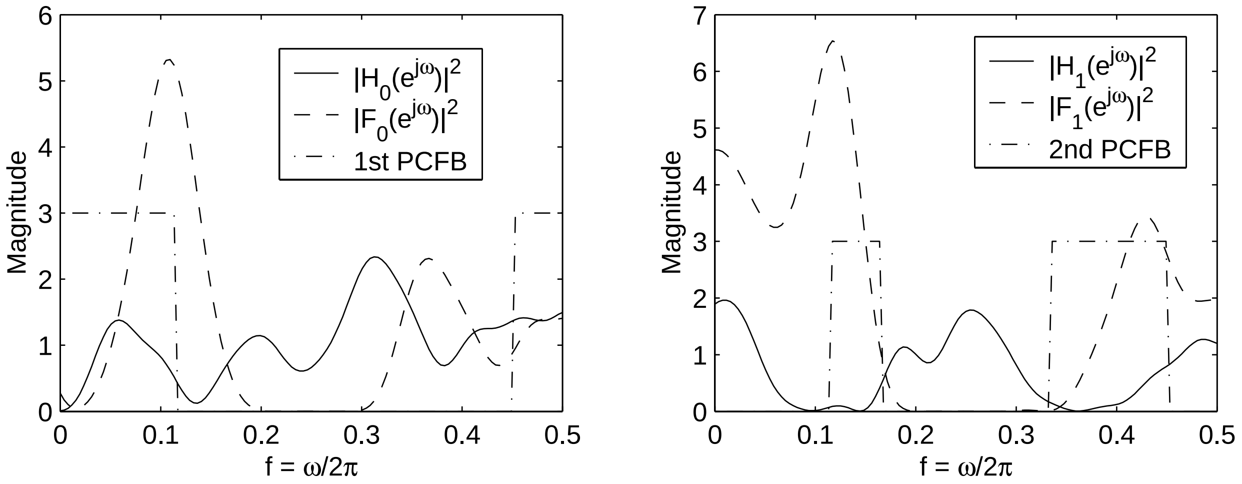

(a)

(b)

Figure 5.10: Magnitude squared responses of the analysis filters $H_k(z)$ and synthesis filters $F_k(z)$ for (a) $k = 0$, and (b) $k = 1$. (Multiple subband example)

In Fig. 5.9(a) and (b), we have plotted the deviation in orthonormality and biorthogonality, respectively. As was the case in Sec. 5.4.1.1, the solution obtained monotonically deviates from orthonormality but appears approximately biorthogonal after some fluctuation.

In Fig. 5.10, we have plotted the magnitude squared responses of the analysis and synthesis filters. For comparison, we have included the corresponding responses of the first two analysis/synthesis filters of the infinite-order PCFB. Note that unlike in Sec. 5.4.1.1, the filters designed do not resemble the PCFB ideal compaction filters.

The designed FIR filters do not individually compact the energy of the input signal but rather *collaborate* to minimize the mean-squared error of the output. It turns out that there is always a nonunique way for the filters to collaborate. To see this, note that in the absence of quantizers, the overdecimated filter bank can be redrawn as in Fig. 5.11, where $\mathbf{T}$ is any $L \times L$ invertible matrix. Clearly, if $\mathbf{H}(z)$ and $\mathbf{F}(z)$ are optimal FIR systems for minimizing the mean-squared reconstruction error ξ, so too are $\widehat{\mathbf{H}}(z) = \mathbf{T}^{-1}\mathbf{H}(z)$ and $\widehat{\mathbf{F}}(z) = \mathbf{F}(z)\mathbf{T}$. As $\mathbf{T}$ need not be diagonal, given any optimal set of analysis/synthesis filters, we can obtain a new set of optimal filters which collaborate with one another to minimize ξ. In the special case where $L = 1$, then $\mathbf{T}$ becomes simply a scale factor, and so in this case, no such collaboration is possible. Hence, the analysis and synthesis filters must individually compact the energy of the input so as to minimize the reconstruction error ξ, which was observed in Sec. 5.4.1.1.

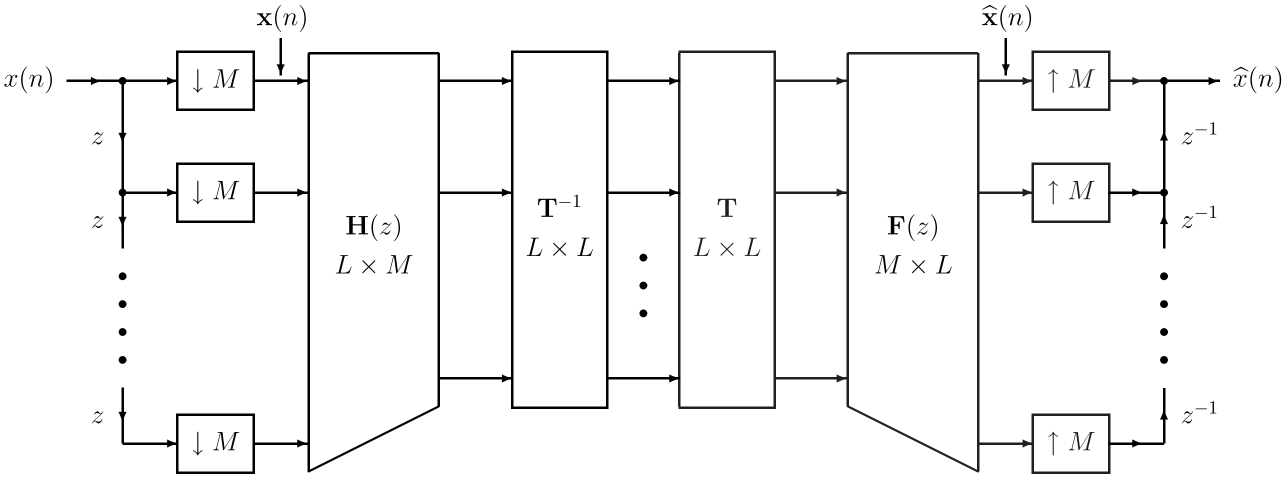

Figure 5.11: Equivalent overdecimated filter bank model in the absence of quantizers.

5.4.2 Quantized Filter Bank Design

In this section, we focus on the design of quantized filter banks. For all of the examples we will consider here, the filter bank will be assumed to be maximally decimated, i.e., $L = M$ here. To gauge the performance of the filter banks designed, we will consider several relevant measures.

The first measure of optimality we consider here is the *coding gain* [25, 67] of the filter banks designed. This quantity measures the improvement in distortion by using a filter bank quantization system as opposed to direct quantization at the same average bit rate. The coding gain G_{code} is defined as the ratio between the distortion incurred by direct quantization and that incurred by using the filter bank system. In other words, we have

$$G_{\text{code}} \triangleq \frac{D_{\text{dir}}}{D_{\text{FB}}} \tag{5.30}$$

where D_{dir} is the distortion incurred from direct quantization given by (5.1) to be

$$D_{\text{dir}} = c2^{-2b}\sigma_x^2$$

where c, b, and σ_x^2 are the quantizer performance factor, average bit rate, and input variance, respectively, and D_{FB} is the *average* distortion incurred by the filter bank system given by

$$D_{\text{FB}} = \frac{1}{M}\xi \tag{5.31}$$

where ξ is the filter bank blocked reconstruction error given in (5.3). Here, in order for G_{code} to be a meaningful measure, we require that the bit rate b of the directly quantized signal be equal to the *average* bit rate of the filter bank quantization system, i.e., we have

$$b = \frac{1}{M} \sum_{k=0}^{M-1} b_k \tag{5.32}$$

Hence, the coding gain is a measure of the improvement in terms of distortion offered by using a sophisticated filter bank quantization scheme as opposed to an unsophisticated single quantizer system at the same bit rate.

In certain special cases, the coding gain can be simplified greatly. For example, if the quantized filter bank system of Fig. 5.1 is a maximally decimated orthonormal or PU filter bank, the coding gain becomes [25, 72]

$$G_{\text{code}} = \frac{c 2^{-2b} \sigma_x^2}{\displaystyle\frac{1}{M} \sum_{k=0}^{M-1} \sigma_{q_k}^2} = \frac{c 2^{-2b} \sigma_x^2}{\displaystyle\frac{1}{M} \sum_{k=0}^{M-1} c_k 2^{-2b_k} \sigma_{w_k}^2}$$

Assuming that all of the subband quantizer performance factors c_k are all equal to c, which occurs if the input pdfs are all the same, then we have

$$G_{\text{code}} = \frac{2^{-2b} \sigma_x^2}{\displaystyle\frac{1}{M} \sum_{k=0}^{M-1} 2^{-2b_k} \sigma_{w_k}^2}$$

It turns out [25, 67] that for any fixed PU filter bank, there is an optimal way to allocate the subband bit rates $\{b_k\}$ subject to the average bit rate constraint of (5.32) to maximize G_{code}. This occurs as a result of using the arithmetic mean/geometric mean (AM/GM) inequality [22, 67]. With optimal bit allocation, the coding gain becomes

$$G_{\text{code}} = \frac{\sigma_x^2}{\left(\displaystyle\prod_{k=0}^{M-1} \sigma_{w_k}^2\right)^{\frac{1}{M}}} = \frac{\displaystyle\frac{1}{M} \sum_{k=0}^{M-1} \sigma_{w_k}^2}{\left(\displaystyle\prod_{k=0}^{M-1} \sigma_{w_k}^2\right)^{\frac{1}{M}}}$$

which is itself the AM/GM ratio of the subband variances. By the AM/GM inequality, we always have $G_{\text{code}} \geq 1$ and so for any PU filter bank, there is always an improvement in terms of distortion if the bits have been optimally allocated. With optimal bit allocation, among all PU filter banks of a certain class, the PCFB, if it exists, exhibits the largest coding gain [1, 68].

Using the proposed iterative greedy algorithm of this chapter, it can be seen from (5.30) and (5.31) that we obtain a filter bank system whose coding gain is *monotonic nondecreasing* with iteration for a *fixed* bit allocation $\{b_k\}$. This is more practical than optimizing the bit allocation for a fixed filter bank, which will often times yield unrealizable noninteger bit allocations [25, 67].

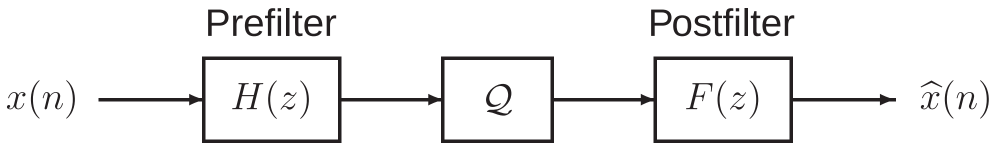

Figure 5.12: Pre/postfiltering quantization system.

Another measure we will focus on here is the distortion itself. It turns out that for a given average bit rate b, there is a minimum distortion $D_{\min}$ which can be achieved using any compression scheme. This bound, known as the *rate-distortion bound* [10, 7] represents an information theoretic limit as to the performance that can ever be achieved. For a Gaussian CWSS(M) input $x(n)$ and for a sufficiently large bit rate b, the rate-distortion bound becomes [25, 67]

$$D_{\min}(b) = \gamma_x^2 2^{-2b} \sigma_x^2 \tag{5.33}$$

where γ_x^2 is the *spectral flatness measure* [25, 31] of the process $x(n)$ given by

$$\gamma_x^2 \triangleq \frac{\exp\left\{\frac{1}{2\pi}\int_0^{2\pi} \log\left[\left(\det\left(\mathbf{S}_{\mathbf{xx}}(e^{j\omega})\right)\right)^{\frac{1}{M}}\right]\, d\omega\right\}}{\frac{1}{2\pi}\int_0^{2\pi} \frac{1}{M}\mathrm{Tr}\left[\mathbf{S}_{\mathbf{xx}}(e^{j\omega})\right]\, d\omega} = \frac{\exp\left\{\frac{1}{2\pi M}\int_0^{2\pi} \log\left[\det\left(\mathbf{S}_{\mathbf{xx}}(e^{j\omega})\right)\right]\, d\omega\right\}}{\sigma_x^2}$$

where $\mathbf{S}_{\mathbf{xx}}(z)$ denotes the psd of the M-fold blocked version of $x(n)$, namely, $\mathbf{x}(n)$. Using (5.33) in (5.30), it follows that the coding gain G_{code} can be upper bounded as follows.

$$G_{\text{code}} \leq G_{\text{code,max}} = \frac{c}{\gamma_x^2} \tag{5.34}$$

where c is the quantizer performance factor of the direct quantization scheme. Through the simulation results we present here, it will be shown that the filter banks designed come closer to the rate-distortion bound and coding gain bound as the filter orders are increased, in line with intuition.

5.4.2.1 Single Channel Example - Pre/Postfiltering in Quantization

The proposed iterative algorithm can be used for the design of an optimal pre/postfiltering quantization scheme such as the one shown in Fig. 5.12. Note that this system is simply a special case of the quantized filter bank system of Fig. 5.1 in which we have $L = M = 1$. The system shown in Fig. 5.12 is often used for lossy data compression applications and the popular quantization scheme *differential pulse code modulation* (DPCM) is itself a special case of this system.

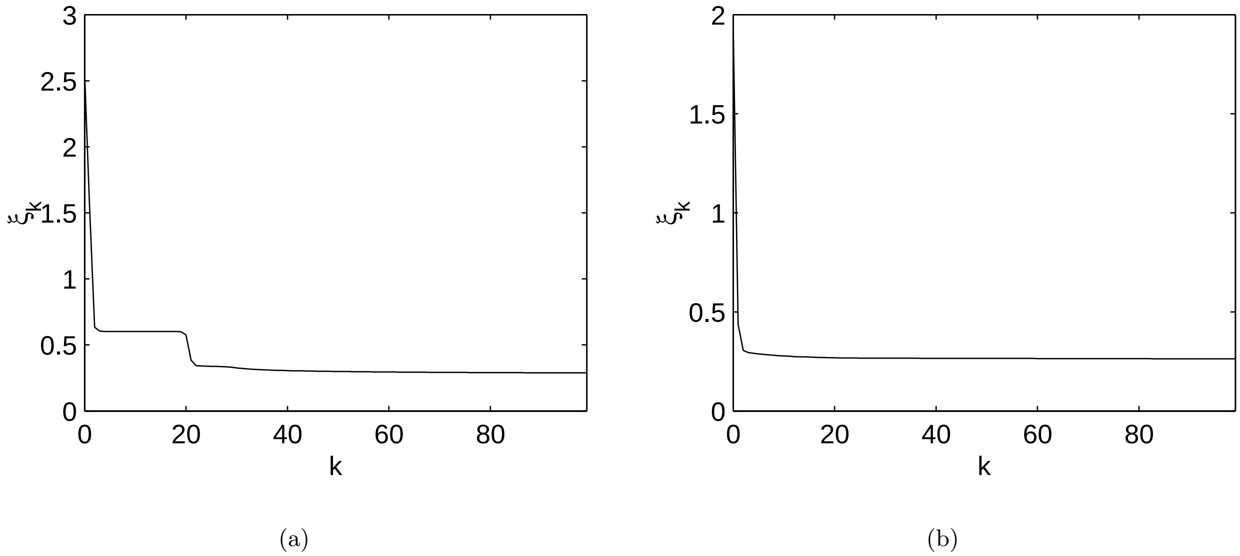

(a)

(b)

Figure 5.13: Mean-squared reconstruction error ξ_k as a function of the iteration index k for (a) $N = 10$ and (b) $N = 20$.

To test the proposed algorithm, we chose the following parameters here.

- Quantizer performance factor – $c_0 = c = 2.71$ (Gaussian pdf)
- Bit rate $b_0 = b$ was varied from 2 to 6 bits.
- Synthesis filter $F_0(z) = F(z)$ was causal FIR and of length N. Analysis filter $H_0(z) = H(z)$ was anticausal FIR and of length N also. Here N was varied from 10 to 20.

For each run of the algorithm, a total of 100 iterations was used. Here, the initial synthesis bank $F_0(z)$ was chosen completely randomly.

In Fig. 5.13, we have plotted the observed reconstruction error ξ_k for a bit rate of $b_0 = b = 2$ as a function of the iteration index k for (a) $N = 10$ and (b) $N = 20$. As can be seen, the error decreases monotonically and appears to saturate as before. For $N = 10$, the error at the last iteration was 0.2884, whereas for $N = 20$, the error was 0.2627. As expected, when N increased here, the steady state error decreased.

In Fig. 5.14 and 5.15 we have respectively plotted the deviation in orthonormality and biorthogonality for (a) $N = 10$ and (b) $N = 20$, respectively. As can be seen, in all of these examples, the solutions appear to become more orthonormal and biorthogonal as the iterations progress. For $N = 10$, we have $\delta_{\perp,k} = 0.3910$ and $\delta_{\mathrm{BIO},k} = 0.0972$ for the last iteration, whereas for $N = 20$, we

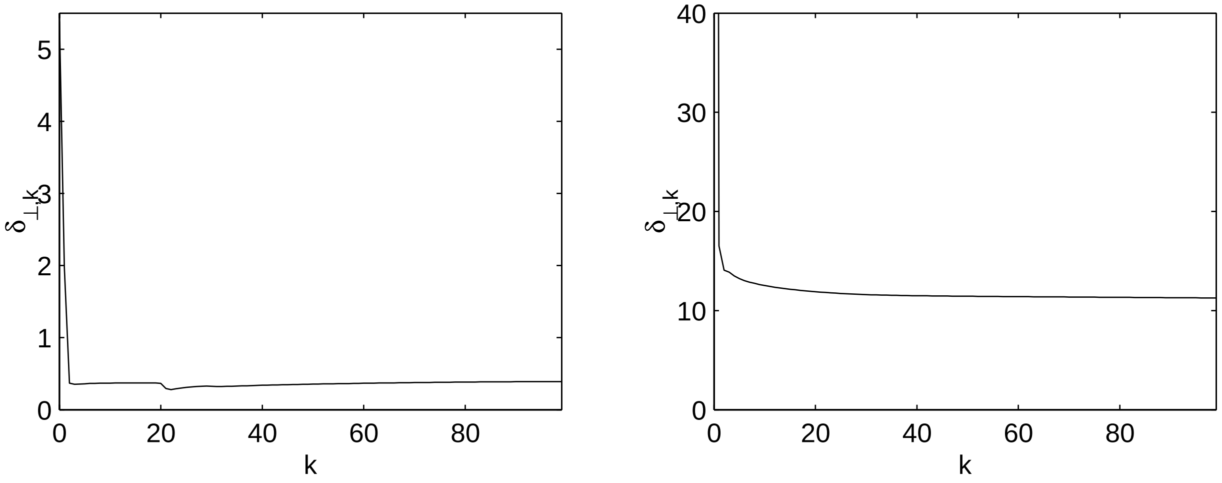

(a)

(b)

Figure 5.14: Deviation from orthonormality $\delta_{\perp,k}$ as a function of the iteration index k for (a) $N = 10$ and (b) $N = 20$.

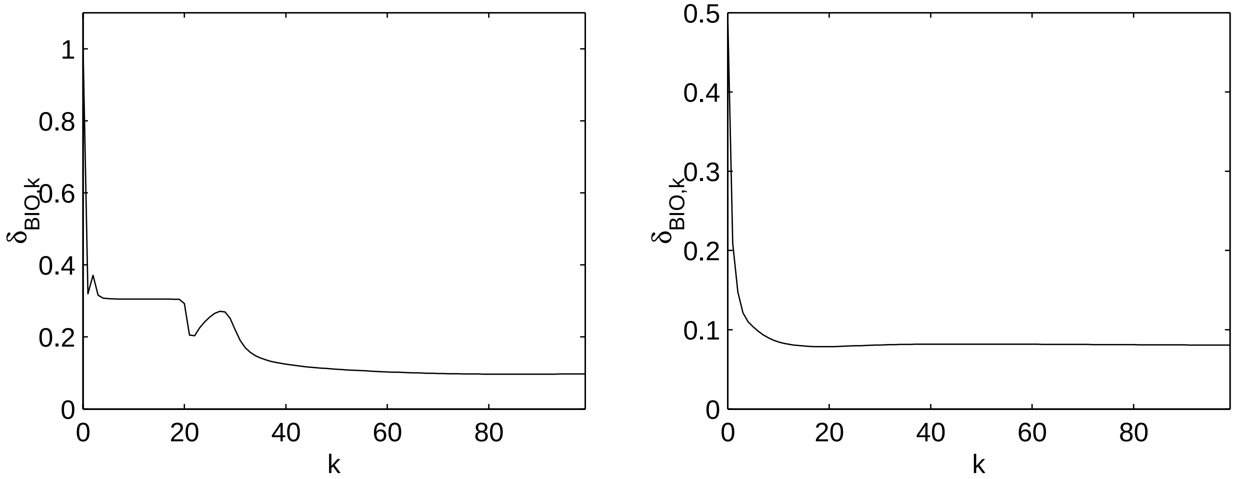

(a)

(b)

Figure 5.15: Deviation from biorthogonality $\delta_{\mathrm{BIO},k}$ as a function of the iteration index k for (a) $N = 10$ and (b) $N = 20$.

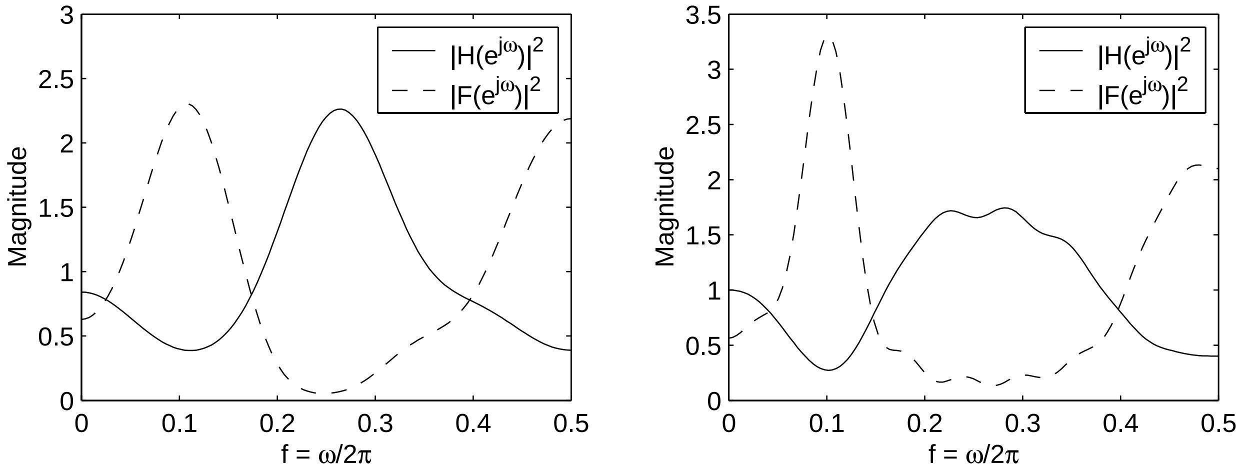

(a)

(b)

Figure 5.16: Magnitude squared responses of the analysis filter $H_0(z) = H(z)$ and the synthesis filter $F_0(z) = F(z)$ for (a) $N = 10$ and (b) $N = 20$.

have $\delta_{\perp,k} = 10.9306$ and $\delta_{\mathrm{BIO},k} = 0.0821$ for the same iteration. Hence, both solutions appear to be approximately biorthogonal but not quite orthonormal. This is in line with intuition, since if the solution were also orthonormal, then the system of Fig. 5.12 would be a simple direct quantization system, which we do not expect to be optimal here.

In Fig. 5.16, we have plotted the magnitude squared responses of the designed pre/postfilters for (a) $N = 10$ and (b) $N = 20$. As can be seen, in both cases the filter responses appear to be very similar to each other in terms of shape and support. This suggests that the algorithm is possibly striving to approximate a globally optimal set of filter responses.

In Fig. 5.17, we have plotted the observed distortion as a function of the average bit rate b for $N = 10$ and $N = 20$. For sake of comparison, we have included the distortion obtained through direct quantization, as well as the rate-distortion bound. As can be seen, the distortion always decreased monotonically with rate and always outperformed direct quantization. Furthermore, as the order increased, the distortion came closer to the rate-distortion bound, as expected.

Finally, in Fig. 5.18, we have plotted the observed coding gain G_{code} as a function of the filter order parameter N for an average bit rate of $b = 2$. As can be seen, the coding gain *monotonically* increased with N, in line with intuition. Furthermore, it came close to the maximum coding gain. Here, we had $G_{\mathrm{code}} = 1.9405$ for $N = 20$ in contrast to the maximum coding gain of $G_{\mathrm{code,max}} = 3.0068$.

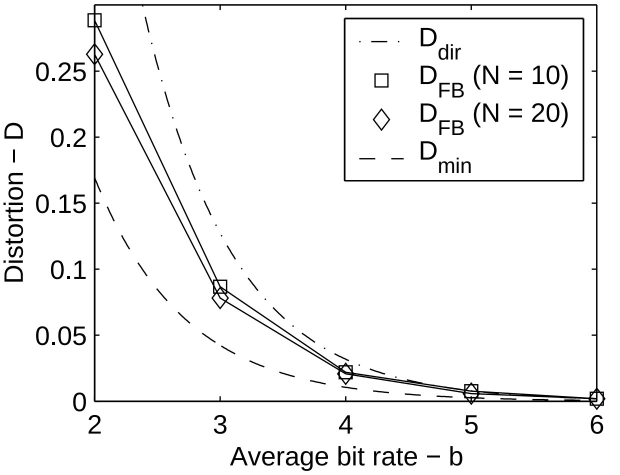

Figure 5.17: Observed distortion D_{FB} as a function of the average bit rate b plotted with the direct quantization and rate-distortion bounds.

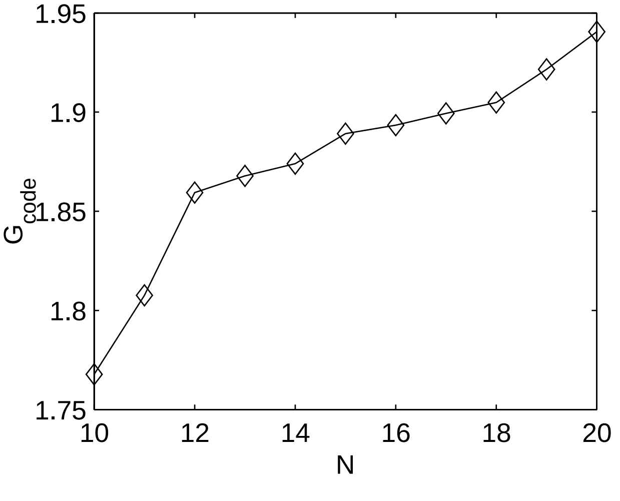

Figure 5.18: Observed coding gain G_{code} as a function of the analysis/synthesis filter order N.

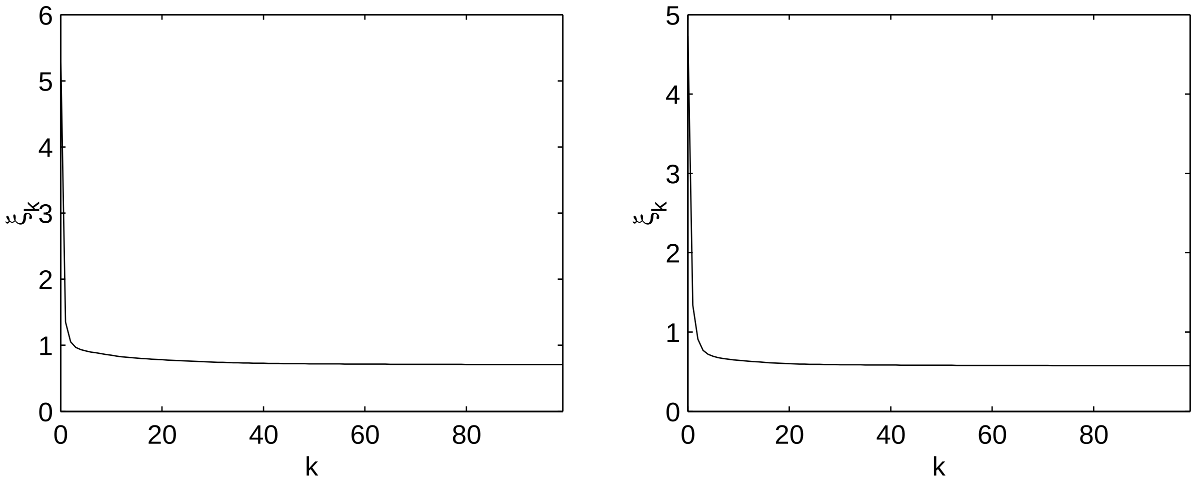

(a) (b)

Figure 5.19: Mean-squared reconstruction error ξ_k as a function of the iteration index k for (a) $N = 3$ and (b) $N = 6$.

5.4.2.2 Maximally Decimated Quantized Filter Bank

In this section, we consider the design of a maximally decimated filter bank with quantizers in the subbands. We chose the following parameters here.

- Number of subbands – $L = 3$. Decimation ratio – $M = 3$
- Quantizer performance factors – $c_k = c = 2.71$ for all k (Gaussian pdf)
- Average bit rate b was varied from 2 to 6 bits. For simplicity, the bits in the subbands were allocated as follows.

$$b_0 = b + 1\,,\ b_1 = b\,,\ b_2 = b - 1$$

- Synthesis polyphase matrix $\mathbf{F}(z)$ was causal FIR and of length N. Analysis polyphase matrix $\mathbf{H}(z)$ was anticausal FIR and of length N also. Here, N was varied from 1 to 6.

As before, the input $x(n)$ considered was the WSS process whose psd $S_{xx}(e^{j\omega})$ is as shown in Fig. 5.4. For each run of the algorithm, a total of 100 iterations was used. Here, the initial synthesis bank $\mathbf{F}_0(z)$ was chosen randomly as was done in the previous section.

In Fig. 5.19, we have plotted the observed reconstruction error ξ_k as a function of the iteration index k for (a) $N = 3$ and (b) $N = 6$. As can be seen, the error decreases monotonically and

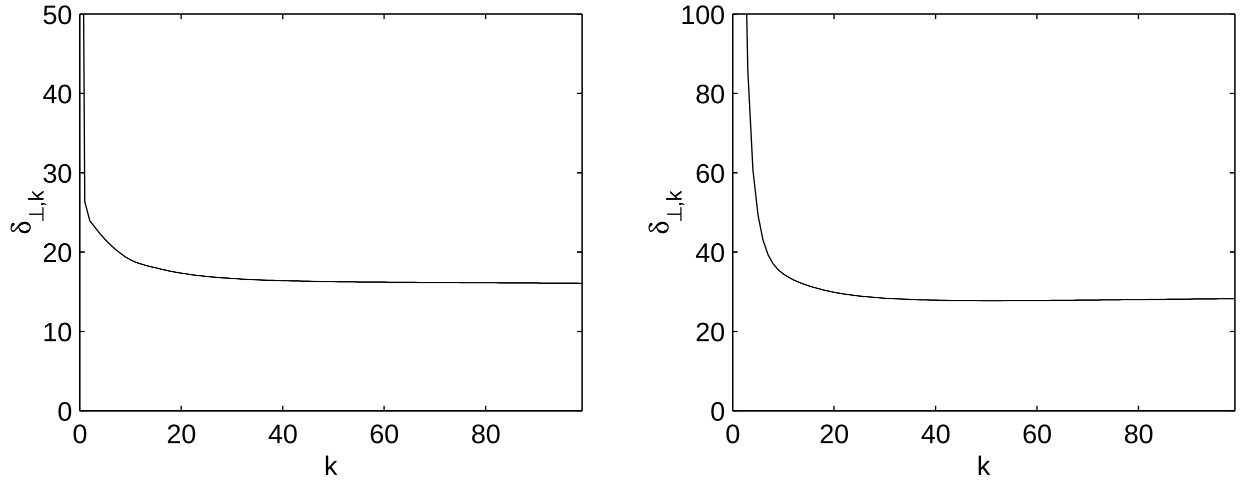

(a)

(b)

Figure 5.20: Deviation from orthonormality $\delta_{\perp,k}$ as a function of the iteration index k for (a) $N = 3$ and (b) $N = 6$.

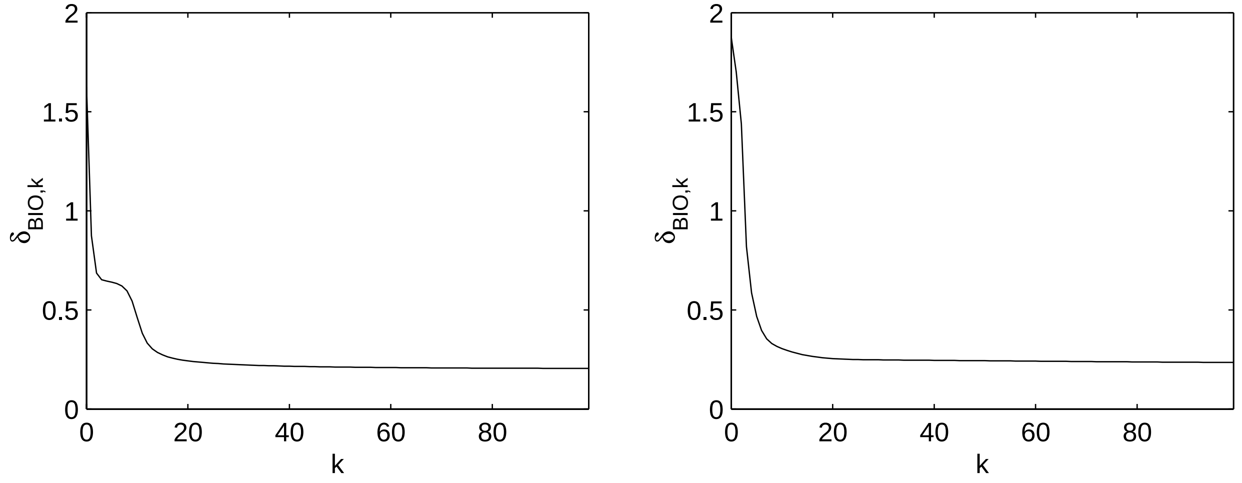

(a)

(b)

Figure 5.21: Deviation from biorthogonality $\delta_{\mathrm{BIO},k}$ as a function of the iteration index k for (a) $N = 3$ and (b) $N = 6$.

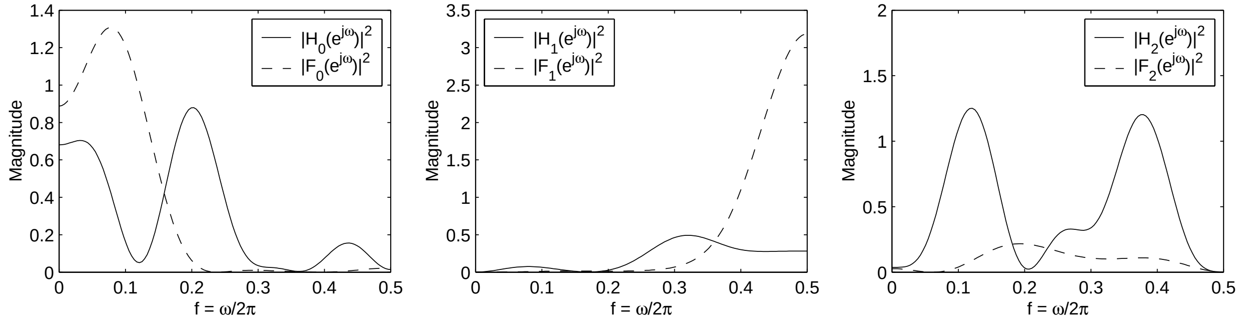

(a) (b) (c)

Figure 5.22: Magnitude squared responses of the analysis and synthesis filters for $N = 3$. (a) $H_0(z)$, $F_0(z)$, (b) $H_1(z)$, $F_1(z)$, (c) $H_2(z)$, $F_2(z)$.

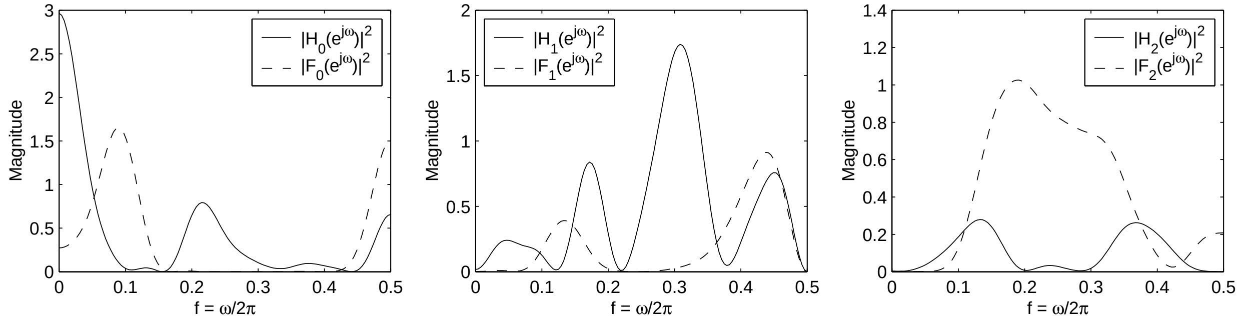

(a) (b) (c)

Figure 5.23: Magnitude squared responses of the analysis and synthesis filters for $N = 6$. (a) $H_0(z)$, $F_0(z)$, (b) $H_1(z)$, $F_1(z)$, (c) $H_2(z)$, $F_2(z)$.

appears to saturate as before. For $N = 3$, the error at the last iteration was 0.2339, whereas for $N = 6$, the error was 0.1919. As expected, when N increased here, the steady state error decreased.

In Fig. 5.20 and 5.21 we have respectively plotted the deviation in orthonormality and biorthogonality for (a) $N = 3$ and (b) $N = 6$, respectively. As can be seen, in all of these examples, the solutions appear to become more orthonormal and biorthogonal as the iterations progress. For $N = 3$, we have $\delta_{\perp,k} = 16.0173$ and $\delta_{\mathrm{BIO},k} = 0.2127$ for the last iteration, whereas for $N = 6$, we have $\delta_{\perp,k} = 28.2432$ and $\delta_{\mathrm{BIO},k} = 0.2347$ for the same iteration. Hence, both solutions appear to be neither orthonormal nor biorthogonal.

In Fig. 5.22 and 5.23, we have plotted the magnitude squared responses of the designed analysis and synthesis filters for $N = 3$ and $N = 6$, respectively. As opposed to the pre/postfiltering quanti-

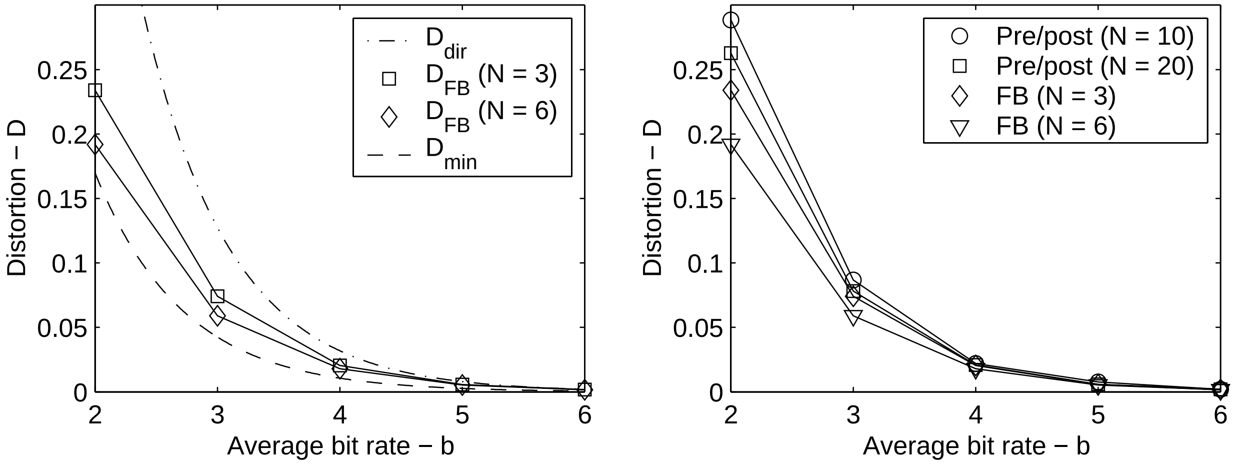

(a)

(b)

Figure 5.24: Observed distortion D_{FB} as a function of the average bit rate b plotted with (a) the direct quantization and rate-distortion bounds, (b) the pre/postfiltering quantization results.

zation system in which the different order solutions looked similar to each other, the corresponding responses here look very different.

In Fig. 5.24, we have plotted the observed distortion as a function of the average bit rate b for $N = 1$ and $N = 6$. For sake of comparison, in Fig. 5.24(a) we have included the distortion obtained through direct quantization and the rate-distortion bound, whereas in Fig. 5.24(b) we have included the results obtained using the pre/postfiltering quantization system analyzed in Sec. 5.4.2.1. As can be seen in Fig. 5.24(a), the distortion always decreased monotonically with rate and always outperformed direct quantization. Furthermore, as the order increased, the distortion came closer to the rate-distortion bound, in line with intuition. More importantly, in Fig. 5.24(b), it can be seen that each filter bank system outperformed both of the pre/postfiltering systems. This justifies the use of a sophisticated filter bank system for quantization as opposed to a less sophisticated pre/postfiltering quantization system.

Finally, in Fig. 5.25, we have plotted the observed coding gain as a function of the polyphase order N for an average bit rate of $b = 2$. As can be seen, the coding gain *monotonically* increased with N, in line with intuition. Furthermore, it came very close to the maximum coding gain in this case. Here, we had $G_{\mathrm{code}} = 2.6576$ for $N = 6$ in contrast to the maximum gain of $G_{\mathrm{code,max}} = 3.0068$. It should be noted that with the filter bank system here, the coding gain came much closer to the maximum possible gain than the pre/postfiltering quantization system considered in Sec. 5.4.2.1.

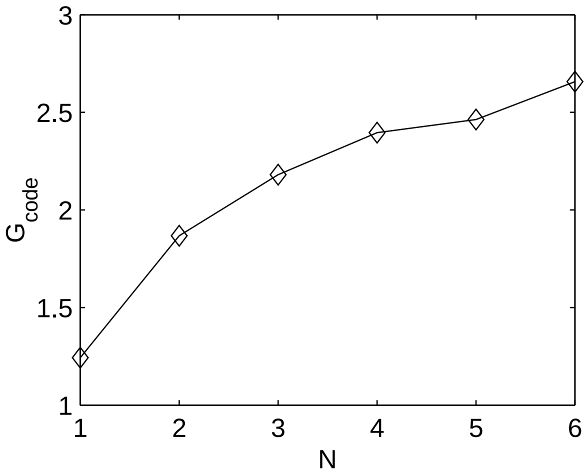

Figure 5.25: Observed coding gain G_{code} as a function of the analysis/synthesis polyphase filter order N.

5.5 Concluding Remarks

In this chapter, we presented a method for the design of purely FIR filter banks for optimal reconstruction with the presence of scalar quantizers in the subbands. Under the high bit rate assumption for the quantizers [25], we showed that the mean-squared error objective was *quadratic* in terms of either the analysis or synthesis filter coefficients and hence could be minimized using the trick of completing the square [22]. By alternately optimizing the analysis and synthesis banks, we proposed an iterative greedy algorithm for the design of such FIR filter banks.

Simulation results presented here brought to light the merit of the proposed iterative algorithm. We showed how the algorithm could be used to obtain minimum mean-squared error overdecimated filter banks. In addition, we showed that sometimes the filter banks designed exhibited behavior similar to the ideal compaction filters of the PCFB.

Afterwards, we focused on the effects of quantization and used the algorithm to design pre/postfiltering quantization schemes as well as general filter bank quantization systems. It was shown that in terms of coding gain and distortion, the systems designed came close to the theoretical bounds established by information theory. In line with intuition, we showed that as the filter order increased, the quantization systems monotonically came closer to these bounds. Furthermore, we showed the advantages of using a sophisticated filter bank quantization system over a simple pre/postfiltering quantization scheme. In particular, it was observed that the filter bank system could come much closer to the optimal information theoretic bounds than the pre/postfiltering system. These phenomena have not previously been formally presented in the literature.

Chapter 6

Eigenfilter Channel Shortening Equalizer for DMT Systems

In this chapter, we show how the eigenfilter technique [74, 56], which was widely used in the optimization algorithms presented for designing signal-adapted filter banks, can be applied to the design of good channel shortening equalizers for discrete multitone (DMT) systems. This chapter differs in theme from the others in that the optimization algorithm is not iterative as the equalizer is designed in one step. The design objective we focus on here takes into account both the effects due to the channel length as well as the noise. We show how our method can be used for the design of fractionally spaced equalizers (FSEs). In contrast to other methods which require a Cholesky decomposition of a certain matrix for every delay parameter chosen, the method presented here only requires one such decomposition, as we show here. As such, this method is lower in complexity than those mentioned above. Despite this decrease in complexity, we show that the method yields nearly optimal performance in terms of bit rate or throughput.

The content of this chapter is mainly drawn from [55] and portions of it have been presented at [53, 51, 52].

6.1 Outline

In Sec. 6.2, we briefly review the channel shortening equalizer design problem and how it relates to DMT systems. A survey of some of the previous work related to the design of such equalizers is given in Sec. 6.2.1.

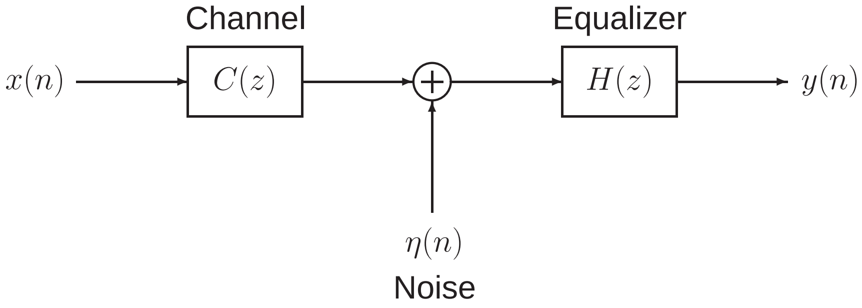

Figure 6.1: Channel shortening equalizer model.

In Sec. 6.3, we introduce the design objective that we will focus on here. The objective considered jointly accounts for the channel shortening objective, as well as the effects due to noise. In Sec. 6.3.1, we analyze the objective function and show how it can be solved using the eigenfilter approach. There, the low complexity advantage of the proposed method is revealed.

In Sec. 6.4, we present simulation results for the proposed channel shortening equalizer design method, along with those of several other methods. There, it is shown that the method outperforms most methods and performs nearly optimally in terms of observed bit rate.

Concluding remarks are made in Sec. 6.5. In the Appendix, we show the equivalence between FSEs and the SIMO-MISO channel/equalizer model we focus on in Sec. 6.3.

6.2 The Channel Shortening Equalizer Problem

Suppose that we have a causal FIR system or channel $C(z)$ of length L_c that we would like to *shorten* to a length $L_d < L_c$. A typical model for the system used to shorten the channel is shown in Fig. 6.1. The goal of the equalizer $H(z)$ is to shorten the *effective channel* $C_{\text{eff}}(z) \triangleq H(z)C(z)$ to a length of L_d. Though this can be done exactly by choosing $H(z) = \frac{A(z)}{C(z)}$, where $A(z)$ is some FIR system of length L_d, there are often problems with this approach. As $C(z)$ may have zeros on or outside the unit circle, the choice of $H(z) = \frac{A(z)}{C(z)}$, which we assume must be causal here, can never be stable. This in turn will result in the undesired phenomenon of spurious noise amplification.

Instead, what is typically done is to choose $H(z)$ to be a causal FIR filter used to *concentrate the energy* of the effective channel $C_{\text{eff}}(z)$ into a window of length L_d. If $H(z)$ is of length L_e, then $C_{\text{eff}}(z) = H(z)C(z)$ is a causal FIR system of length $L_{\text{eff}} \triangleq (L_c + L_e - 1)$. In this case, we can decompose the effective channel impulse response $c_{\text{eff}}(n)$ as a sum of two responses, namely, a desired response $c_{\text{des}}(n)$ which is exactly of length L_d, and a residual response $c_{\text{res}}(n)$ which consists of whatever remains of $c_{\text{eff}}(n)$ after removing $c_{\text{des}}(n)$. This is illustrated in Fig. 6.2. Here, Δ is

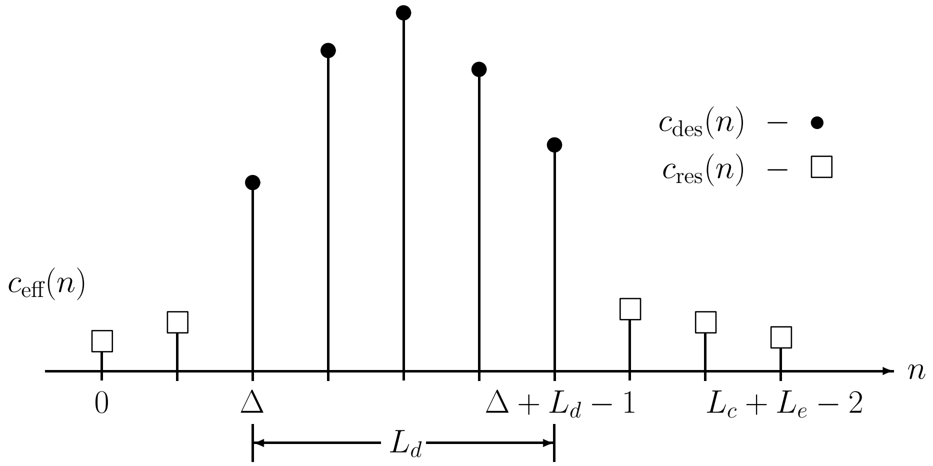

Figure 6.2: Decomposition of the effective channel $c_{\mathrm{eff}}(n)$ into a desired channel $c_{\mathrm{des}}(n)$ and residual channel $c_{\mathrm{res}}(n)$.

a *delay parameter* which satisfies $0 \leq \Delta \leq L_{\mathrm{eff}} - L_d$. As the effects of the equalizer $H(z)$ are most evident in the time domain, it is often referred to as a time-domain equalizer or TEQ [46, 6]. Through proper choice of $H(z)$ here, we can often times not only adequately shorten the channel, but also combat the effects due to the noise as well.

The channel shortening problem arises in DMT systems such as digital subscriber loop (DSL) [46]. A typical DMT system is shown in Fig. 1.14. Perhaps the most important feature of the DMT system is the inclusion of redundancy in the form of a *cyclic prefix*. Essentially, this redundancy allows an FIR channel of length at most equal to one sample more than the cyclic prefix length to be equalized using only FIR components (as discussed in Sec. 1.4). In other words, if L_{CP} denotes the cyclic prefix length, then the DMT system can equalize a channel of length at most $L_d = L_{\mathrm{CP}} + 1$.

The problem with this is that the channel typically encountered in a DMT system is very long. For example, in practical DMT systems such as asymmetric DSL (ADSL), the channel is typically a telephone wire line [46] whose impulse response may be several hundreds of samples long. Instead of increasing the cyclic prefix length to accomodate the long channel, which would result in more redundancy and hence a lower overall rate, a TEQ is used to *shorten* the channel to the desired length $L_d = L_{\mathrm{CP}} + 1$.

Often times, we may know something about the statistics of the noise encountered in a typical DMT system. For example, in ADSL, the noise can sometimes be modeled as a combination of near-end crosstalk (NEXT) and far-end crosstalk (FEXT) [46]. In these cases, we can design the TEQ to jointly shorten the channel and account for the effects due to noise.

For a DMT system, the primary measure of optimality of a TEQ is the overall bit rate or throughput of the system. This measure accounts for both the effects due to the channel length as well as the noise. If f_s denotes the analog sampling frequency and $N_{\rm DFT}$ denotes the size of the DFT matrix used in the DMT system (see Fig. 1.14), then the observed bit rate is given by [6]

$$R_b = \frac{f_s}{N_{\rm DFT} + L_{\rm CP}} \sum_{k \in \mathcal{S}} b_k \tag{6.1}$$

where b_k denotes the number of bits to allocate for the k-th real subcarrier and $\mathcal{S}$ is a subset of the set of real subcarriers $\left\{0, 1, \ldots, \frac{N_{\rm DFT}}{2} - 1\right\}$ that are used. Here, $\mathcal{S}$ is chosen according to the famous "water filling" principle [10, 7], as the subcarriers are modeled as parallel independent Gaussian channels [46]. As such, the number of bits to allocate for the k-th subcarrier is [6]

$$b_k = \log_2 \left(1 + \frac{\text{SNR}_k}{\Gamma}\right)$$

where SNR_k is the signal-to-noise (SNR) ratio for the k-th subcarrier which takes into account the effects due to both the channel length and the noise given by

$$\text{SNR}_k = \frac{S_{xx}(e^{j\omega_k}) \left|C_{\rm des}(e^{j\omega_k})\right|^2}{S_{xx}(e^{j\omega_k}) \left|C_{\rm res}(e^{j\omega_k})\right|^2 + S_{\eta\eta}(e^{j\omega_k}) \left|H(e^{j\omega_k})\right|^2} \text{ , where } \omega_k = \frac{2\pi k}{N_{\rm DFT}}$$

and Γ is an *SNR gap* [46] for achieving the Shannon capacity limit [10, 7] that is assumed to be the same for all subcarriers. Also, $S_{xx}(e^{j\omega})$ and $S_{\eta\eta}(e^{j\omega})$ denote, respectively, the psds of the input to the channel and noise (see Fig. 6.1), which we have assumed are WSS here. The quantity Γ depends on the modulation format used as well as the desired probability of error [46, 6]. For uncoded quadrature amplitude modulation (QAM) [38] with a probability of error of 10^{-7}, $\Gamma = 9.8$ dB [46].

The maximum achievable bit rate is given by the *matched-filter bound* (MFB) [6], which is

$$R_{\rm MFB} = \frac{f_s}{N_{\rm DFT} + L_{\rm CP}} \sum_{k \in \mathcal{S}} \widehat{b}_k \tag{6.2}$$

where $\widehat{b}_k$ is the number of bits allocated to the k-th subcarrier given by

$$\widehat{b}_k = \log_2 \left(1 + \frac{\text{SNR}_{\text{MFB},k}}{\Gamma}\right)$$

and $\text{SNR}_{\text{MFB},k}$ is the MFB SNR given by

$$\text{SNR}_{\text{MFB},k} = \frac{S_{xx}(e^{j\omega_k}) \left|C(e^{j\omega_k})\right|^2}{S_{\eta\eta}(e^{j\omega_k})} \text{ , } \omega_k = \frac{2\pi k}{N_{\rm DFT}}$$

Note that the MFB SNR is only a function of the statistics of the input and noise, as well as the channel response. These are the only *invariants* of the communications system and as such, dictate the maximum possible performance alone.

Prior to presenting our method for TEQ design, we briefly review previous work on the matter.

6.2.1 Overview of Previous Work on Channel Shortening Equalizers

1. *Minimum Mean-Squared Error (MMSE) Methods:* Among the first approaches for the design of channel shortening equalizers were the minimum mean-squared error (MMSE) methods proposed by Al-Dhahir and Cioffi [3, 4]. With these methods, the TEQ $h(n)$ is chosen to be an FIR Wiener filter [48] for the response $b(n) * x(n)$, where $b(n)$ is a *target impulse response* (TIR), which is some FIR system of length L_d. In other words, referring to Fig. 6.1, the equalizer $h(n)$ is chosen to minimize

   $$\xi \triangleq E\left[|y(n) - b(n) * x(n)|^2\right]$$

   For a fixed TIR $b(n)$, the TEQ coefficients of $h(n)$ can be found using the *orthogonality principle* [48].

   Early methods for the design of the TIR $b(n)$ consisted of choosing it such that $b(n)$ satisfied a unit energy or unit tap constraint as shown below [3].

   $$\sum_n |b(n)|^2 = 1 \qquad \text{(Unit Energy Constraint (UEC))}$$

   $$b(n_0) = 1 \text{ for some } n_0 \qquad \text{(Unit Tap Constraint (UTC))}$$

   Though these choices of $b(n)$ are easy to obtain and compute, they often perform poorly with respect to overall observed bit rate. Furthermore, once $b(n)$ has been appropriately computed, the equalizer coefficients of $h(n)$ must still be found using the orthogonality principle.

   Another method for the design of the TIR $b(n)$ perhaps better suited for DMT systems is the geometric SNR (GSNR) method of [4]. In it, the authors obtained an approximate expression for the bit rate and found that increasing the product of $\left|B(e^{j\omega})\right|^2$ at the DFT frequencies $\omega_k = \frac{2\pi k}{N_{\text{DFT}}}$ would increase the bit rate. Formally, the GSNR method consists of maximizing this product, which is equivalent to maximizing the geometric mean of $\left|B(e^{j\omega})\right|^2$ at the DFT frequencies, subject to a mean-squared error constraint $\xi \leq \xi_{\max}$ for some error threshold value $\xi_{\max}$.

   Unfortunately, the GSNR method suffers from several shortcomings. First of all, in their expression for the bit rate, the authors of [4] did not take into account the effects due to intersymbol interference (ISI) (i.e., the effects due to the channel length). Furthermore, they treated the target response $B(e^{j\omega})$ and equalizer $H(e^{j\omega})$ as independent quantities, when in fact $h(n)$ is related to $b(n)$ via the orthogonality principle. Finally, finding the TIR $b(n)$

involves solving a constrained nonlinear optimization problem, and as such, is very high in computational complexity. Though the GSNR method often outperforms the UEC and UTC methods of [3], other methods developed later not only surpass it, but also do so with less computational complexity. Despite this, the GSNR method represented the first attempt to design a TEQ by maximizing the bit rate of a DMT system.

2. *Minimum Shortening SNR (MSSNR) Method:* In [33], Melsa, Younce, and Rohrs developed a method for designing a channel shortening equalizer that delt directly with the TEQ coefficients of $h(n)$. The objective was to maximize the *shortening SNR* (SSNR) given by

   $$\text{SSNR} \triangleq \frac{E_{\text{des}}}{E_{\text{res}}}$$

   where E_{des} and E_{res} denote, respectively, the energy of the effective desired response $c_{\text{des}}(n)$ and residual response $c_{\text{res}}(n)$ (see Fig. 6.2), given by

   $$E_{\text{des}} = \sum_{n} |c_{\text{des}}(n)|^2 \ , \ E_{\text{res}} = \sum_{n} |c_{\text{res}}(n)|^2$$

   To maximize the SSNR, the authors of [33] solved the constrained optimization problem

   $$\text{Minimize } E_{\text{res}}, \text{ subject to } E_{\text{des}} = 1.$$

   They showed that this optimization problem could be solved using the *eigenfilter* technique [74, 56], after computing an appropriate *Cholesky decomposition* [22] of a particular matrix.

   Though this method performs relatively well with relatively low complexity, on account of the fact that the design problem is an eigenfilter-type problem, it suffers from several shortcomings. First, the method does not account for any effects due to noise present in the system. Furthermore, the Cholesky factor obtained from the above-mentioned Cholesky decomposition depends on the delay parameter Δ. If we wish to vary Δ over a certain region to see which value performs the best, which is typically done in practice, then a new Cholesky factor must be computed for each Δ. This results in an extra computational load for each Δ considered. Despite these shortcomings, the MSSNR method of [33] represented the first attempt to pose the channel shortening problem as an eigenfilter-type problem.

3. *Maximum Bit Rate (MBR) and Minimum ISI (Min-ISI) Methods:* Arslan, Evans, and Kiaei [6] were the first to design a TEQ to directly maximize the bit rate given in (6.1). This method, called the maximum bit rate (MBR) method, was shown to perform very well and

often came very close to the MFB maximum achievable bit rate given in (6.2). However, as the bit rate given in (6.1) is a nonlinear, nonconvex function of the TEQ coefficients of $h(n)$, computationally intensive nonlinear optimization techniques had to be employed to maximize the bit rate. Furthermore, these techniques were found to converge slowly to a desired local extrema.

In order to mitigate the effects of this complexity, the authors of [6] proposed a suboptimal method called the minimum ISI (min-ISI) method in which the objective was to minimize a combination of the effects due to ISI as well as those due to noise. As with the MSSNR method of [33], it was shown that the objective could be optimized using the eigenfilter approach after an appropriate Cholesky factor was computed. This method, as it accounted for both ISI and noise, was shown to perform nearly as well as the MBR method with much lower computational complexity. However, as with the MSSNR method of [33], the Cholesky factor needed in the min-ISI method of [6] depends on the delay parameter Δ.

4. *Delay Spread Minimization Method:* Schur and Speidel proposed a unique method for the design of channel shortening equalizers in [44]. In it, the objective was to minimize the *delay spread* of the effective channel $c_{\text{eff}}(n)$, defined as follows.

$$J_{\text{delay}} \triangleq \frac{\displaystyle\sum_n (n-\Delta)^2 \left|c_{\text{eff}}(n)\right|^2}{\displaystyle\sum_n \left|c_{\text{eff}}(n)\right|^2}$$

As with the MSSNR method of [33] and the min-ISI method of [6], it was shown that this problem could be solved using the eigenfilter approach after an appropriate Cholesky factor was computed. However, unlike these methods, the Cholesky factor required for the delay spread minimization method does not depend on the delay parameter Δ. Hence, the method is very low in complexity as only one Cholesky factor must be computed for all Δ.

Despite this significant decrease in complexity, the method suffers from several shortcomings. Though the method was shown to be less prone to synchronization errors than others, it does not account for the desired channel length $L_d = L_{\text{CP}} + 1$ or any knowledge of the noise statistics. Here, we generalize the delay spread minimization method of [44] to account for both of these things. Furthermore, we apply it to a more general model than that shown in Fig. 6.1 which can be used for the design of FSEs for channel shortening.

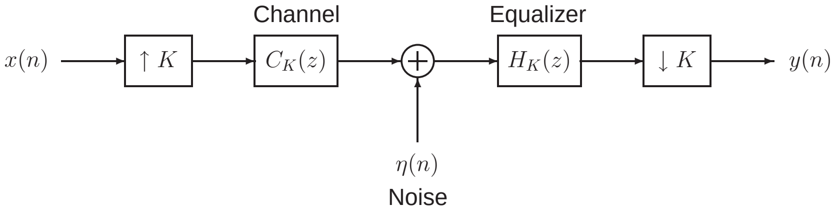

Figure 6.3: Discrete-time model of a K-fold oversampled FSE.

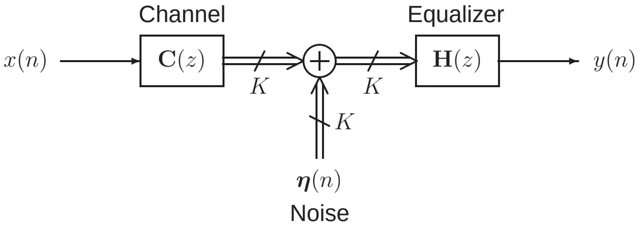

Figure 6.4: SIMO-MISO channel/equalizer model.

6.3 Proposed Eigenfilter Design Method

Consider the system shown in Fig. 6.3. This system is the discrete-time model of an FSE with oversampling ratio K [61]. Here, $C_K(z)$ and $H_K(z)$ represent, respectively, a K-fold oversampled version of the original channel $C(z)$ and equalizer $H(z)$ from Fig. 6.1. Similarly, $\eta(n)$ from Fig. 6.3 represents a K-fold oversampled version of the noise process $\eta(n)$ in Fig. 6.1. In contrast to the symbol spaced equalizer (SSE) shown in Fig. 6.1, the FSE of Fig. 6.3 has a redundancy of a factor of K. As a result of this, channel equalization/shortening and noise suppression with FSEs often become more well conditioned than with SSEs. For example, under certain mild conditions, we can achieve exact channel equalization with FIR filters [76, 78].

If the K-fold oversampled channel $C_K(z)$ and equalizer $H_K(z)$ have the following polyphase decompositions,

$$\begin{aligned} C_K(z) &= \sum_{k=0}^{K-1} z^{-k} E_k\big(z^K\big) \quad \text{(Type I)} \\ H_K(z) &= \sum_{k=0}^{K-1} z^{k} R_k\big(z^K\big) \quad \text{(Type II)} \end{aligned} \tag{6.3}$$

then the FSE system of Fig. 6.3 can be redrawn as in Fig. 6.4 (see the Appendix), where we have

$$[\mathbf{C}(z)]_{k,0} = E_k(z)\,,\ [\mathbf{H}(z)]_{0,k} = R_k(z)\,,\ [\boldsymbol{\eta}(n)]_{k,0} = \eta(Kn+k)\,,\quad 0 \le k \le K-1 \tag{6.4}$$

Hence, the FSE of Fig. 6.3 is equivalent to a single-input multiple-output (SIMO) channel and a multiple-input single-output (MISO) equalizer model. Note that the noise process $\boldsymbol{\eta}(n)$ is simply the *blocked* version of the noise process $\eta(n)$ from Fig. 6.3.

The eigenfilter design method for channel shortening that we propose here will be for the SIMO-MISO channel/equalizer model of Fig. 6.4. We make the following assumptions here.

- The channel $\mathbf{C}(z)$ is a known causal FIR filter of length L_c.
- The equalizer $\mathbf{H}(z)$ is a causal FIR filter of length L_e.
- The input $x(n)$ is zero mean and white with variance σ_x^2.
- The noise $\boldsymbol{\eta}(n)$ is a zero mean WSS random process with autocorrelation $\mathbf{R}_{\boldsymbol{\eta}\boldsymbol{\eta}}(k)$.
- The processes $x(n)$ and $\boldsymbol{\eta}(n)$ are uncorrelated.

Note that the output $y(n)$ can be expressed as $y(n) = x_f(n) + q(n)$, where $x_f(n)$ and $q(n)$ are, respectively, the filtered signal and noise processes given by

$$x_f(n) = c_{\text{eff}}(n) * x(n)\,,\ q(n) = \mathbf{h}(n) * \boldsymbol{\eta}(n)$$

and $c_{\text{eff}}(n)$ is the effective channel given by $c_{\text{eff}}(n) \triangleq \mathbf{h}(n) * \mathbf{c}(n)$.

We want the equalizer to shorten the effective channel $c_{\text{eff}}(n)$ and minimize the noise power σ_q^2 with respect to the signal power $\sigma_{x_f}^2$. To that end, we propose to choose $\mathbf{h}(n)$ to minimize the objective function

$$J \triangleq \alpha J_{\text{short}} + (1-\alpha) J_{\text{noise}}\,,\ 0 \le \alpha \le 1 \tag{6.5}$$

where J_{short} and J_{noise} are defined as follows.

$$J_{\text{short}} \triangleq \frac{\displaystyle\sum_n f(n-\Delta)|c_{\text{eff}}(n)|^2}{\displaystyle\sum_n |c_{\text{eff}}(n)|^2}\,,\ J_{\text{noise}} \triangleq \frac{\sigma_q^2}{\sigma_{x_f}^2} = \frac{\sigma_q^2}{\sigma_x^2 \displaystyle\sum_n |c_{\text{eff}}(n)|^2} \tag{6.6}$$

Here, J_{short} is a channel shortening objective, J_{noise} is the noise-to-signal ratio, and α is a tradeoff parameter between these two objectives. Also, Δ is the delay of the shortened channel as before and $f(n)$ is a "penalty" function which is any nonnegative function used to penalize different values of $c_{\text{eff}}(n)$. The special case where $K = 1$, $\alpha = 1$, and $f(n) = n^2$ corresponds to the objective analyzed by Schur and Speidel in [44].

Though α is arbitrary, one heuristic choice which is well suited for the design of a channel shortening equalizer for DMT systems (see Sec. 6.4) is the value

$$\alpha = \alpha_0 \triangleq \frac{P_{\text{ISI}}}{P_{\text{ISI}} + P_{\text{noise}}} \tag{6.7}$$

Here, P_{ISI} is the intersymbol interference (ISI) power present in $\mathbf{c}(n)$ before equalization, which is σ_x^2 times the difference of the energy of $\mathbf{c}(n)$ and the energy of the $(L_{\text{CP}}+1)$ length window of $\mathbf{c}(n)$ with maximum energy, where L_{CP} is the cyclic prefix length. Also, P_{noise} is the input noise power, namely, $\text{Tr}\,[\mathbf{R}_{\boldsymbol{\eta\eta}}(0)]$. Finding the optimal choice of α for a given criterion is still an open problem. However, for maximizing bit rate, it was found (see Sec. 6.4) that α_0 in (6.7) yielded good results.

To further incorporate the cyclic prefix length in the design, in the simulation results presented in Sec. 6.4, we chose the penalty function to be

$$f(n) = f_{\text{CP}}(n) \triangleq \begin{cases} 0\,, & 0 \le n \le L_{\text{CP}} \\ 1\,, & \text{otherwise} \end{cases} \tag{6.8}$$

Note that $f_{\text{CP}}(n-\Delta)$ penalizes uniformly any samples of $c_{\text{eff}}(n)$ outside of $n \in [\Delta, \Delta + L_{\text{CP}}]$.

6.3.1 Analysis of the Objective Function J

Note that from the above assumptions, the effective channel $c_{\text{eff}}(n) = \mathbf{h}(n) * \mathbf{c}(n)$ is causal and FIR of length $L_{\text{eff}} \triangleq L_c + L_e - 1$. To proceed with analyzing the objective function J from (6.5), let us define the following matrix quantities.

$$\begin{array}{rcll}
\mathbf{h} & \triangleq & \begin{bmatrix} \mathbf{h}(0) & \mathbf{h}(1) & \cdots & \mathbf{h}(L_e-1) \end{bmatrix} & (1 \times KL_e) \\
\mathbf{C} & \triangleq & \begin{bmatrix} \mathbf{c}(0) & \mathbf{c}(1) & \cdots & \mathbf{c}(L_c-1) & \mathbf{0} & \cdots & \mathbf{0} \\ \mathbf{0} & \mathbf{c}(0) & \mathbf{c}(1) & \cdots & \mathbf{c}(L_c-1) & \ddots & \vdots \\ \vdots & \ddots & \ddots & \ddots & & \ddots & \mathbf{0} \\ \mathbf{0} & \cdots & \mathbf{0} & \mathbf{c}(0) & \mathbf{c}(1) & \cdots & \mathbf{c}(L_c-1) \end{bmatrix} & (KL_e \times L_{\text{eff}}) \\
\mathbf{c}_{\text{eff}} & \triangleq & \begin{bmatrix} c_{\text{eff}}(0) & c_{\text{eff}}(1) & \cdots & c_{\text{eff}}(L_{\text{eff}}-1) \end{bmatrix} & (1 \times L_{\text{eff}}) \\
\mathbf{\Lambda}_{\Delta} & \triangleq & \text{diag}\left(f(0-\Delta), f(1-\Delta), \ldots, f((L_{\text{eff}}-1)-\Delta)\right) & (L_{\text{eff}} \times L_{\text{eff}}) \\
\widehat{\mathbf{R}}_{\boldsymbol{\eta}} & \triangleq & \begin{bmatrix} \mathbf{R}_{\eta\eta}(0) & \mathbf{R}_{\eta\eta}(1) & \cdots & \mathbf{R}_{\eta\eta}(L_e-1) \\ \mathbf{R}_{\eta\eta}(-1) & \mathbf{R}_{\eta\eta}(0) & \ddots & \vdots \\ \vdots & \ddots & \ddots & \mathbf{R}_{\eta\eta}(1) \\ \mathbf{R}_{\eta\eta}(-(L_e-1)) & \cdots & \mathbf{R}_{\eta\eta}(-1) & \mathbf{R}_{\eta\eta}(0) \end{bmatrix} & (KL_e \times KL_e)
\end{array}$$

Note that all of the degrees of freedom in the design problem reside in the choice of the row vector $\mathbf{h}$ here. From the convolution equation $c_{\text{eff}}(n) = \mathbf{h}(n) * \mathbf{c}(n)$, note that we have

$$\mathbf{c}_{\text{eff}} = \mathbf{hC} \tag{6.9}$$

Also, from (6.6), we have

$$J_{\text{short}} = \frac{\mathbf{c}_{\text{eff}}\mathbf{\Lambda}_{\Delta}\mathbf{c}_{\text{eff}}^{\dagger}}{\mathbf{c}_{\text{eff}}\mathbf{c}_{\text{eff}}^{\dagger}}\ ,\ J_{\text{noise}} = \frac{\sigma_q^2}{\sigma_x^2\mathbf{c}_{\text{eff}}\mathbf{c}_{\text{eff}}^{\dagger}} \tag{6.10}$$

Substituting (6.9) into (6.10), we get

$$J_{\text{short}} = \frac{\mathbf{h}\mathbf{C}\mathbf{\Lambda}_{\Delta}\mathbf{C}^{\dagger}\mathbf{h}^{\dagger}}{\mathbf{h}\mathbf{C}\mathbf{C}^{\dagger}\mathbf{h}^{\dagger}}\ ,\ J_{\text{noise}} = \frac{\sigma_q^2}{\sigma_x^2\mathbf{h}\mathbf{C}\mathbf{C}^{\dagger}\mathbf{h}^{\dagger}} \tag{6.11}$$

To simplify σ_q^2 from (6.11), recall that we have

$$\sigma_q^2 = \frac{1}{2\pi}\int_0^{2\pi} S_{qq}(e^{j\omega})\,d\omega$$

As $q(n) = \mathbf{h}(n) * \boldsymbol{\eta}(n)$, we have [67]

$$S_{qq}(z) = \mathbf{H}(z)\mathbf{S}_{\boldsymbol{\eta}\boldsymbol{\eta}}(z)\widetilde{\mathbf{H}}(z) = \sum_{m,n}\mathbf{h}(m)\left[\mathbf{S}_{\boldsymbol{\eta}\boldsymbol{\eta}}(z)z^{n-m}\right]\mathbf{h}^{\dagger}(n)$$

and so we get

$$\sigma_q^2 = \sum_{m,n}\mathbf{h}(m)\underbrace{\left[\frac{1}{2\pi}\int_0^{2\pi}\mathbf{S}_{\boldsymbol{\eta}\boldsymbol{\eta}}(e^{j\omega})e^{j\omega(n-m)}\,d\omega\right]}_{\mathbf{R}_{\boldsymbol{\eta}\boldsymbol{\eta}}(n-m)}\mathbf{h}^{\dagger}(n)$$

In light of the FIR assumption on $\mathbf{h}(n)$, we can express σ_q^2 in terms of the row vector $\mathbf{h}$ as follows.

$$\sigma_q^2 = \mathbf{h}\widehat{\mathbf{R}}_{\boldsymbol{\eta}}\mathbf{h}^{\dagger} \tag{6.12}$$

Combining (6.12) with (6.11), we get

$$J_{\text{short}} = \frac{\mathbf{h}\mathbf{C}\mathbf{\Lambda}_{\Delta}\mathbf{C}^{\dagger}\mathbf{h}^{\dagger}}{\mathbf{h}\mathbf{C}\mathbf{C}^{\dagger}\mathbf{h}^{\dagger}}\ ,\ J_{\text{noise}} = \frac{\mathbf{h}\widehat{\mathbf{R}}_{\boldsymbol{\eta}}\mathbf{h}^{\dagger}}{\sigma_x^2\mathbf{h}\mathbf{C}\mathbf{C}^{\dagger}\mathbf{h}^{\dagger}} \tag{6.13}$$

Hence, using (6.13) in (6.5), we get

$$J = \frac{\mathbf{h}\left[\alpha\mathbf{C}\mathbf{\Lambda}_{\Delta}\mathbf{C}^{\dagger} + (1-\alpha)\frac{1}{\sigma_x^2}\widehat{\mathbf{R}}_{\boldsymbol{\eta}}\right]\mathbf{h}^{\dagger}}{\mathbf{h}\mathbf{C}\mathbf{C}^{\dagger}\mathbf{h}^{\dagger}} \tag{6.14}$$

To show that J can be optimized via the eigenfilter approach, we proceed as follows. Assuming $\mathbf{C}$ has a full rank of KL_e, then $\mathbf{A} \triangleq \mathbf{C}\mathbf{C}^{\dagger}$ is strictly positive definite [22]. As such, it has a *Cholesky decomposition* [22] of the form $\mathbf{A} = \mathbf{G}^{\dagger}\mathbf{G}$, where $\mathbf{G}$ is a nonsingular $KL_e \times KL_e$ matrix[1]. Define the $KL_e \times 1$ column vector $\mathbf{v}$ as $\mathbf{v} \triangleq \mathbf{G}\mathbf{h}^{\dagger}$. Then, as $\mathbf{G}$ is nonsingular, we have $\mathbf{h} = \mathbf{v}^{\dagger}\left(\mathbf{G}^{-1}\right)^{\dagger}$, and

[1] If $\mathbf{C}$ is rank deficient, then we can still optimize the objective function J using a Cholesky decomposition, but the details become more complicated [22]. For all of the practical examples considered here in simulations, $\mathbf{C}$ was always of full rank.

so finding the optimal $\mathbf{h}$ is equivalent to finding the optimal $\mathbf{v}$. Substituting $\mathbf{v} = \mathbf{G}\mathbf{h}^\dagger$ into (6.14) yields

$$J = \frac{\mathbf{v}^\dagger \mathbf{T} \mathbf{v}}{\mathbf{v}^\dagger \mathbf{v}}\,, \text{ where } \mathbf{T} \triangleq \alpha \left[\left(\mathbf{G}^{-1}\right)^\dagger \mathbf{C} \mathbf{\Lambda}_\Delta \mathbf{C}^\dagger \left(\mathbf{G}^{-1}\right) \right] + (1-\alpha) \left[\frac{1}{\sigma_x^2} \left(\mathbf{G}^{-1}\right)^\dagger \widehat{\mathbf{R}}_{\boldsymbol{\eta}} \left(\mathbf{G}^{-1}\right) \right]$$

As $\mathbf{T}$ is Hermitian, it follows by Rayleigh's principle [22] that the minimum value of J is λ_{min} where λ_{min} denotes the smallest eigenvalue of $\mathbf{T}$. Furthermore, $J = \lambda_{\text{min}}$ iff $\mathbf{v}$ lies in the eigenspace corresponding to λ_{min}. Thus, the optimization problem here can be solved using the eigenfilter approach [74, 56]. If $\mathbf{v}_{\text{min}}$ denotes any nonzero vector in the eigenspace corresponding to λ_{min}, then the optimal equalizer coefficient vector $\mathbf{h}_{\text{opt}}$ and corresponding optimal objective value J_{opt} are given by

$$\boxed{\begin{array}{rcl} \mathbf{h}_{\text{opt}} & = & \mathbf{v}_{\text{min}}^\dagger \left(\mathbf{G}^{-1}\right)^\dagger \\ J_{\text{opt}} & = & \lambda_{\text{min}} \end{array}}$$

One important point to note is that the Cholesky factor $\mathbf{G}$ does not depend on the delay parameter Δ. Other eigenfilter methods, such as the MSSNR method of [33] and the min-ISI method of [6], require Cholesky factors that do depend on Δ. If we wish to perform an exhaustive search over a range of possible parameters Δ to see which one yields the best performance in terms of bit rate, which is typically done in practice, then these methods are much higher in complexity than the proposed one, which only requires one Cholesky decomposition for all values of Δ.

6.4 Simulation Results

For the reasons mentioned in Sec. 6.2, we opted to compare our proposed TEQ design method with others on the basis of observed bit rate (see (6.1)). Data for the channel and noise was obtained from the `Matlab DMTTEQ Toolbox` [5]. We used the following typical asymmetric DSL (ADSL) input parameters.

- Analog sampling frequency (f_s) – 2.208 MHz, DFT size (N_{DFT}) – 512, Cyclic prefix length (L_{CP}) - 32, SNR gap (Γ) – 9.8 dB
- $K = 1$, $L_c = 512$, $L_e = 16$, $\sigma_x^2 = 21$ dBm
- NEXT noise model with eight disturbers [46] plus additive white Gaussian noise (AWGN) with power density -110 dBm/Hz (see Fig. 6.5 for a plot of the noise psd)

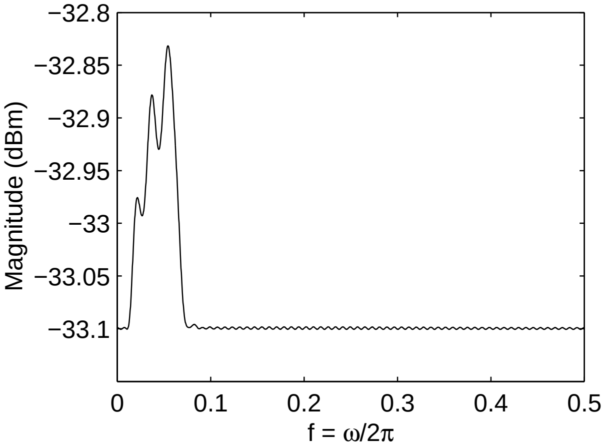

Figure 6.5: Noise psd $S_{\eta\eta}(e^{j\omega})$ corresponding to NEXT noise with eight disturbers [46] plus AWGN with power density −110 dBm/Hz.

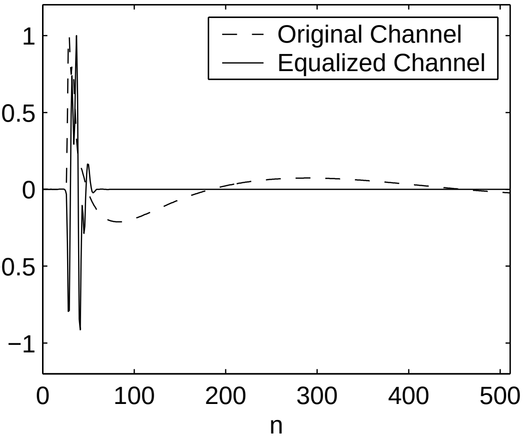

Figure 6.6: Original and equalized channel impulse responses using the proposed eigenfilter method for CSA loop #1.

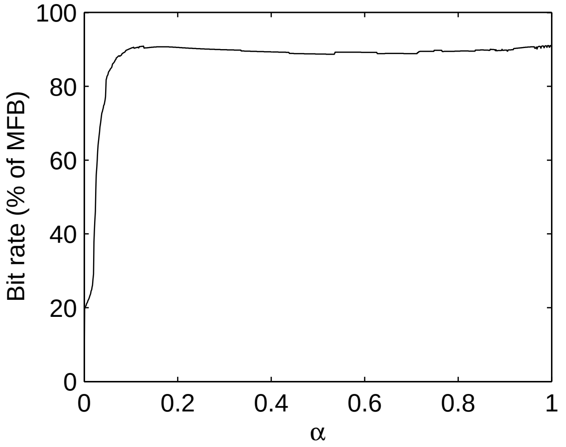

Figure 6.7: Observed bit rate (as a percentage of the MFB bit rate of (6.2)) as a function of the tradeoff parameter α for CSA loop #1.

CSA loop #	*Observed bit rate as a % of the MFB maximum bit rate*							*MFB maximum achievable bit rate*
	MMSE -UTC [3]	MMSE -UEC [3]	GSNR [4]	MSSNR [33]	min-ISI [6]	Delay Spread Minimization [44]	Proposed Method	
1	82.4%	83.3%	84.8%	92.6%	95.0%	77.4%	91.1%	2.844 Mbps
2	81.1%	86.6%	89.3%	86.4%	95.3%	66.8%	91.1%	3.068 Mbps
3	80.3%	81.1%	83.1%	90.4%	95.3%	80.2%	92.3%	2.643 Mbps
4	62.7%	74.9%	74.2%	88.6%	93.2%	51.9%	92.9%	1.933 Mbps
5	79.7%	72.6%	75.2%	81.9%	93.7%	68.5%	89.5%	2.839 Mbps
6	77.8%	80.7%	80.6%	89.5%	94.3%	80.6%	92.8%	2.350 Mbps
7	64.1%	78.2%	79.6%	90.3%	93.9%	72.2%	89.8%	2.519 Mbps
8	69.1%	78.1%	80.7%	88.6%	91.8%	79.0%	90.6%	2.325 Mbps

Table 6.1: Observed bit rates for CSA loops #1-8 using various TEQ design methods. (Bit rates are expressed as a percentage of the MFB maximum achievable bit rate of (6.2) for each loop.)

In Fig. 6.6, we have plotted the original and equalized channel impulse responses for carrier service area (CSA) loop #1 designed using our proposed method. Here, we chose $\alpha = \alpha_0$ as in (6.7) and $f(n) = f_{\text{CP}}(n)$ as in (6.8). We varied the delay parameter Δ from 0 to 40 and chose the one which yielded the best bit rate. As we can see, our method shortened the channel quite well. In Fig. 6.7, we have plotted the observed bit rate (as a percentage of the MFB maximum achievable bit rate from (6.2)) as a function of the tradeoff parameter α. Here, $\alpha_0 = 0.9977$ and yielded a percentage of 91.0819, whereas the optimum α was 0.998 with a percentage of 91.0852. Clearly the heuristic choice of $\alpha = \alpha_0$ from (6.7) yielded nearly optimal results as desired. From Figure 6.7, we can see that performance remained relatively constant for $0.1 \leq \alpha \leq 1$, which heuristically means that for the simulation parameters chosen here, ISI is more of a problem than noise.

In Table 6.1, we have tabulated the observed bit rates from (6.1) for CSA loops #1-8 using the above parameters as a percentage of the MFB bit rate given in (6.2). For each method considered except for the geometric SNR method (GSNR) [4], which requires nonlinear optimization, we varied the delay parameter Δ from 0 to 40 and chose the value that yielded the best bit rate. The optimum MMSE-UEC (unit energy constraint) method of [3] was used as the initial condition for the GSNR method. As was done in [6], the mean-squared error (MSE) parameter used was set to be 2 dB above the MSE obtained from the optimal MMSE-UEC equalizer. From Table 6.1, we can see that our proposed method comes very close to the MFB maximum bit rate and is comparable to the min-ISI method of [6]. However, we should note that our proposed method requires less computational load, as we only require one Cholesky decomposition for all values of Δ, as opposed to the min-ISI method which requires a different such decomposition for each Δ. The MISO equalizers for FSEs designed using our method offer a further improvement over all the methods considered here (see [51] for more details). This improvement, however, comes at the expense of a dramatic increase in redundancy and so for sake of fair comparison, these results have been omitted.

6.5 Concluding Remarks

In this chapter, we generalized the delay spread minimization method of [44] to account for the cyclic prefix length as well as the noise encountered in the system. Furthermore, we showed how the method can be applied to the design of FSEs for channel shortening. In addition, we showed that the proposed eigenfilter method is less complex to implement than other common eigenfilter TEQ design methods in that it only requires one Cholesky decomposition for all delay parameter values. From our simulation results, it was observed that our method came close to MFB maximum bit rate for all CSA loops considered, showing the merit of the proposed TEQ design method.

The proposed eigenfilter channel shortening method not only applies to the SIMO-MISO channel/equalizer model of Fig. 6.4, but also to a more general MIMO model (see [51] for more details). However, as the results in this case are less intuitive and the practical applications are not as clear as for the SIMO-MISO model of Fig. 6.4, we have chosen to omit them here for sake of brevity and clarity. The interested reader is referred to [2, 51] for more details regarding the design of channel shortening equalizers for the general MIMO case.

Appendix: Equivalence between FSEs and the SIMO-MISO Channel/Equalizer Model

Here, we show the equivalence between the discrete time model of the K-fold oversampled FSE shown in Fig. 6.3 and the SIMO-MISO channel/equalizer model of Fig. 6.4. In particular, we will show that if $C_K(z)$ and $H_K(z)$ have the polyphase decompositions given in (6.3), then the system of Fig. 6.3 can be redrawn as in Fig. 6.4 where the components of $\mathbf{C}(z)$, $\mathbf{H}(z)$, and $\boldsymbol{\eta}(n)$ are as in (6.4). This can be done with the help of the noble identities (see Sec. 1.1.3.1).

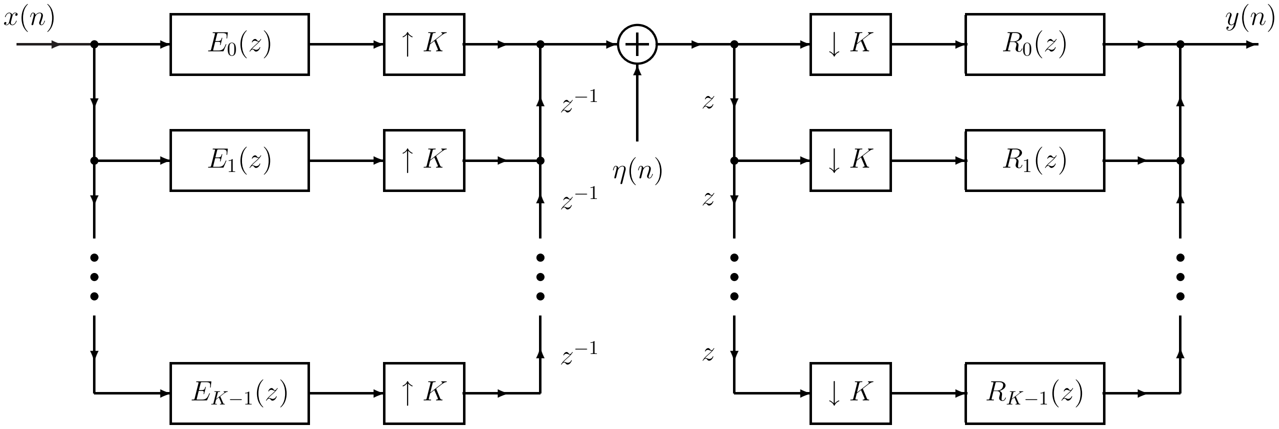

Figure 6.8: Equivalent form of Fig. 6.3 upon using the noble identities.

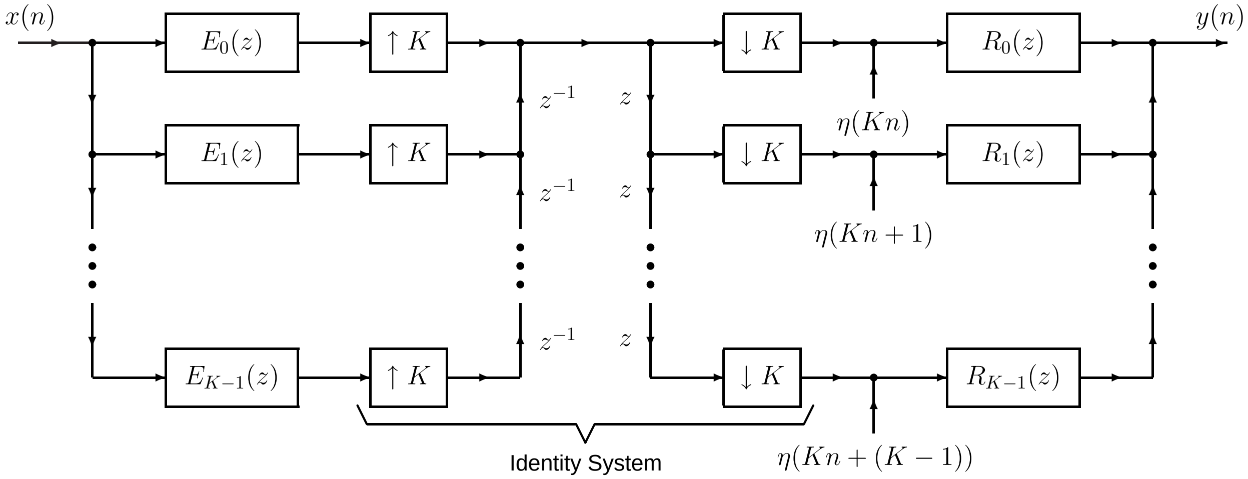

Figure 6.9: Equivalent form of Fig. 6.8 upon moving the noise process $\eta(n)$ past the blocking system.

If $C_K(z)$ and $H_K(z)$ have the polyphase decompositions given in (6.3), then using the noble identities, we can redraw the system of Fig. 6.3 as in Fig. 6.8. It can be seen that just before the noise is added, the signal is *unblocked* by a factor of K, whereas just after the noise is added, the signal is *blocked* by a factor of K (see Sec. 1.1.2).

Note that instead of adding the noise prior to blocking the signal, we can add the noise *after* the signal has been blocked. In other words, the system of Fig. 6.8 can be equivalently redrawn as in Fig. 6.9. Now note that the system comprised of K-fold unblocking followed by K-fold blocking is an identity system, and so we can remove the expanders and decimators from the model entirely as desired. Doing so, we get the system shown in Fig. 6.10.

From Fig. 6.10, it is clear that the original FSE system of Fig. 6.3 is equivalent to the SIMO-MISO model shown in Fig. 6.4, where the quantities $\mathbf{C}(z)$, $\mathbf{H}(z)$, and $\boldsymbol{\eta}(n)$ are as in (6.4).

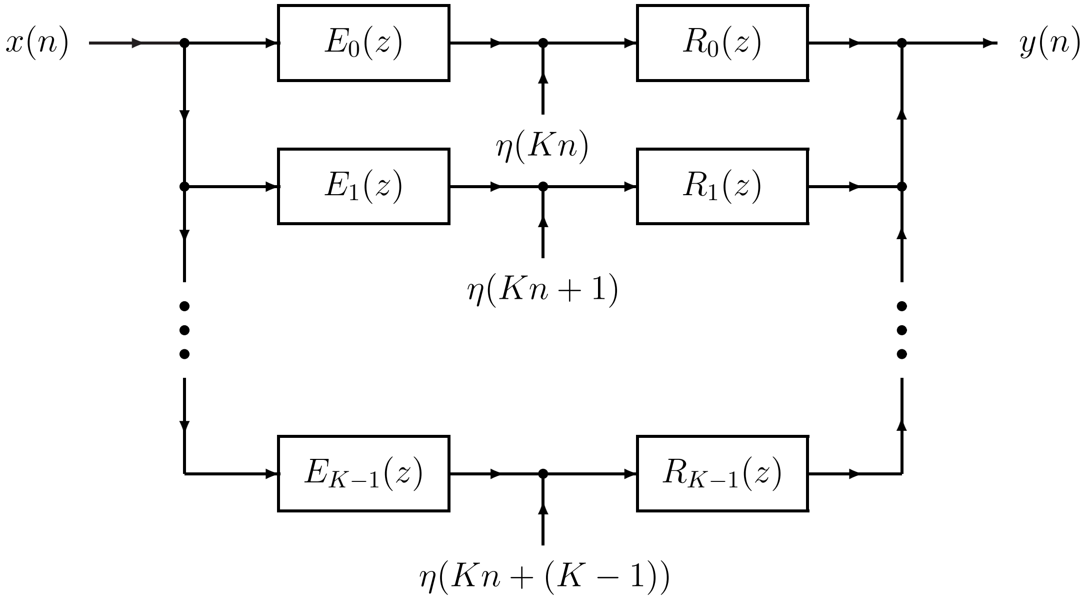

Figure 6.10: Equivalent form of Fig. 6.9 upon removing the unblocking/blocking systems.

Chapter 7

Conclusion

In this thesis we presented a wide variety of optimization algorithms for the design of realizable signal-adapted filter banks. Our focus in the first part of the thesis was specifically on the design of FIR PU signal-adapted filter banks. One of the major contributions was to *bridge the gap* between two theoretically optimal PU filter banks, namely, the zeroth-order PCFB (KLT) and the unconstrained or infinite-order PCFB. This link has previously not been shown in the literature. As opposed to traditional FIR PU signal-adapted filter bank design methods, in which the filter bank is chosen to optimize a specific objective for which the PCFB is optimal, the design goals of the methods presented here were quite different and novel. In particular, in one of the methods proposed, the design objective was to approximate the infinite-order PCFB itself in the least-squares sense with a realizable FIR PU filter bank. Using an important complete characterization of FIR PU systems in terms of degree-one Householder-like building blocks, we showed how to optimize each parameter seperately, which in turn led to an iterative greedy algorithm for solving the original least-squares problem. Simulation results for this and other methods presented here showed that the FIR PU filter banks designed exhibited PCFB-like behavior. The FIR filter banks designed were shown to *monotonically* behave more and more like the infinite-order PCFB as the FIR order increased. This monotonic behavior was shown in terms of numerous objectives for which the PCFB is optimal. These results served to *bridge the gap* between the zeroth-order KLT and infinite-order PCFB which previously had not been reported in the literature.

In the second part of the thesis, we focused on the design of a signal-adapted filter bank in which the analysis and synthesis filters were FIR but otherwise unconstrained. The model considered was a uniform filter bank with scalar quantizers in the subbands. Under the high bit rate assumption, we showed how to obtain either the optimal analysis or synthesis bank using the trick of completing the square. This in turn led to another iterative greedy algorithm in which the analysis and synthesis banks were alternately optimized. The main contribution of the algorithm here was shown through simulations presented here. In particular, the FIR filter banks designed exhibited a monotonic tendency toward information theoretic bounds on distortion and coding gain as the FIR filter orders increased. Though this result is intuitive, it has not formally been shown in the literature until now.

In the third part of the thesis, we showed how some of the optimization techniques used for the design of signal-adapted filter banks could be used for designing channel shortening equalizers. Here, we showed how the eigenfilter method could be used for the design of good TEQs for DMT systems. As opposed to other eigenfilter TEQ design methods which require a different Cholesky factor for every delay parameter considered, the proposed method only required one such factor for all delays. In addition to being low in computational complexity, the proposed method was shown to perform nearly optimally in terms of observed bit rate in simulations presented here.

Matlab code for several of the algorithms presented in this thesis will soon be available at [60].

7.1 Open Problems

Despite the contributions related to the design of realizable signal-adapted filter banks presented here, a number of problems still remain open. First of all, note that all of the algorithms proposed here apply only to uniform filter banks. In several wavelet-based lossy data compression schemes, a *nonuniform* filter bank is commonly used to achieve compression [41, 39]. At this time, it is not known how to generalize the proposed optimization algorithms to nonuniform filter banks. It should be noted that any nonuniform filter bank can be equivalently redrawn as a uniform filter bank with restrictions on the polyphase matrices [67]. Hence, in order to use the algorithms proposed here, we would have to account for these restrictions along with inherent FIR assumption and any other constraints such as the PU condition.

Another problem that also remains open is generalizing the FIR PU design algorithms to the multidimensional case. This may be useful, for example, in image or video processing if we seek an optimal *nonseparable* filter bank for compression. The problem in the general multidimensional case is that there is no known complete parameterization of FIR PU systems in terms of Householder-like degree-one building blocks as in the one-dimensional case. Though FIR PU factorizations similar to those given in Sec. 3.2 exist for the multidimensional case, they do not cover all such systems and are as such incomplete.

On a practical note, one issue which remains unresolved is how the iterative greedy algorithms will perform when the input signal statistics rapidly fluctuate and must be adaptively updated. This phenomenon commonly occurs in audio signal processing where the assumed stationarity is only valid for short periods of time.

Another issue which remains unanswered at this point in time is whether the algorithms proposed here can be used in applications outside of source coding and data compresson. In particular, it is not known if the design methods proposed here can be used for channel coding applications in digital communications. Typically, in digital communications, a redundant transmultiplexer is used and the design objectives are quite different in nature than those considered for data compression. Nevertheless, it would be interesting to see whether the proposed design algorithms could be used for this application. For the FIR PU design algorithms proposed here, this widely depends on whether the theory of PCFBs can be applied to redundant transmultiplexers. The theory of PCFBs, which has been found useful for nonredundant transmultiplexers, has not yet been extended for the redundant case.

Bibliography

[1] S. Akkarakaran and P. P. Vaidyanathan, “Filterbank optimization with convex objectives and the optimality of principal component forms,” *IEEE Trans. Signal Processing*, vol. 49, no. 1, pp. 100–114, Jan. 2001.

[2] N. Al-Dhahir, “FIR channel-shortening equalizers for MIMO ISI channels,” *IEEE Trans. Commun.*, vol. 49, no. 2, pp. 213–218, Feb. 2001.

[3] N. Al-Dhahir and J. M. Cioffi, “Efficiently computed reduced-parameter input-aided MMSE equalizers for ML detection: a unified approach,” *IEEE Trans. Inform. Theory*, vol. 42, no. 3, pp. 903–915, May 1996.

[4] ——, “A bandwidth-optimized reduced-complexity equalized multicarrier transceiver,” *IEEE Trans. Commun.*, vol. 45, no. 8, pp. 948–956, Aug. 1997.

[5] G. Arslan, M. Ding, B. Lu, M. Milosević, Z. Shen, and B. L. Evans. (2003) Matlab DMTTEQ Toolbox. [Online]. Available: http://www.ece.utexas.edu/ bevans/projects/adsl/dmtteq/dmtteq.html

[6] G. Arslan, B. L. Evans, and S. Kiaei, “Equalization for discrete multitone transceivers to maximize bit rate,” *IEEE Trans. Signal Processing*, vol. 49, no. 12, pp. 3123–3135, Dec. 2001.

[7] R. E. Blahut, *Principles and Practice of Information Theory.* Reading, MA: Addison-Wesley, 1987.

[8] H. Caglar, Y. Liu, and A. N. Akansu, “Statistically optimized PR-QMF design,” in *Proc. SPIE 1605, Wavelet Appl. Signal Image Process.*, San Diego, CA, 1991, pp. 86–94.

[9] P. R. Chevillat and G. Ungerboeck, “Optimum FIR transmitter and receiver filters for data transmission over band-limited channels,” *IEEE Trans. Commun.*, vol. COM-30, no. 8, pp. 1909–1915, Aug. 1982.

[10] T. M. Cover and J. A. Thomas, *Elements of Information Theory.* New York, NY: John Wiley & Sons, 1991.

[11] P. Delsarte, B. Macq, and D. T. M. Slock, "Signal-adapted multiresolution transform for image coding," *IEEE Trans. Inform. Theory*, vol. 38, no. 2, pp. 897–904, Mar. 1992.

[12] I. Djokovic and P. P. Vaidyanathan, "Results on biorthogonal filter banks," *Journal of Applied and Computational Harmonic Analysis*, vol. 1, pp. 329–343, 1994.

[13] N. J. Fliege, *Multirate Digital Signal Processing: Multirate Systems - Filter Banks - Wavelets.* Chichester, England: John Wiley & Sons, 1994.

[14] G. B. Giannakis, "Filterbanks for blind channel identification and equalization," *IEEE Signal Processing Lett.*, vol. 4, no. 6, pp. 184–187, June 1997.

[15] G. B. Giannakis, Y. Hua, P. Stoica, and L. Tong, *Signal Processing Advances in Wireless and Mobile Communications, Volume 1: Trends in Channel Estimation and Equalization.* Upper Saddle River, NJ: Prentice-Hall, 2000.

[16] ——, *Signal Processing Advances in Wireless and Mobile Communications, Volume 2: Trends in Single- and Multi-User Systems.* Upper Saddle River, NJ: Prentice-Hall, 2000.

[17] G. B. Giannakis, Z. Wang, A. Scaglione, and S. Barbarossa, "AMOUR-generalized multicarrier CDMA irrespective of multipath," in *Proc. Global Telecommunications Conference*, vol. 1B, Rio de Janeireo, Brazil, Dec. 1999, pp. 965–969.

[18] ——, "AMOUR-generalized multicarrier transceivers for blind CDMA regardless of multipath," *IEEE Trans. Commun.*, vol. 48, no. 12, pp. 2064–2076, Dec. 2000.

[19] A. Hjørungnes, H. Coward, and T. A. Ramstad, "Minimum mean square error FIR filter banks with arbitrary filter lengths," in *Proc. Int. on Image Processing*, vol. 1, Kobe, Japan, Oct. 1999, pp. 619–623.

[20] A. Hjørungnes and T. A. Ramstad, "Algorithm for jointly optimized analysis and synthesis FIR filter banks," in *Proc. IEEE Int. Conf. on Electron., Circuits, and Systems*, vol. 1, Pafos, Cyprus, Sept. 1999, pp. 369–372.

[21] A. Hjørungnes and T. Saramäki, "Minimum mean square error nonuniform FIR filter banks," in *Proc. IEEE Int. Conf. on Acoust., Speech, and Signal Processing*, vol. 6, Salt Lake City, UT, May 2001, pp. 3609–3612.

[22] R. A. Horn and C. R. Johnson, *Matrix Analysis.* Cambridge, U.K.: Cambridge University Press, 1985.

[23] Y. Huang and P. M. Schultheiss, "Block quantization of correlated Gaussian random variables," *IEEE Trans. Commun. Syst.*, vol. C-10, pp. 289–296, Sept. 1963.

[24] O. S. Jahromi, B. A. Francis, and R. H. Kwong, "Algebraic theory of optimal filterbanks," *IEEE Trans. Signal Processing*, vol. 51, no. 2, pp. 442–457, Feb. 2003.

[25] N. S. Jayant and P. Noll, *Digital Coding of Waveforms: Principles and Applications to Speech and Video.* Englewood Cliffs, NJ: Prentice-Hall, 1984.

[26] I. Kalet, "The multitone channel,"*IEEE Trans. Commun.*, vol.37, no.2, pp. 119–124, Feb.1989.

[27] A. Kıraç and P. P. Vaidyanathan, "On existence of FIR principal component filter banks," in *Proc. IEEE Int. Conf. on Acoust., Speech, and Signal Processing*, vol. 3, Seattle, WA, May 1998, pp. 1329–1332.

[28] ——, "Optimality of orthonormal transforms for subband coding," in *Proc. IEEE DSP Workshop*, Bryce Canyon, UT, Aug. 1998.

[29] ——, "Theory and design of optimum FIR compaction filters," *IEEE Trans. Signal Processing*, vol. 46, no. 4, pp. 903–919, Apr. 1998.

[30] J. Kovačević and M. Vetterli, "Perfect reconstruction filter banks with rational sampling factors," *IEEE Trans. Signal Processing*, vol. 41, no. 6, pp. 2047–2066, June 1993.

[31] B. Maison and L. Vandendorpe, "About the asymptotic performance of multiple-input/multiple-output linear prediction of subband signals," *IEEE Signal Processing Lett.*, vol. 5, no. 12, pp. 315–317, Dec. 1998.

[32] S. Mallat, *A Wavelet Tour of Signal Processing*, 2nd ed. San Diego, CA: Academic Press, 1999.

[33] P. J. W. Melsa, R. C. Younce, and C. E. Rohrs, "Impulse response shortening for discrete multitone transceivers," *IEEE Trans. Commun.*, vol. 44, no. 12, pp. 1662–1672, Dec. 1996.

[34] T. K. Moon and W. C. Stirling, *Mathematical Methods and Algorithms for Signal Processing.* Upper Saddle River, NJ: Prentice-Hall, 2000.

[35] P. Moulin, M. Anitescu, K. O. Kortanek, and F. A. Potra, "The role of linear semi-infinite programming in signal-adapted QMF bank design," *IEEE Trans. Signal Processing*, vol. 45, no. 9, pp. 2160–2174, Sept. 1997.

[36] P. Moulin, M. Anitescu, and K. Ramchandran, "Theory of rate-distortion-optimal, constrained filterbanks–application to IIR and FIR biorthogonal designs," *IEEE Trans. Signal Processing*, vol. 48, no. 4, pp. 1120–1132, Apr. 2000.

[37] P. Moulin and M. K. Mıhçak, "Theory and design of signal-adapted FIR paraunitary filter banks," *IEEE Trans. Signal Processing*, vol. 46, no. 4, pp. 920–929, Apr. 1998.

[38] J. G. Proakis, *Digital Communications*, 4th ed. New York, NY: McGraw-Hill, 2000.

[39] D. Salomon, *A Guide to Data Compression Methods.* New York, NY: Springer-Verlag, 2002.

[40] V. P. Sathe and P. P. Vaidyanathan, "Effects of multirate systems on the statistical properties of random signals," *IEEE Trans. Signal Processing*, vol. 41, no. 1, pp. 131–146, Jan. 1993.

[41] K. Sayood, *Introduction to Data Compression*, 2nd ed. San Diego, CA: Academic Press, 2000.

[42] A. Scaglione, G. B. Giannakis, and S. Barbarossa, "Redundant filterbank precoders and equalizers: Part I: unification and optimal designs," *IEEE Trans. Signal Processing*, vol. 47, no. 7, pp. 1988–2006, July 1999.

[43] ——, "Redundant filterbank precoders and equalizers: Part II: blind channel estimation, synchronization, and direct equalization," *IEEE Trans. Signal Processing*, vol. 47, no. 7, pp. 2007–2022, July 1999.

[44] R. Schur and J. Speidel, "An efficient equalization method to minimize delay spread in OFDM/DMT systems," in *Proc. IEEE Int. Conf. on Communications*, vol. 5, Helsinki, Finland, June 2001, pp. 1481–1485.

[45] A. K. Soman and P. P. Vaidyanathan, "On orthonormal wavelets and paraunitary filter banks," *IEEE Trans. Signal Processing*, vol. 41, no. 3, pp. 1170–1183, Mar. 1993.

[46] T. Starr, J. M. Cioffi, and P. J. Silverman, *Understanding Digital Subscriber Line Technology.* Upper Saddle River, NJ: Prentice-Hall, 1999.

[47] G. Strang and T. Nguyen, *Wavelets and Filter Banks.* Wellesley, MA: Wellesley-Cambridge Press, 1996.

[48] C. W. Therrien, *Discrete Random Signals and Statistical Signal Processing.* Upper Saddle River, NJ: Prentice-Hall, 1992.

[49] A. Tkacenko and P. P. Vaidyanathan, "Iterative gradient based greedy algorithm for the design of optimal FIR compaction filters and signal-adapted paraunitary filter banks," submitted to *IEEE Trans. Signal Processing.*

[50] ——, "Iterative greedy algorithm for solving the FIR paraunitary approximation problem," submitted to *IEEE Trans. Signal Processing.*

[51] ——, "Eigenfilter design of MIMO equalizers for channel shortening," in *Proc. IEEE Int. Conf. on Acoust., Speech, and Signal Processing*, vol. 3, Orlando, FL, May 2002, pp. 2361–2364.

[52] ——, "A new eigenfilter based method for optimal design of channel shortening equalizers," in *Proc. IEEE Int. Symp. on Circuits and Systems*, vol. 2, Scottsdale, AZ, May 2002, pp. 504–507.

[53] ——, "Noise optimized eigenfilter design of time-domain equalizers for DMT systems," in *Proc. IEEE Int. Conf. on Communications*, vol. 1, New York, NY, Apr./May 2002, pp. 54–58.

[54] ——, "Iterative eigenfilter method for designing optimum overdecimated orthonormal FIR compaction filter banks," in *Proc. 37th Asilomar Conference on Signals, Systems and Computers*, Pacific Grove, CA, Nov. 2003.

[55] ——, "A low-complexity eigenfilter design method for channel shortening equalizers for DMT systems," *IEEE Trans. Commun.*, vol. 51, no. 7, pp. 1069–1072, July 2003.

[56] ——, "On the eigenfilter design method and its applications: a tutorial," *IEEE Trans. Circuits Syst. II*, vol. 50, no. 9, pp. 497–517, Sept. 2003.

[57] ——, "On the least squares signal approximation model for overdecimated rational nonuniform filter banks and applications," in *Proc. IEEE Int. Conf. on Acoust., Speech, and Signal Processing*, vol. 6, Hong Kong, China, Apr. 2003, pp. 481–484.

[58] ——, “Iterative algorithm for the design of optimal FIR analysis/synthesis filters for overdecimated filter banks,” accepted to *IEEE Int. Symp. on Circuits and Systems*, May 2004.

[59] ——, “Iterative gradient technique for the design of least squares optimal FIR magnitude squared nyquist filters,” accepted to *IEEE Int. Conf. on Acoust., Speech, and Signal Processing*, May 2004.

[60] A. Tkacenko. (2004) Matlab Signal-Adapted Filter Bank Optimization Algorithms. [Online]. Available: http://www.systems.caltech.edu/dsp/students/andre/index.html

[61] J. R. Treichler, I. Fijalkow, and J. C. R. Johnson, “Fractionally spaced equalizers: How long should they really be?” *IEEE Signal Processing Mag.*, vol. 13, no. 3, pp. 65–81, May 1996.

[62] M. K. Tsatsanis and G. B. Giannakis, “Principal component filter banks for optimal multiresolution analysis,” *IEEE Trans. Signal Processing*, vol. 43, no. 8, pp. 1766–1777, Aug. 1995.

[63] D. W. Tufts and J. T. Francis, “Designing digital lowpass filters: comparison of some methods and criteria,” *IEEE Trans. Audio Electroacoust.*, vol. AU-18, pp. 487–494, Dec. 1970.

[64] J. Tuqan and P. P. Vaidyanathan, “A state space approach to the design of globally optimal FIR energy compaction filters,” *IEEE Trans. Signal Processing*, vol. 48, no. 10, pp. 2822–2838, Oct. 2000.

[65] M. Unser, “An extension of the KLT for wavelets and perfect reconstruction filter banks,” in *Proc. SPIE 2034, Wavelet Appl. Signal Image Process.*, San Diego, CA, 1993, pp. 45–56.

[66] ——, “On the optimality of ideal filters for pyramid and wavelet signal approximation,” *IEEE Trans. Signal Processing*, vol. 41, no. 12, pp. 3591–3596, Dec. 1993.

[67] P. P. Vaidyanathan, *Multirate Systems and Filter Banks.* Englewood Cliffs, NJ: Prentice-Hall, 1993.

[68] ——, “Theory of optimal orthonormal subband coders,” *IEEE Trans. Signal Processing*, vol. 46, no. 6, pp. 1528–1543, June 1998.

[69] P. P. Vaidyanathan and S. Akkarakaran, “A review of the theory and applications of optimal subband and transform coders,” *Journal of Applied and Computational Harmonic Analysis*, vol. 10, pp. 254–289, 2001.

[70] P. P. Vaidyanathan and P. Q. Hoang, "Lattice structures for optimal design and robust implementation of two-channel perfect-reconstruction QMF banks," *IEEE Trans. Acoust., Speech, Signal Processing*, vol. 36, no. 1, pp. 81–94, Jan. 1988.

[71] P. P. Vaidyanathan and A. Kıraç, "Cyclic LTI systems and the paraunitary interpolation problem," in *Proc. IEEE Int. Conf. on Acoust., Speech, and Signal Processing*, vol. 3, Seattle, WA, May 1998, pp. 1445–1448.

[72] ——, "Results on optimal biorthogonal filter banks," *IEEE Trans. Circuits Syst. II*, vol. 45, no. 8, pp. 932–947, Aug. 1998.

[73] P. P. Vaidyanathan, Y.-P. Lin, S. Akkarakaran, and S.-M. Phoong, "Discrete multitone modulation with principal component filter banks," *IEEE Trans. Circuits Syst. I*, vol. 49, no. 10, pp. 1397–1412, Oct. 2002.

[74] P. P. Vaidyanathan and T. Q. Nguyen, "Eigenfilters: a new approach to least-squares FIR filter design and applications including Nyquist filters," *IEEE Trans. Circuits Syst.*, vol. CAS-34, no. 1, pp. 11–23, Jan. 1987.

[75] P. P. Vaidyanathan, T. Q. Nguyen, Z. Doğanata, and T. Saramäki, "Improved technique for design of perfect reconstruction FIR QMF banks with lossless polyphase matrices," *IEEE Trans. Acoust., Speech, Signal Processing*, vol. 37, no. 7, pp. 1042–1056, July 1989.

[76] P. P. Vaidyanathan and B. Vrcelj, "Biorthogonal partners and applications," *IEEE Trans. Signal Processing*, vol. 49, no. 5, pp. 1013–1027, May 2001.

[77] B. Vrcelj and P. P. Vaidyanathan, "Least squares signal approximation using multirate systems: multichannel nonuniform case," in *Proc. 35th Asilomar Conference on Signals, Systems and Computers*, vol. 1, Pacific Grove, CA, Nov. 2001, pp. 553–557.

[78] ——, "MIMO biorthogonal partners and applications," *IEEE Trans. Signal Processing*, vol. 50, no. 3, pp. 528–542, Mar. 2002.

[79] B. Xuan and R. H. Bamberger, "FIR principal component filter banks," *IEEE Trans. Signal Processing*, vol. 46, no. 4, pp. 930–940, Apr. 1998.